Finite Element Method Based Design Approach for Low Volume Roads Using Dynamic Cone Penetrometer Results

by

JACOB ADEDAYO **ADEDEJI**

Doctoral thesis submitted in partial fulfilment of the requirement for the degree

DOCTOR OF ENGINEERING IN CIVIL ENGINEERING

at the

Central University of Technology

Faculty of Engineering, Built Environment and Information Technology,

Department of Civil Engineering, Bloemfontein Campus,

Free State

Supervisor: Prof. Mohamed M H Mostafa (University of KwaZulu-Natal, South Africa)

Co-Supervisor: Prof. Yali Woyessa

NOVEMBER 2025

Bloemfontein

Copyright Notice

Disclaimers

The presentation of this thesis contains colour images meant to present the results visually in a more understandable form. While printing or viewing the thesis in greyscale (black and white) is possible, it is recommended that for clarity, the thesis be viewed (or printed) in full-colour format.

Dedication

This thesis is dedicated to all my family members for their unwavering support and love. I also dedicate this work to my future children, with hopes and prayers for the bright and promising lives they will lead.

Declaration

This research, as presented in this thesis, is original work and has not been presented for any other university award. Knowledge derived from other sources has been clearly indicated, with acknowledgement and reference to the literature.

This study was conducted under the guidance of Professor Mohammed Mostafa Hassan, Department of Civil Engineering at Central University of Technology, Free State, South Africa.

Jacob Adedayo Adedeji

Signature: _____

Date: 03-11-2025

In our capacity as the supervisors of this thesis, we certify that the above statements are true to the best of our knowledge.

Prof. Mohamed Mostafa Hassan

Signature: _____

Date: 03/11/2025

Prof. Yali Woyessa

Signature: _____

Date: 03/11/2025

Preface and Acknowledgements

With a grateful heart, I first give thanks to Almighty God for His unwavering love, grace, strength, wisdom, knowledge, and understanding. His constant presence and guidance made the completion of this research study possible.

I extend my deepest gratitude to my supervisor, Prof. Mohamed Mostafa. Your mentorship has been instrumental in my growth as a researcher, and I am profoundly thankful for your invaluable contributions to this study. I also extend my gratitude and appreciation to my co-supervisor, Prof. Yali Woyessa, for his academic advice and support throughout this journey.

To my beloved parents, Mr. Isaac Adedeji and Mrs. Rachel Adedeji, I am eternally grateful for your love, prayers, and unwavering encouragement. A heartfelt thank you to my uncle, Mr. Taiwo Ogundana, and his wife, Fadesayo Ogundana, for your care and support.

I also wish to acknowledge my colleagues who have become like family here in South Africa. Your companionship and support have been truly invaluable. I extend my heartfelt gratitude to the Central University of Technology and the Durban University of Technology (DUT) for their financial support, and my sincere appreciation to my colleagues at DUT for their continued encouragement and collaboration.

Last, I would like to express my deepest appreciation to my beloved wife, Wendy Kgaphudi Adedeji, for her unwavering support, love, and understanding throughout this journey. Your encouragement has been my greatest source of strength. To my precious daughters, IfeOluwasimi and IyanuOluwa Adedeji, your presence has been a constant reminder of the joy and purpose in my life. I dedicate this work to both of you with all my love.

Abstract

Road networks are fundamental to national development, but their provision should prioritise structural efficiency and long-term sustainability rather than accessibility alone. Despite significant global advances in road construction, a large proportion of roads, particularly in developing and emerging economies, remain unsealed and prone to rapid deterioration. South Africa exemplifies this challenge: although it has the continent's longest road network (764,978 km), almost three-quarters of its proclaimed roads are unpaved. Sustainable and cost-effective upgrading of such networks to sealed low-volume roads is therefore a pressing need, particularly under financial constraints.

The aim of this study was to develop a Finite Element Method (FEM) model that utilises existing Dynamic Cone Penetrometer (DCP) correlations to improve the efficiency and cost-effectiveness of low-volume road (LVR) design, benchmarked against conventional empirical methods. Trial sections were established in two climatically distinct provinces—Northern Cape (dry) and KwaZulu-Natal (wet)—to enable material collection and in-situ testing representative of different geotechnical environments.

The methodology integrated in-situ testing, laboratory characterisation, and computational modelling. DCP testing was undertaken across the trial sections to establish penetration resistance profiles, which were correlated with laboratory-derived parameters obtained from grain size distribution, Atterberg limits, California Bearing Ratio (CBR), and repeated load triaxial tests (RLTT). AfCP-LVR software was used to establish empirical DCP–CBR–modulus relationships, while comparative pavement designs were produced using CBR charts, AASHTO 1993, TRH 20, Odemark's method, mePADS, and FEM simulations. FEM models (2D and 3D) were developed in Abaqus®/CAE to simulate pavement responses under traffic loading, incorporating both unsealed and sealed surface conditions.

The findings indicate that while existing design guides such as TRH 20:2009 remain valuable references for unsealed road design, their limitations in accounting for surfacing seal effects underscore the need for integrated analytical approaches. In this study, the FEM model was developed to incorporate material parameters derived from DCP correlations, enabling a mechanistic evaluation of pavement performance under

various loading and environmental conditions. This integration provided more consistent and realistic predictions of structural behaviour, particularly with respect to pavement deflections, stresses, and service life, than conventional empirical approaches. Model validation demonstrated strong agreement between mePADS, 2D FEM and 3D FEM Abaqus® simulations, confirming the robustness of the developed modelling framework. Furthermore, the inclusion of surface seals, both single and double treatments, significantly reduced critical tensile strains and extended pavement service life, emphasising the influence of binder stiffness and temperature on overall performance.

This study concludes that the integration of DCP testing with FEM modelling offers a robust, field-applicable, and cost-effective approach for the design and upgrading of low-volume roads in South Africa. The research further delivers a simplified design model that incorporates new construction and rehabilitation options, supporting the use of surface seals as alternative wearing courses to achieve durable and economical LVR solutions.

Keywords: Low-volume roads, Mechanistic-empirical design, Dynamic cone penetrometer, Finite element method, Surface seal

List of Abbreviations and Acronyms

AASHTO	American Association of State Highway
AfCAP	Africa Community Access Partnership
ALD	Average Least Dimension
BN	Balance Number
CBR	California Bearing Ration
CPT	Cone Penetration Test
CSIR	Council of Scientific and Industrial Research
DCP	Dynamic Cone Penetrometer
DCPI	DCP penetration index
DN	Penetration Rate
DOF	Degree of Freedom
DP	Drucker-Prager
ERA	Ethiopian Roads Authority
FEM	Finite Element Method
GDP	Gross Domestic Product
KZNS	KwaZulu-Natal Soil
LVR	Low Volume Road
MC	Mohr-Coulomb
MDD	Maximum Dry Density
MISA	Million Standard Axles
MR	Resilient Modulus

NCS	Northern Cape Soils
OMC	Optimum Moisture Content
SAICE	South African Institute of Civil Engineering
SANRAL	South African National Road Agency
SAPDM	South African Pavement Design Method
SPBC	Standard Pavement Balance Curve
SPT	Standard Penetration Test
TRH	Technical Recommendation for Highway
UCS	Unconfined Compressive Strength

Table of Contents

List of Figures

List of Tables

List of Publications

As an outcome of this research, the author of this thesis is the first author of the currently published paper listed below.

- Adedeji, J. A., & Mostafa Hassan, M. (2019). Performance Evaluation of Ultra-Thin Pavement Seals in Low-Volume Roads. In *Recent Developments in Pavement Design, Modelling and Performance: Proceedings of the 2nd GeoMEast International Congress and Exhibition on Sustainable Civil Infrastructures, Egypt 2018–The Official International Congress of the Soil-Structure Interaction Group in Egypt (SSIGE)* (pp. 1-14). Springer International Publishing.

Chapter 1 : Introduction

1.1 Background

A road network constitutes a fundamental component of a nation's infrastructure, playing a critical role in socio-economic development. Over the past century, significant advancements have been made globally in road construction (Balaguera, Carvajal, Albertí, & Fullana-i-Palmer 2018; Rensburg & Krygsman 2020). However, a substantial proportion of these roads remain unsealed and are progressively deteriorating. While this issue is observed worldwide, it is particularly pronounced in developing and emerging economies. This trend is especially evident in Africa, where the total length of unpaved roads generally exceeds that of paved networks (Paige-Green & Pinard 2012).

South Africa has the longest road network, with a total length of 764,978 kilometres, and equally represents the continent as the 10th longest in the world (Rensburg & Krygsman 2020; Kannemeyer 2013; South African National Roads Agency Ltd 2013). However, although South Africa is at the forefront of the continent, almost three-quarters of the proclaimed road network, accounting for over 500,000km of roads, is unpaved (Kannemeyer 2013; Paige-Green 2005). These roads have contributed to retarding the country's economic growth in terms of the agricultural sector and social services as highlighted by (Pooni, Robert, Giustozzi, Gunasekara & Setunge 2022; Nkomo, Desai & Peerbhay 2016; Jagtap & Nagrale 2013; DoT 1996).

Franzen & Thorpe (2020), Paige-Green & Pinard (2012), and Paige-Green 2005, further highlight that unsealed roads constrain mobility, significantly increase vehicle operating costs and maintenance costs, increase accident rates and the generation of unnecessary dust, which is hazardous to human health, and the unsustainable loss of gravel material, which is quantified at 30-60 million cubic meters annually. Additionally, it can contribute to increased transportation challenges and may exacerbate issues such as limited access, economic hardship, poor health services, and low educational attainment in rural communities (Burningham & Stankevich 2005). Considering these challenges, sustainable and economical upgrading of unsealed roads to low-volume

sealed roads is needed. Similar to the conventional design principle for new roads, the in-situ conditions of unsealed roads need to be assessed. Notably, a simple and cost-effective dynamic cone penetrometer (DCP) test device can be used for this task. In addition, the DCP results have been extensively used in rehabilitation design for a variety of roads, which makes it relevant in this situation.

Overall, the current global trend in pavement design has shifted from traditional empirical methods to mechanistic-empirical design methods (ME-DMs). These modern approaches often incorporate advanced numerical techniques—such as the Finite Element Method (FEM)—to simulate pavement behaviour with greater accuracy. In the context of upgrading unsealed roads to sealed standards, it is essential to consider these developments. Although the use of FEM offers significant advantages in terms of modelling accuracy and design optimization, its applicability to low-volume roads (LVRs) may be questioned due to perceived cost implications. However, recent studies (Jagtap & Nagrale 2013; Gerald, Andrewski & Gallivan 2009) have demonstrated that FEM-based modelling can reduce the overall cost of road construction by enabling more efficient material use and structural optimization. Accordingly, this study focuses on applying FEM to model LVRs using Dynamic Cone Penetrometer (DCP) test results.

1.2 Problem Statement

Rural roads are the key to increasing living standards in poor rural areas; however, these rural roads are primarily categorized as low-volume roads that are not in good condition (mostly unsealed). These poor conditions of low-volume roads have contributed significantly to increased vehicle operating costs, increased accident rates, excessive dust, and unsustainable loss of gravel materials, and they have further contributed to human and property costs. Although this is a global issue, the case of developing countries in Africa is alarming, as three-quarters of the population does not have access to all-weather roads. Additionally, South Africa's case is not different, as almost three-quarters of the road network remains unpaved.

Over the years, researchers have been looking for the most economical way of constructing low-volume roads to meet society's needs. One of the greatest successes recorded was the use of the DCP test to analyse the initial condition of the unsealed roads, thereby designing the roads via traditional empirical methods. However, the

use of this conventional empirical method has been questioned because of its drawbacks (Jagtap & Nagrale 2013; Gerald et al. 2009; Paige-Green & Pinard 2012). Thus, pavement design continues to experience a global shift, with the resilient modulus and similar parameters being increasingly institutionalized within mechanistic-empirical design frameworks (Committee of State Road Authorities 1984; AASHTO 2002). Considering this, one of the best, simplest, and most cost-effective practices for designing and analysing low-volume roads is needed. Therefore, this study focuses on developing a FEM approach for designing low-volume roads based on DCP test results, as an alternative to traditional empirical methods.

1.3 Research Aim and Objectives

This research aims to develop a FEM model that utilises existing DCP correlations to improve the efficiency and cost-effectiveness of low-volume road design. To achieve this aim, the following specific objectives are considered:

- To analyse the factors influencing DCP results and establish correlations with laboratory-derived parameters to improve reliability in LVR structural assessments.
- To evaluate existing LVR design methods, including DCP-based approaches, and compare their performance using site-specific datasets.
- To develop a FEM model for predicting LVR deformation and compare its outputs with empirical and mechanistic-empirical design approaches.
- To develop a simplified design model for low-volume roads, incorporating both new construction and rehabilitation options, including the use of surface seals as alternative wearing courses.

1.4 Delimitation of the Study

This study focuses on designing and evaluating LVRs based on DCP correlations using FEM. The scope is limited to unsealed LVRs, particularly in developing countries such as South Africa, where maintaining and upgrading these roads is costly because of the high proportion of unpaved roads.

The research excludes high-volume roads, as their traffic volumes and construction needs are distinct. However, it emphasizes the application of the FEM in LVR design, specifically for unbound granular aggregates, and considers the application of surface

seals, which are commonly used in LVR construction. This study does not address materials such as asphalt or concrete, which are typical of high-volume roads, nor does it cover the entire design methodology. It compares the FEM with traditional empirical and mechanistic-empirical methods currently used for LVR design.

The study is also limited by the number of test specimens and scenarios, acknowledging that larger sample sizes might alter the findings. Conducted under South African climatic and geological conditions, the conclusions are most applicable to similar contexts where LVRs are prevalent, and DCP testing is a practical tool for road analysis.

1.5 Significance of the Study

This study contributes meaningfully to the ongoing discourse on sustainable infrastructure development by introducing an innovative, cost-effective methodology for designing LVRs using DCP data within a FEM model. Unlike conventional empirical approaches, which often lack adaptability and precision, the proposed method integrates site-specific in-situ data to produce more accurate and resource-efficient road designs.

The relevance of this research lies in its potential to bridge the methodological gap between traditional DCP analysis and modern mechanistic-empirical pavement design. By translating DCP data into input parameters for FEM, this study offers a new perspective on road design that reduces reliance on extensive and expensive laboratory testing while enhancing structural accuracy and long-term performance.

Furthermore, the models developed here is particularly tailored for use in resource-constrained environments like those prevalent in many parts of Africa, including South Africa. It addresses critical challenges such as material scarcity, high construction costs, and inadequate road performance by offering a streamlined process for assessing and upgrading unsealed roads. The potential outcomes include enhanced road safety, reduced maintenance costs, and improved access to essential services for underserved populations. This study not only fills a vital research gap but also lays a foundation for future integration of smart and adaptable tools in rural infrastructure development. Its findings are expected to inform both policy and practice in pavement

engineering, making it a valuable resource for engineers, planners, and decision-makers in the transportation sector.

1.6 Outline of Thesis

The remainder of this thesis is organised as follows:

Chapter 2 presents a review of literature on LVRs and their global and African context. It highlights the differences between sealed and unsealed roads, their economic and social significance, and the challenges posed by leaving LVRs unpaved. The chapter also examines the definitions of LVRs across regions and discusses cost-effective approaches such as the use of in-situ materials and sealing options.

Chapter 3 continues the literature review with a focus on material testing and design methods for LVRs. Both laboratory tests (Atterberg limits, compaction, CBR) and in-situ methods (particularly the Dynamic Cone Penetrometer, DCP) are discussed, alongside their applications in material classification and strength assessment. The chapter also reviews empirical design methods (CBR, AASHTO 1993, TRH 20) and mechanistic-empirical methods (Odemark, MePADS, FEM), highlighting their advantages and limitations for LVR applications.

Chapter 4 outlines the research methodology. It describes the selection of study areas in South Africa (Northern Cape and KwaZulu-Natal), the field and laboratory investigations undertaken (soil index properties, compaction, CBR, triaxial testing), and the DCP testing programme. The chapter also explains the development of FEM models and the comparative framework applied to evaluate different design approaches using consistent datasets.

Chapter 5 presents the laboratory test results and material characterisation for the study areas. The results include grain size distribution, Atterberg limits, compaction behaviour, and resilient modulus values derived from triaxial testing. Correlations between DCP results and laboratory-derived parameters (CBR and modulus) are established, providing the basis for integrating field data into FEM analysis.

Chapter 6 evaluates existing LVR design methods by applying empirical (CBR, AASHTO 1993, TRH 20, Odemark) and mechanistic-empirical approaches (MePADS and FEM) to the site-specific datasets. The chapter compares the predicted pavement

structures, stresses, strains, and design lives, and validates the FEM outputs against MePADS elastic theory and laboratory data. The findings demonstrate the strengths and weaknesses of each method and emphasise the role of DCP-informed models in capturing realistic field variability.

Chapter 7 develops FEM models for predicting LVR deformation and compares their outputs with conventional approaches. The chapter highlights the limitations of elastic models in capturing yielding and bulging, and shows how non-linear models (Drucker–Prager and Mohr–Coulomb) provide results more consistent with experimental data. Rutting predictions expressed as the number of load repetitions to failure are also presented, demonstrating the improved predictive capacity of FEM over conventional methods.

Chapter 8 focuses on the modelling of surface seals for LVRs at the mesoscale. It analyses the interactions between aggregate, binder, and base layers under different loading and temperature conditions. The chapter evaluates performance in terms of deflections, strains, and failure mechanisms, showing the benefits of single and double seals and the importance of binder stiffness. These findings provide the basis for a simplified design model for incorporating surface seals in both new construction and rehabilitation.

Chapter 9 presents the overall conclusions and recommendations of the study. Each conclusion is aligned with the specific objectives, addressing the developed correlation between DCP and laboratory results, the evaluation of existing design methods, the performance of FEM models, and the simplified model for surface seals. Recommendations for practice and areas for further research are also outlined, with the aim of improving the reliability, cost-effectiveness, and sustainability of LVR design.

Chapter 2 : Literature Review – Low-Volume Roads

2.1 Introduction: Global Rationale for Low-volume Road

A reduction in travel time and cost of travel, as well as increased traffic safety, are the ultimate deliverables of a well-designed road system in global transportation. To address these targets, efforts have been made in material technology, sustainability, traffic management, improved design methods, construction practices, and information services for highway engineering standards (Brito 2011). However, these targets are yet to be met, as there is a continuous increase in travel time and vehicle operation cost, especially when travelling on low-volume roads (LVRs), which constitute more than 80% of the world road network (Franzen & Thorpe 2020; Jing, Nowamooz & Chazallon 2017; Chowdary, Ramulu, Shankar & Prasad 2012; Faiz, Faiz, Wang & Bennett 2012).

LVRs provide essential links to highway transportation systems and significant links between raw materials and markets. Thus, these roads constitute a substantial length of road networks throughout the world; for example, the USA, Canada, the UK, India, France and South Africa have approximately 65%, 75%, 95%, 80%, 85% and >75% of LVRs, respectively (Gupta 2017; Jing *et al*. 2017; Doré 2014; Cook, Petts & Rolt 2013; Faiz *et al*. 2012; Brito 2011; Paige-green 2007; Hall & Bettis 2001). Nevertheless, the need for LVRs for economic development and poverty alleviation in a country cannot be overemphasized; however, the larger percentage of LVRs around the world remains unsealed, especially in developing countries.

Different agencies or geographical locations have variously defined the concept of LVRs. Daily traffic volume has been commonly used as a parameter to define what a LVR stands for. In the USA, for example, a road that carries fewer than 500 vehicles per day (vpd) is considered an LVR, whereas the South Africa National Road Agency Limited (SANRAL) describes any road that carries an average traffic of less than 400–500 vpd (Chowdary *et al*. 2012; Hall & Bettis 2001). However, in Ethiopia, LVRs are considered to carry less than 300 vpd (Table 2-1). These roads are further classified into rural, recreational, and resource development roads (Doré 2014).

.

Table 2-1 Global view of low volume (Author's compilation)

Country Name	***Low Volume Definition per Country***	***Total Length of Road Network (km)***	***Total Length of LVRs (km)***	***Percentage of LVRs (%)***	***Percentage of Unsealed (%)***	***Reference (s)***
Angola	< 300 vpd	76,000	-	-	80	Springer Nature Limited 2021
Canada	<200 vpd	1.04 Million	800,000	-	78.3	Douglas 2018; Doré 2014; Roads and Transportation Association of Canada 1986
Ethiopia	< 300 vpd	126,773	56,732	44.75	86	Ethiopian Roads Authority 2018
India	< 450 commercial vehicles per day	5.9 Million	2.7 million	80	-	Mathew & Isaac 2014; Gupta, Kumar & Rastogi 2011; Paul, Biswas, Mondal & Sahis 2024
Malawi	<300 vpd	15,451	8,969	-	74	The World Bank Nov 2009
Nigeria	<300 vpd	200,000	130,000	-	-	Mostafa Hassan 2018
South Africa	400 - 500 vpd	764,978	591,879	> 75	95	Chowdary *et al*. 2012; Paige-green 2007; Hall & Bettis 2001
UK	< 400vpd	393,473	346,455	87.3	-	Department for Transport 2018; Douglas 2018
USA	< 400vpd	6.8 million	-	69	35	Douglas 2018; Apronti, Ksaibati, Gerow & Hepner 2016

Owing to the limited traffic volume per day on the basis of their functionalities, these roads are not a primary focus of the transportation industry or the government. Although these roads carry less traffic, they deteriorate rapidly due to non-traffic-related factors, such as climate, soil conditions, topography or terrain, soil conditions, and a lack of maintenance. This results in limited access and high transportation costs (Pinard *et al*. 2003).

Furthermore, 95% of unsealed roads in South Africa are low in volume (Paige-green 2007). LVRs are considered to carry traffic less than 200,000 equivalent standard axles (ESAs) over a 20-year design life. In South Africa, these roads are taken to have daily traffic of fewer than 500 vpd and basically fall under road categories C and D, which are described as "*light trafficked rural roads, strategic roads*" and "*rural access roads*," respectively, and are regarded as "*less important*" roads. Other characteristics of these road types include the typical pavement class: < ES0.03–ES3; total equivalent traffic loading (E80/lane): < 3 million depending on the design strategy (SANRAL 2013).

Additionally, unsealed roads have constrained mobility in terms of travel time, significantly increase vehicle operating costs and maintenance costs, increase accident rates, contribute to dust generation, which is hazardous to human health, and cause unsustainable loss of gravel material, which is quantified at 30-60 million cubic meters annually (Paige-Green & Pinard 2012; TRH 20 2009; Paige-Green 2005). Furthermore, unsealed roads contribute to associated human and property costs and aggravate rural communities' isolation, poverty, poor health, and illiteracy. Considering these challenges, sustainable and economical upgrading of unsealed roads to sealed LVRs through chip seal or chip sealing techniques seems to be the way out.

Given that LVRs constitute a significant portion of the overall road network, particularly in rural areas and developing countries, they have increasingly attracted the attention of road authorities and developers (Roads Authority Malawi 2020). Coupled with the linkages it provides between production and market areas for the economic development of a country. The importance of roads, especially LVRs, engenders their provision in all regions of the world, including the African continent

2.2 African Context Rationale on LVR

The African continent is characterized by a large population living in rural areas. Several social and economic activities exist in these areas, such as farming, trading, and meetings. These social and economic activities are carried out effectively, depending on the nature of the available road networks in the area. Berg, Blankespoor & and Selod (2018) noted that the growth of African markets and gross domestic product (GDP) from 1971 to 2010 was associated with continuous improvement in the provision of rural roads on the continent. However, most rural roads and some urban roads in Africa are LVRs.

Some low-volume urban roads in Africa are sealed. However, rural areas are mostly constructed as unsealed roads owing to challenges such as inadequate funds, poor engineering design, and poor construction practices, which affect the provision of high-quality roads. The surfaces of rural unpaved roads on this continent are exposed to rainfall and surface water runoff. The surface water runoff and traffic movement on unsealed roads cause rapid deterioration of many low-volume unsealed African roads (Ngezahayo, Burrow & Ghataora 2021). Despite the contributions of LVRs to social and economic development, the conditions of the available road networks on the African continent still leave a gap in effective transportation systems, which slows the development required in the area.

The condition of the road network is critical for the effective transportation of goods and services for production. This shows that for an area to be economically viable, it must have roads that are in good condition to facilitate mobility and that do not damage vehicles. However, some scholars have noted that LVRs in Africa are in distress, associated with poor drainage systems on roads and poor maintenance services (Nkomo *et al*. 2016). Despite the LVR conditions, these roads are the most common and provide accessibility to African urban or rural settlements. In view of the importance of LVRs to settlement accessibility, various countries in Africa, such as Nigeria, Ethiopia, South Africa, etc., should make LVRs construction and maintenance a top priority.

2.2.1 Case Study of Nigeria

Nigeria, as one of the developing countries in Africa, has road networks as the commonest mode of transportation. Road networks connect cities, towns, and rural settlements in the country. Most of her settlements in the networks are linked by LVRs, which are either sealed or unsealed, paved or unpaved (Table 2-2). These LVRs facilitate improvements in the income of rural dwellers in Nigeria. This improvement depends on the quality of LVRs connecting people's economic and social activities, such as farming, trading, healthcare services, education, and security services (Kakwagh 2018). Owing to the criticality of LVRs for national development, Campbell (2009) noted that Nigeria's local, state, and federal governments are committed to providing these roads. This has made it possible for LVRs to be roads that connect most settlements, tourist centres, and places for social activities.

Table 2-2 Road network and structure of ownership in Nigeria (Mostafa Hassan 2018)

Road Type	Federal	State Roads	Local Roads	Total
Paved main roads	26500	10400	0	36900*
Unpaved main Roads	5600	20100	0	25700
Urban roads	0	0	21900	21900
Main rural roads	0	0	72800	72800
Village Access Roads	0	0	35900	35900
Total	32100	30500	130600	193200*

Despite the availability of LVRs in Nigeria, various researchers have reported that they are in poor condition. Kakwagh (2018) and Adeniyi, Akinrinmade & Abiodun (2018) reported that Nigerian unsealed surface LVRs are mostly worn away by erosion during the rainy season. The poor condition of road surfaces has created transportation challenges, such as increasing travel costs and making roads inaccessible during the rainy season (Adeniyi *et al*. 2018; Kakwagh 2018; Usman 2014). The failure of roads, which can cause mobility problems, can be attributed to the use of substandard construction materials, failure in engineering designs, or the effect of expansive soils on road pavements in some parts of the country. The political, geotechnical, and weather influences on the condition of LVRs in Nigeria, a developing African country, can be similar to those in other countries on the continent.

2.2.2 Case Study of Ethiopia

Ethiopia is one of the most populated countries in Africa, with lockedness and mountainous terrain (Mostafa Hassan 2018). Like in most other countries worldwide, the most common mode of transportation in Ethiopia is by road. This attempts to connect various places in human settlements and connect their citizens to economic and social activities. Road networks are the key determinants of household income and facilitators of national gross domestic product (Wondemu & Weiss 2012). The presence of road networks in the country has created employment opportunities for people by facilitating small businesses and industries as well as providing temporary work during the construction process (Terefe, Lorenzo & Bedi 2012). The economic importance of roads in the country engenders federal and regional governments to ensure that all areas with high economic development potential are linked.

However, one of the challenges in the country is the lack of decent road networks, which has a negative effect on economic growth. In rural areas, for example, most roads are characterized as unpaved, with either gravel or earth wearing course. Such a wearing course is usually exposed to road failure caused by erosion or water permeability. Gobena & Lollo (2016) and Terefe *et al*. (2012) noted that the Ethiopian Roads Authority (ERA) defines most rural roads as LVRs.

The ERA has LVRs that are roads with ATRs of less than 300 vehicles. Gobena & Lollo (2016) further noted that unpaved gravel roads in the country suffer surface loss of approximately 25–30 mm gravel depth for every 100 ADT over one year. Importantly, the influence of weather and traffic on the condition of roads should be considered during planning, design, and construction. This determines the material choice and maintenance plan. Some LVRs in Ethiopia do not receive maintenance attention for proper water drainage. Some roads grow with vegetation via road shoulders, which block side drains and increase water permeability into road pavements, resulting in rutting, cracking, or potholes (Otto, Rolt & Mukura 2020). It is estimated that the road network in the country is approximately 33 km/1000 km^2, with 22 km/1000 km^2 of which is rated good or fair (Wondemu & Weiss 2012). In providing more road networks in the country, adequate maintenance of road networks is needed.

2.2.3 Case Study of South Africa

South Africa is one of the fastest-growing economies on the African continent. This country has a large road network linking various rural and urban settlements. The provision of large road networks by South African government agencies (Figure 2-1) is an attempt to pursue economic development to meet the needs of the country's growing population. In Rensburg & Krygsman (2020), it is noted that the country has approximately 750,000 km of road network, which places it as the 11th largest road network in the world (Table 2-3). However, rural roads and some parts of urban roads can be described as LVRs.

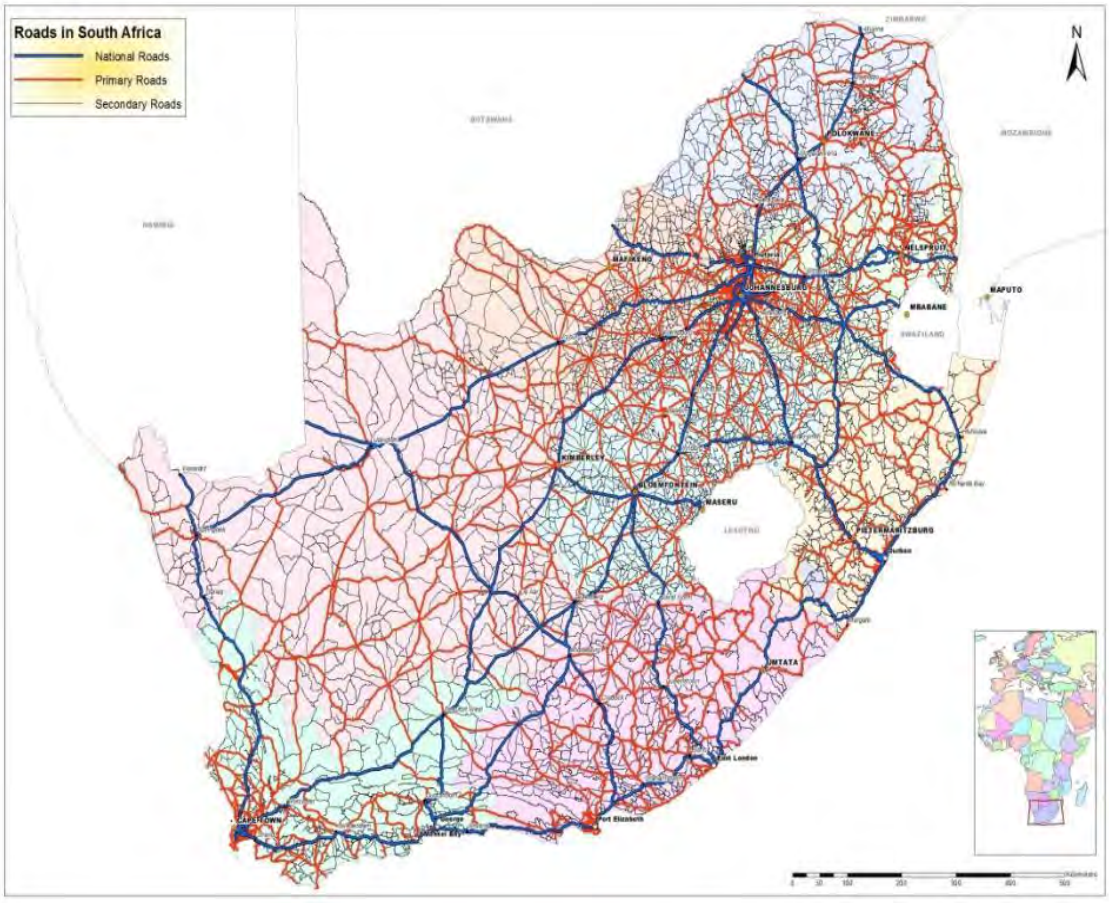

Figure 2-1 South African road network map (Kannemeyer 2013)

Table 2-3 Total South Africa Roads Network (SANRAL, 2024)

Authority	Paved (km)	Gravel (km)	Total (km)
SANRAL	24 026	135	24 162
Provinces - 9	44 759	226 138	270 897
Metros - 8	51 682	14 461	66 143
Municipalities	37 657	219 223	256 880
Total	158 124	459 957	618 081
Un-Proclaimed (Estimate)		131 919	131 919
Estimated Total	158 124	591 876	750 000

Low-volume roads in South Africa are roads with ADT that are less than 400 vehicles/day (Chowdary *et al*. 2012; van Zyl, Visser & du Plessis 1995). However, according to TRH 20, LVRs are “mainly applicable to roads carrying less than approximately 200 vpd, with less than 60 of these being heavy vehicles (axles legally permitted to carry 80 kN loadings), although much of the discussion applies to roads carrying up to 400 lights vpd or more” (TRH 20 2009). Overall, this type of road is characterized by low daily traffic, paved or unpaved, and sealed or unsealed, spanning settlements or facility services. Visser and Krygsman (2017) noted that LVRs in South Africa are designed according to standards specified in the design manual (DoT 1996), which shows that the stone base of the road crushed stone is less than 12% passing through a 0.075 mm sieve size and that the maximum particle size is 37.5 mm. The base course of LVRs is usually constructed with a 150 mm or 120 mm thickness, depending on the road design available. Inappropriate construction, such as poor drainage and compaction, has caused some early failed roads through rutting or cracking. Overall, LVRs in South Africa still surpass 75%, and the majority remain unsealed and in a devastating state with a rating of D to E according to (SAICE 2022) (Figure 2-2).

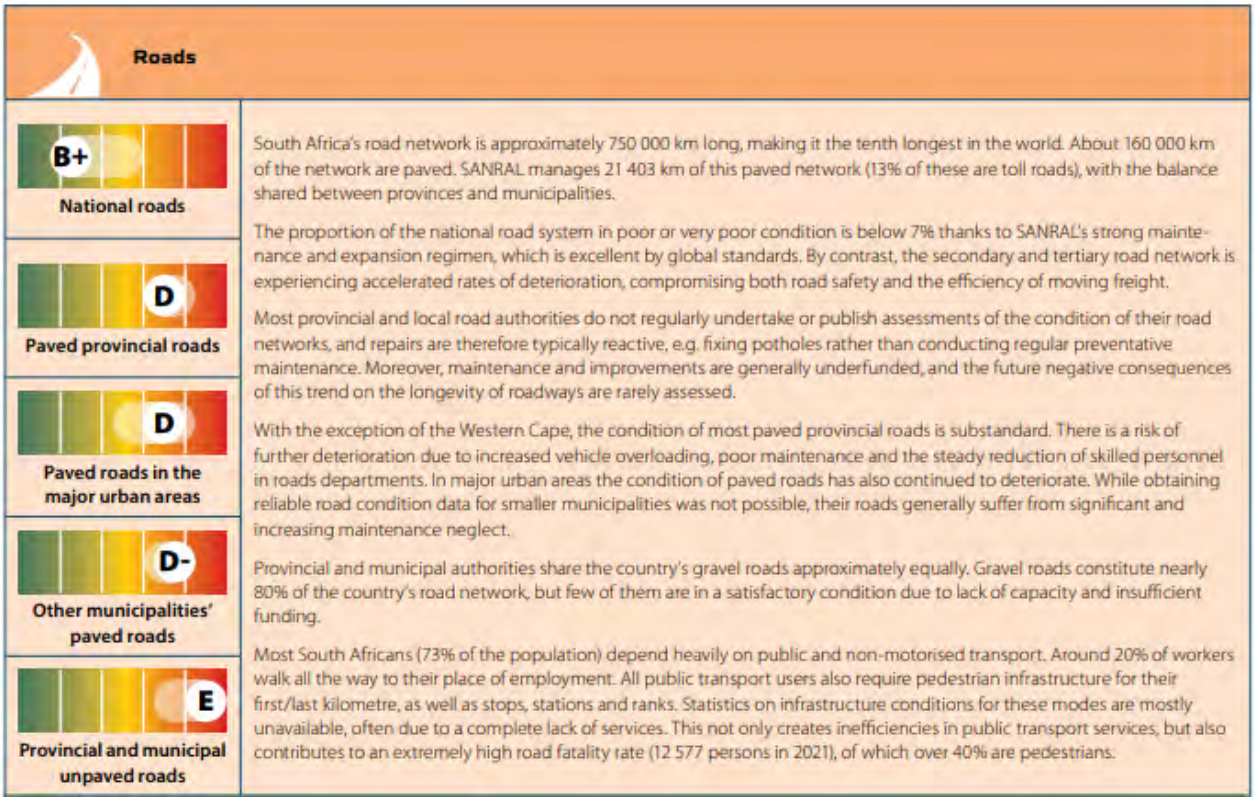

Figure 2-2 Infrastructure scorecard for Road infrastructure in South Africa (South African Institution of Civil Engineering (SAICE) 2022).

2.3 LVR Pavement Infrastructure

Pavement is a combination of layers used to effectively distribute the loads imposed by traffic down to the in-situ soil below a roadway. The combination of layers essentially depends on the type of load intended, the existing foundation, the material type to be used, the environmental conditions, and the life span expected of the road (Douglas 2018). Consequently, this determines the cost of constructing the pavement structure. With the growing demand for transportation worldwide, the need to construct more road networks is increasing. Thus, roads have been seen as a national asset, representing one of most countries' largest public infrastructure investments. For example, maintenance costs in South Africa exceed two trillion Rands (Kannemeyer 2013). Thus, as road transportation is continuously becoming the preferred means of transportation, there is a need to seek for a more cost-effective construction method. The unavailability of the surface layer in a pavement structure drastically reduces construction costs, but this is not without its disadvantages. Nevertheless, the majority of the roads in African countries remain unpaved.

2.3.1 Unsealed Road *Versus* Sealed Roads

Unsealed roads, also referred to as unpaved roads, lack a permanent waterproof surfacing layer (Figure 2-3) (Henning, Kadar, and Bennett 2006). These roads may be classified as unformed or earth roads, formed roads, and gravelled roads (Pooni *et al*. 2022). Unformed roads have no defined cross-section or drainage, while formed roads include grading and drainage, and gravelled roads include an additional gravel surface placed according to engineering principles. In contrast, sealed roads incorporate a bound surfacing layer (e.g., bitumen or asphalt) that provides weather resistance, reduced dust, and improved serviceability (Henning *et al*. 2006; Paige-Green 2005).

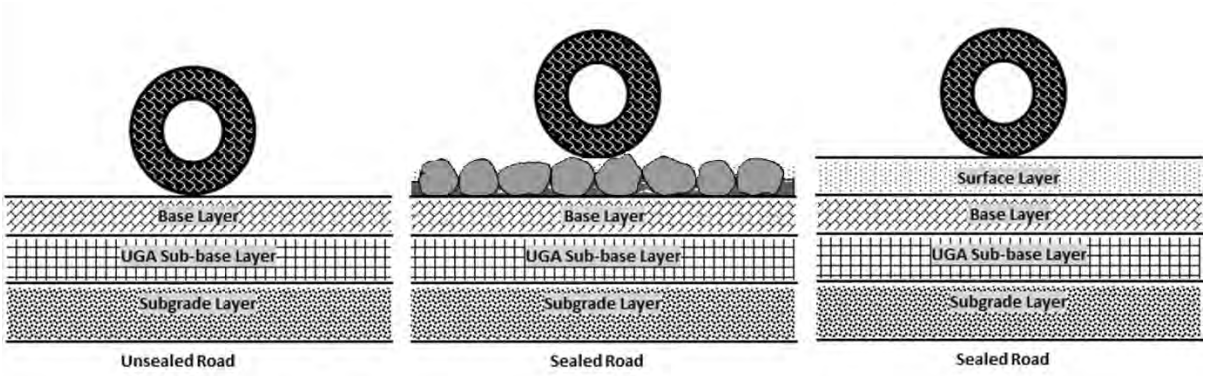

Figure 2-3 Unsealed road versus sealed road (Author's compilation)

Recent studies highlight that unsealed networks remain extensive in developing regions due to financial constraints, but they present growing sustainability challenges in terms of vehicle operating costs, safety, and climate resilience (Otto, Rolt & Mukura 2020; Pooni *et al*. 2022). Low-volume sealed roads, typically designed for less than 200,000 equivalent standard axles (ESAs) over a 20-year life (Pinard, Paige-Green & Hongve 2015), provide a compromise by adopting thin bituminous surfacing over granular bases. Contemporary research has shown that the performance of these LVRs depends primarily on the strength and durability of the unbound granular base and subbase layers rather than the thin surface seal (Gupta 2017; Debrah & Anochie-Boateng 2022).

This distinction is central to the present study, as the in-situ performance of unsealed and lightly sealed roads is often evaluated using the DCP. Recent work has investigated correlations between DCP-derived indices and pavement performance, particularly for granular layers in LVRs (Garcia *et al*. 2024; Pinard *et al*. 2021). By

situating sealed and unsealed roads within this framework, the section underlines the importance of reliable DCP interpretation in guiding cost-effective decisions between maintaining unsealed roads, upgrading with gravel, or sealing with thin surfacing.

2.3.2 LVR Pavement Design Conceptualization

The pavement design concept includes the following aspects: material and material testing (Paige-Green 2015; Paige-Green & Pinard 2012), traffic, pavement thickness design (Douglas 2018), and construction practices (Franzen & Thorpe 2020). Thus, the performance of a pavement structure is influenced by the factors mentioned earlier.

2.3.2.1 Materials and Material Testing for Low Volume Roads

Previously, road construction has depended mainly on the use of conventional materials from borrow pits. However, owing to the difficulty of obtaining suitable borrow pits and the increasing cost of hauling, the use of non-conventional materials and improvements of in situ materials are increasing. Overall, the type of soil or material used in road construction is defined by the size and shape of the particles, but generally, the engineering properties of soil can be defined by the interaction between the particles, the air and water contents (Roy & Bhalla 2017; Roy, Chattopadhyay & Roy 2010). Furthermore, when introducing nonconventional materials, such materials need to be tested to evaluate their true mechanical characteristics (Khajeh, Jamshidi Chenari & Payan 2020).

Various forms of material testing include sieve size analysis, plasticity, and strength in terms of the Californian bearing ratio (CBR), unconfined compressive strength (UCS), and isotropic compression test. Furthermore, several methods, such as uniaxial strain tests, indirect tensile strength tests, triaxial tests, nuclear gauge tests, standard penetration tests (SPTs), cone penetration tests (CPTs), and Dynamic Cone Penetrometers (DCPs), have been used. These methods are used to determine the properties of soil or other materials, such as the gradation size, moisture content, density, strength, and resilient modulus. Some of these tests are carried out in the laboratory, whereas others are conducted directly at the construction site (in-situ). One of the most popular laboratory tests in road construction is the CBR; however, it has several drawbacks (Jagtap & Nagrale, 2013). In most cases, laboratory tests are

destructive and, consequently, less preferred. In contrast, most in-situ tests are non-destructive, which has led to their steadily increasing use over the years.

In-situ penetration tests are among the most commonly used in-situ tests (Robertson 2012). These tests have been widely used for site investigations in support of material analysis and road design. Penetration test such as CPTs are often used in practice. Nevertheless, the DCP test combines the previously mentioned features, giving it an edge over them (Robertson 2012; Salgado & Yoon 2003).. This is coupled with the fact that DCP is cost-effective, easy to operate, and essentially a non-destructive process. Thus, a safer and easier alternative, such as DCP, is desired (Paige-Green 2015; Paige-Green & Pinard 2012; Salgado & Yoon 2003). Overall, since the roads in question are LVRs and already exist, appropriate and cost-effective testing with a simple DCP test device can be used to assess in-situ conditions (Paige-Green & Pinard 2012), and the layers of existing roads that have developed strength over time should be used as much as possible with minimal disruption.

2.3.2.2 Traffic Load Determination for LVR Surfaces

Traffic is a major factor in pavement design, as it determines the loads that the pavement will be subjected to over its service life (Selsal, Karakas & Sayin 2022). The volume and weight of traffic and the type of vehicles using the pavement are important considerations in the design process. High-volume roads typically require thick pavement layers to withstand higher stress levels and prevent deformation. On the other hand, LVRs can often be accommodated with thinner pavement layers (DoT 1996). The type of vehicles that use the pavement is also important, as different vehicles carry different loads that impact the pavement (DoT 1996).

Although describing the pavement's design life in years is convenient, the total traffic loading during service determines the actual design life of the pavement (Jihanny, Subagio, Yang, Karsaman & Hariyadi 2021; SANRAL 2013). For low-volume roads, the design period is usually ten years, whereas for medium- to high-volume roads, the design period is 15 to 25 years (DoT 1996). The adoption of a 10-year design life for LVRs is generally intended to allow for subsequent rehabilitation or reconstruction; however, in practice this provision is rarely realised. However, in most cases, because of the rapid increase in population or demand for road networks, LVRs do not need to reach their design life before deteriorating or before reconstruction. Low-volume roads

also serve heavy trucks that haul agricultural products from rural areas to urban centres. However, the issue of traffic overload is still a major concern on a global scale (Jihanny *et al*. 2021; Hamim & Hoque 2019). Overall, traffic can be determined by carrying out traffic surveys and predicting traffic growth on the basis of historical trends or by using transportation models (Jain, Joshi & Goliya 2013; Ekwulo & Eme 2009). Nonetheless, the traffic estimated for roads determines the road class and subsequently affects the pavement structure thickness design.

2.3.2.3 LVR Pavement Thickness Design: Current Trends

Pavement thickness design refers to the processes used to determine the road or runway surface thickness required to support expected traffic loads and resist deformation and failure (Douglas 2018). The design considers factors such as traffic volume and weight, pavement construction materials, and environmental factors. Current practices in pavement thickness design use various methods and models, including the American Association of State Highway and Transportation Officials (AASHTO) guide for the design of pavement structures, the mechanistic-empirical design method (ME-DM), and the 1993 AASHTO Guide for the Design of Pavement Structures, among others (Adedeji 2015). The thicknesses of the pavement layers, such as the surface, base, subbase, and subgrade layers, are critical components of the overall design process and must be thick enough to ensure long-term durability and safety.

The use of ME-DM over traditional methods has continually gained interest for decades (Kim 2007), with fewer applications to the design of LVRs. This results from the inaccuracy of design and failure experienced in the use of conventional methods (Jain *et al*. 2013; Huang 2004) and the advantages of using ME-DMs, which are able to determine stress and strain, analyse static and time-dependent problems, incorporate nonlinear material characterization, large strains/deformations, perform dynamic analysis and other sophisticated features. ME-DM analysis is based on inputs such as pavement thickness, material properties, loading conditions (static and dynamic), and other factors that interact with the pavement structure. Thus, to model pavements correctly, it is necessary to use numerical methods, such as the finite difference method, the boundary element method, and the finite element method (FEM) (Rojimol & Umashankar 2022; Ameri, Salehabadi, Nejad & Rostami 2012).

However, the FEM is the most commonly adopted method in pavement analysis and will be considered.

The FEM has been applied extensively in road engineering over the years (Peng & He 2009). To date, it is the most versatile of all analysis techniques, with capabilities for 2D and 3D geometric modelling, and is able to analyse stable (static), time-dependent problems, nonlinear material characterization, large strains/deformations, dynamic analysis, and other sophisticated features (NCHRP 2004). However, the application of the FEM to solve any problem consists of three separate stages: pre-processing (modelling), processing (evaluation), and post-processing (simulation). However, the use of 3D appears to be the best approach (Adedeji 2015; Shafabakhsh, Motamedi & Family 2013; Rahman, Mahmud & Ahsan 2011; Sukumaran 2004; Wang 2001).

Various studies have focused on the layers in flexible pavement via the FEM (Gupta & Kumar 2014). However, granular materials do not feature strongly, as more focus is given to designing the asphalt layer and subgrade conditions (Tiliouine & Sandjak 2014; Araya 2011; Adu-Osei 2001). Similarly, only limited work has been undertaken on the stabilized base and subbase layers (Peng & He 2009). Nevertheless, various sources of error in pavement performance predictions are more difficult to control than the response model (NCHRP 2004). Therefore, a reality check through the validation of results with field tests or available results is important.

However, the FEM has been successfully used to analyse the major forms of failure in pavement structures, such as rutting and fatigue cracking in different layers (Al-Khateeb, Saoud & Al-Msouti 2011; Walubita and van de Ven 2009). Additionally, it has been used to determine the accurate positioning of geogrid materials (Al-Azzawi 2012), the thickness of each layer (Sinha, Chandra & Kumar 2014; Shafabakhsh *et al*. 2013) and the interaction between the pavement and its instrumentation (Yin 2013; Zafar, Nassar & Elbella 2005). Recently, researchers have started considering the use of the FEM for the design of LVRs. In a study by Jagtap & Nagrale (2013), the application of the FEM in LVR design was shown to reduce construction costs by 11–15%. Building on these findings, it is important to incorporate FEM-based design approaches for LVRs, as they can contribute to achieving more durable and cost-effective pavement structures.

2.3.2.4 LVR Construction Practices

LVR construction practices are critical issues affecting pavement structures' structural life and overall performance (Franzen & Thorpe 2020). However, this issue has been extensively explored by providing various construction guides for road work. However, unlike high- and medium-traffic roads, there is considerable relaxation in terms of rules around the material requirements concerning LVRs (DoT 1996). Furthermore, the use of labour-intensive construction methods, rather than traditional mechanistic methods, is always encouraged for LVRs, as it helps with employment and skill transfer to women, youth, and people living with disabilities within the community through training. Nonetheless, there are various disadvantages associated with using labour-intensive construction methods, including poor-quality contracts, broken contractual agreements, false claims for funding to purchase materials, and inexperienced contractors (Van Amsterdam 2014). Thus, proper monitoring of the use of labour-intensive LVR construction is necessary.

On the other hand, the majority of LVRs lack proper maintenance activities. Although the issue of maintenance is not unique to LVRs, it is not of major concern to governments, as they are still behind in the maintenance of prioritized roads (medium- to heavy-traffic roads) (Mostafa Hassan 2018). Nevertheless, the design of LVRs with paved surfacing layers is essential, as unpaved roads require more maintenance, which can drastically increase the life cycle of LVRs.

2.4 Economic Importance of Sealing Low Volume Roads

In most African countries, unsealed LVRs make up a substantial proportion of the road network and impact the lives of most regional populations who live and work in rural areas (Pinard *et al*. 2003). Although these roads constitute a considerable portion of the road network, they remain unsealed for economic reasons. On the other hand, unsealed roads require continual maintenance, which is significantly affected by weather conditions or the nature of traffic.

Unsealed LVRs have several defects that affect road roughness and safety. These defects are peculiar not only to unsealed roads but also to sealed roads. These include dustiness, potholes, stoniness, corrugations, ruts, cracks, ravelling, erosion, slipperiness, impassability, and loss of surfacing or wearing course (TRH 20 2009; Committee of State Road Authorities 1990). Thus, the sealing of LVRs, in addition to

the advantages of pavement life-cycle costs, contributes to reducing poverty in the communities around roads and improving agricultural growth, which in turn creates new job opportunities (Nakamura, Bundervoet & Nuru 2020; Berg, Deichmann, Liu & Selod 2017; Riverson, Gaviria & Thriscutt 1991). Other benefits of sealing LVRs include savings on vehicle operating costs, travel time, and safety improvements (Chowdary *et al*. 2012; Geoffroy 1998; Committee for State Road Authorities 1990).

2.5 Surfacing Options for Unsealed Low Volume Roads

The percentage of unsealed road networks on a global scale (Figure 2-4) and the majority of the unsealed networks are LVRs, which are the connecting links between rural and urban communities. The surface plays a major role in the life cycle of the pavement structure, as it prevents gravel loss, eliminates dust, improves skid resistance, and reduces water ingress into the underlying layers (Roads Authority Malawi 2020). Significant progress has been made with respect to various surfacing options.

Additionally, innovations have led to different surfacing options that can be considered economical rather than conventional asphalt (Figure 2-5) or concrete surfacing, especially surface treatment options; however, these options are affected by various factors that can further affect their selection for use. These factors include climate and topography conditions, environmental and socioeconomic impacts, safety, engineering suitability, and the durability of surfacing. The various factors affecting these options and selection considerations are presented in Table 2-4
(Doré 2014; Henning *et al*. 2006; DoT 1996).

Furthermore, selection considerations are also based on cost and performance, which are further divided as follows: cost: initial cost (IC), maintenance cost (MC), and rehabilitation cost (RC); and performance: service life (SL), level of service (LOS), and structural capacity (SC). A project's cost is determined by the initial construction cost, routine and periodic maintenance costs, road user costs, and the salvage value of the facility (Committee for State Road Authorities, 1990). Notably, higher costs are involved in the use of bituminous and concrete surfaces; however, the performance tends to outweigh these costs, and vice versa for gravel surfacing. However, the application of bituminous surfaces, chip seals or sprayed seals is more economical in the case of LVRs.

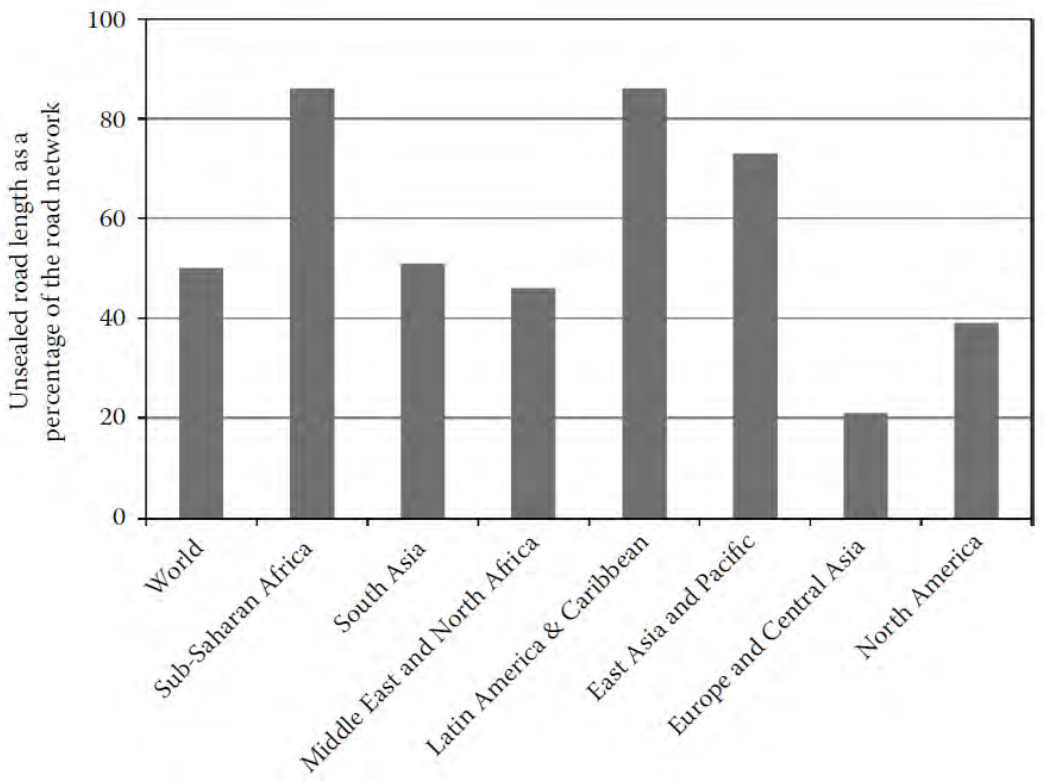

Figure 2-4 Proportion of unsealed roads by global region—the percentage of network (Douglas 2018)

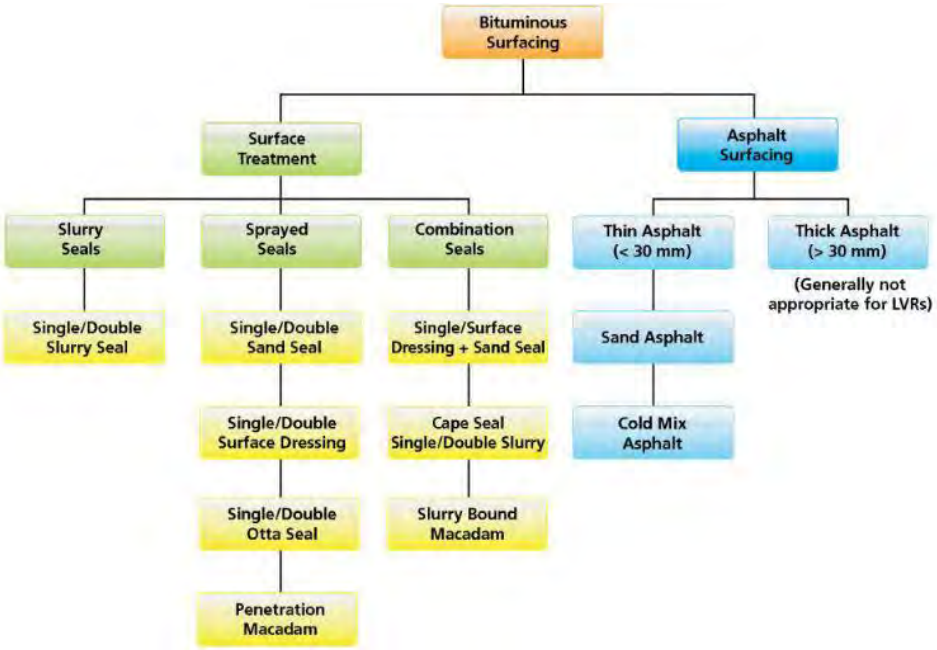

Figure 2-5 Bituminous surfacing options for LVR (Roads Authority Malawi 2020)

Table 2-4 Surfacing options for pavement structures and their selection considerations (Adedeji & Hassan 2018; Doré 2014; Henning et al. 2006)

Surfacing Type	***Description***	***Selection Consideration#***					
		Cost			***Performance***		
		IC	***MC***	***RC***	***SL***	***LoS***	***SC***
Natural Surfacing	Engineered earth roads or natural surfaces. Generally, have poor geometry and drainage.	1	4	1	1	1	1
Gravel	Typically, 150-250 mm thick natural gravel or other imported layer worn down by traffic and the environment.	1	4	2	1	1	1
Dust Suppressants	Additionally, for good construction and mechanical stabilization, dust can be controlled with chemical additives, such as Wetting Agents, Salts/Chlorides, Natural Polymers, Wax Agents, et cetera.	2	2	3	2	3	1
Stone	Crushed stone layers can be placed with machines or manually. The former requires heavy equipment for compaction. The latter may be prepared without heavy compaction equipment.	3	2	3	3	2	3
Bricks	Usually prepared from high-quality clay bricks. Pavements are very durable and can present a very tight, relatively smooth surface.	3	2	3	3	3	3
Concrete	Very durable, but mostly require minimum thickness for high volume roads. A special application is concrete block pavement, which behaves and performs similarly to brick and clay bricks.	5	2	5	5	4	5
Bituminous Surfaces	Classified into two groups: Seals (bitumen film and stone embedded) and Bituminous mixes (asphalt layers)	4	1	4	4	4	4
Other Surfaces	Recycled rubble, concrete or asphalt mix.	3	2	3	3	3	4

*Where: 5–very high; 4-high; 3-moderate; 2-low; 1-very low

Overall, the use of bituminous surfaces in LVRs will make these roads cost-effective, improve surface texture, reduce the amount of noise generated, improve ride qualities, assist in waterproofing of the underlying layers, and reduce dust generation and the loss of aggregate (Yetkin Yildirim 2015; Sandberg *et al*. 2011). Nevertheless, the total cost of upgrading an unsealed road to a sealed road standard will be kept as low as possible. This can, however, be achieved by (i) making optimal use of in-situ materials, thus minimizing the number of imported materials and reducing environmental impact (Paige-Green & Pinard 2012); (ii) using simple, inexpensive and effective material

testing methods such as dynamic cone penetrometers (Paige-Green & Pinard 2012; Salgado & Yoon 2003); (iii) considering the use of labour-intensive construction practices (Pinard *et al*. 2015; DoT 1996); and (iv) incorporating their design in the current pavement design manual trend (FEM) for validation and estimation of possible structural maintenance/renovation (Du Plessis, Kilian & Mngaza 2014). Based on this study's scope, the design of the LVRs will be considered using the current design trend.

2.6 Bituminous Surfacing Concept

Bituminous surface techniques have been developed and refined in South Africa since the 1930s to meet the need for cost-effective and durable pavement maintenance solutions. These techniques, which originated in Europe, were developed to restore the surface properties of roadways without the need for extensive structural repairs (Alaswadko, Hassan, Meyer & Mohammed 2019) and can also be used for the construction of new roads, particularly those with lower traffic volumes. The use of bituminous pavements has attracted interest worldwide, including in countries such as Australia, France, and South Africa, with applications to low-volume roads and a lack of funds being of particular interest (Pavement Interactive 2024). Bituminous pavements can be divided into surface treatments (also called seals) and asphalt-wearing courses, as shown in Figure 2-5. The surface treatments or seals can be further subdivided into spray, slurry, and combination seals (Van Zyl, Beukes, Bredenhann, Fourie & Greyling 2021). There are various types of seals, including single seals, double seals, cape seals, slurry seals, sand seals, geotextile seals, split seals, chocked seals, inverted double seals, and graded aggregate seals (Figure 2-6 and Figure 2-7). However, not all of the seals mentioned are used frequently (Figure 2-7).

The concept of sprayed seal coating primarily involves the application of bitumen-based treatments that provide various benefits, such as a waterproof layer to protect the underlying pavement, increased skid resistance, a filler for existing cracks or bevelled surfaces, an antiglare surface in wet weather, and a more reflective surface for night driving (Guirguis & Buss 2017; Hoffmann & Potgieter 2007). These treatments can be categorized into different systems, including chip sealers, spray sealers, slurry

seals, and combination seals, which vary in thickness depending on their intended use (Gerber & Jenkins 2017; Kodippily, Henning & Ingham 2012).

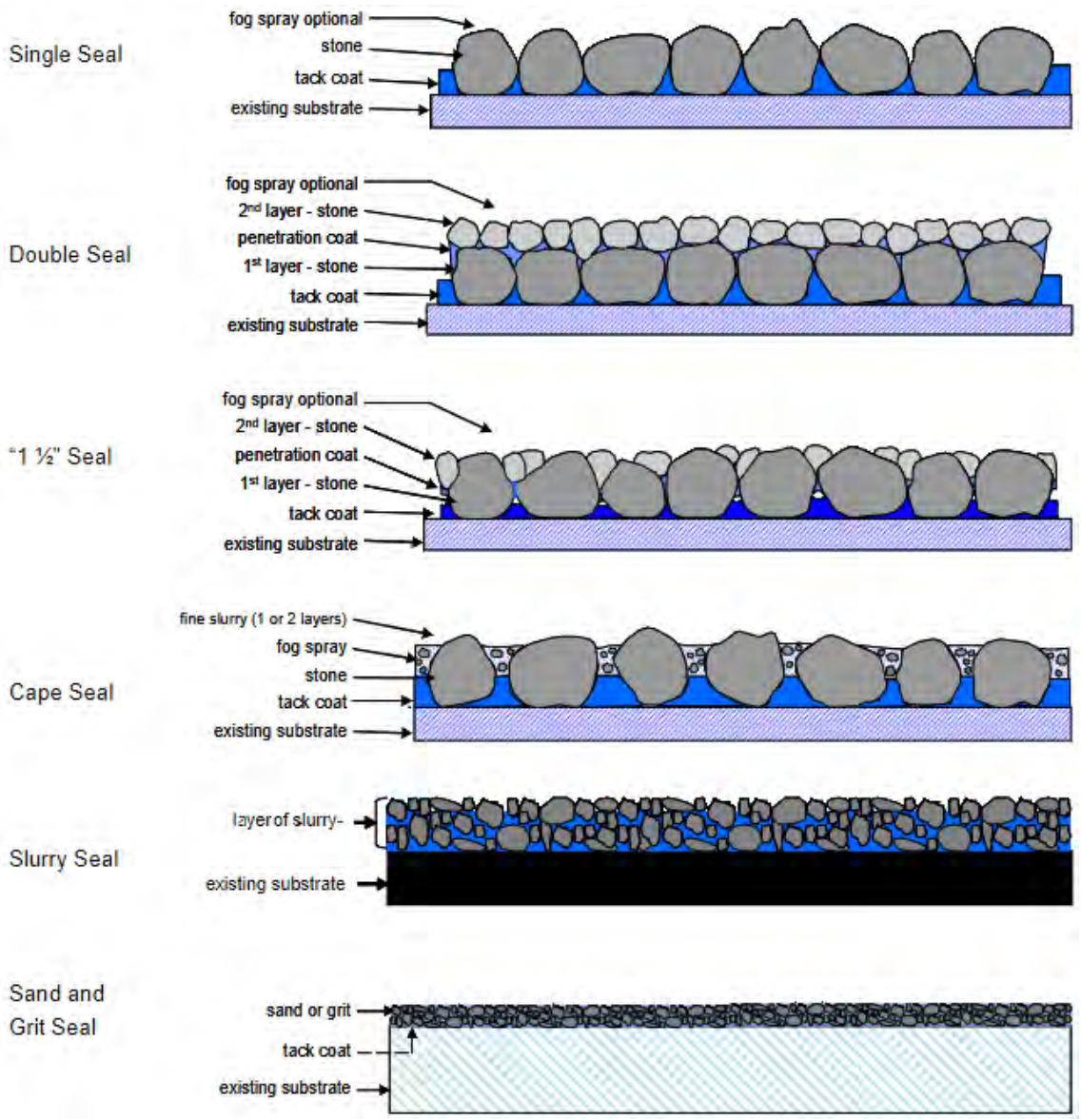

Figure 2-6 Schematic illustration of seal structure Part A (Van Zyl et al. 2021)

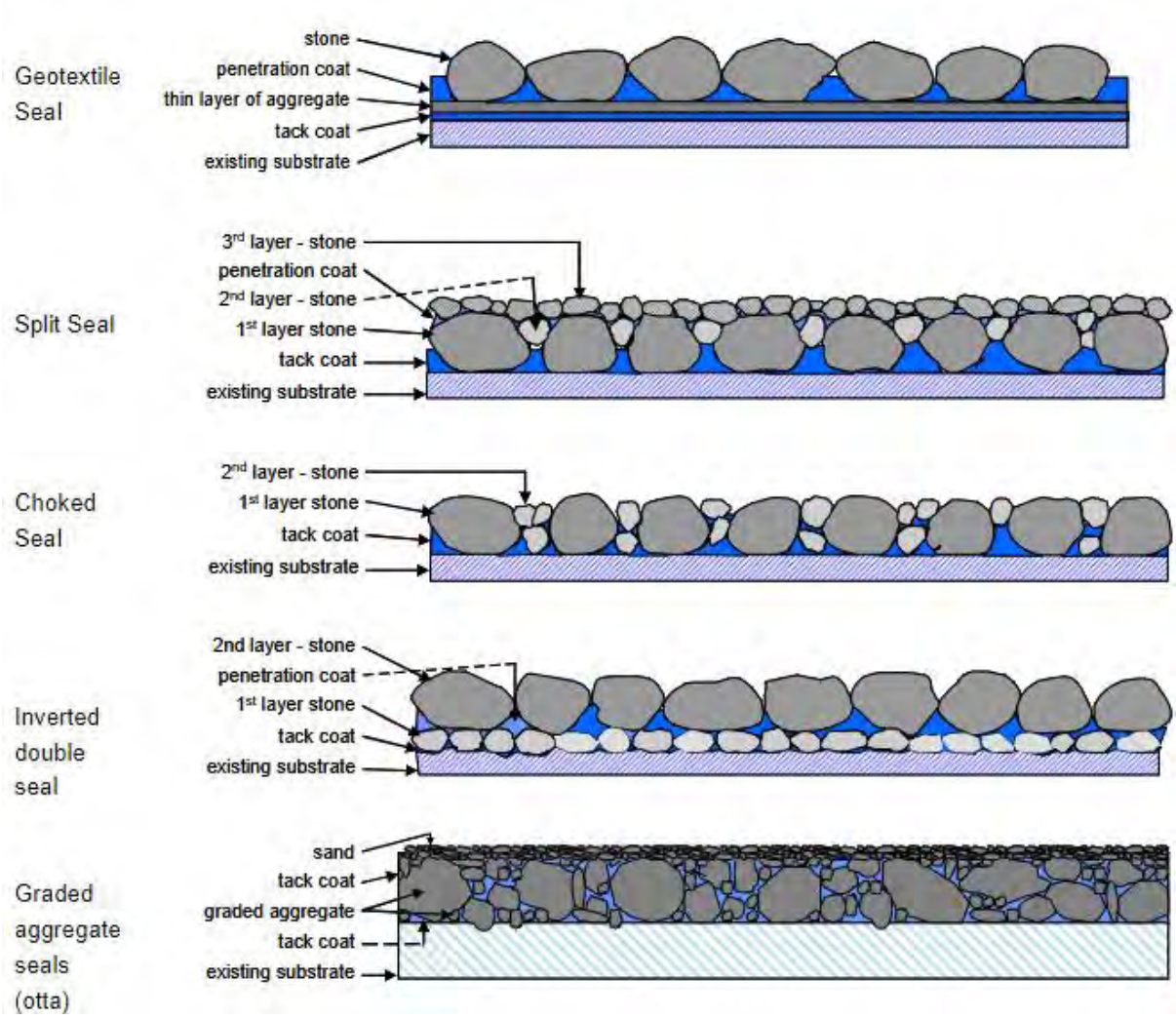

Figure 2-7 Schematic illustration of seal structure Part B (Van Zyl et al. 2021)

Two main materials are generally used for spray seals: Bitumen (bituminous binder, cutback, or bitumen emulsion) and a top aggregate. In its simplest form, a spray seal consists of a layer of bituminous binder that is sprayed onto the road surface and then covered with a layer of aggregate (stone or sand). The layer thickness is between 12 mm and 15 mm, depending on the type of aggregate used, the average least dimension (ALD), and the type of seal, e.g., single or double seal. However, thicker layers of up to 25 mm can be applied to achieve the desired performance characteristics (Praticò, Vaiana & Iuele 2015, 2016; Federation of Canadian Municipalities and National Research Council 2005). While these treatments do not significantly increase the structural strength of the pavement, they improve the smoothness of the surface, protect against premature deterioration, reduce shallow

rutting, and help delay fatigue cracking (Hwayyis, Hassan & Fahey 2022; Kumbargeri, Kutay & Boz 2018).

The use of bituminous pavements has increased due to continued technological advances and their cost-effectiveness (Merritt, Lyon & Persaud 2015). Although traditionally associated with bitumen, the application of bituminous materials in the maintenance of roads is expanding to include other innovative treatments that offer economic and environmental benefits (Du Plessis et al. 2014; Groenewald & Wijk 2010).

Chip seals, a common form of bituminous surfacing, are often used because they form a protective wear layer and extend the life of the pavement. This involves spraying on a bitumen binder and then applying an aggregate, which is then compacted to form a durable surface (Zheng et al. 2022). The performance of such treatments is influenced by factors such as aggregate properties, aggregate embedment, base course thickness, road slope, climatic conditions, and binder type, which have been the subject of various studies to optimize their effectiveness (Jin, Yin, Xin & You 2023; Van Zyl et al. 2021; Ozdemir, Kutay, Hibner, Lanotte & Kumbargeri 2018).

Overall, bituminous surfacing continues to evolve into a reliable and efficient method for pavement maintenance and the cost-effective construction of low-volume roads that meet current and future requirements for sustainable infrastructure solutions.

2.7 Chapter Summary

Chapter two presents a literature review on low-volume road infrastructures and highlights the differences between unsealed and sealed roads. Additionally, looks at the design concept for LVRs regarding materials, traffic loading, and construction practices. Furthermore, this chapter presents a literature review on the current state of LVRs at the global scale and in the African context. The literature shows that LVRs constitute a large portion of road networks around the world. The literature further shows that despite the larger portion of road networks is made of LVRs, these roads are in very poor condition, and the majority are left unpaved and are not given proper attention as a result of cost.

Additionally, in this chapter, the definition of low-volume roads varies or differs from country-to-country. Overall, less traffic uses such roads and hence tends to be

neglected in plans for infrastructural development by governments. However, low-volume roads are missing links between urban and rural developments and constitute a critical puzzle for the advancement of the rural economy. Therefore, upgrading unsealed LVRs is necessary. Various options have been discussed in the literature, and more emphasis has been placed on the use of in-situ materials to reduce the total cost of constructing LVRs (Paige-Green & Pinard 2012; Salgado & Yoon 2003). In LVRs, the goal of reducing construction costs starts with using appropriate and cost-effective methods of testing materials to be used and using alternative and current methods for the design of pavement.

Chapter 3 : Literature Review – Material Testing and Design Methods

3.1 Introduction

Material testing and selection are vital aspects of pavement design, as in most cases, there is a need to know the strength of the in-situ soil and each material to be used to construct a pavement structure (Islam, Gassman & Rahman 2020; DoT 1996). The strength of a pavement structure comes from various materials that form the surfacing, base, subbase, and subgrade layers, depending on the road type in question. Pavement design determines the economically required thickness of various pavement layers to protect the given or determined in-situ soil conditions for a given wheel load in terms of magnitude and volume (Douglas 2018; DoT 1996). Hence, material testing is inevitable and necessary for pavement design. Material testing for disturbed soil samples can be conducted onsite and in the laboratory. The method of testing has a significant effect on the overall cost of pavement construction. After testing, the selection process of materials must satisfy the following conditions (DoT 1996; van Zyl *et al*. 1995):

- adequate bearing capacity under any individual applied load
- adequate bearing capacity to resist progressive failure under repeated individual loads
- the ability to retain that bearing capacity with time (durability) and
- the ability to retain bearing capacity under various environmental influences (which relates to material moisture content and, in turn, to climate, drainage, and moisture regime).

Thus, this chapter aims to check the structural capacity of existing LVRs via various testing methods. This chapter focuses on selecting road material for experimental testing and the fundamental geotechnical properties of the study samples.

3.2 Laboratory Testing for Low Volume Roads

The laboratory for disturbed soil samples is a facility equipped to handle and analyse soil samples that have been disturbed during collection or transportation. Disturbed soil samples are those that have undergone some alteration in their natural state and

structure, which may occur during excavation, handling, or transportation from the field to the laboratory (Vakili, Salimi & Shamsi, 2021; Islam *et al*., 2020). These samples are commonly used for a wide range of geotechnical and environmental testing purposes.

The laboratory's primary function is to conduct various tests and analyses on disturbed soil samples to determine their engineering properties, classification, and suitability for specific applications. Some of the common tests conducted on disturbed soil samples include the following (Vakili *et al*. 2021; Islam *et al*. 2020; Mathur, Kumar, Pandey & Choudhary 2017; Ji, Siddiki, Nantung & Kim 2014):

- Soil index properties and soil classification
- Compaction tests
- Shear strength tests
- Permeability tests
- California bearing ratio (CBR) test
- Unconfined compression test
- Consolidation test

3.2.1 Soil Index Properties and Soil Classification

Soil index properties, such as grain size distribution and Atterberg limits, are commonly used for soil classification and can provide preliminary insight into engineering behaviour (Ikechukwu, Emeka & Hassan 2019; Aneke 2018; Ikechukwu 2018; Mathur et al. 2017; Rahim & George 2004). These soil tests are fundamental tests that help identify and classify soils for general or basic engineering purposes. Standard soil index tests were conducted on remoulded soil samples to determine their composition, such as the relative percentages of gravel, sand, silt, and clay present within each sample, and to evaluate the suitability of the materials for reuse in the construction of the proposed roads (Islam *et al*. 2020; Rahim 2005; Rahim & George 2004). The tests conducted include the following:

- Grain size analysis
- Atterberg limit analysis

The results from the soil index property tests are thereafter used in the classification of soil. Soil classification aims to reflect the diversity of soils and their internal and external relationships; it inventories natural resources and provides information on their protection and use (Van Huyssteen, Turner & Le Roux 2013). Various soil classifications exist, such as the Unified Soil Classification System, American Society for Testing and Materials, American Association of State Highways and Transportation Officials, Group Index, TRH14 soil classification, and COLTO (Fouche 2021; Netterberg & Elsmere 2015). However, the index properties and the class of soil encountered at the site are elementary or preliminary indicators of the behaviour of the soil. Nevertheless, it is difficult to judge the engineering characteristics of such soil.

3.2.1.1 Grain Size Analysis

Grain size analysis is pivotal in understanding granular materials' physical properties and behaviour across various scientific disciplines (Ikechukwu et al. 2019; Mamatha & Dinesh 2017; Mathur et al. 2017). The distribution of particle sizes within a material offers insights into its origins, transport processes, and potential applications. Researchers (Mamatha & Dinesh 2017; Mathur et al. 2017; Roy et al. 2010; George 2004; DoT 1996) have employed diverse methodologies to conduct grain size analysis and obtained valuable information.

The particle size distribution is a common measure of a material:

- A well-graded distribution enables each particle to fit into the voids created by interparticle contacts of larger sizes, resulting in a maximum density and minimum number of voids.
- Poorly graded material is limited in compaction since it cannot obtain a close-packed geometric arrangement.
- An excess of fines reduces mechanical interlocking, so it reduces strength, presents a slippery surface when wet, is dusty, is less stiff, and is often sensitive to water.
- The internal friction, void content, wear resistance, and permeability depend on the distribution size.

Overall, the behaviour of soils depends on the relative sizes of the particles and, in turn, their surface areas (Roads Authority Malawi 2020).

3.2.1.2 Atterberg Limit Analysis

The Atterberg limit test aims to determine the upper and lower limits of the range of water content at which fine-grained soil exhibits plastic behaviour and for primary material classification (Islam *et al*. 2020; George 2004). The test, which was carried out on a soil sample exhibiting plasticity (ability to undergo unrecoverable deformation at a constant volume without crumbling), was performed in accordance with TMH5 (Norther Cape Samples) (Ikechukwu et al. 2019; Aneke 2018) and SANS 3001 (KwaZulu-Natal Samples). The conditions that must be met before the Atterberg limit test is carried out are as follows:

- Non-Plastic Soil (NP): An Atterberg limit test is not carried out if the soil is non-plastic. This is evident if the soil cannot be moulded or rolled. It is also possible that after completion of the Atterberg limit test, the plastic limit is greater than the liquid limit. This type of soil is classified as non-plastic.
- High Fine Content: Soil sample particles must pass through a 425 µm (micron) sieve and, when needed, material passing through a 75 µm sieve. The results from the test on material passing through the 75 µm sieve should be identified from the grain size analysis (SANS 3001) to avoid confusion.

3.2.2 Compaction Characteristics

3.2.2.1 Modified AASHTO Compaction

Several types of tests are used to determine the compactability of soil, of which the Modified AASHTO, Standard Proctor, and Modified Proctor tests are commonly used. The aim is to establish the optimum moisture content (OMC) at which soil becomes densest, known as its maximum dry density (MDD) (Obe, de Brito, Silva & Lye 2019; Aneke 2018). The test uses one standard compaction effort (mass of tamper = 4.536 kg, dropping distance of 457.2 ± 2 mm, 55 blows per 5 layers) to compact soil samples at varying moisture contents. After the second layer has been compacted, a representative sample is taken from the material in the basin and placed in a suitable container to determine the moisture content (TMH1 1986).

3.2.2.2 California Bearing Ratio (CBR) Tests

The CBR test is a penetration test used to assess the subgrade strength of roads and pavements, and the results are used in the design of road structures (Ikechukwu et al. 2019; Roy et al. 2010). The CBR of a material is the load required to penetrate a circular piston of 1935 mm^2 into the surface of a compacted material at a rate of 1.27 mm/min to depths of 2.54, 5.08, and 7.62 mm expressed as a percentage of the California standard values for these depths, which are 13 344, 20 016, and 25 354 N, respectively, as described in TMH1 Method 8 (Aneke 2018; Du Plessis & Paige-Green 2009). In summary, the test comprises the compaction of three soil samples at three successively lower compaction efforts, usually resulting in densities of 100%, 95%, and 90% of the modified AASHTO maximum.

3.2.3 Shear Strength Tests

Shear tests are crucial for understanding the behaviour of soils under different loading and stress conditions (Sadek, Chen & Liu 2011). Soil shear testing methods can be divided into those with a forced shear plane (direct shear) and those with a free shear plane (indirect shear) (El Hariri, Elawad Eltayeb Ahmed & Kiss 2023; Stefanow & Dudziński 2021; Bareither, Benson & Edil 2008). Direct shear methods, such as translation and rotational shearing, exert direct shearing on the soil surface, whereas indirect methods are mostly based on soil compression; they involve penetration testing, which, with the use of certain empirical dependencies, allows an estimation of the shear strength of the soil (El Hariri *et al*. 2023; Stefanow & Dudziński 2021; Dudziński 2019) (Figure 3-1). The direct methods include direct shear, double direct shear, simple shear, shearing grousers, shearing grouser tracks, and cycloidal shearing grousers. On the other hand, indirect methods include indirect compression methods, such as unconfined compression, biaxial compression, squeeze tests, triaxial compression, true triaxial compression and torsion, hollow cylinder torsional simple shear and indirect penetration methods, such as cone penetrometers, pocket penetrometers, ball penetrometers and T-bar penetrometers (Stefanow & Dudziński 2021; Dudziński 2019). Nevertheless, direct methods are not without disadvantages, such as non-uniform deformation and stress fields; the interface area diminishes during shearing, and the principal stresses are not known and have limited applicability to cohesive soils (Kozicki, Niedostatkiewicz, Tejchman & Muhlhaus 2013). Overall, the shear strength results are greater than those from simple shear tests or triaxial tests

(Kozicki *et al*., 2013). However, there are still no established rules for choosing soil shear strength test methods (Stefanow & Dudziński 2021).

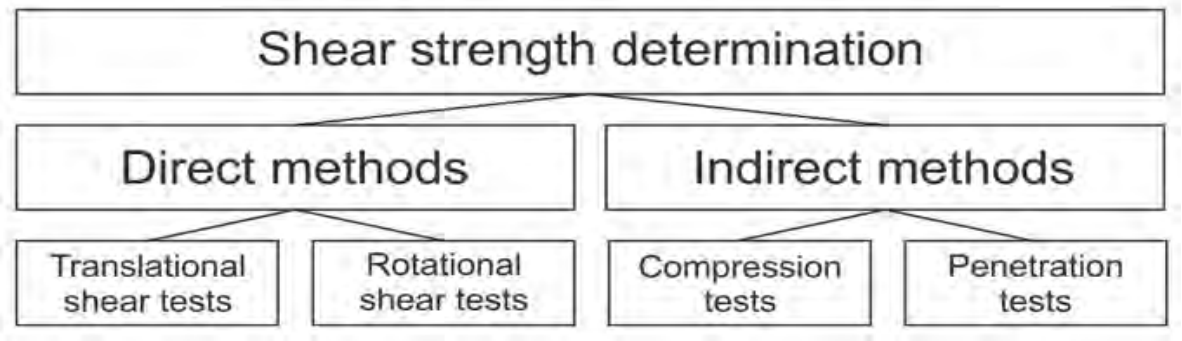

Figure 3-1 Types of methods for determining the soil shear strength (Stefanow & Dudziński 2021)

3.3 In-Situ Material Testing for LVRs

In-situ material testing is crucial for low-volume road construction and is used to assess the engineering properties of the existing soil and materials at a project site. Unlike laboratory testing, which involves testing disturbed soil samples, in situ testing evaluates the in-situ characteristics of the soil and materials directly at the construction site (Sagar, Badiger, Mamatha & Dinesh, 2022). This type of testing is beneficial for low-volume roads, where transportation and logistics may limit the availability of laboratory facilities or where the representative sampling of disturbed soil samples may be challenging.

The state of the art in the mechanical characterization of compacted aggregates continues to make significant progress, and the gap with the state of practice in transportation and geotechnical engineering continues to widen. However, determining the in-situ mechanical properties of foundation materials is a continuous challenge; hence, several methods have been developed (Zhalehjoo, Tolooiyan, Mackay & Bodin 2018; Mohammadi, Nikoudel, Rahimi & Khamehchiyan 2008)). These methods include soil stiffness gauge (SSG), light falling weight deflectometer (LFWD), falling weight deflectometer (FWD), and dynamic cone penetrometer (DCP); nevertheless, there is a need for appropriate correlations of their results with those of standard laboratory tests (Lee, Kim, Woo & Lee 2014). Overall, the standard penetration test (SPT) and the cone penetration test (CPT) are two typical in situ penetration tests and the DCP test shows features of the CPT and the SPT. DCP is

one of the most versatile methods overall (Zhalehjoo *et al*. 2018; Paige-Green & Pinard 2012; Robertson 2012; Mohammadi *et al*. 2008; Salgado & Yoon 2003).

3.3.1 Dynamic Cone Penetrometer (DCP)

Scala (1985) developed a dynamic cone penetrometer in Australia, and further work on its development has continued in South Africa (Paige-Green & Pinard 2012; Paige-Green 2011; Du Plessis & Paige-Green 2009). DCP measures the in-situ shear strength and has been used in the characterization of materials in pavement worldwide (Zhalehjoo *et al*. 2018; Mohammadi *et al*. 2008; Mohammad, Herath, Abu-Farsakh, Gaspard & Gudishala 2007). The original design of the DCP consists of a 9 kg mass dropping 508 mm and knocking a cone with a 30° point into the materials being tested; however, in the 1970s, the South Africa standard had a mass of 8 kg, a fall distance of 575 mm and a cone of 60° (Figure 3-2). Usually, the depth of investigation of DCP is 800 mm to 2000 mm or to the point of refusal, which measures the shear strength using the penetration index with units of mm/blow (Pinard, Paige-Green, Hongve & Mukandila 2021; Du Plessis & Paige-Green 2009; Mohammadi *et al*. 2008). Additionally, the DCP device can be either manually or automatically operated (Parker, Hammons & Hall 1998; Livneh, Ishai & Livneh 1992, 1995). The manual DCP is operated by two people, with one person operating the device and the other recording the readings from the device. Although the automated DCP device is recommended as an efficient substitute for the manual device (Livneh *et al*. 1992, 1995), manual DCP is still widely used.

DCPs, which are devices for in-situ testing, have been applied to various types of materials ranging from soft soil to hard soil, non-cohesive to cohesive soil, base courses to subgrade layers in pavement structures and find applications in the laboratory testing of pavement materials (Pinard *et al*. 2021; Islam *et al*. 2020; Lakshmi, Priya, K & N 2019; Zhalehjoo *et al*. 2018; Zumrawi 2014; Paige-Green 2011; Mohammadi *et al*. 2008; Mohammad *et al*. 2007; Livneh *et al*. 1995).

In the design of roads, the DCP is a practical test used for onsite measurement of road material strength. The test results can be correlated with the CBR, resilient modulus, elasticity coefficient, uniaxial compressive strength, cohesion and friction angle by applying a formula, the results of which can be correlated with laboratory tests conducted on soils from the same location (Pinard et al. 2021; Vakili et al. 2021; Paige-

Green & Van Zyl 2019; Zhalehjoo et al. 2018; Du Plessis & Paige-Green 2009; Mohammadi et al. 2008). Overall, the DCP results are influenced by the existing moisture regime of the pavement (Paige-Green & Van Zyl 2019; Zhalehjoo et al. 2018; South African National Roads Agency Ltd 2013).

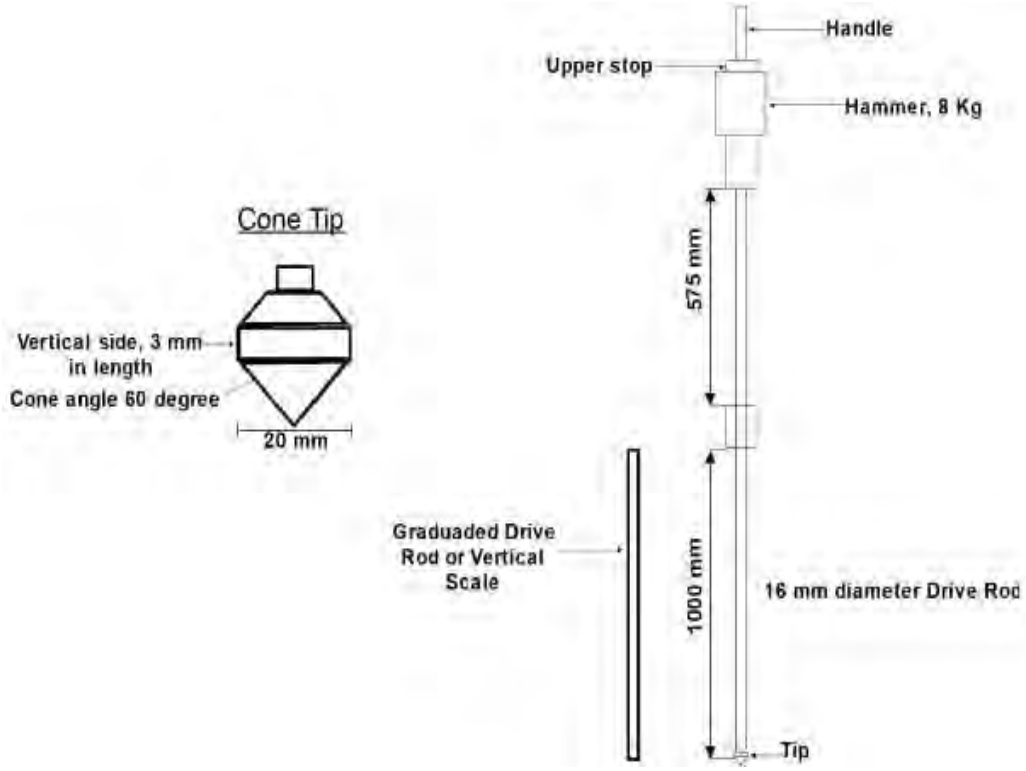

Figure 3-2 Schematic of a dynamic cone penetrometer device (Paige-Green & Van Zyl 2019; Mohammadi et al. 2008).

3.3.2 DCP Results and Interpretation

The DCP result is the number of blows against the depth of penetration; hence, the DCP result is represented as the DCP penetration index (DCPI). DCPI is the slope of the curve and defines the relationship between the number of blows and the depth of penetration at a given linear depth. This can be calculated via Equation 3-1.

Equation 3-1

$$DCPI = \frac{Diff\ Depth\ of\ penetration}{Diff\ Number\ of\ blows}$$

Furthermore, the results of DCP tests can be used in conjunction with computer software to gauge the pavement's structural capacity and to estimate in situ material properties, such as the CBR, UCS, and dynamic modulus. The calculations used to estimate the structural capacity of the pavement are based on the number of blows

required to probe to a depth of 800 mm, known as DSN800. When it was not possible to penetrate a layer (refusal), in the DSN800 calculation, it is necessary to allocate a penetration rate (DN) to the refusal layer (South African National Roads Agency Ltd 2013).

3.4 DCP for the Prediction of In-Situ Strength Low Volume Roads

Over the past decade, the use of the resilient modulus (MR) in the design of pavement has increased, which has resulted from the use of mechanistic-empirical design methods in the design of pavement structures. The material characterization model in the ME-DM uses the MR to predict the behaviour of pavement under the action of a load. Nevertheless, the prediction of the resilient behaviour of pavement material is a dunning task, a very expensive and destructive test using the triaxial laboratory testing method. Thus, these challenges have raised awareness of using simple, cost-effective, and non-destructive testing methods.

Overall, through the use of correlation equations, various simpler testing methods, such as the California bearing ratio (CBR), unconfined compressive strength (UCS), and dynamic cone penetrometer (DCP), have been used to predict the MR of the pavement layer. Nevertheless, the aforementioned DCP is the cheapest and has been found to be extensively used in new and rehabilitation designs for all kinds of roads. Furthermore, considering the nature or class of the road's “low volume” in question, DCP is relatively cheaper and will reduce the overall geotechnical cost of the road and the overall design cost.

3.4.1 Resilient Modulus in Pavement Design

In the design of a pavement structure, the mechanical properties of the underlying foundation are crucial and vital, as they significantly impact the behaviour of the whole structure (Hossain, Singh & Zaman 2015). Additionally, the overall objective of pavement design is to protect the foundation, which is known as the subgrade, from any form of failure as a result of the expected load and climate conditions. Failures such as deformation, stress, and strain levels in the subgrade layer should be reduced to a minimum so that the pavement can perform efficiently during the design period. Thus, the mechanical properties of the subgrade need to be measured directly or indirectly through different testing methods, ranging from laboratory tests to in situ tests, which include soil index property tests, triaxial tests, oedometer tests, shear

tests, isotropic compression tests, uniaxial strain tests, indirect tensile strength tests, California bearing ratio (CBR) tests, unconfined compressive strength (UCS) tests, standard penetration tests, back-calculations from deflection measurements, and dynamic cone penetrometer (DCP) tests (El-Ashwah, Mousa, El-Badawy & Abo-Hashema 2022; Islam et al. 2020; Zhalehjoo et al. 2018; Hossain & Kim 2015; Adedeji 2015; Ji et al. 2014; Toohey, Mooney & Bearce 2013; Mohammadi et al. 2008; Rahim 2005; Kim & Siddiki in press). All the aforementioned tests indicate that testing materials in road construction contribute greatly to the overall cost of constructing pavement structures. Thus, minimal testing with great reliability of the results for pavement design is needed.

Furthermore, with the advent of new methods for designing pavement structures, the use of MR in the design of pavement is increasing. The MR is one of the essential inputs alongside Poisson's ratio for all the pavement layers, especially in the ME-DM. Additionally, parameters affect the overall behaviour in terms of deformation, stress, and strain of the pavement (Islam et al. 2020; Hossain & Kim 2015; Adedeji 2015; Ji et al. 2014; Huang 2004). The MR is directly determined through repeated load tests and is frequently used to characterize the soil subgrade. However, owing to the cost and complexity or difficulties related to cyclic testing, approximate methods are often used for design estimates of MR. Some of these approximate methods include deflection measurements, CBR, UCS, and DCP test results, but few methods have been used in estimating the MR for aggregates used in the base, subbase and subgrade of the pavement structure (Dione, Fall, Yves, Benboudjema & Michou 2015; Hossain et al. 2015; Cary & Zapata 2011; Drumm, Boateng-Poku & Johnson Pierce 1990; Kim & Siddiki in press).

3.4.2 CBR - Resilient Modulus Relationship

The CBR test is widely used worldwide, especially on the African continent. The studies of material strength are based practically entirely on the CBR test and form the basis for most pavement design methods (El-Ashwah *et al*. 2022; Taskiran 2010; Paige-Green 2003; DoT 1996). CBR is an empirical strength property and an indirect measure that compares the strength of subgrade material to the strength of standard crushed rock mentioned in percentage values (El-Ashwah *et al*. 2022; Taskiran 2010). Additionally, CBR is a relatively simple laboratory test that is easy to perform, not time-

consuming, and not too expensive (Dione *et al*. 2015). Thus, the CBR is common and has been extensively used to estimate the resilient modulus. Over the years, various models have been developed to correlate the CBR results with the resilient modulus with various applications in different types of materials and, recently, black cotton soil (Mamatha & Dinesh 2017). Some of these correlation models are recommended by the AASHTO design guide (Hossain & Kim 2013), Mechanistic-Empirical Pavement Design Guide, MEPDG (Gungor, Al-Qadi, Gamez & Hernandez 2017; Hossain et al. 2015), and Austroads pavement design guide (Austroads 2012) (Table 3-1).

Overall, despite the wide application of the CBR for determining the resilient modulus of pavement layers, various studies have reported that the use of the CBR correlation model leads to an overestimation of the resilient modulus value and is not suitable for estimating the resilient modulus (Nguyen & Mohajerani 2016; Hossain & Kim 2015; George 2004; Sukumaran, Kyatham, Shah & Sheth 2002; Hall & Thompson 1994). However, correlations for the resilient modulus have been suggested for improved soil index properties (Rahim 2005; George 2004). Nevertheless, many agencies still rely on these correlations to determine the resilient modulus (El-Ashwah *et al*., 2022).

3.4.3 Soil Index-Resilient Modulus Relationships

Soil properties such as the percentages of material passing through the No. 4, No. 40, and No. 200 sieves; the percentage of silt or clay; the Atterberg limits; the optimum moisture content (OMC); the maximum dry density (MDD); the uniformity coefficient (Cu); and the specific gravity have been used to develop correlation models for the resilient modulus (Zumrawi & Awad 2017; Hossain *et al*. 2015; Yan, Xu & Shen 2014; Hossain 2009). Janoo & Bayer II (2001) and Lekarp, Isacsson & Dawson (2000) established that there is a relationship between particle size and resilient modulus (Janoo, Bayer Jr & Benda 2004). Table 3-2 suggested some correlation for predicting the resilient modulus on the basis of the soil index (Aneke 2018). However, local soils are best represented by soil-property-based modulus estimates when the methodologies described are applied specifically to local conditions rather than when generic or blanket relationships developed for a wide range of soils are relied upon. (Hall & Thompson 1994). Additionally, Hossain & Kim (2015) and Sukumaran *et al*. (2002) suggested the use of unconfined compressive tests for the estimation of the resilient modulus; these correlations cater to the use of stabilizer layers in pavement.

Table 3-1 Correlation equations for the CRB and MR

Equation No.	Correlation	Reference	Application Area
1	$M_R(MPa) = 16.2(CBR)^{0.70}$ $M_R(MPa) = 22.4(CBR)^{0.50}$	NAASRA (1950)	Subgrade and Granular Materials
2	$M_R\ (psi) = 1565\ X\ CBR$	Heukelom and Foster (1960)	Fine-grained soils with a soaked CBR between 5% and 10%
3	$M_R(MPa) = 10(CBR)$	Heukelom and Klomp (1962)	Fine Grained Materials
4	$M_R(MPa) = 37(CBR)^{0.711}$	Green and Hall (1975)	Base, Subbase and Subgrade Materials
5	$M_R(MPa) = 19.59(CBR)^{0.68}$ $M_R(MPa) = 21.39(CBR)^{0.62}$	Paterson (1978)	Base, Subbase and Subgrade Materials
6	$M_R(MPa) = 22.6(CBR)^{0.60}$	Freeme *et al*. (1982)	Subgrade soils (Gravel)
7	$M_R(MPa) = 17.6(CBR)^{0.64}$	Powell *et al*. (1984)	Subgrade and Base/Subbase Materials
8	$M_R(MPa) = 91.226 + 0.017(CBR)^2$	Uzan (1985)	Granular Materials
9	$M_R(MPa) = 21.48(CBR)^{0.478}$	Webb and Campell (1986)	Fine-Grained Subgrade Soils
10	$M_R(MPa) = 17.914(CBR)^{0.874}$	Hopkins (1994)	Cohesive Subgrade Soil
11	$M_R(MPa) = 21.48(CBR)^{0.49}$	Georgia Department of transportation (2004)	Granular Materials (Stabilized Limestone)
12	$M_R(MPa) = 92.720 + 0.019(CBR)^2$	NCHRP 2004	
13	$M_R(MPa) = 21(CBR)^{0.65}$	South Africa Council on Scientific and Industrial Research (CSIR)	Granular Materials
12	$M_R(MPa) = 17.6\ XCBR^{0.064}$	Transportation and Road Research Laboratory	

Table 3-2 Correlation equations for the soil index properties and MR

Equation No.	Model	R^2	Reference	Comments
1	$\log(M_R)\,(ksi) = 0.1328(M_c) + 0.0134(S) + 2.319$	0.94	Jones and Witczak (1977)	Disturbed sample
2	$\log(M_R)\,(ksi) = -0.1111(M_c) + 0.0217(S) + 1.179$	0.45	Jones and Witczak (1977)	Undisturbed sample
3	$\log(M_R)\,(ksi) = 0.5323 - 0.025(M_c) + 0.544(\log\theta) + 0.173\,(SM) + 0.197\,(GR)$	-	Carmicheal and Struart (1896)	Coarse grain soils
4	$M_R(ksi) = 37.431 - 0.4566(PI) - 0.6179(M_c) - 0.1424(P_{200}) + 0.1797\,(\sigma_d) + 36.722(CH) + 17.097(MH)$	-	Carmicheal and Struart (1896)	Fine grain soils
5	$M_R(ksi) = 6.90 + 0.0064\,(C) + 0.216(PI) + 1.970(OC)$	0.76	Hall and Thompson (1994)	Inorganic soils
6	$M_R = 16.75\left\{1\left(\frac{LL}{M_c x\,\gamma_{dr}}\right)^{2.06} + \left(\frac{P_{200}}{100}\right)^{-0.59}\right\}$	0.91	Rahim and George (2004)	Fine-grained soils in Mississippi
7	$M_R = 172.29\left\{\left(\frac{LL}{M_c + 1}\,X\,\gamma_{dr}\right)^{2.18} + \left(\frac{P_{200}}{100}\right)^{-0.069}\right\}$	0.70	Rahim (2005)	Fine grain soils
8	$M_R = 324.14\left(\frac{\gamma_{dr}}{M_c + 1}\right)^{0.8998}\left(\frac{P_{200}}{\log C_u}\right)^{-0.4652}$	0.75	Rahim (2005)	Coarse grain soils

3.4.4 UCS - Resilient Modulus Relationship

Compared with the resilient modulus test, the UCS test is simple and relatively inexpensive. Additionally, UCS testing is more common and popular because its data are readily available (Hossain & Kim 2013; Rao et al. 2012) and can predict the design better (George 2004). Furthermore, the UCS test is simply a triaxial (quick shear) test without confinement and thus has been widely applied in the determination of MR for pavement layer materials. Overall, the UCS has been widely used for stabilized layers of pavement structures (Toohey *et al*. 2013; Hall & Thompson 1994). Table 3-3 suggested several equations to estimate MR with results from UCS tests. Nevertheless, most correlation equations have been developed for specific stress levels; thus, the role of the stress state on the resilient modulus is not included in the models (Ozel & Mohajerani 2011).

Table 3-3 Correlation equations for the UCS and MR

Equation No.	Correlation	R^2	Reference	Application Area
1	$M_R(ksi) = 0.214UCS(psi) + 9.98$	-	Thompson (1966)	Lime-stabilized soils
2	$M_R(psi) = 1200UCS(psi)$	-	Barenberg (1977)	Cement-stabilized coarse-grained sandy soils
3	$M_R(psi) = 440UCS(psi) + 0.28UCS^2(psi)$	-	Barenberg (1977)	Cement-stabilized fine-grained soils
4	$M_R(ksi) = 0.307UCS(psi) + 0.86$	-	Thompson and Robnett (1979)	Fine-Grained soil
5	$M_R(ksi) = 500 + UCS(psi)$	-	American Coal Ash Pavement Manual (1990)	Lime-cement-fly ash stabilized soils
9	$M_R(ksi) = 45.8 + 0.0052\left(\frac{1}{a}\right) + 0.188(q_u) + 0.45(PI) - 0.216(\gamma_d) - 0.25(S) - 0.15(P_{200})$	0.83	Drumm *et al*. (1990)	Various soils (Tennessee)
10	M_R (ksi) = $(a' + b'\sigma_d)/\sigma_d$ $M_R(ksi) = \frac{a' + b'\sigma_d}{\sigma_d}$	0.73	Drumm *et al*. (1990)	Various soils (Tennessee)
6	$M_R(psi) = 0.25UCS^2(psi)$		McClelland Engineers (unpublished)	Lime-cement-fly ash mixtures
8	$M_R(MPa) = 695.4\ X\ (S_{u1\%}) - 5.93\ X\ (S_{u1\%})^2$	0.97	Lee *et al*. (1997)	Fine cohesive soil
7	$M_R(MPa) = 2240UCS^{0.88}(MPa) + 110$		Australian Road Research Laboratory (1998)	Cemented natural gravel
11	$\frac{M_R}{P_a} = 2494.2 + 0.6(PI) - 8.66(P_{200}) + 16.4\ (GI) + 165.53(MCR) - 1961(DR) + 185.29\left(\frac{q_u}{P_a}\right)$	0.44	Hossain *et al*. (2011)	Soils (Oklahoma)
12	$M_R = 657\ X\ (S_{u1\%}) - 6.75\ X(S_{u1\%})^2$	0.97	Hossain and Kim, 2014	

3.4.5 DCP-Resilient Modulus Relationship

DCP is a highly cost-effective technique for quickly acquiring large quantities of data on subsurface material strength and thickness, essentially in a non-destructive process (Paige-Green 2011). Owing to its non-destructive and cost-efficient nature, it has been applied in the determination of the resilient modulus of soil through correlation equations (Nguyen & Mohajerani 2012, 2016, 2017; De Beer & van Rensburg 2016; Mohammad *et al*. 2007; Herath, Mohammad, Gaspard, Gudishala & Abu-Farsakh 2005; Gudishala 2004; Rahim & George 2002; George & Uddin 2000; Chen, Hossain & Latorella 1999; Hassan 1996). Additionally, using DCP allows the soil's natural density and moisture content to be tested (Mousavi, Gabr & Borden 2018). Nevertheless, these correlations may be bound by locations or conditions of development (Mohammad et al. 2007), and these correlations provide only the resilient modulus at a specific stress state (Mousavi *et al*. 2018). Table 3-4 presents the list of available correlation models and their applications.

Table 3-4 Correlation equations for DCP and MR

Equation No.	Model	R^2	Reference	Comments
1	$M_R(MPa) = 7013.065 - 2040.783\ \ln(DCPI)$	0.80	(Hassan 1996)	Fine-grained soils at OMC
2	$M_R(MPa) = 338\ X\ (DCPI)^{-0.39}$	0.42	(Chen *et al*. 1999)	Subgrade soil
3	$M_R(MPa) = 532\ X\ (DCPI)^{-0.492}$	0.40	(George & Uddin 2000)	Fine-grained soils and coarse-grained soils in Mississippi
4	$M_R(MPa) = \frac{1100\ X\ (DCPI)^{-0.44}}{M_c + 2.39\ X\ (\gamma_d)}$	0.68	(Gudishala 2004)	Subgrade soil
5	$M_R(MPa) = 520.62\ X\ (DCPI)^{-0.738} + 0.4\ X\left(\frac{\gamma_d}{M_c}\right) + 0.44\ X\ (PI)$	0.78	(Herath *et al*. 2005)	All types of soil
6	$M_R(MPa) = 151.8\ X\ (DCPI)^{-1.096}$ $M_R(MPa) = 165.5\ X\ (DCPI)^{-1.147} + 0.097\ X\ \left(\frac{\gamma_d}{M_c}\right)$	0.91	(Mohammad *et al*. 2007)	All types of fine-rained subgrade soil and granular materials
7	$\log M_R(MPa) = 2.176 - 0.847$	0.70	(Nguyen & Mohajerani 2017)	Fine-grained soils

Equation No.	Model	R^2	Reference	Comments
8	Log (Eeff) = 3.04758 – 1.06166 x log (DN)	-	(De Beer & van Rensburg 2016)	All types of soil

With the advent of technology, the DCP software package was developed and launched in 1989, with regular updates. AfCAP LVR-DCP software calculates the weighted average DCP penetration rate (DN) in mm/blow, the UCS, the CBR, and Young's modulus of the soil (De Beer & van Rensburg 2016). The first version of the DCP software package was launched in 1989 and has been regularly updated since. AfCAP LVR-DCP v1.03 automatically calculates the weighted average DCP penetration rates (DN) in mm/blow. These rates are calibrated against unconfined compressive strength (UCS) and the California bearing ratio (CBR). The software classifies the pavement into various DCP categories on the basis of the principle of structural strength–balance of pavements (De Beer & van Rensburg 2016). The DCP information is displayed graphically in a report-ready format, featuring layer strength diagrams, balance curves, redefined layers, and E-moduli *vs*. depth for all DCP plots (Ikechukwu et al. 2019).

3.5 Design Methods for LVRs

The design of low-volume roads does not differ from the design concept for other road categories except for minimising cost and relaxing material requirements under conditions in which the drainage and moisture regimes are suitable. The minimization of cost depends on the use of locally available materials, less expensive materials for the construction of the surface layer, and a reduction in the number of layers or thickness. Overall, the fundamentals of any pavement design include traffic in terms of magnitude and volume, the strength of materials in each layer, and climate/environmental factors. However, with all pavement design methods, the four main activities of the design procedure are as follows (Pinard & van Zyl 2019; DoT 1996):

- Assessing the subgrade strength
- Assessing the design traffic loading
- Selection of pavement materials
- Determination of pavement layer requirements (thickness/strength)

3.6 Empirical Design of Low Volume Roads

The design of pavement has evolved slowly over the past 50 years and has traditionally relied heavily on empirical practices (Brown 2013). An empirical design method relies on the results of experiments or experiences (Ekwulo & Eme 2009). However, the experiments conducted in the laboratory simulate the field behaviour of the soil in question, and the observations over time make up the experiences used to develop the empirical design. However, these design methods are limited by the climate conditions, traffic type, and material type; thus, the design is no longer valid when the conditions change. Nevertheless, these design methods still find application because they are relatively simple and widely known in their application, especially in the design of low-volume roads. With low-volume roads, the cost of empirical testing is considered low, as these tests require basic engineering tests for pavement materials.

3.6.1 CBR Method

The CBR method of pavement design was first used in the California Division of Highways, America, as a result of extensive investigations of pavement failure between 1928 and 1929 (Vásquez-Varela & García-Orozco 2020; Roy et al. 2010; Ekwulo & Eme 2009). Thus, a relationship was established between the CBR value and the subgrade and the required pavement thickness of construction above the level. This guideline was based on the subgrade strength (CBR) and traffic (in terms of commercial vehicles per day) (Indian Road Congress 2012). Design curves relating the CBR to the pavement overlying thickness were produced, from which the required layer thicknesses could be determined (Figure 3-3). The CBR method curves evolved when the US Corps of Engineers adopted it, and various design parameters, such as wheel loads, the shear stress of the CBR, and the design traffic class (Roy *et al*. 2010), need to be incorporated. The relationship between the pavement thickness and the CBR is shown in Equation 3-2.

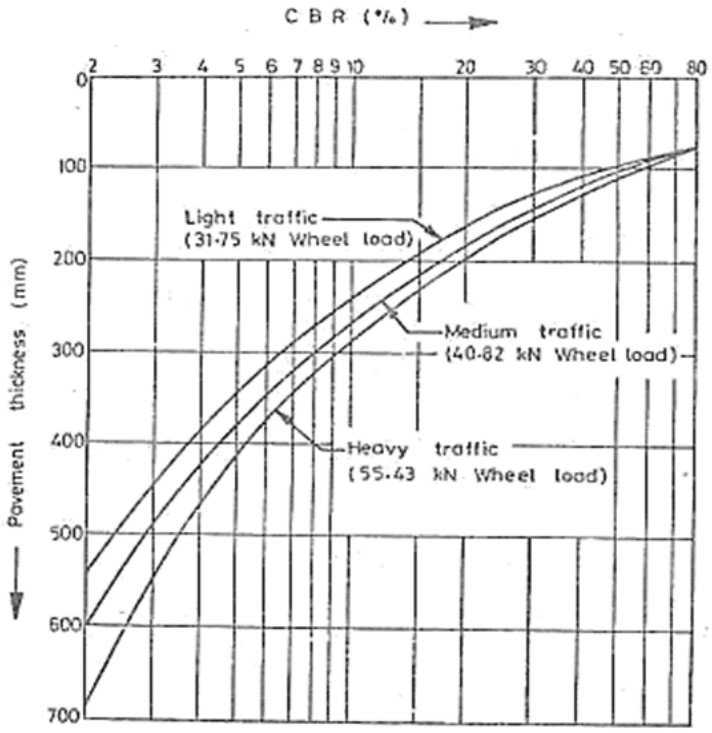

Figure 3-3 CBR design curve for determining the pavement thickness (Peddaiah, Burman & Sreedeep 2018)

Equation 3-2

$$t = \sqrt{W\left[\frac{1}{8.1CBR} - \frac{1}{p\pi}\right]}$$

where t = thickness of the pavement layer

W = wheel load

P = tire pressure

As research on pavement design has developed, the shortcomings of the CBR method have become apparent. The CBR method determines the thickness of asphalt pavement but does investigate the fatigue and rutting strains that cause failure in asphalt pavement. No specific provision has been made for the number of load repetitions, which does not directly include the environmental conditions since it is intended for relatively low traffic volumes and for construction that is largely dependent on unbound granular materials with or without a relatively thin asphalt layer above (Brown 2013; Roy *et al*. 2010; Ekwulo & Eme 2009; DoT 1996). Nevertheless, the use of the CBR procedure is still gaining ground in some developing tropical countries even when the original owners of the procedures have long begun the application of the

mechanistic approach to pavement design (Brown 2013; Ekwulo & Eme 2009). Overall, the CBR cover curve method (Figure 3-4) is applicable to South African conditions, including road embankments (DoT 1996).

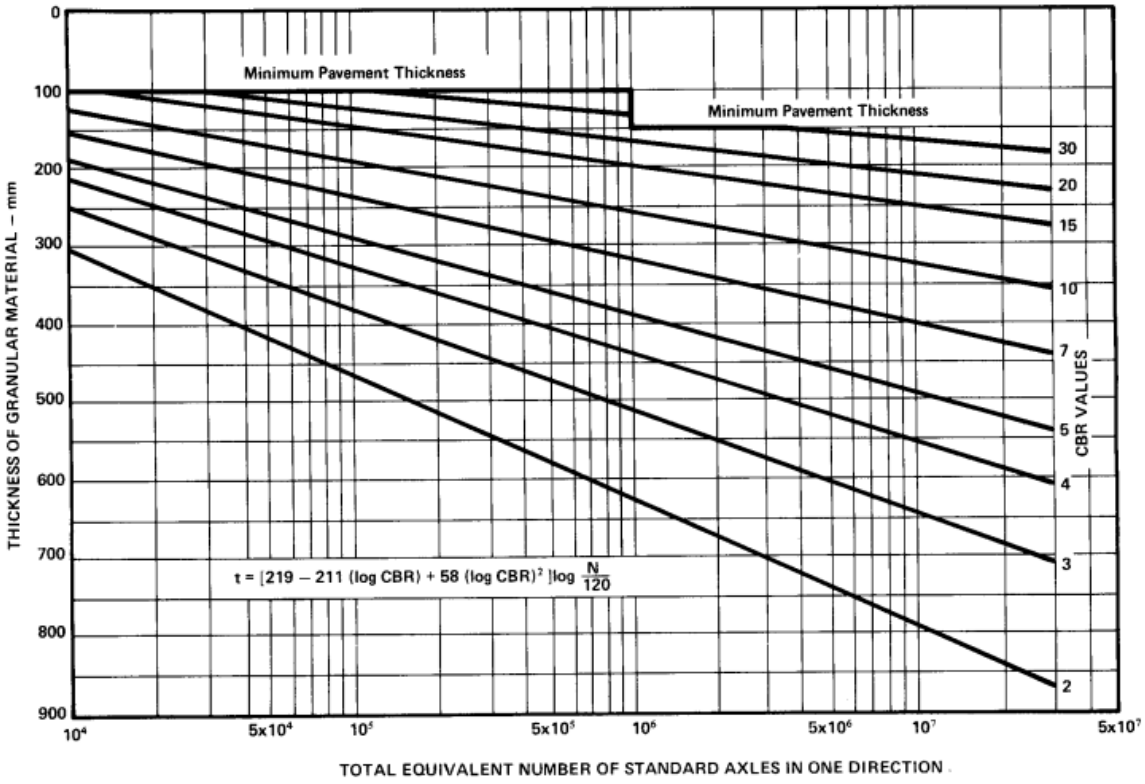

Figure 3-4 CBR design curves for pavements with thin asphalt surfaces (Jameson 1996)

The CBR method requires design parameters such as the CBR value for the subgrade, subbase, base course, and wheel load to read the pavement thickness. On the other hand, when the design formula is used, tyre pressure is needed. From the curves, the thickness design is performed by entering a graph corresponding to the appropriate traffic category, for example, medium traffic, and reading the total pavement thickness required for a material of a certain CBR. The thicknesses of the base and subbase can also be obtained from this curve since it is necessary to place a material of a certain thickness over a material with a certain CBR. However, no provision was made to obtain the thickness of the bituminous surfacing (Appendix A).

3.6.2 AASHTO Method (1993)

Evolving from the AASHTO1961 draft, 1972, 1986, and 1993, this method is sometimes referred to as the structural number method. The AASHTO method is based on the results of the AASHTO road test conducted in Ottawa, Illinois (Garber & Hoel 2018; Douglas 2018; Adedeji 2015; South African National Roads Agency Ltd 2013; Brown 2013; Papagiannakis & Masad 2012). It has been widely applied in new and rehabilitated pavement designs. In this method, the subgrade material, class of road, predicted traffic through equivalent 80 kN axles (E80), drainage, environmental conditions, and reliability for the design of pavement are considered. These are the advantages of AASHTO over the CBR method. Overall, the major changes in 1993 involved the overlay design procedure (Garber & Hoel 2018). Each edition of the guide specifically mentions that the design procedure presented cannot possibly include all conditions related to any specific site. It is therefore recommended that, when the guide is used, local experience be used to augment the procedures given in the guide (Garber & Hoel 2018).

The structural capacity of pavement is calculated via the basic formula (Equation 3-3) or the use of a nomograph chart (Appendix A). The design procedure is summarized in Appendix A.

Equation 3-3

$$log_{10}(SC) = Z_R \, X \, S_o + 9.36 \, X \, log_{10}(SN + 1) - 0.2 + \frac{log_{10}\left(\frac{\Delta PSI}{4.2-1.5}\right)}{0.40 + \frac{1094}{(SN+1)^{5.19}}} + 2.32 \, X \, log_{10}(M_R) - 8.07$$

where SC = Predicted number of 80 kN ESALs

Z_R = Standard normal deviation

S_o = Combined standard error of the traffic and performance predictions

SN = Structural number of the total pavement thickness

ΔPSI= Difference between the initial (PSI_0) and terminal (PSI_t) serviceability indices

M_R = Subgrade resilient modulus (in psi)

SN = Structural number of the total pavement thickness (Equation 3-4)

Equation 3-4

$$SN = a_1D_1 + a_2D_2m_2 + a_3D_3m_3$$

where a = i[th] layer coefficient (per inch) (*see Table 43 by* SANRAL, 2013)

D = i[th] layer thickness (inches)

m = i[th] layer drainage coefficient; assumed = 1.0

3.6.3 TRH 20 Design Method

The Technical Recommendation for Highways (TRH) 20, developed in South Africa, provides guidelines for the design, construction, and maintenance of unsealed roads (TRH 20 2009; Committee of State Road Authorities 1990). In TRH 20, low-volume roads (LVRs) are defined as those carrying traffic volumes ranging from less than 50 vehicles per day (vpd) to more than 500 vpd, with a heavy vehicle component exceeding 20%. The guidelines specifically apply to the design of unsealed roads with low traffic volumes that feature a gravel-wearing course layer. In the earlier version of TRH 20 (1990), the design of the gravel-wearing course was based on Equation 3-5:

Equation 3-5

$$T = t + \left(1 + \left(\frac{C_t}{100}\right)\right) x \left(GL_p \; x \; L_d\right)$$

Where:

t = Required thickness for subgrade protection at a minimum (mm)

C_t = Compaction induced by traffic (%)

GL_p = Estimated annual gravel loss (mm)

L_d = Design life of the road or frequency of regravel (years)

In the updated draft of TRH 20 (2009), a simplified design catalogue for gravel roads was introduced (Figure 3-5) to estimate the additional structural depth required for low-volume roads (LVRs). The primary purpose of the pavement design thickness in TRH 20 is to create a gravel-wearing course that provides a maintainable surface that is as skid-resistant, dust-free, and impermeable to moisture as possible. The design catalogue serves as the foundation for selecting an appropriate pavement structure, with special considerations given to the moisture regime, in situ material classification, and existing pavement strength.

- The design traffic (typically 7–10 years for unsurfaced roads, but depending on the potential upgrading strategy) is calculated.
- Select an appropriate pavement structure from the catalogue (Figure 3-5) and draw a layer strength diagram.
- Plot the DCP layer-strength diagram on a similar scale
- The DCP layer strength diagram (in situ CBR values) was adjusted to reflect the expected moisture conditions under which each layer/part of the pavement structure would operate.

Existing moisture condition	**In situ CBR from DCP (top 300 mm) (%)**				
Dry	< 15	16 – 25	26 – 45	46 – 80	> 80
Moist	< 10	11 – 15	16 – 25	26 – 45	> 45
Wet	< 5	6 – 10	11 – 15	16 – 25	> 25
Pavement class	**Additional structure required (depth in mm)**				
ES 0.003	WC, 200 G7	WC. 150 G7	WC, 100 G7	WC	WC
ES 0.01	WC, 250 G7	WC, 200 G7	WC, 150 G7	WC	WC
ES 0.03	WC, 275 G7	WC, 225 G7	WC, 175 G7	WC	WC
ES 0.1	WC, 150 G6, 150 G7	WC, 125 G6, 125 G7	WC, 100 G6, 100 G7	WC, 100 G6	WC
ES 0.3	WC, 150 G5, 150 G7	WC, 125 G5, 125 G7	WC, 100 G5, 100 G7	WC, 100 G5	WC

Notes
1. This catalogue is conservative and does not take into account the strength of the wearing course layer.
2. The use of low cohesion materials in the layer supporting the wearing course is risky and should only be considered if the road will be upgraded or regravelled before this layer is exposed to traffic.
3. Example 1: Testing a dry existing structure and obtaining say 20% in situ CBR would require, for ES 0.003 traffic category (3 000 80 kN axles), an additional 150 mm G7 material before placement of the wearing course.
4. Example 2: Testing a moist existing structure and obtaining say 30% in situ CBR would require, for ES 0.03 traffic category (30 000 80 kN axles), no additional layer before placing of the wearing course

Figure 3-5 Simplified design catalogue for gravel roads

Furthermore, to determine the wearing course thickness, the following approach was proposed:

- Decide on an appropriate regravelling frequency (typically 7-10 years)
- Calculation of the estimated gravel loss over this period (Equation 3-6)
- The sensitivity of the supporting material and the typical maximum thickness of the wearing course material were evaluated to obtain a buffer thickness (typically 25–50 mm).

Equation 3-6

$$AGL = 3.65 * [ADT * (0.059 + 0.0027N - 0.0006P26) - 0.367N - 0.0014PF + 0.0474P26]$$

where ADT = average daily traffic

N = Weinert N value

P26 = percentage passing through the 26.5 mm sieve*

PF = product of the plastic limit and per cent passing through a 0.075 mm sieve*

* - All grading analyses are to be normalized for 100% passing 37.5 mm.

Overall, the recommended wearing course thickness should at least match the expected gravel loss, plus an additional buffer thickness. TRH 20 suggests a minimum compacted thickness of 100 mm, with a maximum thickness of 200 mm recommended for placement in a single layer.

Additionally, selecting appropriate materials for the wearing course is crucial to the successful design of unsealed roads. TRH 20 highlights various material specifications for different types of unsealed roads, including rural, urban, and haul roads. For unpaved rural roads, the following material specifications are recommended (TRH 20 2009) (Table 3-5).

Table 3-5 Recommended material specifications for unsealed rural roads (TRH 20 2009)

Maximum size (mm)	37.5
Oversize index (I_o)[a]	0.05
Shrinkage product (S_p)[b]	100 - 365 (max. of 240 preferable)
Grading coefficient (G_c)[c]	16 - 34
Soaked CBR (at 95 per cent Mod AASHTO compaction)	>15%

Treton impact value (%)	20 – 65
[a] Io = Oversize index (per cent retained on 37.5 mm sieve	
[b] Sp = Linear shrinkage x per cent passing 0.425 mm sieve	
[c] Gc = (Percentage passing 26.5 mm - percentage passing 2.0 mm) x percentage passing 4.75 mm)/100	

3.7 Mechanistic Design of Low Volume Roads

Mechanistic design methods are theoretically based methods that consider pavement as a mechanism with various layer interactions in response to loading (Paul et al. 2024; Du Plessis & Paige-Green 2009). In the global context, various mechanistic design methods exist and are applicable to LVRs, such as Odemark's Method 1940 and the Asphalt Institute Method. These methods simplify the multi-layered system to an equivalent single-layer model and simplify the computation of stress and strain. The method of multilayer systems is widely used but assumes homogeneous, isotropic layers and does not fully capture the real non-linear cross-anisotropic behaviour of materials. The Asphalt Institute Method for rigid pavements focuses on empirical data and layered elastic theory. The AASHTO Design Guide combines empirical data with mechanistic principles in the context of predicting pavement performance (Paul et al. 2024; Saudy, Breakah, El-Badawy & Khedr 2021; Biswas, Sahis, Mondal & Majumdar 2016; El-Badawy & Kamel 2011).

In South Africa, great contributions have been made through the development of the South African Mechanistic-Empirical Design Method (SAMDM), which is now known as the South African Pavement Design Method (SAPDM) (South African National Roads Agency Ltd 2013; Theyse, De Beer & Rust 1996). The SAMDM analysis for flexible pavement is based on linear elastic multilayer theory, and here, the structural pavement layers are assumed to be isotropic (Steyn, Maina & Repsold 2013). Although SAMDMs are sound in principle and have been applied successfully to the design of pavement, this method faces the intense challenge of its inability to cater to the cross-anisotropic behaviour of materials (Steyn *et al*. 2013) and its oversensitivity to changes in the input variables, which leads to inadmissible and counterintuitive results and provides unrealistic pavement design (Theyse, de Beer, Maina & Kannemeyer 2011). These, in turn, have contributed to increases in scrutiny and criticism in the recent past (Jooste 2004). However, for SAMDM to achieve more

realistic values of the predicted life for the pavement section, it must include cross-anisotropic analysis (Steyn et al. 2013); as a result, SAMDM is being revised (South African National Roads Agency Ltd 2013).

Overall, considerable efforts have been reported regarding linear elastic simulations of pavement structures, yet the assumptions on which this approach works make it inappropriate for real pavement properties and actual scenarios onsite. Such assumptions are (Huang 2004; Wang 2001);

- Each layer is homogeneous, isotropic, and linearly elastic with a finite thickness.
- The material is weightless.
- Circular uniform pressure is applied on the surface.
- Continuity and frictionless interface conditions.

3.7.1 Odemark's Method

Many adaptations and refinements have been made to Odemark's method over the years, although it was the pioneering concept in mechanistic pavement design. Recent studies on the design of low-volume flexible road pavements have led to further development of the principles laid down by Odemark (Paul et al. 2024; Sahis & Biswas 2021; Saudy et al. 2021; Biswas et al. 2016). Some of these studies (Paul et al. 2024; Saudy et al. 2021) focused on the inherent rutting problem that affects the subgrade layers by strain. A common approach to this process is the reduction of multi-layered pavement structures to a single equivalent layer for simple analysis and design with reasonable accuracy (Paul et al. 2024). The latter significantly relies on the stress-based design approach, considering the restriction of the vertical stress limitation of the interface on top of the subgrade. Empirical relations that favour this approach include those proposed by Huang (2004). One of the critical equations (Equation 3-7) found in this methodology is as follows:

Equation 3-7

$$\sigma_z = \left[\frac{Nr}{4.783 \times 10^{-5} \times E_4}\right]^{\left\{-\frac{1}{3.734}\right\}}$$

where σ_z represents the vertical stress at the interface of the subgrade, Nr represents the cumulative number of repetitions by an axle load, and E_4 represents the elastic modulus of the natural subgrade. This relation ensures that the amount of stress applied to the subgrade remains within the limit allowed so that it does not have the effect of deformation or failure under too much pressure. In addition to stress, the strain-based methodology can be used in the design procedure, where the vertical compressive strain is used as an indicator of rutting failure. This method is extremely important in the field for assessing long-term performance under repeated loading on pavements. Equation 3-8 is used to estimate the vertical compressive strain.

Equation 3-8

$$\varepsilon_v = \left[\frac{4.1656 \times 10^{-8} \times Nr}{1}\right]^{\left\{\frac{1}{4.5337}\right\}}$$

where ε_v is the vertical compressive strain at the soil–pavement interface, and where Nr is the number of load repetitions before rut failure occurs. Therefore, from this strain-based approach, good judgment can be made regarding the durability of the pavement, especially under different subgrade conditions. Such contemporary applications have built upon the link of Odemark's transformation procedure with Boussinesq's hypothesis on stress distribution (Paul et al. 2024). Thus, a multi-layered pavement structure was transformed into an overall volume, during which the analysis of the vertical stress and strain was simplified.

The equivalent layer thickness, which forms the essence of this conversion via Odemark's method, is determined via the following repeated transformation of the layer, as presented in Equation 3-9:

Equation 3-9

$$h_{eq} = f \cdot h \cdot \left(\frac{E_2}{E_1}\right)^{\left\{\frac{1}{3}\right\}}$$

where h_{eq}= equivalent thickness f = factor of correction by Odemark h = thickness of original layer E_1 and where E_2 are elastic moduli for any one of the layers. The principles of Odemark's theories allow the derivation of overall stress- and strain-based methodologies, which basically form a strong framework for the mechanistic-

empirical design of pavement structures. This methodology ensures that pavements are designed to carry traffic loads and that environmental stresses are imposed on them, especially for low-volume roads with guaranteed cost-effective and durable solutions. Recent comparisons with other design guidelines, such as AASHTO, have shown good levels of convergence, thus validating the effectiveness of these methodologies in practical applications (Paul et al. 2024; Sahis & Biswas 2021).

3.7.2 mePADS Software

During the early 1990s, Prof. Lynne Irwin of the USA introduced an update on ELSYM5, with some improvements in the integration algorithms close to the tyre contact area. In the late 1990s, a metric version of this package (ELSYM5M, 1995) was released to industry as well as tertiary institutions and is still used today (together with CHEV15) as the main software for mechanistic layered road pavement design and analysis. At the turn of the century, ELSYM5 was integrated into a package called Mechanistic-Empirical Pavement Design and Analysis Software (mePADS) by (Theyse & Muthen 2000).

mePADS is mechanistic pavement design software that combines a stress-strain computational engine with pavement material models and is capable of analysing pavement for bearing capacity. mePADS generates outputs of pavement layer lives and contour plots of stresses and strains (CSIR Built Environment, 2009). Although various multilayer linear elastic software programs exist, mePADS was selected based on its availability and suitability for South African pavement design.

3.7.3 FEM Approach

Pavement design for low-volume roads typically involves evaluating the structural capacity of the pavement to support expected traffic loads and prevent excessive deformation, cracking, or other forms of distress (Adedeji & Hassan 2018). The finite element method (FEM) is one of the most commonly used approaches for pavement design and analysis, as it can simulate the behaviour of the pavement structure under a range of loading conditions and provide detailed information on stress and strain distributions within the layers of the pavement (Fiorentini, Huang, Cuciniello, Leandri & Losa 2023; Peng & He 2009).

In the FEM approach, the pavement structure is divided into discrete elements, each of which is assigned a set of material properties (e.g., stiffness, density, and thickness) on the basis of the characteristics of the underlying materials (e.g., soil, subgrade, base course, and surface layer) (Fiorentini et al. 2023; Tsige, Korita & Beyene 2022). The elements are connected at nodal points, and the interactions between them are described by a system of equations that reflects the mechanical behaviour of the pavement under loading.

To apply the FEM approach to pavement design, the following steps are typically followed:

- The soil and other materials underlying the pavement are characterized, and their engineering properties (e.g., strength, stiffness, and density) are determined.
- The pavement structure, including the number and thickness of each layer, as well as the type and quality of the materials used, is defined.
- The loading conditions that the pavement is expected to experience are established on the basis of the anticipated traffic volume, vehicle type, and climate conditions.
- A finite element analysis software package is used to create a computational model of the pavement structure on the basis of the inputs from steps 1-3.
- The model was run to simulate the behaviour of the pavement under the expected loading conditions, and the resulting stress and strain distributions within the pavement layers were analysed.
- The performance of the pavement structure under the simulated loading conditions is evaluated, and the design parameters are adjusted as needed to achieve the desired level of performance.
- The design is verified via field tests and observations, and the design is refined as needed based on the actual performance of the pavement.

Overall, the FEM approach can provide a robust and flexible tool for pavement design (Adedeji & Hassan 2018; Adedeji 2015; Peng & He 2009), as it can consider a wide range of factors that can affect the performance of the pavement, including material properties, loading conditions, and environmental factors. However, the FEM approach does require specialized expertise and software tools to implement

effectively and may be more complex and time-consuming than other design approaches, particularly for low-volume roads where resources and budgets may be limited.

3.8 Non-Linear Material Characterization for Soils

Proper material characterization is a major aspect of the FEM-based design of pavement for accurate response prediction, as the reliability of pavement design depends on it (Gkyrtis 2023; Liu, Gu, Ren, Wang & Dong 2022; Adedeji, Abejide & Mostafa 2021; Adedeji 2015). However, accurate material characterization is the selection or formulation of proper constitutive equations to represent the behaviour of the materials under loading (Kim 2007). Qualitative choice is needed in material characterization, and it is important that the model captures the major features of material behaviour, while minor features may be ignored in the model (Abaqus 2019). Furthermore, the resilient modulus (MR) is an important input alongside Poisson's ratio and is a primary material property for characterizing all unbounded layers and soils in any FEM model for flexible pavement design (Gkyrtis 2023; Ji et al. 2014; Kim & Siddiki in press). MR values may be estimated directly from laboratory tests, such as triaxial, oedometer and shear tests (level 1 input), indirectly through correlation with other laboratory/field tests (CBR, isotropic compression test, uniaxial strain test, indirect tensile strength and UCS) (level 2 input) or back-calculated from deflection measurements (level 3 input) (Islam et al. 2020; Ji et al. 2014; Rao et al. 2012).

Although the use of triaxial, oedometer, and shear test results as material characterization is level 1 input, which is considered more accurate (El Hariri et al. 2023; Rao et al. 2012), as a result of these tests' unavailability, it is considered second in research studies. The use of direct testing results (level 1 inputs) in material characterization provides a more realistic constitutive model, which consequently provides a better understanding of the mechanical behaviour of the material (in terms of material non-linearity) (Abaqus 2019; Sahoo & Reddy 2010). However, level 2 (correlation input methods) methods provide only room for obtaining limited parameters (such as the MR and Poisson's ratio), which results in the use of linear material characterization and is basically considered for preliminary studies. Using any of the direct test results requires at least one to two laboratory tests for calibration in the FE model. Additionally, these test results are used to obtain the MR and are further

input into various constitutive models in the FE model for the characterization of the material in question.

Two material constitutive models are used in pavement structures: elastic and viscoelastic models and plasticity models: viscoelastic, Drucker–Prager (D-P), Mohr-Coulomb (M-C), modified Cam–Clay, and modified Cap models (Ahmad 2023; Abaqus 2019; Robert 2017; Hernandez & Al-Qadi 2015; Shafabakhsh et al. 2013). However, out of the various plasticity models (viscoelastic, D-P, M-C, modified Cam-Clay, modified cap model, etc.), the D-P and M-C plasticity models have been considered to be better representations of base, subbase, and subgrade layer materials in pavement.

3.8.1 Drucker–Prager Plasticity Model for Pavement Layers

The D–P model is a plasticity model and a modified version of the von Mises criterion, which is approximate to the Mohr-Coulomb criterion for simulating frictional materials (Abaqus 2019; Jing et al. 2017; Peng & He 2009; Hadi & Bodhinayake 2003). In this model, there is a period of purely elastic response, after which some material deformation is not recoverable (plastic); thus, it should be used along with elasticity models, which make this model elastoplastic in nature (Abaqus 2019; Jing et al. 2017; Shafabakhsh et al. 2013). The D–P model has three different yield criteria: linear, hyperbolic, and a general exponent (Abaqus 2019). Nevertheless, the most common of the three yield criteria is the exponent form, which provides the most flexibility in matching triaxial test data, such that Abaqus® determines the material parameters required for this model directly from the triaxial test data, thus minimizing the relative error (Abaqus 2019). However, D-P is not non-linear; however, according to (Rodriguez-Roa 2003), there is not much difference between non-linear elastic and elastoplastic behaviour; thus, elastoplastic models such as D-P can be used as a close representation of non-linearity in pavement materials.

Furthermore, the yield criteria for the general exponent form provide the most general yield criteria available, which are expressed in Equation 3-10. Overall, other parameters used in the D–P model, such as the dilation angle (ψ) and flow–stress ratio (K), can be determined via the M–C model.

Equation 3-10

$$F = aq^b - p - p_t = 0$$

where: F = Yield surface

ab = Constant with respect to stress

p = Mean normal stress

p_t = Hardening parameter that represents the hydrostatic tensile strength of the material

q = Mises equivalent stress

3.8.2 Mohr-Coulomb Model for Pavement Layers

The Mohr-Coulomb model is a soil strength model that specifically simulates the behaviour of subgrade materials (Duris & Hrubesova 2020; Jawad, Almuhanna & Shaban 2020). This model, characterized by its linear relationship between shear stress and normal stress, approximates the shear strength behaviour of soils through the parameters of cohesion and internal friction angle, which are crucial for assessing the stability and load-bearing capacity of subgrades (Ahmad & Mahboubi 2023; El Hariri et al. 2023; Notash, Dabiri, Hajialilue Bonab, Khodadadi & Behrouz Sarand 2022; Park & Park 2017; Robert 2017). In this model, the failure criterion is expressed by the following equation:

Equation 3-11

$$\tau_f = c' + \sigma' \tan \phi'$$

where τ_f is the shear stress, c' represents the cohesion, σ' is the normal stress, and ϕ' denotes the internal friction angle.

The Mohr-Coulomb model assumes a linear elastic–perfectly plastic response, meaning that the material behaves elastically up to the yield point, beyond which plastic deformation occurs, and the material does not recover fully after unloading (La Ragione, Prantil & Sharma 2008). This elastic-perfect plastic nature makes the Mohr-Coulomb model suitable for use in conjunction with elasticity models to simulate the elastoplastic behaviour of subgrade soils (Ahmad & Mahboubi, 2023). The model is widely adopted for subgrade analysis because of its simplicity and effectiveness in predicting soil behaviour under various loading conditions (Ahmad & Mahboubi, 2023; Jawad et al., 2020)(Jawad *et al*., 2020; Ahmad, 2023).

Despite its advantages, the Mohr-Coulomb model has limitations, particularly in capturing the non-linear behaviour of certain soils, such as soft clays, under different stress states (Notash et al. 2022; La Ragione et al. 2008). The linear assumption in the model does not account for strain softening, where the soil strength decreases after peak stress, a critical aspect in subgrade materials that can undergo large deformations (Park & Park 2017; Robert 2017). Therefore, while the Mohr-Coulomb model approximates the actual behaviour of subgrade soils, it may not fully capture the complexity of the non-linear and time-dependent behaviours observed in some soil types (Goh, Teh & Wong 1997).

Furthermore, recent studies have introduced modifications to the Mohr-Coulomb model, such as non-linear extensions, to better represent the stress-strain behaviour of soils under varying loading conditions, offering improved accuracy in subgrade analysis (Li, Zhao, Cheng, Huang & Zuo 2020; Yu & Carter 2002). Despite these enhancements, the basic parameters of the Mohr-Coulomb model, including cohesion and internal friction angle, remain critical in the design and assessment of subgrades (Notash et al. 2022; Bareither et al. 2008). Overall, while the Mohr-Coulomb model is not inherently non-linear, it serves as a close representation of the soil behaviour under typical subgrade conditions and continues to be a valuable tool in geotechnical engineering (Notash et al. 2022; Sivakugan, Das, Lovisa & Patra 2014).

3.8.3 Viscoelastic Model for Surface Layer

Viscoelastic materials, such as asphalt binders, can respond to time in both elastic and viscous ways. These materials' behaviours are typically modelled via the Maxwell viscoelastic model. As shown in Figure 3-6 (Djenane, Demagh & Hammoud 2022; Tapia Romero, Dehonor Gomez & Lugo Uribe 2020), the model is composed of a dashpot (which represents the viscous component) and a spring (which represents the elastic component).

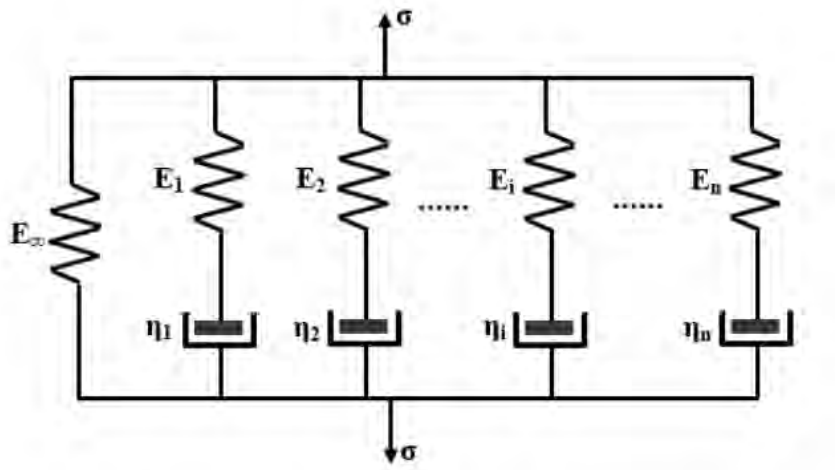

Figure 3-6 Generalized Maxwell model (Djenane et al. 2022)

The model can be described in terms of the relaxation modulus via the following equation:

Equation 3-12

$$G_i(t) = G_i e^{\frac{-t}{t_i}}$$

where G_i is the spring constant and where t_i is the relation time of the element, which can be defined as *Equation 3-13*.

Equation 3-13

$$t_i = \frac{h_i}{G_i}$$

where t_i is the dashpot constant. The relaxation modulus of the complete model is the sum of the relaxation moduli of all the Maxwell elements connected in parallel, as follows:

Equation 3-14

$$G(t) = \sum_i G_i e^{\frac{-t}{t_i}}$$

When t $\rightarrow \infty$ in the case of materials that have a solid-like behaviour such as asphalt, G(t) approaches a finite value Ge, and equation (3) can be rewritten as *Equation 3-15,* which is known as the Prony series equation.

Equation 3-15

$$G(t) = G_e + \sum_i G_i e^{\frac{-t}{t_i}}$$

The phase angle and its norm |G*|, which are dependent on both the temperature and the loading frequency, characterize the dynamic shear results that were obtained from laboratory tests. This modulus is made up of two parts: an imaginary component G'', known as the loss modulus, and a real part G', also known as the storage modulus, which quantifies the elastic energy that has been stored in the material. Nevertheless, the dynamic modulus, frequency, and phase angle are usually the outcomes of laboratory tests. To obtain the values for the storage modulus and loss modulus, the relationship between the dynamic modulus, storage modulus, and loss modulus is established by Equation 3-16 to Equation 3-20.

Equation 3-16

$$G^* = G' + iG''$$

Equation 3-17

$$G' = G^*.\cos d$$

Equation 3-18

$$G'' = G^*.\sin d$$

Equation 3-19

$$G'(w) = \{G_e\} + \sum_i \frac{G_i w^2 {t_i}^2}{1+w^2 {t_i}^2}$$

Equation 3-20

$$G''(w) = \sum_i \frac{G_i w t_i}{1 + w^2 {t_i}^2}$$

Using adhesive zones, which describe the strength of the bond between these materials, the interaction between the binder and aggregates was simulated. This is an important step in assessing probable adhesive failure (Gerber 2016).

3.9 Distress Prediction in Mechanistic Design

Distress prediction models are derived from observations of pavement performance in relation to observed failure and initial strain under various loads, thereby computing the number of loading cycles to failure (Pavement Interactive 2024; Mamlouk & Mobasher 2004; NCHRP 2004). Various distress prediction models exist; nonetheless, two are widely recognized: fatigue cracking in asphalt and permanent deformation in the subgrade (Pavement Interactive 2024; South African National Roads Agency Ltd 2013; Ekwulo & Eme 2009). Furthermore, the Asphalt Institute

damage model (Asphalt Institute 1982) is commonly accepted (Pavement Interactive 2024; Ekwulo & Eme 2009). Asphalt Institute models are presented in Equation 3-21 (Fatigue criterion) and Equation 3-22 (Rutting criterion).

Additionally, in rigid pavement, the effective fatigue life is used to estimate the lifespan of the cemented or concrete layer to failure. The horizontal tensile strain at the bottom of the layer is used in Equation 3-23 with other established constants (South African National Roads Agency Ltd 2013). Overall, the distress prediction models are used to define the point at which failure occurs in a pavement by determining the incremental damage.

Equation 3-21

$$N_f = 0.0796(\varepsilon_t)^{-3.291}(E)^{-0.854}$$

where N_f = the number of repetitions for fatigue cracking; ε_t = the tensile strain at the bottom of the asphalt layer under microstrain; and E = the resilient modulus of the asphalt in psi.

Equation 3-22

$$N_r = 1.365x10^{-9}(E_c)^{-4.477}$$

where N_r = number of repetitions for subgrade rutting failure and where E_c = compressive strain on top of the subgrade (South African National Roads Agency Ltd 2013).

Equation 3-23

$$N_{eff} = SF \times 10^{c\left(1-\frac{\square}{d\square_b}\right)}$$

where N_{eff} = effective fatigue life; SF = shift factor for crack propagation; ε = horizontal tensile strain at the bottom of the layer under microstrain; $\square_b$ = strain-at-break; and c,d = constants (South African National Roads Agency Ltd 2013). Note that the assumption for rigid pavement is taken from SANRAL 2013.

3.10 Comparative Analysis of LVR Pavement Design Methods

Table 3-6 comparatively analyses the various LVR pavement design methods discussed in the study, focusing on how each method considers different design criteria. These methods are categorized into empirical and mechanistic design approaches, each with distinct strengths and limitations.

The comparative analysis highlights that while empirical methods such as the CBR and AASHTO are easier to apply and require less computational effort, they may fall short in scenarios demanding careful consideration of environmental and structural factors. Mechanistic methods, particularly the FEM approach and MEPADS software, provide a more detailed and accurate assessment of pavement performance. These methods are better suited for designing pavements that are expected to endure variable and demanding conditions over their design life.

The choice of design method depends largely on the specific project requirements. For LVRs, empirical methods may suffice. However, for projects where long-term durability, adaptability to environmental changes, and precise load predictions are critical, mechanistic methods are the preferred choice. Overall, Table 3-6 emphasizes the need for careful selection of pavement design methods on the basis of the complexity of the project and the specific design criteria that are most relevant to the expected performance and longevity of the pavement.

Table 3-6 Cross-reference table of design criterion consideration in relation to pavement design methods

Pavement Design	Design Criteria Considerations									
	Subgrade Strength	Traffic Loads	Defined Traffic Type Path	Pavement Layers Characteristics	Climate and Environment	Design Life	Thickness Design	Structural Design	Drainage	Cost-effectiveness
EMPIRICAL DESIGN										
CBR Method	✓	✓	**C**	**-**	**-**		✓	**-**	✓	✓
AASHTO Method (1993)	✓	✓	**C**	**-**	✓	✓	✓	✓	✓	✓
TRH 20	✓	✓		✓	✓	✓	**P**	✓	**-**	✓
MECHANISTIC DESIGN										
ODEMARK'S Method	✓	✓	**C**	**-**	**-**	✓	**P**	✓	**-**	✓
MEPADS Software	✓	✓	**C**	✓	✓	✓	**P**	✓	✓	✓

FEM Approach	✓	✓	**V**	✓	✓	✓	**P**	✓	✓	**-**

Notes: C= Circle; V= Various Shapes; P= Prescribed

3.11 Chapter Summary

Chapter Three presents literature that addresses the importance of material testing and selection in the design of road pavements, particularly LVRs. The chapter emphasized that the strength of pavement structures is highly dependent on the quality of the materials used for the pavement, base course, subbase, and subgrade. These materials must be tested both in the laboratory and in the field to ensure durability and sufficient load-bearing capacity. Laboratory testing focuses on disturbed soil samples that have been altered during extraction or transportation. The key tests include soil index properties, compaction properties, Atterberg limit analyses, and CBR tests. These tests help classify and determine soil suitability for construction purposes.

The grain size analysis and Atterberg limit analysis provide information on the physical properties of the soil, whereas compaction tests help to determine the OMC and MDD of the soil. In-situ testing, on the other hand, evaluates the soil and materials directly on site and is, therefore, particularly useful for LVRs, which have limited laboratory capacity and limited economic resources. The DCP test is highlighted as an important in-situ method for measuring the shear strength of soils. The DCP results can be correlated with other properties, such as the CBR, modulus of elasticity, and uniaxial compressive strength, to evaluate the structural capacity of pavements.

This chapter also reviews the literature on the design of LVR, which includes both empirical and mechanistic-empirical design methods. For the empirical method, the CBR, AASHTO 1993, and TRH 20 designs of the LVR were considered. For the mechanistic-empirical method, the Odemark method, the FEM approach, and the MEPADS software were also examined.

Overall, the chapter emphasizes the need for comprehensive testing to ensure that the selected materials meet the required standards for durability, load-bearing capacity, and resistance to environmental influences, thus guaranteeing the long-term performance of the road structure.

Chapter 4 : Research Methodology

4.1 Introduction

This chapter presents the comprehensive methodology adopted to achieve the research objective of developing a Finite Element Method (FEM) based pavement design model for Low Volume Roads (LVRs), guided by Dynamic Cone Penetrometer (DCP) test results, and benchmarking its performance against conventional empirical design approaches. The methodology integrates field investigations, laboratory testing, and computational modelling to evaluate and predict pavement responses under varying subgrade conditions.

The experimental programme commenced with the selection of representative materials from LVR sites. Two study locations, situated in distinct geographical regions, were chosen to capture a broad spectrum of geotechnical behaviours. The collected materials underwent a suite of standardised geotechnical tests in accordance with established South African civil engineering protocols, ensuring both reliability and repeatability of results. The laboratory testing programme focused on quantifying fundamental soil properties known to influence pavement performance.

The following tests were conducted on all selected materials:

- Soil Index Properties and Soil Classification
- Standard Proctor Compaction Test
- California Bearing Ratio (CBR)
- Repeated Load Triaxial Test (RLTT)

In parallel, field-based DCP testing was conducted to establish empirical correlations between in-situ penetration resistance and laboratory-derived strength parameters. These correlations formed the basis for translating DCP measurements into FEM input parameters, enabling the development of a practical, field-applicable design tool (Figure 4-1).

Subsequently, FEM simulations were performed using the acquired geotechnical data to model pavement responses. A comparative analysis of FEM-based designs versus

traditional empirical methods was undertaken, highlighting the FEM potential advantages in reliability, adaptability, and precision when addressing variable subgrade conditions.

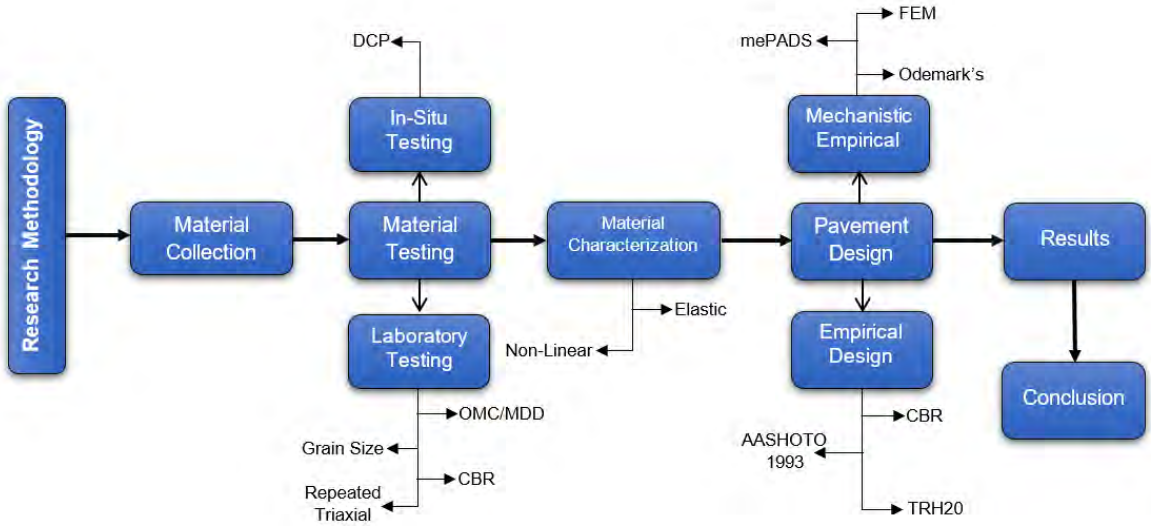

Figure 4-1 Flowchart: research methodology

4.2 Materials

4.2.1 Materials Location/Collection

In this study, low-volume roads from two provinces in South Africa, Northern Cape and KwaZulu-Natal, were investigated. Apart from the availability of access to these sites, the sites are located in different climatic regions. The Northern Cape is a dry climatic region, whereas KwaZulu-Natal is a wet region; thus, it is dynamic in terms of the types of materials encountered (Figure 4-2) (Weinert 1980). The soil samples were labelled according to the province from which they were collected, such as Northern Cape soil (NCS) and KwaZulu-Natal soil (KZNS). The soils were subjected to in situ testing, and samples were collected and transported to the laboratory for laboratory testing.

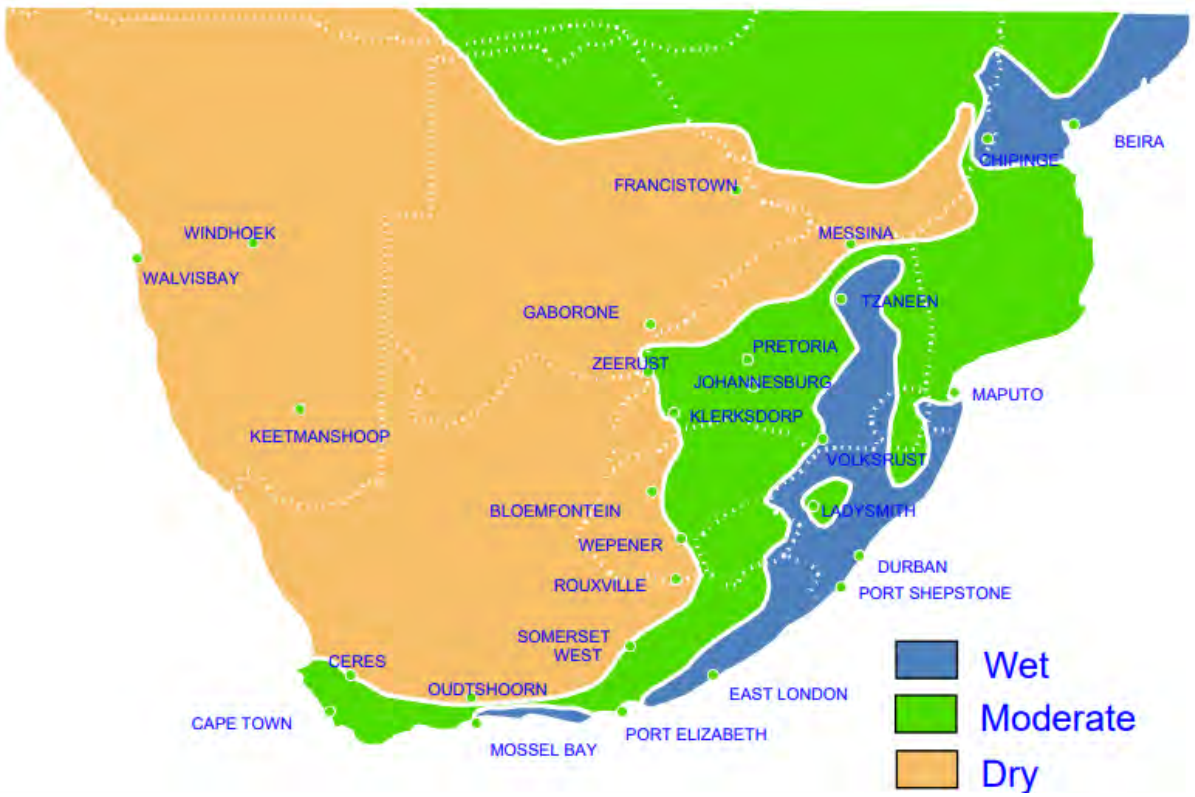

Figure 4-2 Macroclimatic regions of Southern Africa (South African Road Federation, 2022)

4.2.1.1 Study Area 1: Northern Cape Site

The study area in the Northern Cape is located within the far eastern portions of the Northern Cape Province, approximately 70 km west of the province's capital, i.e., Kimberley. On a more local scale, the study area incorporates the town of Schmidtsdrift. Schmidtsdrift is situated west of the prominent Vaal River landform and directly north of National Road 8 (N8). The study area is easily accessible via Regional Road 370 (R370), which forms the eastern boundary of the town (Figure 4-3). The site for this investigation is composed of multiple gravel roads, all of which form part of the internal road network of Schmidtsdrift. The roads, which form the focal point of this investigation, are located within the central to South Eastern portions of the abovementioned settlement and have a combined length of approximately 1.80 km.

4.2.1.2 Study Area 2: KwaZulu-Natal Site

The study area in KwaZulu-Nata is situated approximately 15 km east of Greytown, KwaZulu-Natal. The site for this investigation is composed of a 5 km gravel road, and

road D77 is accessible via Road P160 at km 15+000 or via R74 from Greytown to Kwadukuza 2 km before town Ahrens (Figure 4-3).

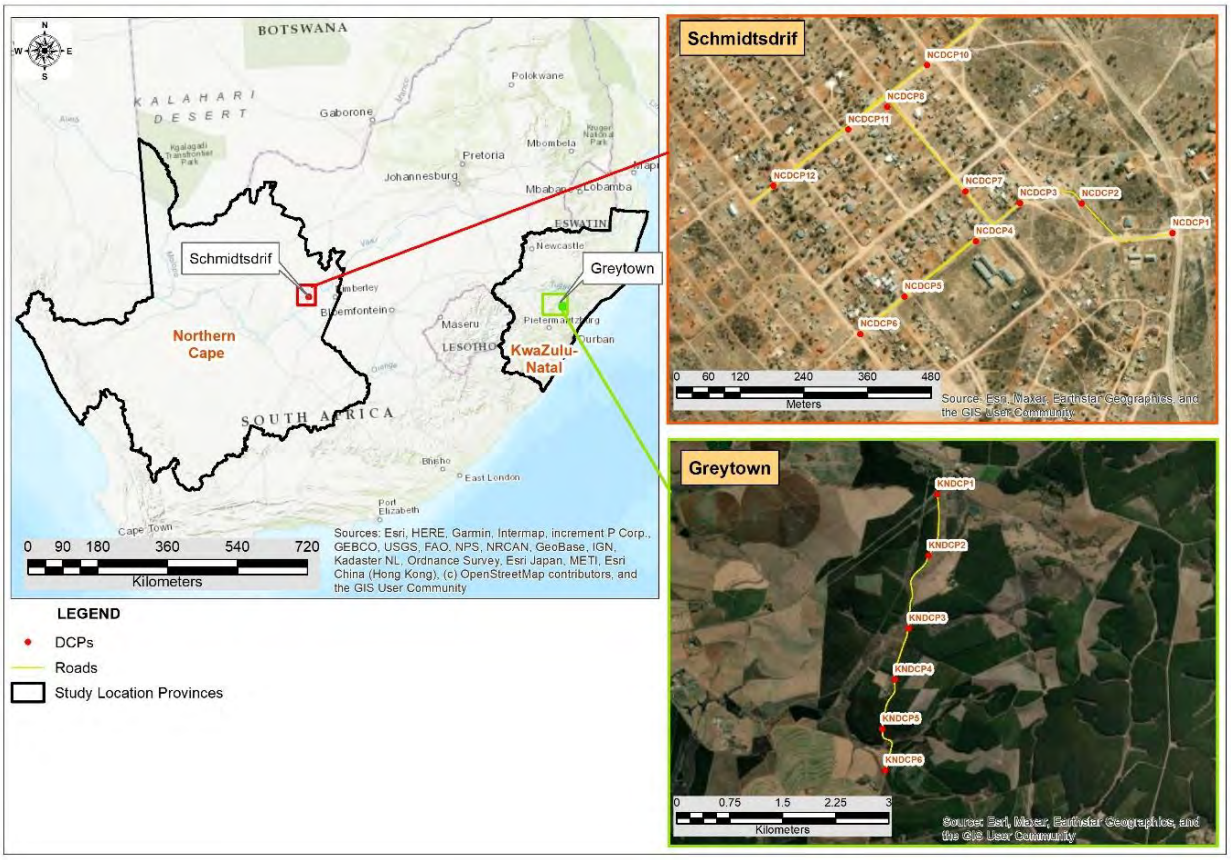

Figure 4-3 Map indicating the study sites (Author's compilation)

4.2.1.3 Material Collection

Soil samples from each site were systematically collected at a depth of approximately 1.0 m below the existing ground level or at refusal. The test pits were excavated within each of the existing gravel roads under investigation, and the points of collection coincided with the location of the DCP test to expose the various soil horizons underlying the site. The soils were transported to the Simlab geotechnical laboratory and the Council of Scientific and Industrial Research (CSIR) laboratory for testing.

4.3 Laboratory Testing Programme

The laboratory testing programme was undertaken at Simlab Geotechnical Laboratory on soil samples collected during the fieldwork phase. Its primary aims were to determine the geotechnical properties of the soils, assess their suitability for use in the

proposed road construction, and generate reliable parameters for FEM-based analysis.

4.3.1 Soil Index Properties

Soil indicator tests were performed on disturbed soil samples to determine composition specifically the proportions of gravel, sand, silt and clay, and to assess compliance with South African road construction requirements. The following tests were conducted in accordance with relevant South African National Standards (SANS 3001):

4.3.1.1 Grain Size Distribution

Conducted to determine particle size distribution, grading modulus, dust content, and coarse sand ratio (SANS 3001-PR5: 2011). Samples were oven-dried (≤ 110 °C) for 24 hours per SANS 3001-GR20: 2010, then sieved through a nested stack ranging from 50 mm to 0.075 mm. Retained material was weighed (± 1 g) to determine grading metrics.

4.3.1.2 Atterberg Limits

Atterberg limits test was conducted in accordance with SANS 3001-GR10: 2011, to determine the plasticity characteristics of fine-grained soils. The Liquid Limit (LL) is obtained using a Casagrande cup or cone penetrometer method, while the Plastic Limit (PL) is found by rolling soil threads until they crumble at 3 mm diameter. The Plasticity Index (PI) is calculated as the difference between LL and PL, indicating the range of moisture contents where the soil exhibits plastic behaviour. Linear Shrinkage (LS) measures volumetric change upon drying. These parameters are critical for assessing soil expansiveness, workability, and susceptibility to shrink-swell movements, directly influencing pavement performance and material suitability.

4.3.2 Compaction and Strength Tests

To assess site-won subsoils' potential for use in road construction, compaction and strength tests were performed using standardised SANS methods:

4.3.2.1 Maximum Dry Density (MDD) and Optimum Moisture Content (OMC)

Determined in accordance with SANS 3001-GR30: 2010, this test establishes the relationship between dry density and moisture content for a given soil or aggregate. Samples are compacted in a mould at varying moisture contents using a specified compaction energy. The MDD is the highest dry density achieved, and the OMC is the

moisture content corresponding to that density. These parameters are critical for specifying compaction requirements in the field, ensuring adequate strength and durability. Achieving compaction close to MDD at OMC minimises settlement, improves load-bearing capacity, and enhances resistance to moisture-related deterioration in road pavement layers.

4.3.2.2 California Bearing Ratio (CBR)

Conducted in accordance with SANS 3001-GR40: 2013, the CBR test measures the load-bearing capacity of subgrade soils and granular pavement materials. A compacted specimen is penetrated by a standard plunger at a fixed rate, and the resistance is expressed as a percentage of the resistance of a standard crushed rock. Testing may be performed under soaked conditions for four days to simulate in-situ moisture states and the readings were taken on daily basis (SANS 3001-GR40: 2013). CBR values are used directly in empirical pavement design methods and serve as calibration data for mechanistic-empirical and FEM models.

4.3.3 Repeated Load Triaxial Test

Performed in accordance with CSIR Protocol TR 2002/21 and aligned with AASHTO T307, the Repeated Load Triaxial Test (RLTT) determines the resilient modulus of unbound granular and subgrade materials under simulated traffic loading. Cylindrical specimens are subjected to a sequence of axial load pulses under constant confining pressure, replicating wheel-load stress conditions. The recoverable (elastic) strain response is recorded, and the resilient modulus is calculated as the ratio of applied stress to recoverable strain. This parameter is critical for mechanistic-empirical and FEM-based pavement design, enabling accurate prediction of layer performance under cyclic loading. RLTT results enhance the reliability of structural pavement models and guide optimal material selection. Detailed sample preparation and test procedures are presented in subsequent sections.

4.3.3.1 Test Materials and Sample Preparation

Test Materials

The laboratory test was performed on two samples of unbound granular aggregate materials sourced from Northern Cape Site and KwaZulu-Natal Site. Materials were selected based on their previous performance in terms of index properties and compaction characteristics. Only two materials were selected because of the cost associated with triaxial testing.

Sample Preparation

A total of four (4) samples were prepared, each weighing between 11 and 12 kilograms. The samples were oven-dried to achieve a consistent mass. Allowing for a 10% margin for waste, a sufficient mass of dry material was weighed to prepare the four triaxial samples. The dry material was then transferred into an appropriate mixer. Subsequently, the volume of water required for the four triaxial compression tests was calculated. The material was mixed until the water was evenly distributed throughout. Thereafter, the mixture was sealed and left to stand for one hour to allow the aggregates to absorb the water.

The materials were compacted in five layers of equal weight in a steel mould via the vibratory compaction method at specific moisture contents and densities determined via compaction tests. The compaction force was generated via an electric vibratory hammer in accordance with the CSIR protocol (TR 2002/21) and AASHTO Standard T307-99 to produce a cylindrical sample 300 mm in height and 150 mm in diameter.

Furthermore, the "Harmonized test methods for laboratory determination of the resilient modulus for flexible pavement design" call for a 0.2-second heave load pulse and a 0.8-second rest period. The applied deviator stress and total resilient axial deformation response were measured. The loading system is a function of three different confining pressures, with five different cyclic deviatoric stresses applied at each confining pressure; however, this study used seven different cyclic deviatoric stresses. Furthermore, each sample was subjected to 15 different stress states during testing. During the conditioning stage, a total of 1000 cycles were applied to remove imperfections on the top and bottom surfaces that may have occurred during compaction.

A sine-wave movement-shaped load pulse was used to apply the cyclical load, and this loading sequence most accurately mimics the loading circumstances experienced by a pavement structure when subjected to vehicle or rail track loading. The deviatoric stress is divided by the recoverable strain to obtain the resilient modulus (MR = d/R). The resilient modulus for each loading sequence is determined by taking the average of the last five cycles of that sequence.

4.3.3.2 Test Procedure for Repeated Load Triaxial

Static triaxial testing procedure

A set of three static triaxial tests was performed for each density/moisture content combination. Each test was conducted on a new sample. The confining pressures applied during these tests were typically 50, 100, and 150 kPa. All samples were sealed airtight for the duration of testing using rubber membranes. The static tests were conducted without on-sample instrumentation, and each sample was deformed at a constant vertical displacement rate of 2 mm per minute until shear failure occurred, indicated by a decrease in vertical load. After testing, the samples were taken for moisture content determination.

Dynamic testing procedure

A set of six (6) dynamic triaxial tests was performed for each density/moisture content combination. Each test in the set was conducted on a new sample. The confining pressures applied during the tests were 200, 150, 100, 50, and 20 kPa. The samples were sealed airtight for the duration of the tests using rubber membranes. The vertical load for each test was determined based on the shear strength of the material obtained from the static triaxial test. The dynamic tests were conducted using on-sample instrumentation, including three LVDTs and clip gauges. Each dynamic triaxial test was carried out for 28,000 load repetitions (Table 4-1).

Table 4-1 Loading sequence for the resilient modulus test

Seq	Phase	Confinement pressure (kPa)	SR sequence	Deviator stress	Cycles
1	Conditioning (AM0)	200	20%	247	100
2			40%	494	100
3			60%	741	100
4	1 (AM1)	200	20%	247	100
5			30%	371	100
6			40%	494	100
7			50%	618	100
8			60%	741	100
9	2 (AM2)	150	20%	214	100
10			30%	320	100
11			40%	427	100
12			50%	534	100
13			60%	641	100

14	3 (AM3)	100	20%	180	100
15			30%	270	100
16			40%	360	100
17			50%	450	100
18			60%	540	100
19	4 (AM4)	50	20%	147	100
20			30%	220	100
21			40%	293	100
22			50%	367	100
23			60%	440	100
24	5 (AM5)	20	20%	126	100
25			30%	190	100
26			40%	253	100
27			50%	316	100
28			60%	379	100

4.4 In-Situ Testing - Dynamic Cone Penetrometer

Performed in accordance with TMH6: 1984 – Methods A8 and A10, the DCP test is used to evaluate the in-situ strength of pavement layers and subgrades by measuring the rate of penetration of a standard cone into the material under repeated impacts from a falling weight (Table 4-2). The penetration per blow is recorded to produce a penetration index, which can be correlated with strength parameters such as the CBR and resilient modulus. This rapid, cost-effective method enables continuous profiling of layer strength with depth. DCP results are integral to this study for developing correlations with laboratory-derived parameters and generating FEM input datasets.

Table 4-2 Summary of Laboratory Testing and In-Situ testing

Test	Purpose	SANS Standard Reference
Grain-Size Distribution	Composition, grading, dust content	PR5 (2011)
Moisture Content	Water content determination	GR20 (2010)
Atterberg Limits, Linear Shrinkage	Plasticity, shrink-swell behaviour	GR10 (2011)
MDD vs. OMC	Optimal compaction characteristics	GR30 (2010)
CBR	Subgrade bearing capacity	GR40 (2013)
Repeated Load Triaxial	Resilient modulus under cyclic loading for mechanistic-empirical	CSIR protocol (TR 2002/21)/ AASHTO T307-99
DCP	In-situ strength profiling and correlation with laboratory parameters	TMH6: 1984 (Methods A8, A10)

4.5 Pavement Design Method

In this study, a range of pavement design methods for low-volume roads (LVRs) was applied using identical site-specific input parameters obtained from field investigations, laboratory testing, and material characterisation. The aim was to evaluate and compare the performance and suitability of each method for the study conditions.

The selected methods were: the California Bearing Ratio (CBR) method, the AASHTO 1993 design method, the TRH 20 method, Odemark's method, the mechanistic-empirical Pavement Design System (mePADS), and the Finite Element Method (FEM) approach. For each method, the relevant design procedures were followed in accordance with their published guidelines or software specifications.

The process began by preparing a consistent dataset including traffic loading parameters, subgrade strength indicators (e.g., CBR and resilient modulus), climatic considerations, and layer material properties. These datasets were then input into each method sequentially:

- CBR method: design charts were used to determine the required pavement thickness based on subgrade CBR values.
- AASHTO 1993 method: the pavement structural number was calculated using traffic, reliability, and performance criteria.
- TRH 20 method: the South African design catalogue was consulted to select layer configurations appropriate for the measured material properties.
- Odemark's method: was applied using equivalent thickness calculations derived from layered elastic theory.
- mePADS software: was used to run mechanistic-empirical analyses incorporating the South African calibration factors.
- FEM approach was implemented within Abaqus® to model pavement responses under the same loading and material conditions.

The outputs from each method, including required layer thicknesses, stress–strain responses, and estimated service lives, were compared directly.

4.6 Development of Pavement Model

Abaqus® analysis modules begin with a batch process designed to assemble an input file that fully describes the problem, enabling Abaqus® to perform the required analysis (Liang, 2000). The input file consists of two key components: model data, which define the FEM geometry, element properties, material characteristics, and all details specifying the model; and history data, which describe the sequence of loading, analysis procedures, time integration controls, and output requests (Liang, 2000; Britto, 2010; Abaqus, 2013) (Figure 4-4).

These data can be defined either through a user-prepared input file or by using the Abaqus®/CAE graphical interface. In this study, the Abaqus®/CAE method was selected because of its simplicity, reduced requirement for manual coding, and efficient model management. Once the model parameters are defined, Abaqus® automatically controls the time steps and load increments, recording all relevant messages and results throughout the analysis. Post-processing is then performed in the visualisation module to review and interpret the computed outputs.

The pavement model developed for this study consisted of a three-layer flexible pavement system, comprising a surface layer, a base layer, and a subgrade. This configuration was selected to enable focused analysis of the stabilised base layer without the influence of an additional sub-base layer.

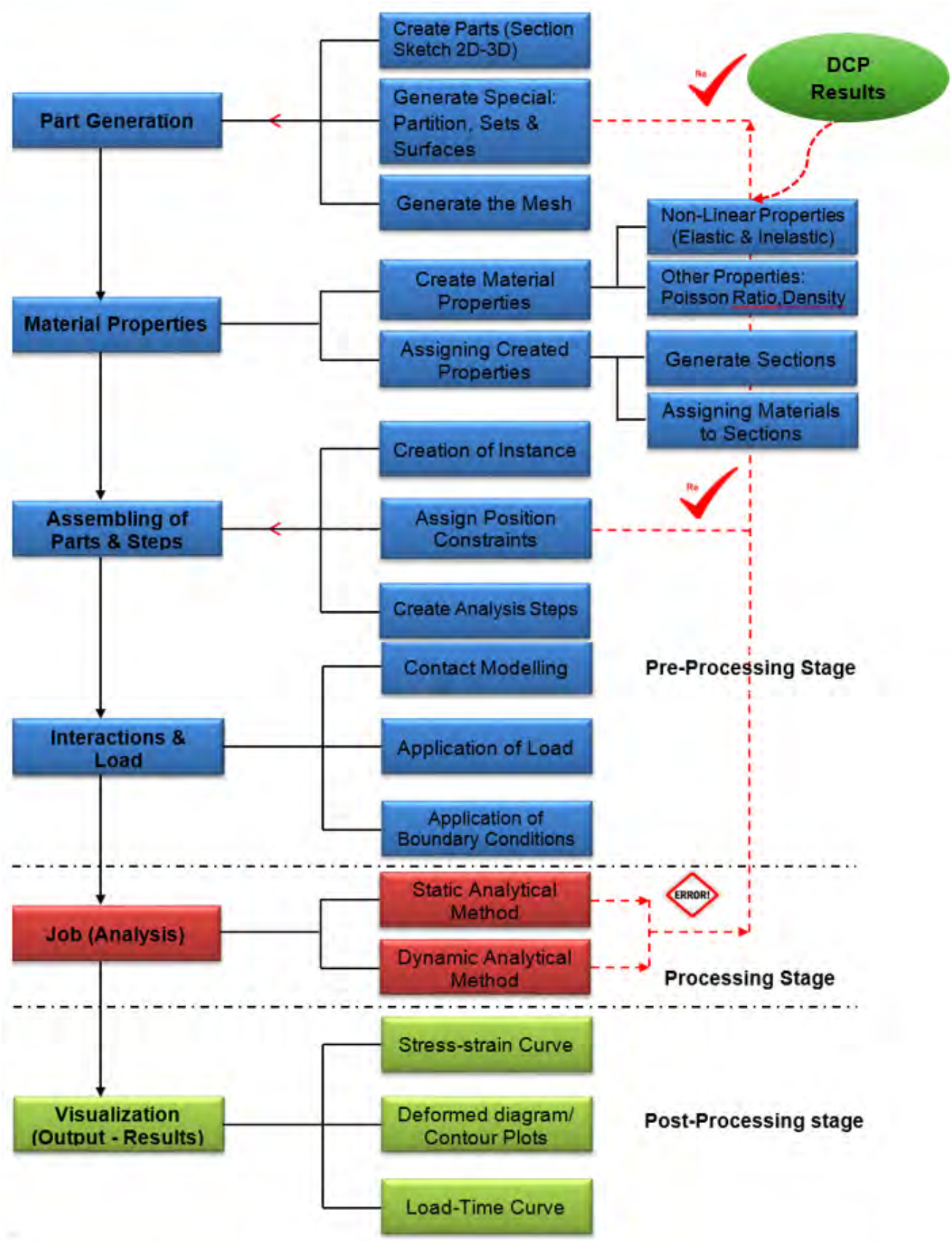

Figure 4-4 General steps for the development of flexible pavement (Abaqus®/CAE usage) (Adapted from Adedeji, 2015).

The modelling process in Abaqus®/CAE began with the definition of each pavement layer's geometry in the part module, where two-dimensional sketches were created and then extruded into three-dimensional solids. Partitioning, mesh generation, and the assignment of named sets were undertaken to ensure precise control over the model elements. Material properties for each layer, such as elastic modulus, Poisson's ratio, and density, were defined in the property module based on laboratory-derived data. These parts were then assembled in the assembly module to form the complete pavement structure.

Loading stages and boundary conditions were specified within the step module to capture variations in applied loads and constraints during the simulation. Interactions between the layers, including contact definitions and load transfer mechanisms, were configured in the interaction module, while the load module was used to apply traffic loading as a surface pressure and to assign realistic field boundary conditions. The model was then submitted for computation through the job module, with progress monitored closely to identify and resolve any warnings or errors.

Following completion of the analysis, the visualisation module was employed to extract results, including stress distributions, strain responses, and displacements within the pavement layers. These outputs were subsequently used to evaluate performance and compare the FEM-based design outcomes with those derived from traditional empirical methods. Careful attention was paid throughout the modelling process to ensure accurate representation of in-situ conditions and to maintain the reliability of the simulation results.

4.7 Chapter Summary

This chapter outlined the comprehensive methodology adopted to develop a FEM based pavement design for LVRs, using DCP data and benchmarking it against conventional empirical methods. The study commenced with the selection of representative materials from two geographically and climatically distinct sites in South Africa, Northern Cape and KwaZulu-Natal, followed by in-situ testing and systematic sample collection.

Laboratory investigations, undertaken at Simlab geotechnical laboratory and the CSIR laboratory, included soil index property determination, compaction testing, CBR

testing, and Repeated Load Triaxial Testing in accordance with the relevant SANS standards and CSIR protocols. DCP tests were performed on site to establish empirical correlations with laboratory derived parameters for FEM input.

A range of pavement design methods, CBR, AASHTO 1993, TRH 20, Odemark's, mePADS, and FEM will be applied using identical datasets to enable direct comparison of predicted layer thicknesses, stresses, strains, and service lives. The FEM modelling will be undertaken using Abaqus®/CAE to simulate pavement responses under traffic loading, with careful attention given to geometry definition, material property assignment, boundary conditions, load application, and result interpretation.

The methodology ensured consistent data acquisition, rigorous testing, and systematic model development, thereby enabling reliable comparative analysis and validation of the proposed FEM based for LVR design.

Chapter 5 : Material Characterisation Results

5.1 Introduction

This chapter presents results on soil samples from the Northern Cape and KwaZulu-Natal regions of South Africa to conduct a geotechnical investigation of the materials used in low-volume roads (LVRs). These areas were chosen to enable a comparative study of the geotechnical characteristics of the materials because of different climate conditions, KwaZulu-Natal is wet, whereas the Northern Cape is dry. Samples of soil were collected from certain sites in these areas and tested in the laboratory for several parameters, such as compaction properties, Atterberg limits, grain size distributions, and in situ dynamic cone penetrometer results. Additionally, triaxial testing results were also represented and thereafter correlated with the DCP results. The results offer insights into the suitability of these materials for road construction, emphasizing the importance of site-specific testing and material classification.

5.2 Results of the Laboratory Testing Methods

5.2.1 Soil Index Properties and Soil Classification Results

5.2.1.1 Grain Size Results

The main objective of grain size analysis is to quantify the size of grains in a type of soil and thus understand the behaviour and interactions within the soil. The samples collected from the sites were subjected to testing. Figure 5-1 and Figure 5-2 show the results of the grain size analysis of the soils. The percentage of samples passing through different sieve sizes was determined to determine the uniformity of the soil and its gradation. From the graph, it can be deduced that the gravel soils are made up of gravel, sand, and silt.

In addition, Table 5-1 and Table 5-2 show the results of the other grain size analysis terms, such as the diameter corresponding to 60%, 30%, and 10% fines in the grain size distribution (D_{60}, D_{30}, and D_{10}, respectively), coefficient of uniformity (C_u), and coefficient of gradation (C_c). The grain size analysis results revealed that the soils from Northern Cape Province are well-graded, whereas the samples from KwaZulu-Natal are poorly graded and feature few gap-graded soils.

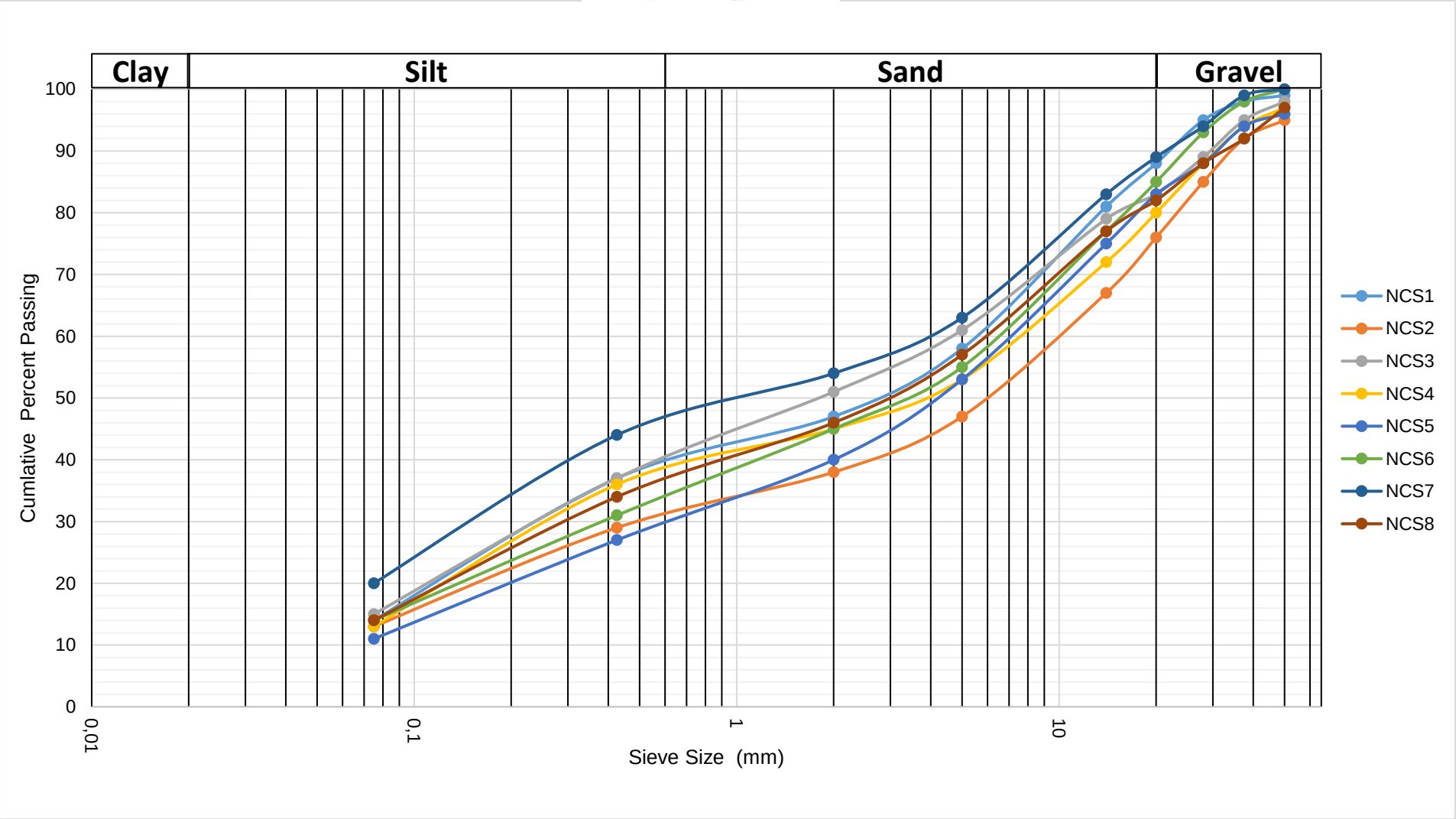

Figure 5-1 Northern Cape Samples (NCS) grain size distribution curves

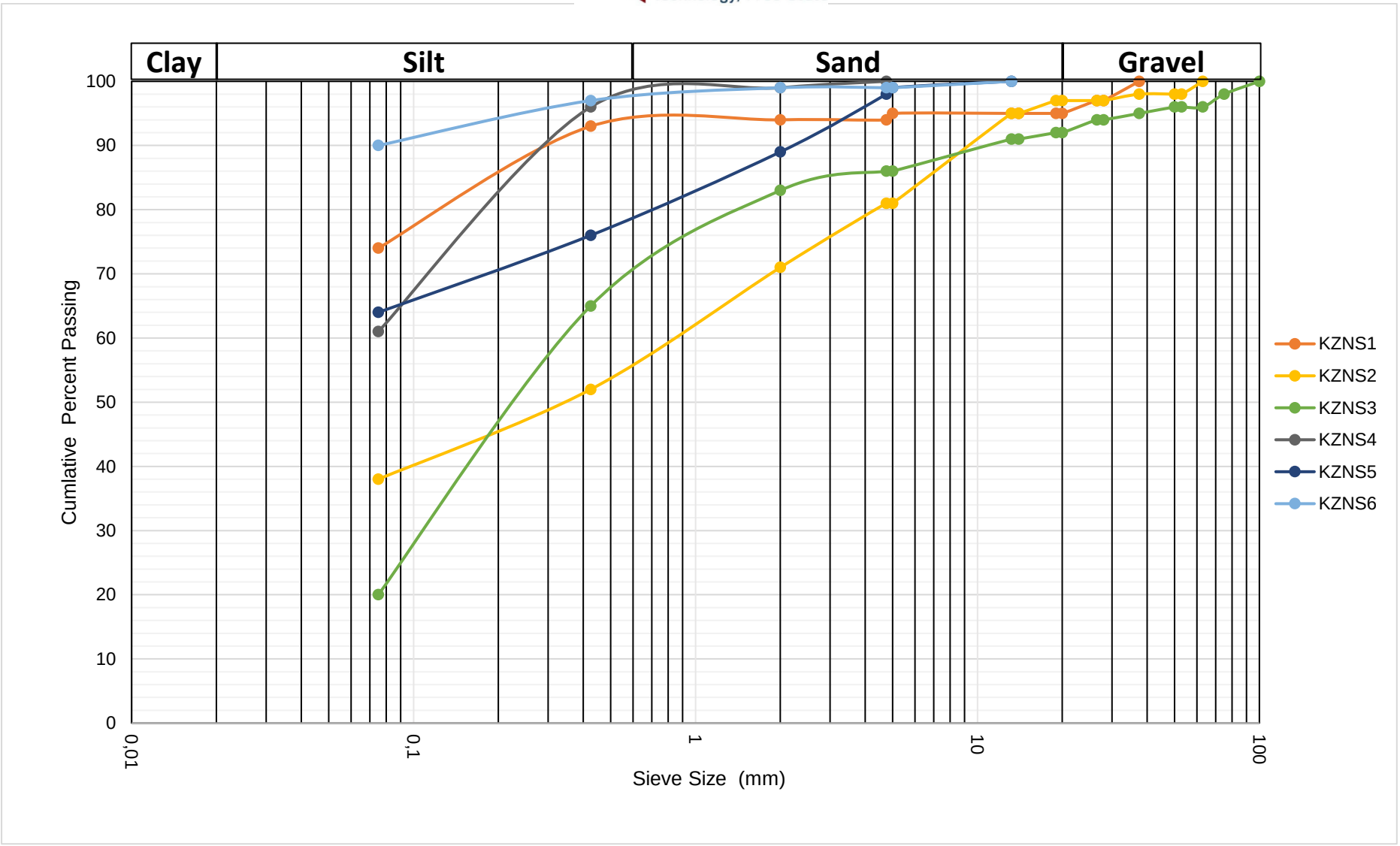

Figure 5-2 KwaZulu-Natal Samples (KZNS) grain size distribution curves

The C_u values for NCSs 1 to 8 ranged between 12.0 and 217.7, with an average of 132.48, which indicated that the soils were well-graded. The KZNS 1-6 Cu soils range from 3.0-52.9 and are considered poorly graded and well-graded soils. Furthermore, the particle size shapes are determined by the C_c. In Table 5-1 and Table 5-2, the values obtained for the investigated soils are compiled. The C_c values for the NCS samples range from 0.04-0.86. Because the value of C_c does not fall within the accepted range of 1-3, the NCS samples displayed an irregular particle form. The KZNS samples had irregular shapes because their C_c values ranging from 0.16-0.8 were outside the acceptable range owing to the wide range of particle shapes.

Table 5-1 Index properties for NCS

Index Property	NCS1	NCS2	NCS3	NCS4	NCS5	NCS6	NCS7	NCS8	Average
Coarse sand (<2,0>0,425 mm)	20	24	27	21	32	29	18	26	25
Fine Sand (<0,425>0,075 mm)	51	42	43	50	41	39	45	42	44
Materials (<0,075 mm)	29	34	30	29	27	31	37	31	31
D10	0,04	0,045	0,375	0,049	0,06	0,041	0,028	0,04	0,085
D30	0,25	0,5	0,25	0,28	0,6	0,39	0,17	0,3	0,34
D60	5,4	9,8	4,5	7,2	7	6,15	3,75	5,9	6,21
Cu	135,00	217,78	12,00	146,94	116,67	150,00	133,93	147,50	132,48
Cc	0,29	0,57	0,04	0,22	0,86	0,60	0,28	0,38	0,41

Table 5-2 Index properties for KZNS

Index Property	KZNS1	KZNS2	KZNS3	KZNS4	KZNS5	KZNS6	Average
Coarse sand (<2,0>0,425 mm)	2	26	21	4	14	2	12
Fine Sand (<0,425>0,075 mm)	19	20	55	34	14	7	25
Materials (<0,075 mm)	79	54	24	62	72	91	64
D10	0,014	0,017	0,028	0,015	0,014	0,013	0,017
D30	0,023	0,05	0,12	0,028	0,027	0,02	0,045
D60	0,05	0,9	0,35	0,074	0,065	0,039	0,246
Cu	3,57	52,94	12,50	4,93	4,64	3,00	13,60
Cc	0,76	0,16	1,47	0,71	0,80	0,79	0,78

5.2.1.2 Atterberg Limit Results

The results for the Atterberg limit test are shown in Table 5-3 and Table 5-4. The soil sample test results and accompanying plasticity charts for the NCS and KZNS samples are shown in Figure 5-3 and Figure 5-4, respectively. The Universal Soil

Classification System (USCS) was applied to provide typical soil descriptions for each symbol.

The NCS samples generally exhibit low plasticity, with liquid limits ranging from non-plastic to 41% and plasticity indices typically between 4% and 8%. On the Casagrande chart, the samples plot above the A-line but within the low-plasticity range, corresponding to ML and CL–ML soil types under USCS. According to AASHTO classification, they fall mainly within the A-1-a, A-1-b, and A-2-4/5 groups, which represent granular soils of good quality, further confirmed by a group index (GI) of 0. In South African terms (COLTO, 1998), these soils correspond to the G6–G9 material classes, indicating good to fair quality gravels, suitable for use in subgrade and subbase layers of low-volume roads.

The KZNS samples, by contrast, show moderate to high plasticity, with liquid limits ranging from 35% to 56% and plasticity indices between 16% and 24%. These soils plot above the A-line with PI > 4%, classifying them primarily as CL and MH under USCS. AASHTO classification places them in the A-6, A-7-5, and A-7-6 groups, which are typically clayey soils with poor subgrade quality. The relatively high group indices (up to 24) further reflect their weak performance potential. In the South African COLTO classification, most KZNS soils are listed as ND (not defined), except for one sample classified as G7, indicating that they are unsuitable in their natural state and would require treatment or stabilisation prior to use in pavement structures.

Furthermore, the results obtained from sieve analysis and Atterberg limit tests are used for classifying soil via the AASHTO classification method (Table 5-3 and Table 5-4) (Equation 5-1).

Equation 5-1

$$GI = (F - 35)[0.2 + 0.005(LL - 50)] + 0.01\,(F - 15)(PI - 10)$$

Where:

GI: Group Index

F: Fine content (per cent passing through the #200 sieve)

LL: Liquid limit

PI: Plasticity Index (LI - PL)

Table 5-3 Atterberg limit properties for NCS

Atterberg Limits	NCS1	NCS2	NCS3	NCS4	NCS5	NCS6	NCS7	NCS8
Liquid Limit (%)	NP	31	40	28	24	32	24	41
Plastic Limit (%)	NP	24	32	23	20	27	19	33
Plastic Index (%)	NP	7	8	5	4	5	5	8
Shrinkage Limit (%)	0	3,4	4	2,7	1,8	2,5	2,3	4
USCS	-	ML	ML	ML	CL-ML	ML	CL-ML	ML
AASHTO	A-1-b	A-2-4	A-2-4	A-1-b	A-1-a	A-1-b	A-1-b	A-2-5
Group Index	0	0	0	0	0	0	0	0
COLTO: 1998	G8	G6	G7	G6	G6	G8	<G9	<G9

Table 5-4 Atterberg limit properties for KZNS

Atterberg Limits	KZNS1	KZNS2	KZNS3	KZNS4	KZNS5	KZNS6
Liquid Limit (%)	49	39	NP	35	56	50
Plastic Limit (%)	26	22	NP	19	32	27
Plastic Index (%)	23	17	NP	16	24	23
Shrinkage Limit (%)	12,5	8	0	8,5	12	12
USCS	CL	CL	-	CL	MH	CL
AASHTO	A-7-6	A-6	A-2-4	A-6	A-7-5	A-7-6
Group Index	17	0	0	7	15	24
COLTO: 1998	ND	ND	G7	ND	ND	ND

Notes: ND=Not Defined

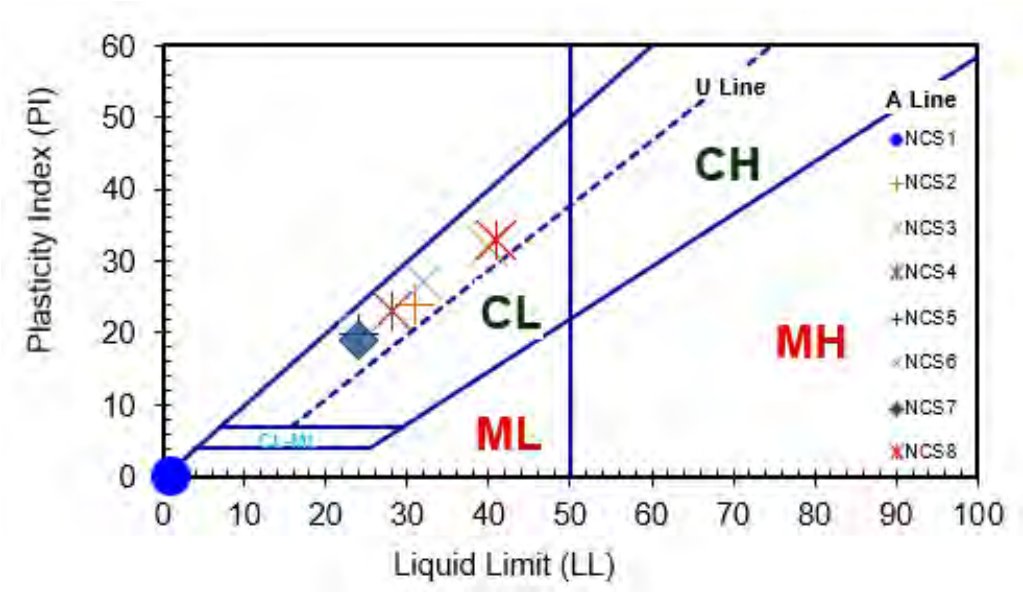

Figure 5-3 Casagrande plasticity chart for an NCS

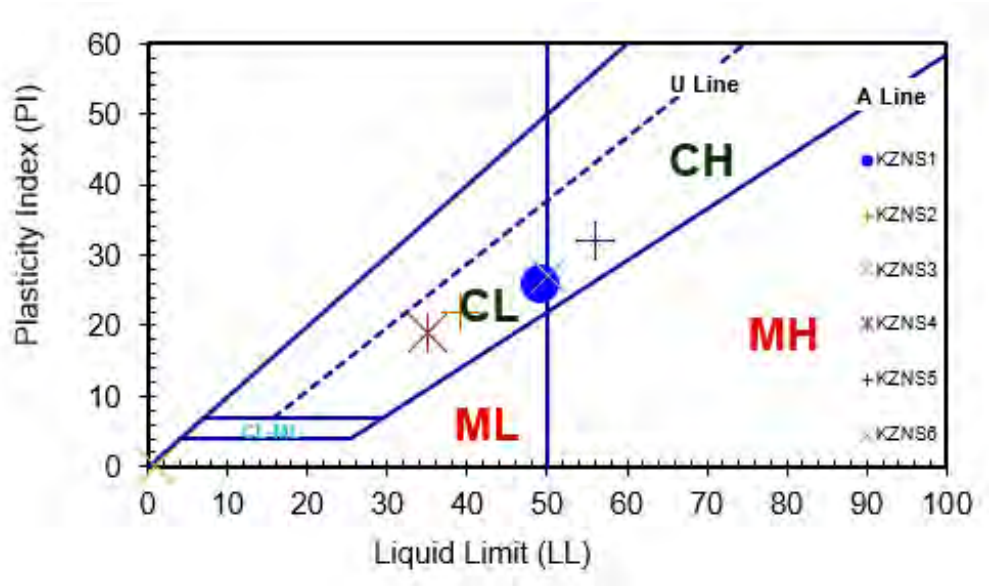

Figure 5-4 Casagrande plasticity chart for KZNS

5.2.2 Compaction Characteristics Results

The compaction properties of KZNS and NCS were investigated via the modified Proctor compaction method in accordance with the TMH1 method A7 guidelines. The moisture–density relationships of the NCS and KZNS samples were determined and are presented in Table 5-5 and Table 5-6, respectively. These relationships show how the OMC and MDD vary between samples, indicating the influence of moisture content on the compaction behaviour of the soil (Figure 5-5).

For the NCS samples, the OMC ranged from 8.2% to 14.6%, whereas the MDD varied from 1839 to 2053 kg/m³. In general, soil density increases with moisture content until reaching the OMC, where maximum compaction and stability are achieved. Beyond this point, additional moisture leads to a more dispersed soil structure and reduced density. This behaviour is consistent with soil compaction theory, which describes a parabolic relationship between moisture content and dry density, with the peak at the OMC.

Table 5-5 Compaction characteristics of the NCS

Compaction Characteristics	NCS1	NCS2	NCS3	NCS4	NCS5	NCS6	NCS7	NCS8	Average
OMC (%)	14,6	9,9	10,2	9,2	10,4	12,1	8,2	9,9	10,6
MDD (kg/m3)	1839	1972	2038	1852	1908	1858	2053	1973	1937
CBR Value	35	48	35	98	55	40	20	49	55

Table 5-6 Compaction characteristics of KZNS

Compaction Characteristics	KZNS1	KZNS2	KZNS3	KZNS4	KZNS5	KZNS6	Average
OMC (%)	22,3	14,5	9,1	13,2	20,4	21,5	16,8
MDD (kg/m3)	1646	1747	2054	1870	1714	1695	1788
CBR Value	9,3	11	38	13	15	8,5	15,8

The KZNS samples exhibited similar trends but with slightly different compaction parameters. The OMC for KZNS ranged from 9.1% to 22.3%, whereas the MDD varied from 1646 kg/m³ to 2054 kg/m³. These results suggest that KZNS may have a broader range of moisture contents at which compaction occurs, possibly due to its varied mineral composition, particle size distribution, and likely moist environment. The higher OMC values observed in some KZNS samples may indicate a greater requirement for water to achieve optimal compaction, as finer particles require more water to aid in particle rearrangement and reduce voids.

In addition to the compaction characteristics, the CBR values obtained at OMC and MDD provide further insight into the strength performance of the soils (Table 5-5 and Table 5-6). The NCS samples, which achieved relatively high maximum dry densities and low plasticity indices, also recorded higher CBR values ranging from 20% to 98%, confirming their adequacy as competent subgrade materials for LVRs. In contrast, the KZNS samples, which exhibited lower maximum dry densities and higher plasticity indices, yielded comparatively low CBR values between 8.5% and 38%. These outcomes indicate that while NCS soils are generally suitable for pavement support, the KZNS soils are problematic in their natural state and would require stabilisation or replacement to meet design requirements

The variation in the CBR values for both the NCS and KZNS samples provides additional evidence for the observed differences in compaction behaviour. The CBRs for the NCS samples ranged from 20% to 98%, whereas those for the KZNS samples ranged from 8.5% to 38%. The lower CBRs in some KZNS samples may be attributed to suboptimal compaction at either lower or higher moisture contents, leading to a less stable soil structure.

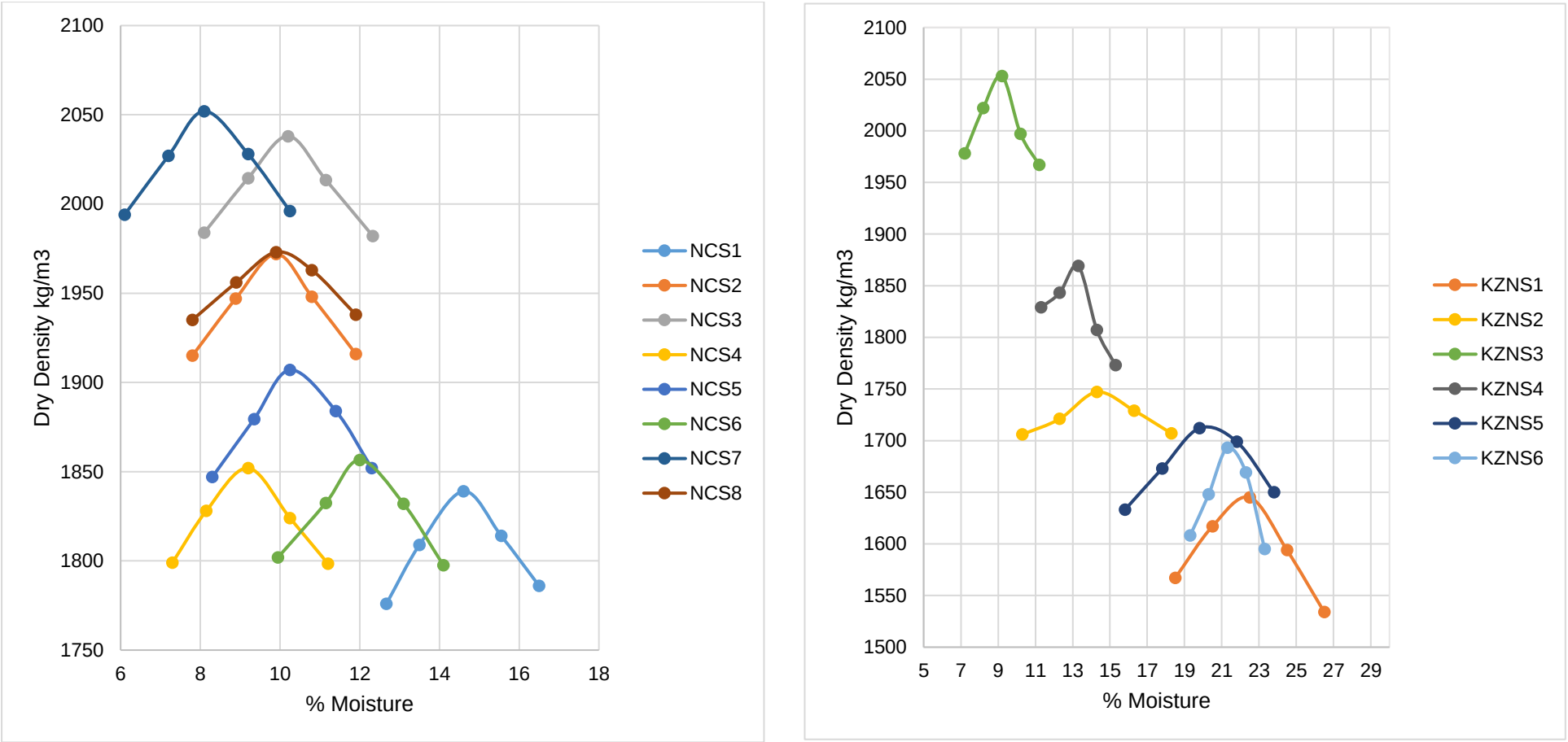

Figure 5-5 Standard proctor test results for NCS and KZNS

Overall, the results emphasize the importance of precisely controlling the moisture content during compaction to achieve optimal soil strength and density. They highlight the necessity of site-specific compaction settings to ensure the desired geotechnical properties, particularly when working with different soil types such as NCS and KZNS.

5.2.3 Repeated Load Triaxial Test Results

The maximum dry density (MDD) and optimum moisture content (OMC) of the soil samples tested from each region were characterized according to SANS 3001-GR30. The MDD and OMC test results are shown in Table 5-7. The bulk density (BD), apparent density (AD), and water absorption (WA) from each region were determined for the soil material via the SANS 3001-AG21 test methods. Notably, the test results obtained are similar to those obtained previously.

Table 5-7 Index properties of the RLT samples

Property	Test Results	
	NCS	KZNS
OMC (%)	11,1	12,3
MDD (kg/m3)	1938	1886
AD (kg/m3)	2438	2490
BD (kg/m3)	2192	2093
WA (%)	4,6	7,6

5.2.3.1 NCS5 Sample

A summary of the sample compaction properties for the determination of shear strength and shear strength results is shown in Table 5-8 and Table 5-9, respectively. The graphs of load *vs* time for the samples tested and of shear stress *vs* principal stress are shown in Figure 5-6.

Table 5-8 Specimen compaction properties for shear strength determination

NCS5	OMC (%)	MDD (kg/m3)	Compacted Mass (kg)	Target Mass (kg)	Sample height (mm)	Curing days
NCS5-S1	11.1	1938	11.603	11.609	307	1
NCS5-S2			11.598	11.609	307	1
NCS5-S3			11.604	11.609	307	1

Table 5-9 Summary of the shear strength results

NCS5	MC at testing	Confining pressure	Failure load	Failure stress	Total displaceme	Saturation (%)	Cohesion (kN)	Friction angle

	(%)	(kPa)	(kN)	(kPa)	nt (mm)			(Deg.)
NCS5-S1	11.1	51	13.4	736	7.6	**19.9**	**135.5**	**38.8**
NCS5-S2	11.1	101	16.4	905	7.2			
NCS5-S3	11.1	152	19.5	1075	7.96			

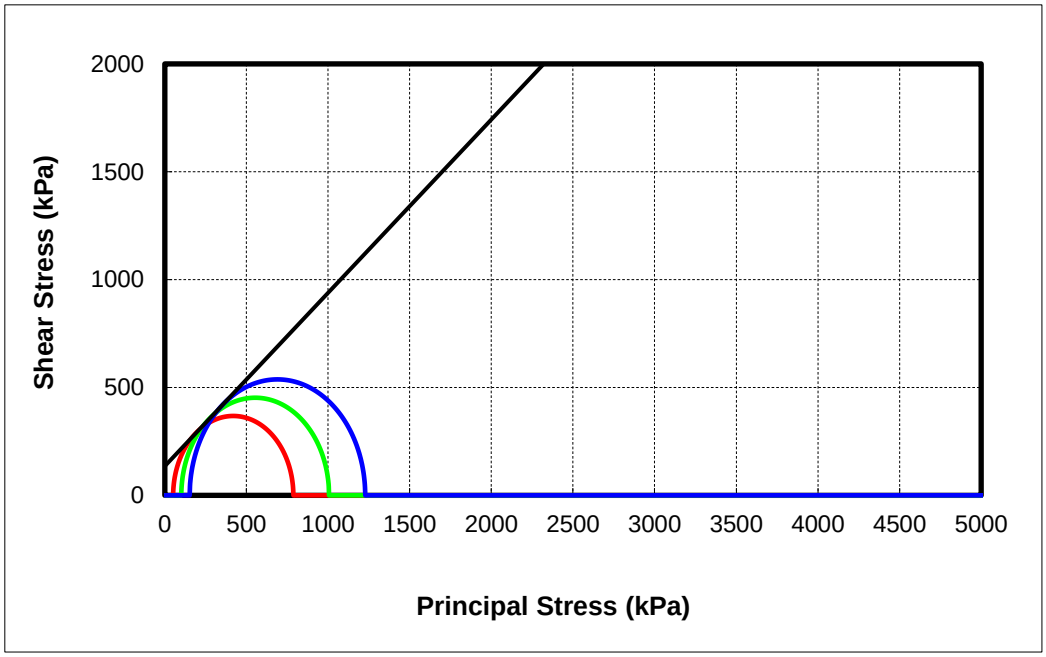

Figure 5-6 Shear stress vs principle stress for NCS5

NCS5 Resilient Modulus Test

A summary of the sample compaction properties used for the determination of the resilient modulus is shown in Table 5-11, and the resilient modulus, shear modulus, and Poisson's ratio graphs are shown in Figure 5-7 to Figure 5-9. As shown in Figure 5-7, the resilient modulus (MR) test results analysis indicates a distinct correlation between MR and confinement pressure. A higher confinement pressure results in an increase in the resilient modulus, which shows that the material stiffens and becomes more resistant to deformation under repeated loading. This behaviour is explained by greater confinement-induced densification and a decrease in the void ratio, which improve particle interaction and overall stiffness. The relationship between the Poisson's ratio and confinement pressure is depicted in Figure 5-8, where the Poisson's ratio slightly decreases as confinement increases. This implies that the material is more rigid and stable because it shows less lateral expansion than axial compression.

The decrease in Poisson's ratio can be linked to the reduced lateral movement of the particles due to increased friction and interlocking. As the confinement pressure increases, Figure 5-9 demonstrates that the shear modulus (G) also increases, resulting in enhanced resistance to shear deformation. This pattern demonstrates the material's improved resistance to shear stresses and structural integrity at increased confinement. These results highlight the important impact of confinement pressure on the mechanical characteristics of the tested material, especially in terms of increasing stiffness and decreasing deformability.

Table 5-10 Specimen compaction properties for determination of the resilient modulus

NCS5	OMC (%)	MDD (kg/m3)	Compacted Mass (kg)	Target Mass (kg)	Sample height (mm)	Curing days
NCS5-S4	11.1	1938	11.595	11.609	306	1

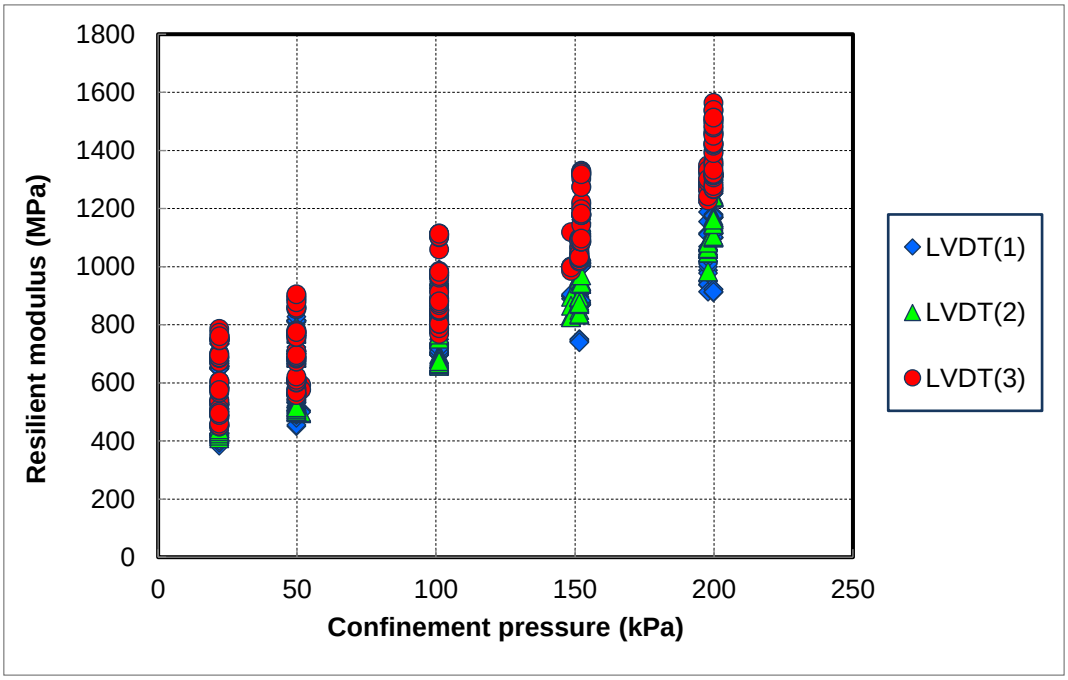

Figure 5-7 Resilient modulus vs. confinement pressure for NCS5

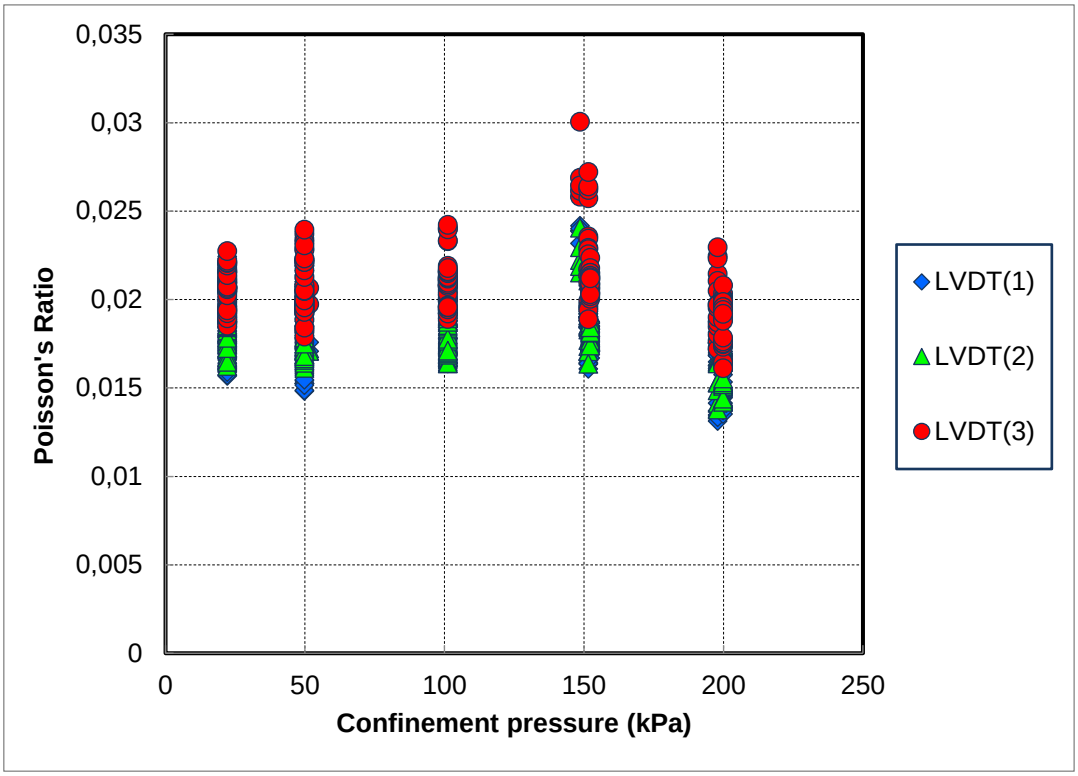

Figure 5-8 Poisson's ratio vs. confinement pressure for NCS5

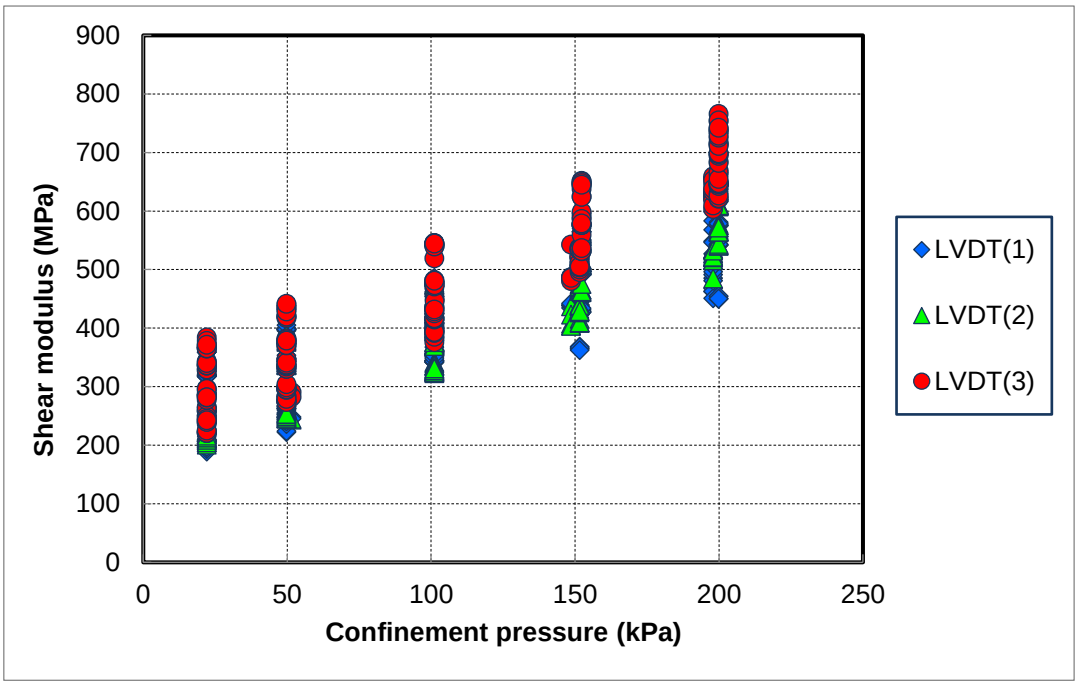

Figure 5-9 Shear modulus vs confinement pressure for NCS5

5.2.3.2 KZNS4 Sample

A summary of the sample compaction properties for the determination of shear strength and shear strength results is shown in Table 5-11 and Table 5-12, respectively. The graphs of load *vs* time for the samples tested and of shear stress *vs* principal stress are shown in Table 5-12.

Table 5-11 Specimen compaction properties for shear strength determination

KZNS4	OMC (%)	MDD (kg/m^3)	Compacted Mass (kg)	Target Mass (kg)	Sample height (mm)	Curing days
KZNS4-S1	12.3	1886	11.362	11.416	310	1
KZNS4-S2			11.392	11.416	306	
KZNS4-S3			11.386	11.416	308	

Table 5-12 Summary of the shear strength results

KZNS4	MC at testing (%)	Confining pressure (kPa)	Failure load (kN)	Failure stress (kPa)	Total displacement (mm)	Saturation(%)	Cohesion(kN)	Friction angle (Deg.)
KZNS4-S1	12.3	50.47	11	622	7.96	12.1	52.3	50.7
KZNS4-S2	12.5	101.32	18	1019	12.52			
KZNS4-S3	12.4	150.81	23	1302	13.99			

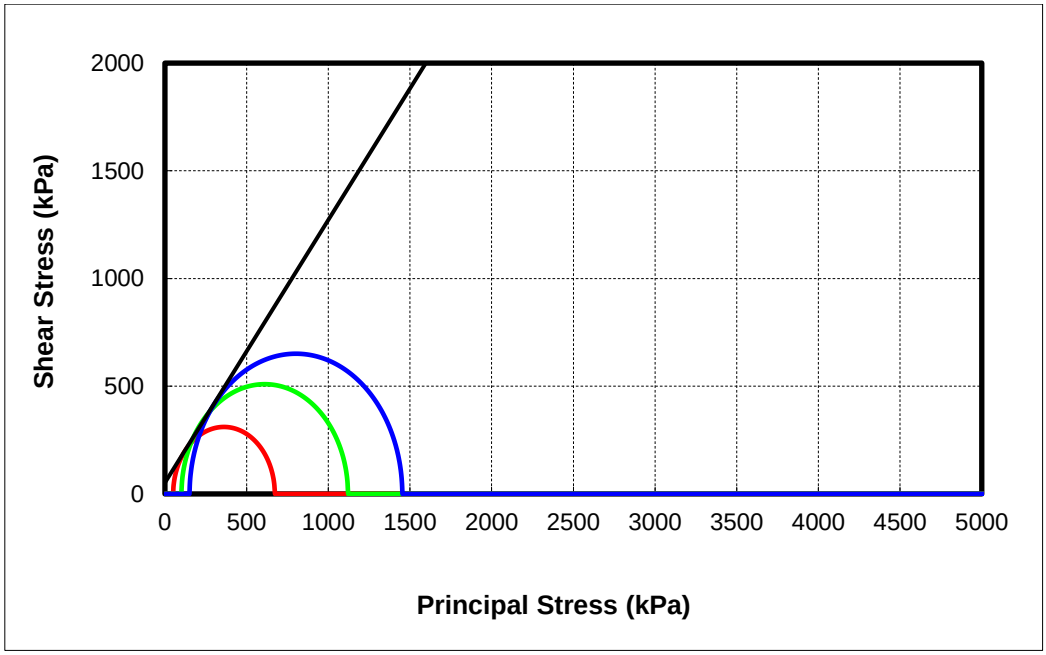

Figure 5-10 Graph of shear stress vs. principal stress for KZNS4

KZNS4 Resilient modulus test

A summary of the sample compaction properties for the determination of the resilient modulus is shown in Table 5-13, and the resilient modulus, Poisson's ratio, and shear modulus graphs are shown in Figure 5-11 to Figure 5-13. During the MR test, the average vertical deformation of the samples was monitored and recorded by using three external variable displacement transducers (LVDTs) placed on the top of the triaxial cell. These LVDTs provided precise measurements of the vertical displacement, which are crucial in determining the resilient modulus values at each confinement pressure. The resilient deformation of the last five deviatoric cycles was averaged to obtain the MR values. The test results indicated that the MR of the soils was highly dependent on the confinement pressure, with an increase in confining pressure leading to a decrease in MR values for KZNS. Furthermore, the KZNS samples exhibited permanent deformation under cyclic loading, which reduced MR values.

The LVDTs provided detailed displacement data, allowing for the analysis of how different confining pressures affect the resilient properties of soils. The MR values plotted as a function of these pressures revealed the high sensitivity of the soil samples, particularly under varying moisture conditions. This highlights the importance of considering both stress conditions and moisture content when evaluating the resilient behaviour of soils for road pavement structures.

Table 5-13 Specimen compaction properties for determination of the resilient modulus

KZNS4	OMC (%)	MDD (kg/m3)	Compacted Mass (kg)	Target Mass (kg)	Sample height (mm)	Curing days
KZNS4-S4	12.3	1886	11.392	11.416	306	1

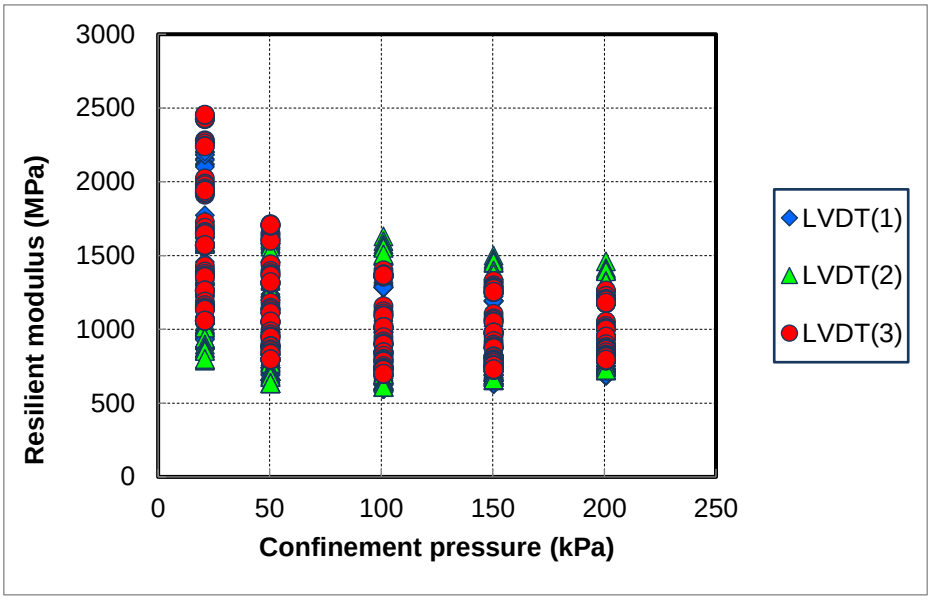

Figure 5-11 Resilient modulus vs. confinement pressure for KZNS4

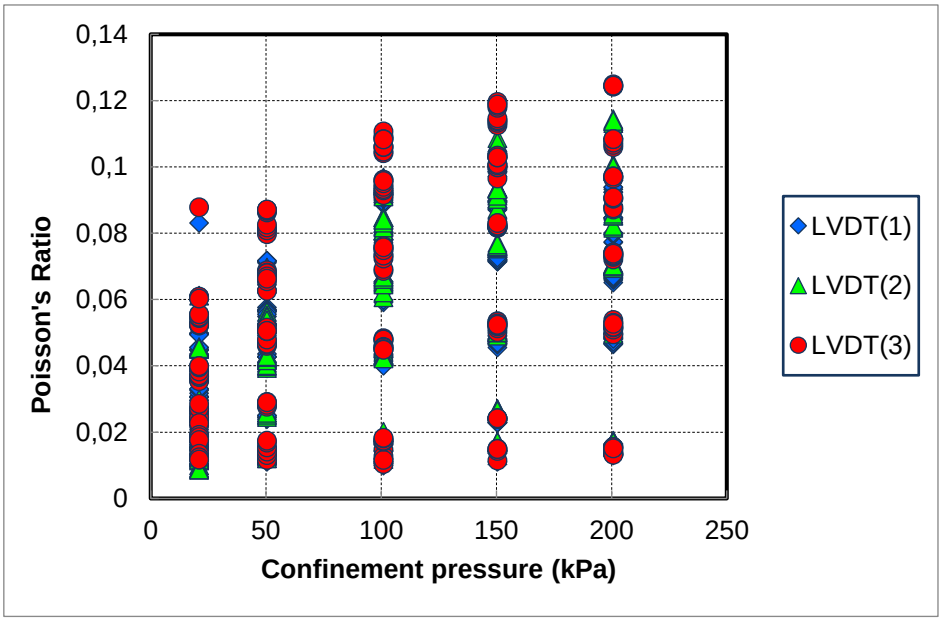

Figure 5-12 Poisson's ratio vs. confinement pressure for KZNS4

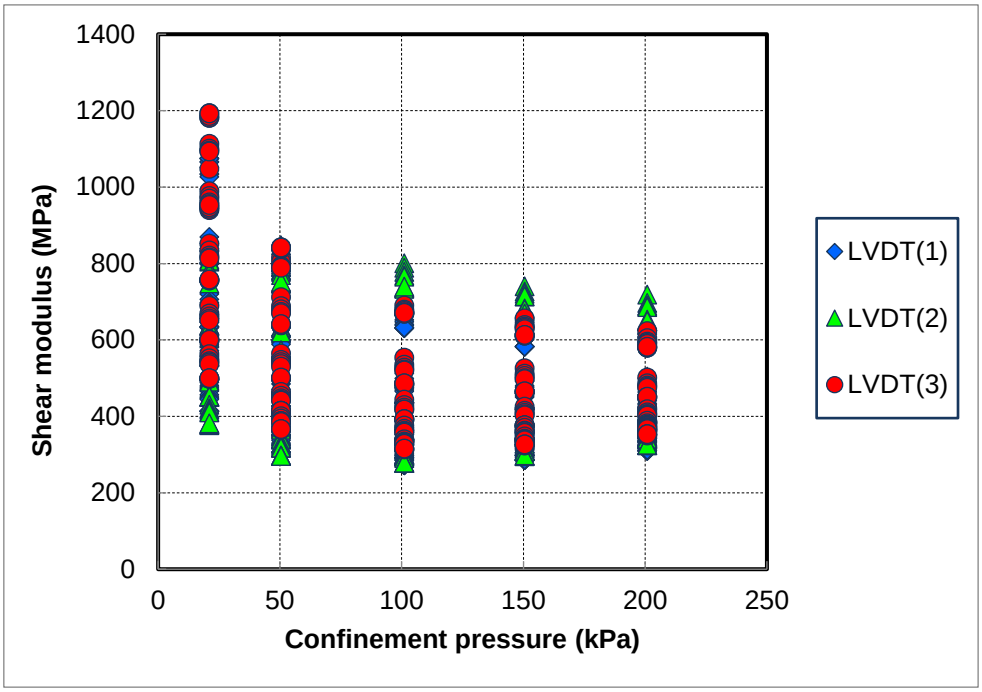

Figure 5-13 Shear modulus vs. confinement pressure for KZNS4

5.3 Results of In-Situ Material Testing

In-situ DCPI is influenced by soil stiffness, dry unit weight, and water content under natural conditions (Khalid, Rehman, Mujtaba & Farooq, 2022). Figure 5-14 and Figure 5-15 illustrate the correlations between cumulative blows and cumulative penetrations for the NCS and KZNS samples, respectively. The samples exhibiting higher stiffness and greater resistance to penetration demonstrated lower cumulative penetration values for a given number of blows, whereas specimens of lower stiffness and reduced strength capacity exhibited greater cumulative penetration under the same loading conditions. Using the aforementioned technique and Equation 3-1, the DCPI values of the samples were estimated. The DCPI values ranged from 10 mm/blow to 200 mm/blow.

Equation 5-2

$$DCPI = \frac{Diff\ Depth\ of\ penetration}{Diff\ Number\ of\ blows}$$

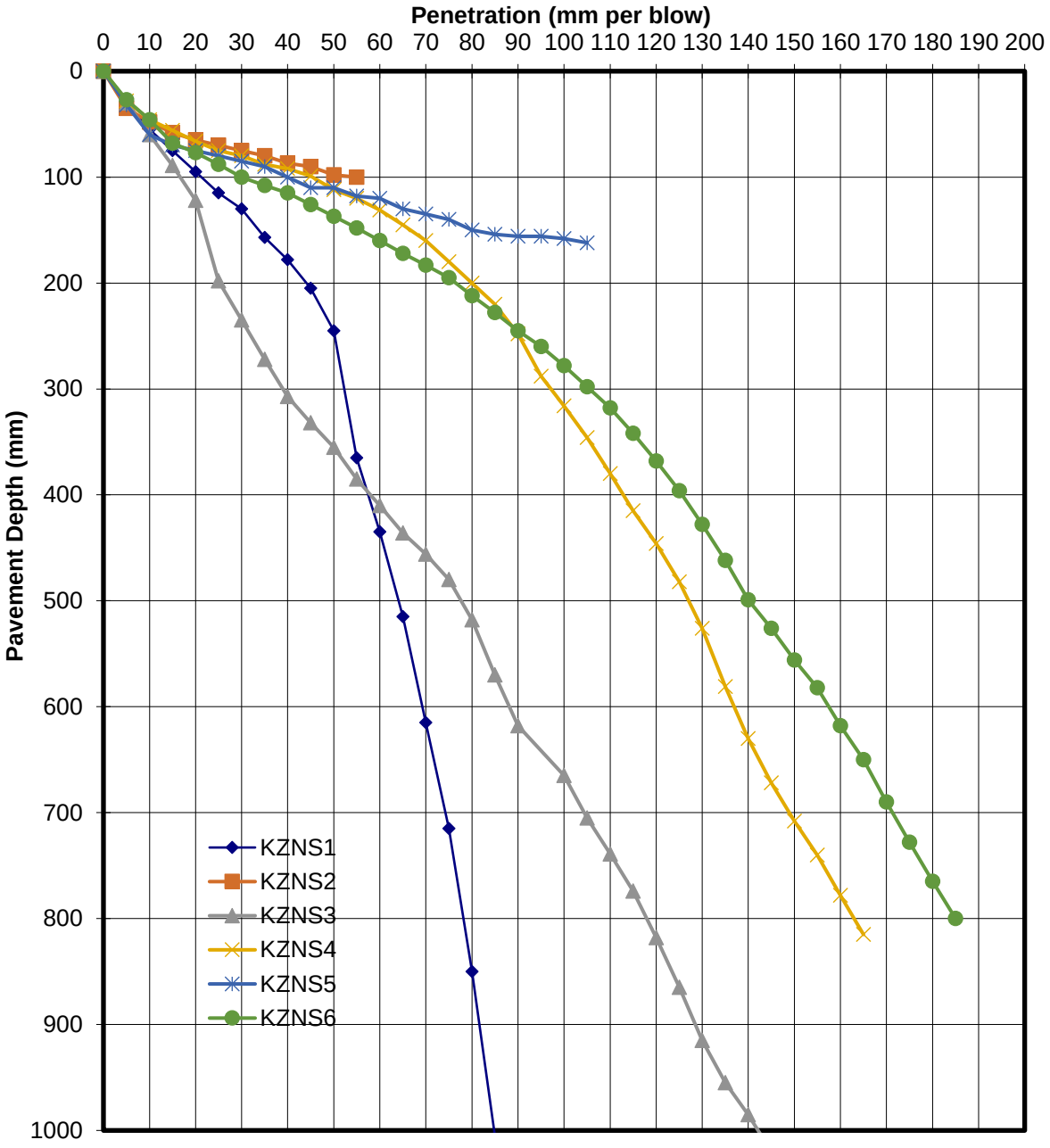

Figure 5-14 In-situ *DCP profile of KZNS sample soils*

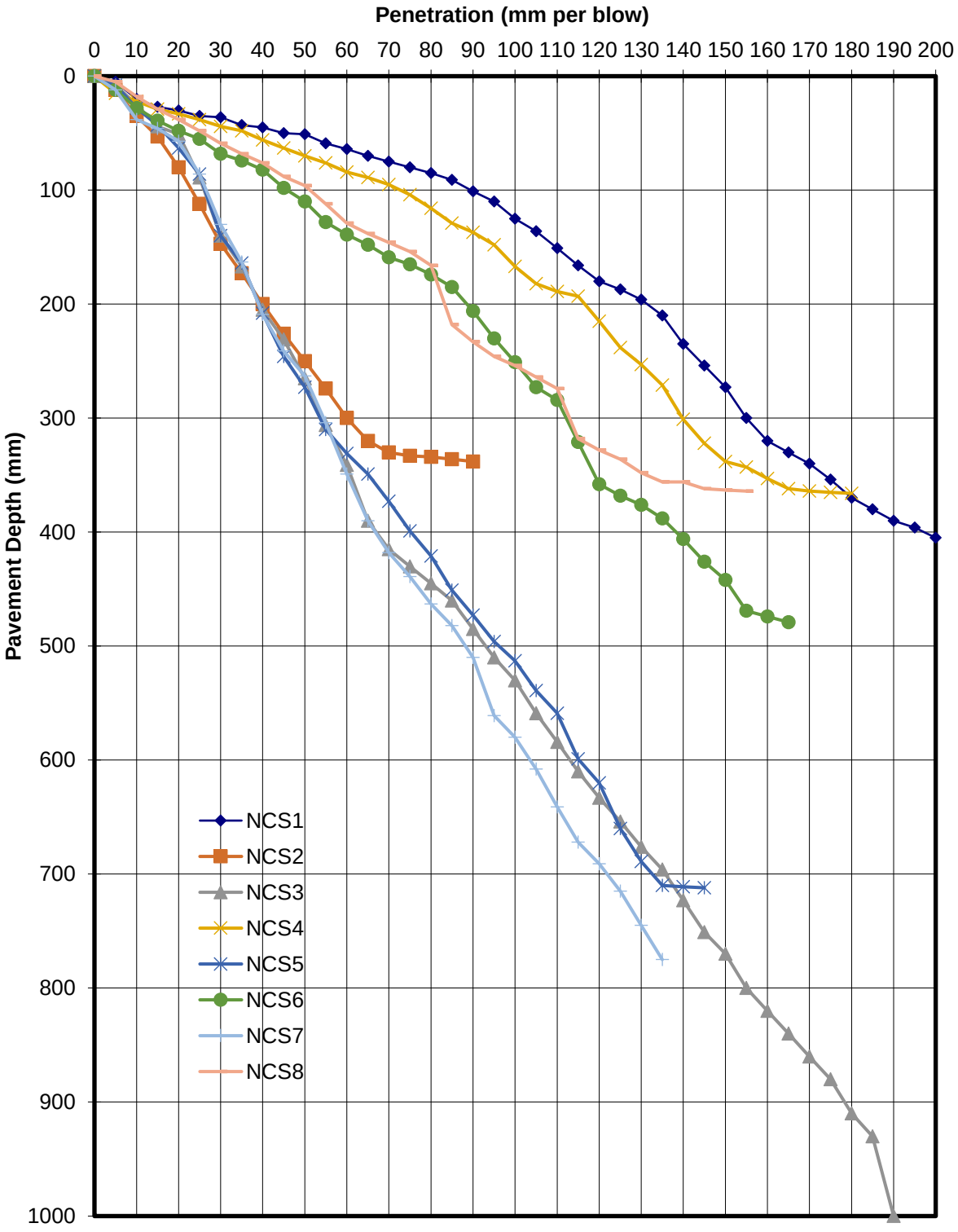

Figure 5-15 In-situ *DCP profile of NCS samples*

5.4 Analysing the DCP Results

The AFCP-LVR-DCP software represents a significant advancement in the management and analysis of road infrastructure within Sub-Saharan Africa. Developed under the Africa Community Access Partnership (AfCAP) initiative, this software is tailored to address the unique challenges of road maintenance and management in the region; however, it has been applied outside of regions and in different material types (Pinard et al. 2021; Ikechukwu et al. 2019; Mousavi et al. 2018; Zumrawi 2014; Mohammad et al. 2007). A critical application of AFCP-LVR-DCP is in the analysis of dynamic cone penetrometer (DCP) data, which are essential for assessing the bearing capacity and structural condition of existing pavement structures (Zhalehjoo et al. 2018; Mohammadi et al. 2008; Mohammad et al. 2007).

In pavement design, it is crucial for the pavement structure to be well designed and constructed over its design life, which allows for proper transfer of the traffic load to the subgrade. The pavement strength should deteriorate consistently with depth from the surface, a concept known as strength balance (Ikechukwu et al. 2019). The change in the strength of pavement layers with depth is an indicator of the strength balance of the pavement structure. A smooth decrease in strength without discontinuities is considered well-balanced, and DCP design analysis is based on this concept.

However, some pavement structures, especially low-volume roads (LVRs) with limited pavement layers over the subgrade, utilize in situ materials. Analysis via the software revealed that the NCS was poorly balanced to average balanced inverted structures Figure 5-16 to Figure 5-17 (Appendix B1). In contrast, the KZN structures are identified as average balanced deep to average inverted structures Figure 5-18 to Figure 5-19 (Appendix B1) because the strength of the pavement layers in the study area decreases gradually without discontinuities. The pavement balance at any depth is determined via the formula proposed by (Kleyn, De Wet & Savage 1989) (Equation 5-3):

Equation 5-3

$$DSN(\%) = \frac{D[400B + (100 - B)^2]}{[4BD + (100 - B)^2]}$$

Where:

- DSN = Number of pavement structures (%)
- B = parameter defining the standard pavement balance curve (SPBC)
- D = pavement depth (%)

This equation accommodates a series of developed curves for various pavement structure numbers and depths, presented in standard pavement balance curves (SPBC), as shown in Figure 5-20 through Figure 5-23 (Appendix B2).

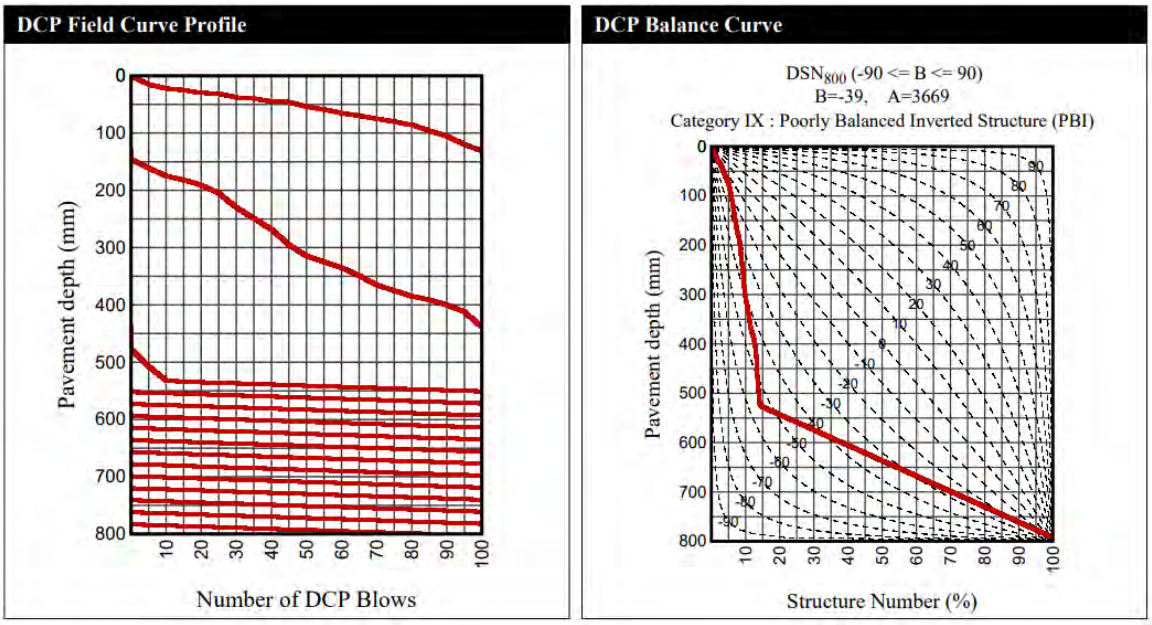

Figure 5-16 Penetration against the number of blows and the DSN curve for NCS1

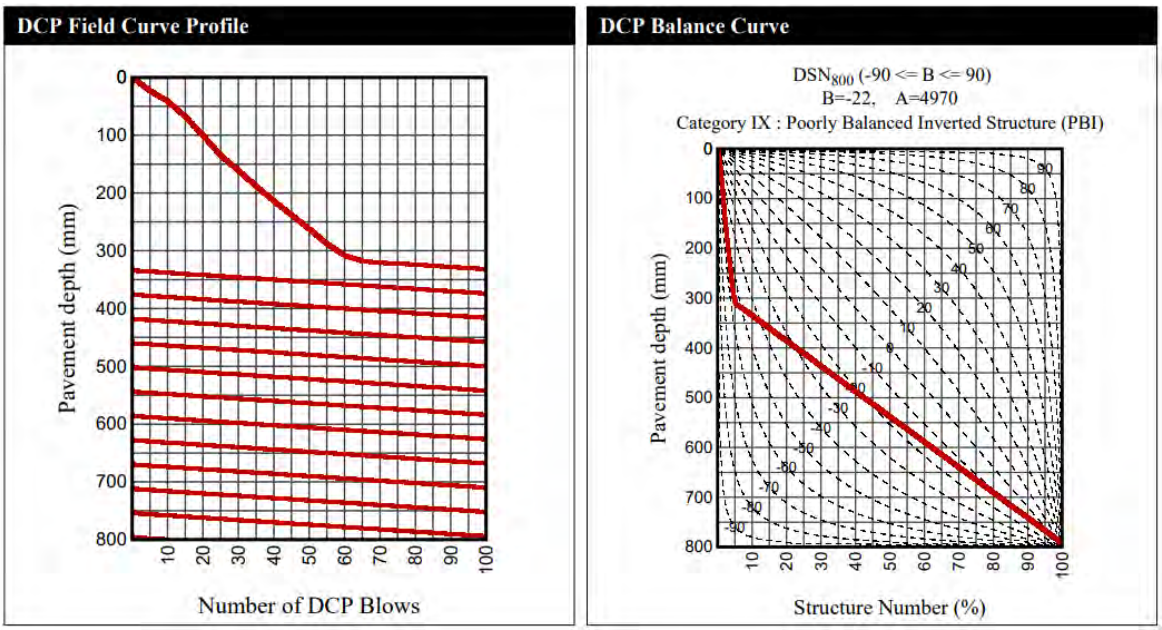

Figure 5-17 Penetration against the number of blows and the DSN curve for NCS2

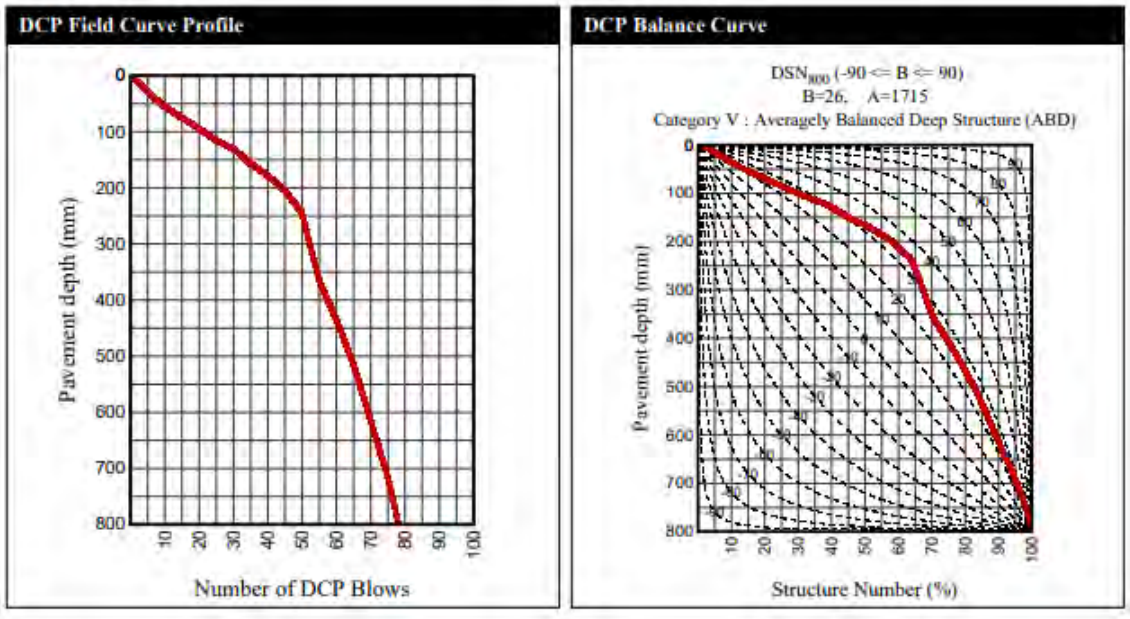

Figure 5-18. Penetration against no blows and the DSN curve for KZNS1

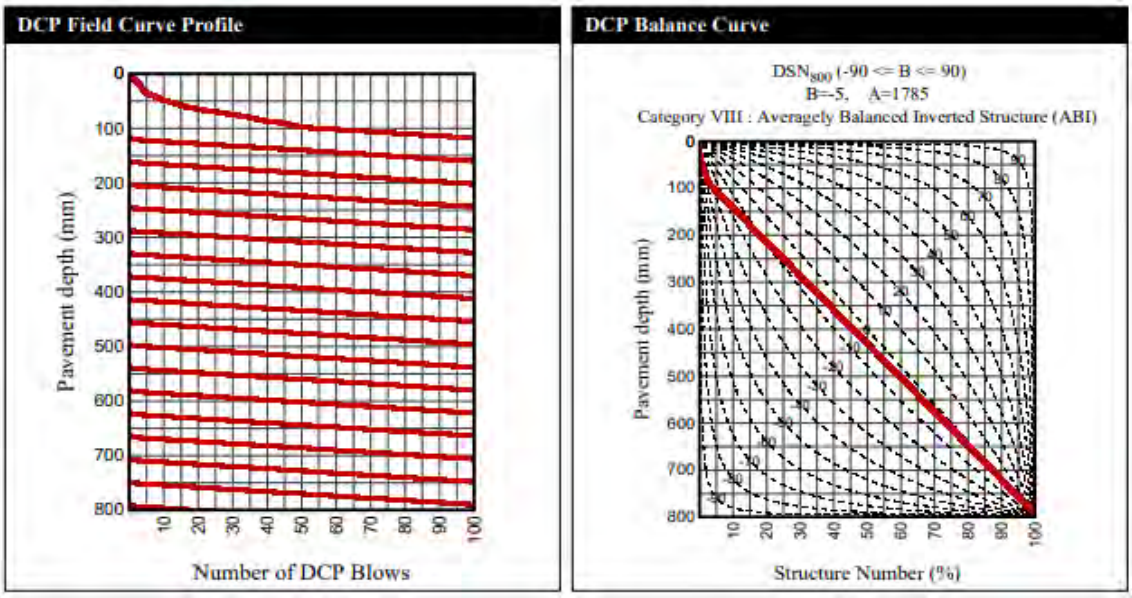

Figure 5-19 Penetration against no blows and the DSN curve for KZNS2

5.4.1 Layer Strength Diagram

In the AFCP-LVR-DCP software, details concerning the structural behaviour of the existing pavement layer, as tested by the DCP device, are provided. The DCP analysis data provide adequate strength performance of various pavement layers when fitted into the software via the layer strength diagram interface (Ikechukwu et al. 2019).

The layer strength diagram illustrates the in-situ strength of the pavement materials at every depth Figure 5-20 through Figure 5-23 (Appendix B2). The rate of penetration

is then compared with minimum specified standards called DCP master curves. The evaluation of pavement adequacy at various depths for the expected future traffic load is used for DCP profiling Figure 5-24 through Figure 5-23 (Appendix B3). The structural number (DSN800) is the number of blows the DCP requires to reach a certain depth for a balanced pavement, expressed as a percentage, and it is the balance number (BN) at that depth.

A classification system was developed using pavement strength balance curves. The pavement is classified in terms of the balance curve (B), which is the balance curve followed by the measured balance curve of the pavement, and the deviation (A) between the standard pavement balance curve (SPBC) and the measured curve. The dotted legend lines in Figure 5-20 through Figure 5-23 (Appendix B2), with changes in direction, indicate changes in the layer properties influenced by the layer thickness.

The processed data from the AFCP-LVR software are presented graphically, with the SPBC on the horizontal axis and the penetration depth on the vertical axis. According to this information, a first attempt at layer interface recognition was made by considering changes in the slope of the graph. Figure 5-20 through Figure 5-23 (Appendix B2) reported four discerned structural layers: a medium-strength wearing course to a depth of 150 mm for both NCS and KZNS, with the exception of a few weak wearing courses, a strong base with a depth of 450 mm, and a subbase extending to a depth of 800 mm. The ranges are recognized for SPBC in %. When the SPBC is greater than 40, the pavement is considered shallow; when it is between 0 and 40, it is designated deep; and when it is less than 0, it is inverted. The investigated pavement is confirmed to have a wearing course of 150 mm of deep pavement because the curve at each section is between 0 and 40 mm (Figure 5-20 through Figure 5-23 (Appendix B2)). Therefore, this confirms that the existing subgrade at each segment is adequate for low-volume road traffic.

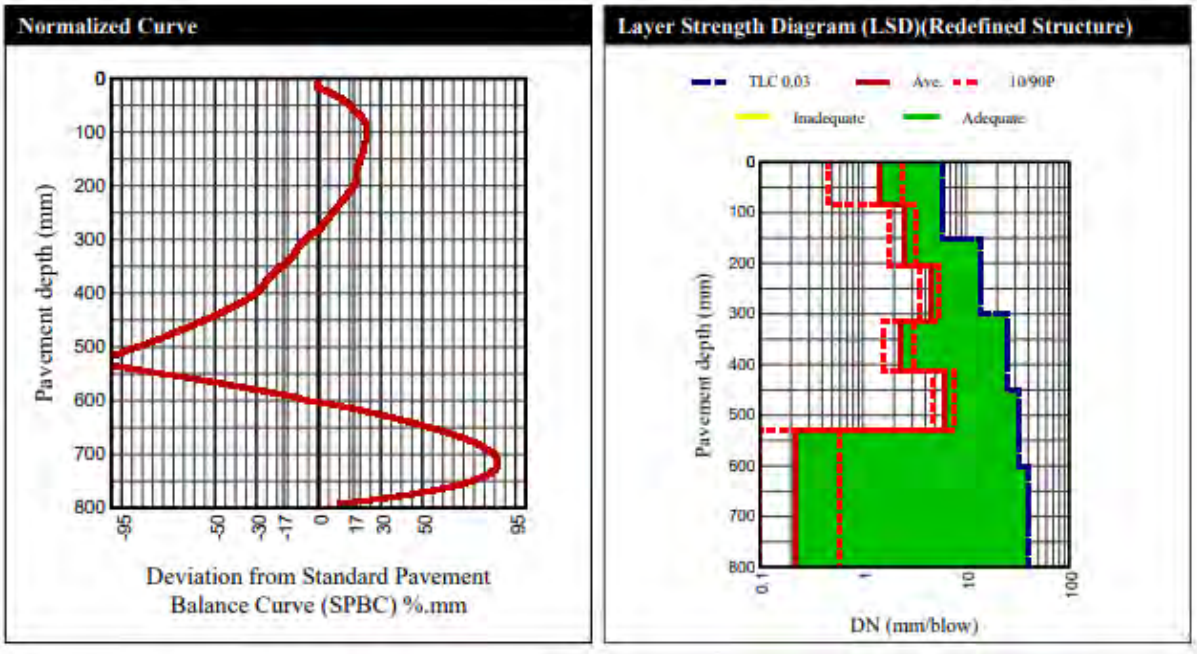

Figure 5-20 Normalized curve and layer strength diagram NCS1

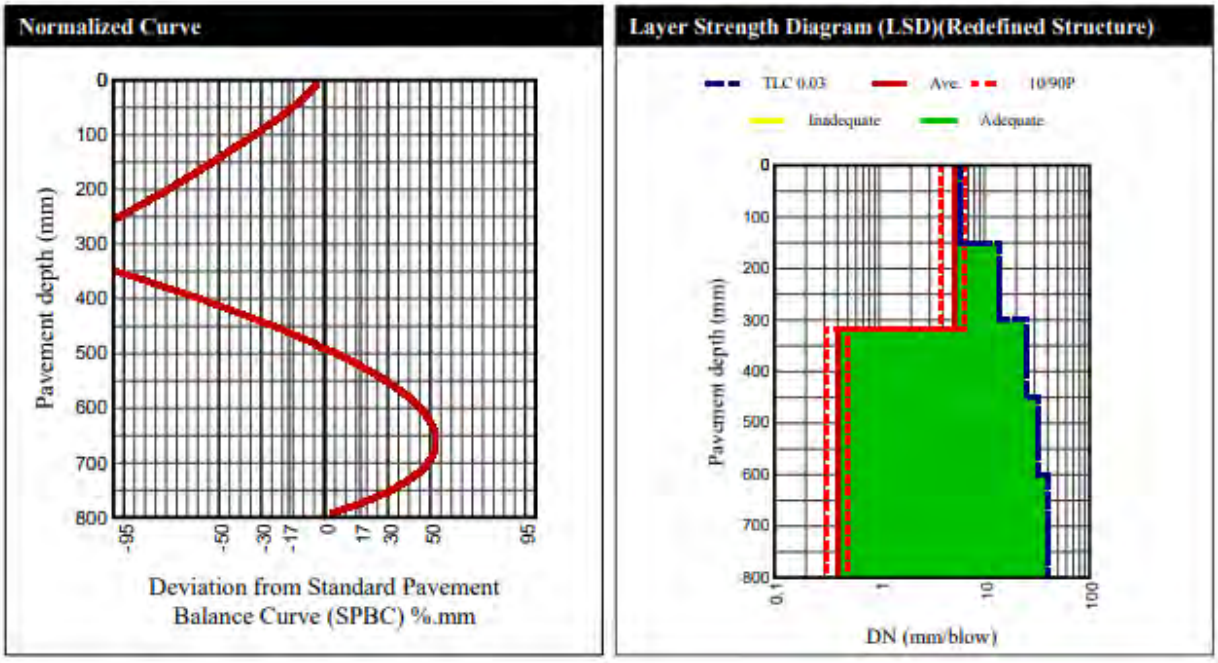

Figure 5-21 Normalized curve and layer strength diagram NCS2

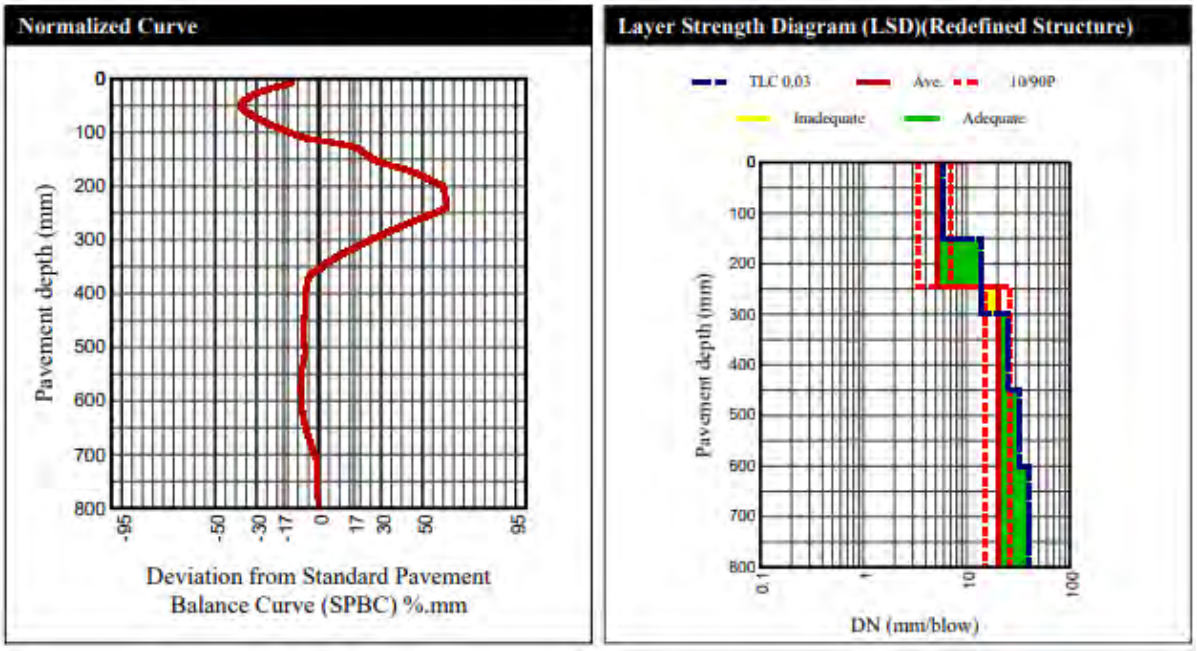

Figure 5-22 Normalized curve and layer strength diagram of KZNS1

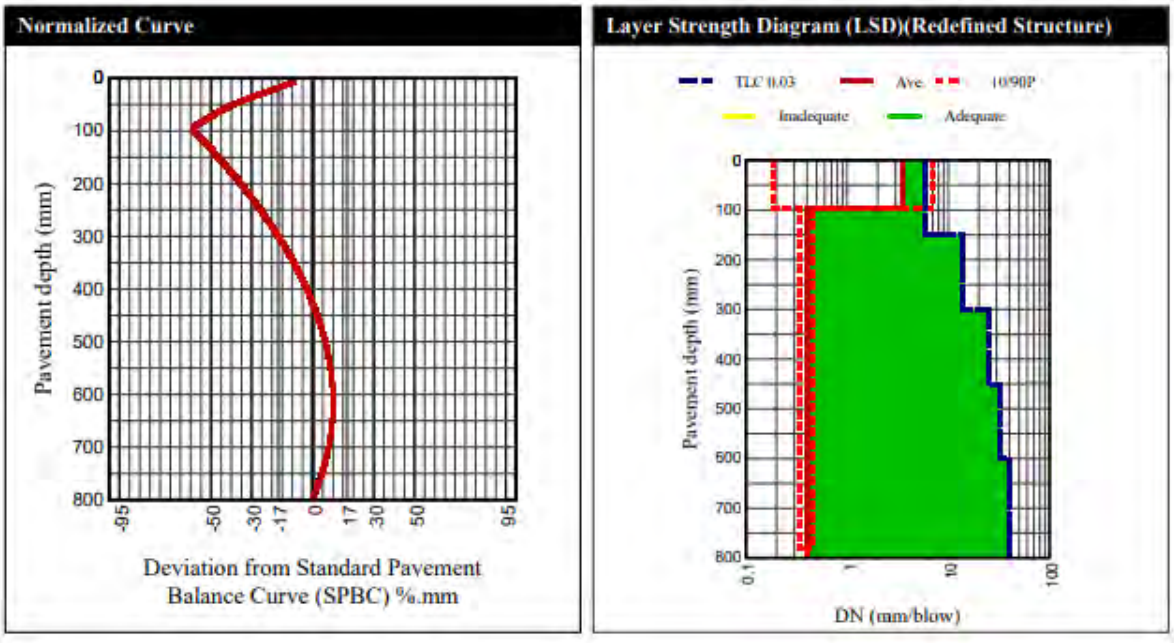

Figure 5-23 Normalized curve and layer strength diagram of KZNS2

5.4.2 Elastic Modulus Analysis

The three classes of pavement design expressed in million standard angles (MISAs) are as follows (COLTO, 1998):

- Light traffic: less than 200,000 E80s
- Medium traffic: between 200,000 and 800,000 E80s
- Heavy traffic: between 800,000 and 12 million E80s.

To investigate the required structural strength of the existing pavement, DCP field data expressed in terms of the DCP layer–strength diagram was projected to the appropriate DCP master curve, as shown in Figure 5-24 through Figure 5-23 (Appendix B2). The field data plotted on the left side of the design curves indicate that the pavement foundation has adequate structural strength for the low-traffic class. However, if the plot is located on the right-hand side of the design curve, this indicates that a region of the pavement structure has insufficient resilient strength.

In addition, DCP data curves plotted on the left side of a particular design curve, showing the area between the DCP field curve and the selected design curve, are coloured in green. This implies that adequate resilient strength is provided for the selected traffic class at the required depth. When the DCP field data curve is positioned to the right of the design curve, the corresponding area is highlighted in yellow, signifying that the pavement structure at that depth has insufficient structural capacity to accommodate the specified traffic load.

Overall, there are few yellow legend lines on the curves, implying that the existing pavement foundation is adequate for low traffic loading. Figure 5-24 through Figure 5-23 (Appendix B2) illustrate the distress mechanism of existing pavement with respect to traffic loading. The field data of the existing pavement plotted in red indicate that the pavement was designed not to carry more than 200,000 standard E80 traffic load applications. In contrast, the light traffic class is indicated by blue dotted lines (Figure 5-24 through Figure 5-23 (Appendix B2)). The results in Figure 5-24 through Figure 5-23 (Appendix B2) illustrated the DCP field data for all layers plotting to the left of the selected design curve, as presented by the green areas, which signifies that the pavement has adequate strength to carry at least between 200,000 and 800,000 E80s traffic load applications.

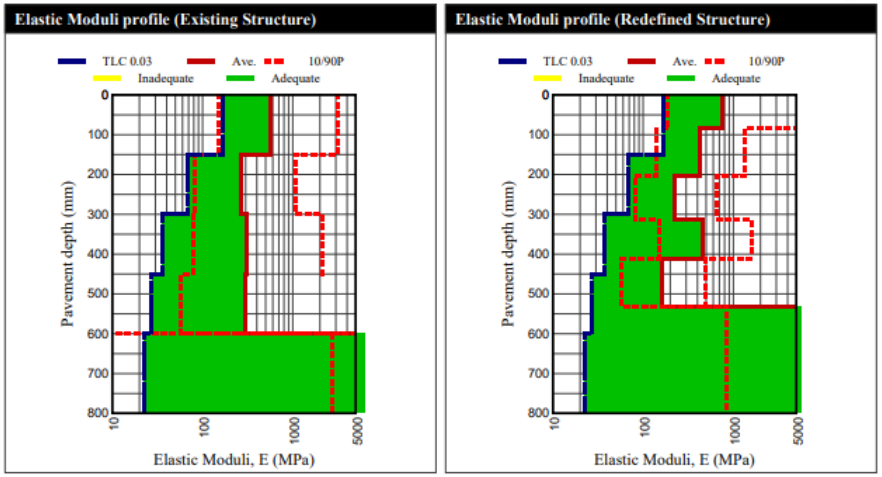

Figure 5-24 Elastic moduli versus the pavement depth NCS1

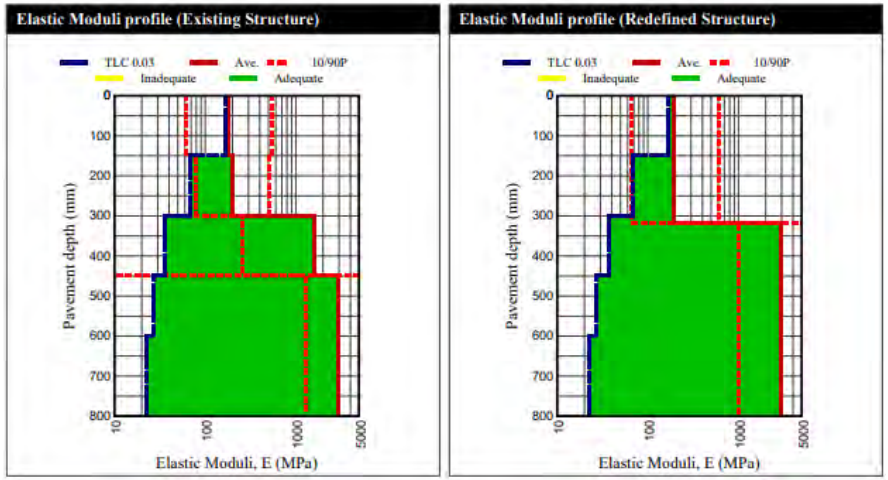

Figure 5-25 Elastic moduli versus the pavement depth NCS2

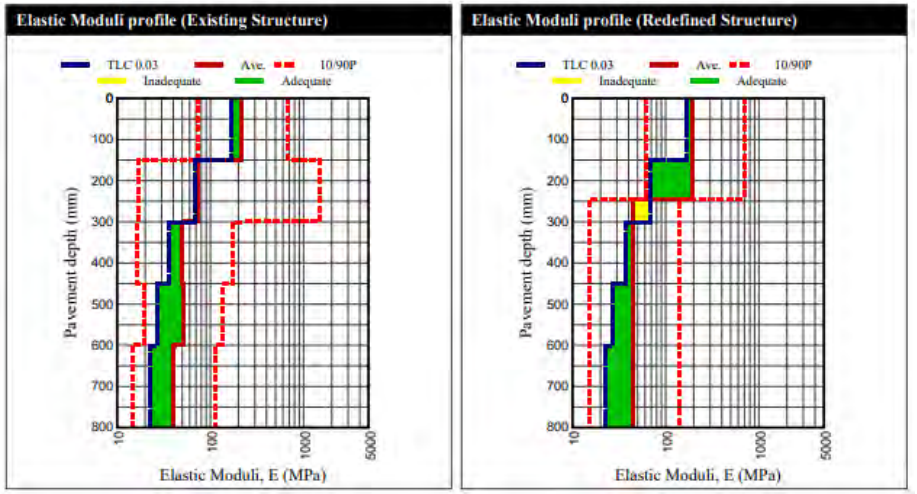

Figure 5-26 Elastic moduli versus pavement depth for KZNS1

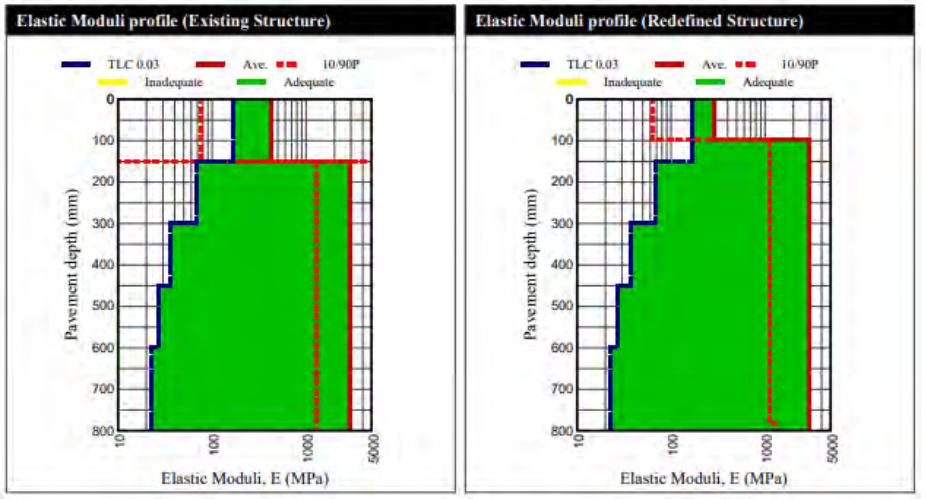

Figure 5-27 Elastic moduli versus pavement depth for KZNS2

5.5 Analysis of DCP, CBR, and Triaxial Results

The results of the laboratory resilient modulus and DCP tests confirmed that the evaluated subgrade possesses adequate strength and stiffness to provide a suitable foundation for the pavement layers of LVRs. These results are consistent with the results of the CBR laboratory tests. The predicted CBR values deviated by an average of 28% (Table 5-14). When the predicted values were compared with the measured laboratory values, the CBR results revealed a difference of 5.6% for NCS5. Similar studies, including Ikechukwu et al. (2019) and Daleiden, Killingsworth, Simpson & Zamora (1994), have reported this magnitude of result deviation. The resilient modulus results did not match those of the DCP test, as indicated in Table 5-14 because only a few triaxial tests were performed in this study. Ikechukwu et al. (2019) noted that testing a small number of samples would lead to poor correlation between the results. Therefore, the sample size should be increased in further studies to improve reliability and accuracy.

5.6 Chapter Summary

This chapter presents the results of soil samples from the study areas subjected to extensive laboratory testing. A grain size study revealed that the KwaZulu-Natal soils are poorly graded and that the Northern Cape soils are well-graded. According to the Atterberg limits, KwaZulu-Natal soils have greater plasticity and are finer-grained than the majority of Northern Cape soils, which are coarser-grained. Compaction tests revealed that the MDD and OMC of the soils varied, with Northern Cape soils typically having a greater MDD and lower OMC than KwaZulu-Natal soils. This chapter also presents the findings of many triaxial tests, which reveal a relationship between the resilient modulus and confinement pressure, with more confinement resulting in stiffer materials with better resistance to deformation. The results highlight the importance of considering local soil features while building and maintaining LVRs. Furthermore, the results presented will be used in the design of LVRs in the following chapters.

Table 5-14 Comparative analysis of the DCP results and laboratory MR/CBR

NCS5							
Material Description	**Depth**	**Ave Estimated E-Moduli @ Depth**	**Measured MR**	**E-Moduli Range (MPa)**	**Estimated CBR @ Depth**	**Measured CBR**	**UCS**
	(mm)	***(MPa)***	***(MPa)***	***10P-90P***	***(%)***	***(%)***	***(kPa)***
	0-150	142		40-713	35		341
	151-300	141		51-407	34		338
	301-450	155	**397**	43-816	39	**52**	373
	451-600	201		76-540	53		492
	601-800	209		75-609	55		513
KZNS4							
	Depth	**Ave Estimated E-Moduli @ Depth**	**Measured MR**	**E-Moduli Range (MPa)**	**Estimated CBR @ Depth**	**Measured CBR**	**UCS**
	(mm)	***(MPa)***	***(MPa)***	***10P-90P***	***(%)***	***(%)***	***(kPa)***
	0-150	362		93-2546	106		912
	151-300	185		56-738	48		415
	301-450	154	**594**	61-393	38	**13**	372
	451-600	126		47-350	30		300
	601-800	103		37-298	24		244

Chapter 6 : Low-Volume Road Pavement Design Results

6.1 Introduction

This chapter evaluates the performance and suitability of different pavement design methods for low-volume roads (LVRs). The methods considered include the California Bearing Ratio (CBR) method, the AASHTO 1993 method, the TRH 20 method, Odemark's method, mePADS software, and the finite element method (FEM) approach. Each of these methods applies distinct principles and computational techniques to address critical design factors such as soil conditions, material behaviour, and load-carrying capacity.

The comparison of these methods is necessary to achieve the research aim because it enables a direct assessment of how reliably conventional and advanced design approaches perform when applied to site-specific datasets. By analysing their outputs side by side, this study is able to identify the strengths, limitations, and practical implications of each method in the context of LVRs. Such evaluation is particularly important for methods incorporating Dynamic Cone Penetrometer (DCP) data, as it demonstrates the extent to which DCP-based approaches provide accurate and cost-effective solutions for LVR design.

Through this comparison, the study not only benchmarks existing methods but also highlights the most reliable and economical approach for ensuring long-term pavement durability under low-traffic volume scenarios.

6.2 LVR Pavement Design via Empirical Design Methods

6.2.1 CBR design, AASHTO 1993, TRH 20 and Odemark's input parameters

The design input parameters and criteria necessary for flexible pavement design were defined in accordance with the guidelines provided in the CBR, AASHTO, and TRH 20 design guides. For the CBR, TRH 20, and Odemark methods, the pavement layer properties are considered on the basis of the CBR value, whereas in the AASHTO design, they are considered on the basis of the MR value. Table 6-1 presents a

summary of the design input parameters and the various methods applicable to the input parameters. The expected cumulative traffic over the design life of 10-15 years is also presented. Input parameters such as the initial and terminal serviceability, layer coefficients, and design reliability are among those listed in Table 6-1. The initial serviceability of a newly built pavement was set at 4.2, and at the end of the design life, the terminal serviceability was specified as 2.0. These parameters were established via recommendations from AASHTO (Garber & Hoel 2018; Papagiannakis & Masad 2012).

The layer coefficients represent another important group of input variables, determined according to the characteristics of the available materials. For sandy gravel, which was the in-situ material in this study, AASHTO recommends a typical coefficient value of 0.07. In addition, the design reliability was set at 80%, consistent with AASHTO guidelines for low-volume roads.

Table 6-1 Pavement design input values used in CBR, AASHTO, TRH20 and Odemark's methods

Parameter	Design values		Comments
	NCS5	KZNS4	
Expected ESAL, SCw18	0,892/1.488 x 10^6	0,892/1.488 x 10^6	CBR, AASHTO, TRH20, DCP, Odemark
Structural Design Period	10/15 years	10/15 years	CBR, AASHTO, TRH20
Reliability, R	80%	80%	AASHTO, TRH20
Zr	- 0.841	- 0.841	AASHTO
So	0.45	0.45	AASHTO
MR base (CBR)	142 MPa (35)	362 MPa (106)	CBR, AASHTO, TRH20, DCP, Odemark
MR subbase (CBR)	155 MPa (39)	185 MPa (48)	
MR subgrade (CBR)	201 MPa (52)	154 MPa (13)	
Layer coefficients	a2: 0.07 (Sand gravel)		AASHTO
Pi	4.2	4.2	AASHTO
Pt	2.0	2.0	AASHTO
PSI = (Pi – Pt)	2.2	2.2	AASHTO
Weinert N-values	2	10	AASHTO, TRH20,

Parameter	Design values	Comments
Tyre Load and Radius of contact	80 kN and 195 mm	Odemark

6.2.2 CBR Design, AASHTO and TRH 20 Pavement Thickness

According to the design criteria listed in Table 6-1, two comparative pavement design alternatives were developed using the CBR method, namely the AASHTO and TRH 20 approaches. The AASHTO 1993 provides an empirical design equation for flexible pavement, which builds upon the CBR method. Table 6-2 provides information on the final design thicknesses for the granular subbase and granular base layers. With a robust subgrade material and minimal traffic, NCS5 can achieve the minimum design thickness, as shown in Table 6-2. This could be attributed to the climate of the region, which is drier than that of KZNS4, a wet region. According to the CBR method, the granular base and granular subbase for NCS5 have design thicknesses of 0 mm and 120 mm, respectively. In contrast, the AASHTO method produces a design thickness of 150 mm for each layer for both NCS5 and KZNS4. On the other hand, the results from the TRH20 method produce layer thicknesses of 125–150 mm for the granular base and granular subbase for both NCS5 and KZNS4, with the provision of a double surface seal layer as the surface material.

Thus, only the TRH 20 method considers the provision of a gravel-wearing layer, as it directly addresses the design of pavement for LVRs. Overall, these design methods considered LVRs should be without bituminous surfaces. However, the TRH 3 design of the seal surface covers the application of the seal as rehabilitation or for the new design, especially LVRs. The empirical methods considered in this study did not include the provision of a seal surface. However, designers often include an ultrathin layer of 30 mm, which is considered a non-structural layer.

Furthermore, when Odemark's stress-based method was used, the thicknesses of the granular base and subbase were 100 mm and 150 mm for NCS5 and 80 mm and 120 mm for KZNS4, respectively. Notably, Odemark's method is a mechanistic-empirical approach that considers the strength of the granular layer but does not account for environmental factors. Overall, the results presented by Odemark's method agree with those of Paul et al. (2024).

Table 6-2 Pavement design thickness established via the CBR, AASHTO 1993, TRH 20 and Odemark methods for different cases

Design Method	Case Description	Surface Layer (mm)	Granular Base Thickness (mm)	Granular Subbase Thickness (mm)
CBR	NCS5	-	-	120
	KZNS4	-	-	280
AASHTO 1993	NCS5	-	150	150
	KZNS4	-	150	150
TRH 20	NCS5	WC (80)	100 G5	-
	KZNS4	WC (90)	100 G5	100 G7
Odemark's Stress-Based Method	NCS5	-	100	150
	KZNS4	-	80	120

6.3 LVR Pavement Design Using 2D and 3D FEM Modelling Analysis for Unseal LVRs

In South Africa, a typical light pavement structure for low-volume roads (LVRs) usually consists of four layers: a surface seal (thickness varies depending on the type of seal), a granular base of 150 mm, a stabilized subbase of 150 mm, and a subgrade, which includes both a selected subgrade and an in-situ subgrade (Vaughan 2014; Horak 2008; DoT 1996). Owing to cost implications, these roads are often left unpaved. Therefore, in the model, three layers were analysed without the surfacing layer.

Two different material characterizations were used in the model, employing both 2D and 3D models in Abaqus for the two different study areas. In the 2D model, the pavement was considered a three-layered system with a compacted subgrade (Figure 6-1). The pavement section consists of a 150 mm granular base and a 150 mm subbase resting on a 2000 mm natural subgrade, which acts as its foundation, as designed according to AASHTO (6.2.2).

Furthermore, in the 3D model analysis, the layers were consistent with those in the 2D model. These models highlight the effects of unsealed pavement. Similarly, all the models were also analysed in MePADS for validation and comparative study.

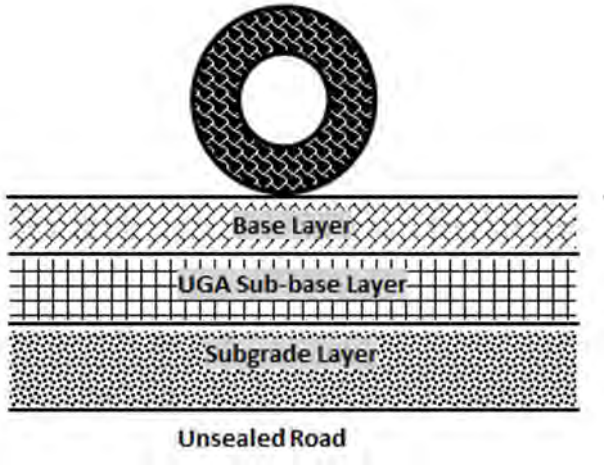

Figure 6-1 Model scenarios of the pavement structure

For any successful FEM simulation, factors such as model geometry, material characterization, element type and mesh size, boundary conditions, and loading type need to be carefully considered (Al-Khateeb et al., 2011). The next section details the factors for this study.

6.3.1 Model geometry, Element Types, and Mesh Size

The models were simulated via the axisymmetric approach in Abaqus with dimensions of 3000 mm on the horizontal axis. The depth on the vertical axis remained constant at 2300 mm. However, the depths of the base and subbase were 150 mm each, and the subgrade layer depth was 2000 mm. In terms of element types, for the 2D model, four-node axisymmetric elements (CAX4 and CAX4R) were used, whereas a solid continuum 8-node element with reduced integration (C3D8R) was used for the 3D models. The mesh size around the loading area was 5 mm throughout the layers, gradually increasing to 500 mm at distances away from the applied load to ensure an efficient model (Adedeji & Hassan 2018; Tiliouine & Sandjak 2014) (Figure 6-2). Using the bias factor method for meshing in Abaqus, the number of elements along the length of the layer thickness is presented in Table 6-3.

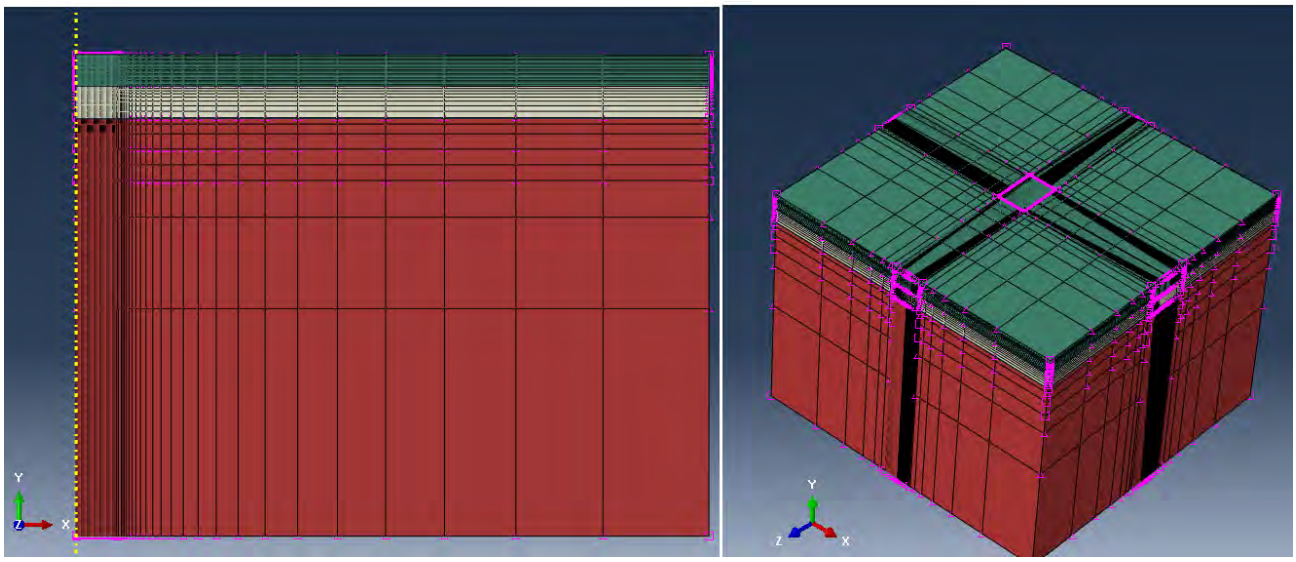

Figure 6-2 Pavement layer meshing configuration and bias factor meshing for 2D and 3D models.

In MePADS, flexible pavement is modelled as an axisymmetric structure subjected to a circular load with linear elastic materials (Sanchez 2021; Fabrice, Abejide, Adedeji & Mostafa 2020; Adedeji & Hassan 2018). Furthermore, MePADS was used as a control to determine the mesh configuration of the finite element model. This model in Abaqus was developed after conducting a mesh sensitivity analysis. When the entire model meshed with the same seeding as that of the tyre path, the results remained consistent. Overall, the results were similar to those obtained from other pavement multi-layered elastic design software, such as MePADS.

Table 6-3 Abaqus model mesh configuration analysis

Pavement Structures	***2D model***	***3D model***	***2D model***	***3D model***
	No. of Elements along the layer thickness	No. of Elements along the layer thickness	Total Number of Elements CAX4R	Total Number of Elements C3D8R
Gravel Base	41	12	4346	271272
Granular Subbase	8	7	848	158242
Subgrade	8	6	848	135636

6.3.2 Material Characterization

All the layers of the pavement are assumed to be linearly elastic in behaviour for simplicity, and the effects of material characterization on the FEM models are

determined. Additionally, two different material characterizations were used in the two-study area model: material characterization based on the obtained DCP test results and resilient modulus test results. The material characteristics of the gravel base, subgrade, and subgrade are closely related to those presented in (South African National Roads Agency Ltd 2013); these material characteristics are presented in Table 6-4.

Table 6-4 Material characterizations used in the models

Study Area	***Pavement Layer***	***Material code (TRH4, 1996)***	***Layer Thickness (mm)***	***Density (kg/m3)***	***Triaxial Resilient Modulus (MPa)***	***DCP Elastic Modulus (MPa)***	***Poisson's Ratio***
NCS5	Gravel	G4	150	1908	362	142	0.02
	Gravel	G5	150			141	
	Subgrade	G7	2000			155	
KZNS4	Gravel	G4	150	1870	185	362	0.12
	Gravel	G5	150			185	
	Subgrade	G7	2000			154	

6.3.3 Boundary Condition, Loading and Contact Modelling

In terms of boundary and loading conditions, the models were subjected to a static load in a linear perturbation analysis. The models were restrained in the horizontal direction (i.e., degrees of freedom 1 and 3), with the subgrade restrained in all directions. In the Abaqus axisymmetric model, the load contact area was assumed to have a radius of a circle (195 mm) with a wheel pressure of 0.67 MPa for simplicity (Fabrice, Abejide, Adedeji & Mostafa 2020; Adedeji & Hassan 2018; Rahman et al. 2011), as this study does not focus on pavement responses close to the surface. Additionally, tie constraints were assumed for the interaction between the interfaces of the layers, meaning that the layers were fully bonded with no friction for control purposes. In contrast, in MePADS, the load contact area was 119,355 mm² (285x419 mm) with a load of 80,000 N.

6.4 Modelling Results and Discussion

In this analysis, the structural importance of the granular base was evaluated by considering material characterization on the basis of the results of the DCP test and resilient modulus test. The decision to leave these pavements unsurfaced is justified

by the need to minimize the cost of low-volume roads while maximizing the strength and performance of the granular base in the design of LVRs. To assess the impact of the granular base, critical areas such as the compressive vertical strain and stress at the top of the subgrade were analysed as part of the pavement verification process.

6.4.1 Effect of Material Characterization on an Unsealled Surface Utilizing DCP Results and Triaxial Mr Results

Technically, the use of DCP test results should provide a better option for pavement design, as it shows a balanced structure of the pavement layers, especially for the KZNS5 result (Figure 6-3, Figure 6-4, and Figure 6-5) in terms of the stress, strain, and deflection developed in the pavement layers. However, this was not the case, as the triaxial elastic material performed better. It could be argued that the elastic modulus for the triaxial Mr model is greater than that of the DCP model. Nevertheless, the redistribution of stress and strain resulting from the input of the DCP elastic model needs to be better understood (Figure 6-6).

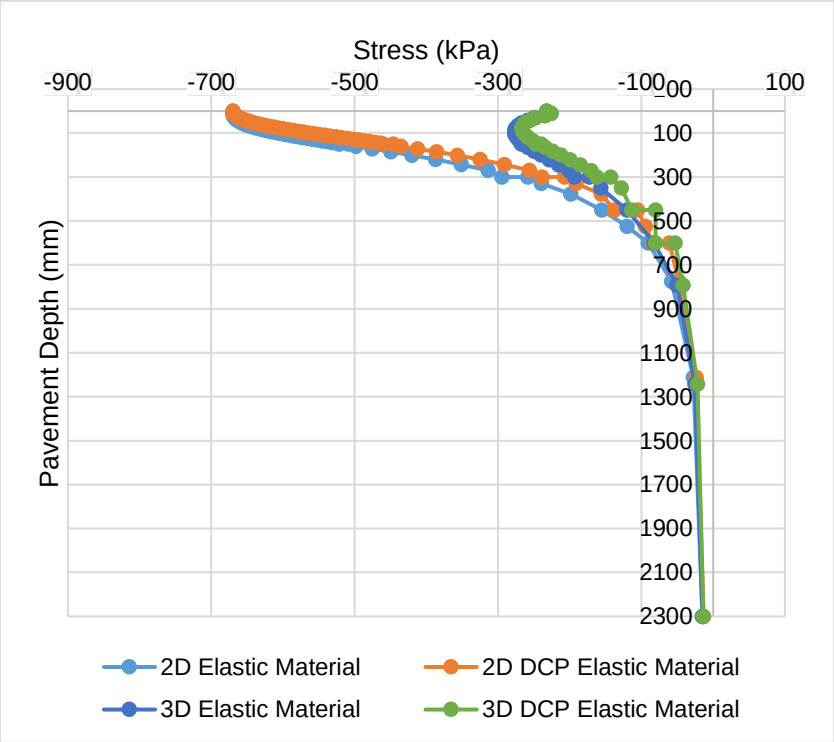

Figure 6-3 Comparative analysis of stress responses for 2D and 3D models via elastic and DCP elastic models (KZNS5)

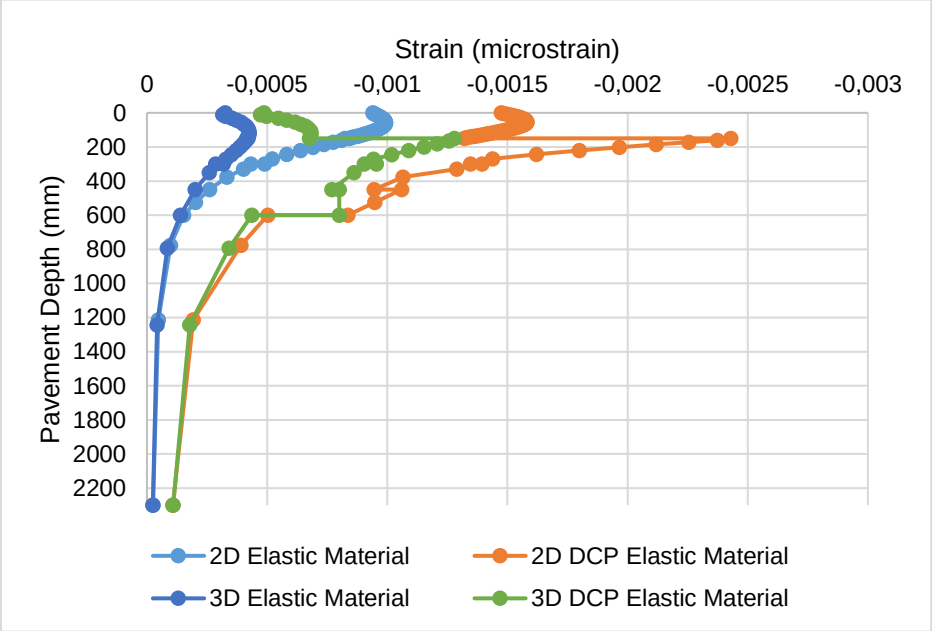

Figure 6-4 Comparative analysis of strain responses for 2D and 3D models via elastic and DCP elastic models (KZNS5)

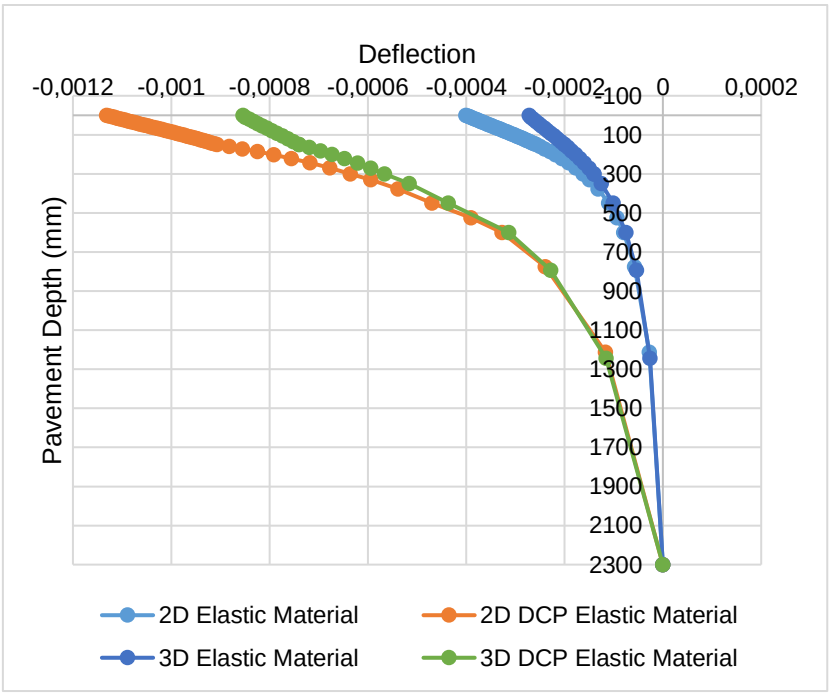

Figure 6-5 Comparative analysis of deflection responses for 2D and 3D models via elastic and DCP elastic models (KZNS5)

The analysis in this study revealed that the compressive vertical strain/stress at the top of the subgrade was drastically lower (from 1395×10^{-6} to 432.0×10^{-6}) in the elastic model (triaxial test results) than in the DCP elastic model (Figure 6-7) (supplementary results for NC are illustrated in Appendix C). Although the DCP elastic model showed a larger area affected by strain/stress, this reflects the effect of changes in layer properties, which more accurately depicts the pavement layer structure in real-life scenarios. This subsequently affects the structural capacity of the subgrade layer (DCP elastic model: 8.29×10^{3}, and elastic model: 1.57×10^{6} ESALs).

Overall, when designing low-volume roads, the DCP elastic model needs to be considered, as it provides a closer depiction of real-life pavement structures. However, a proper correlation between the DCP elastic model and the elastic (triaxial resilient modulus) model needs to be established. According to Ikechukwu et al. (2019), Pezo, Nazarian & Picornell (1996) and Daleiden, Killingsworth, Simpson & Zamora, (1994), there is a close correlation between the in situ DCP and triaxial test results in terms of material characterization. Therefore, the use of a single elastic modulus for pavement layer design tends to lead to overdesign of the pavement structure.

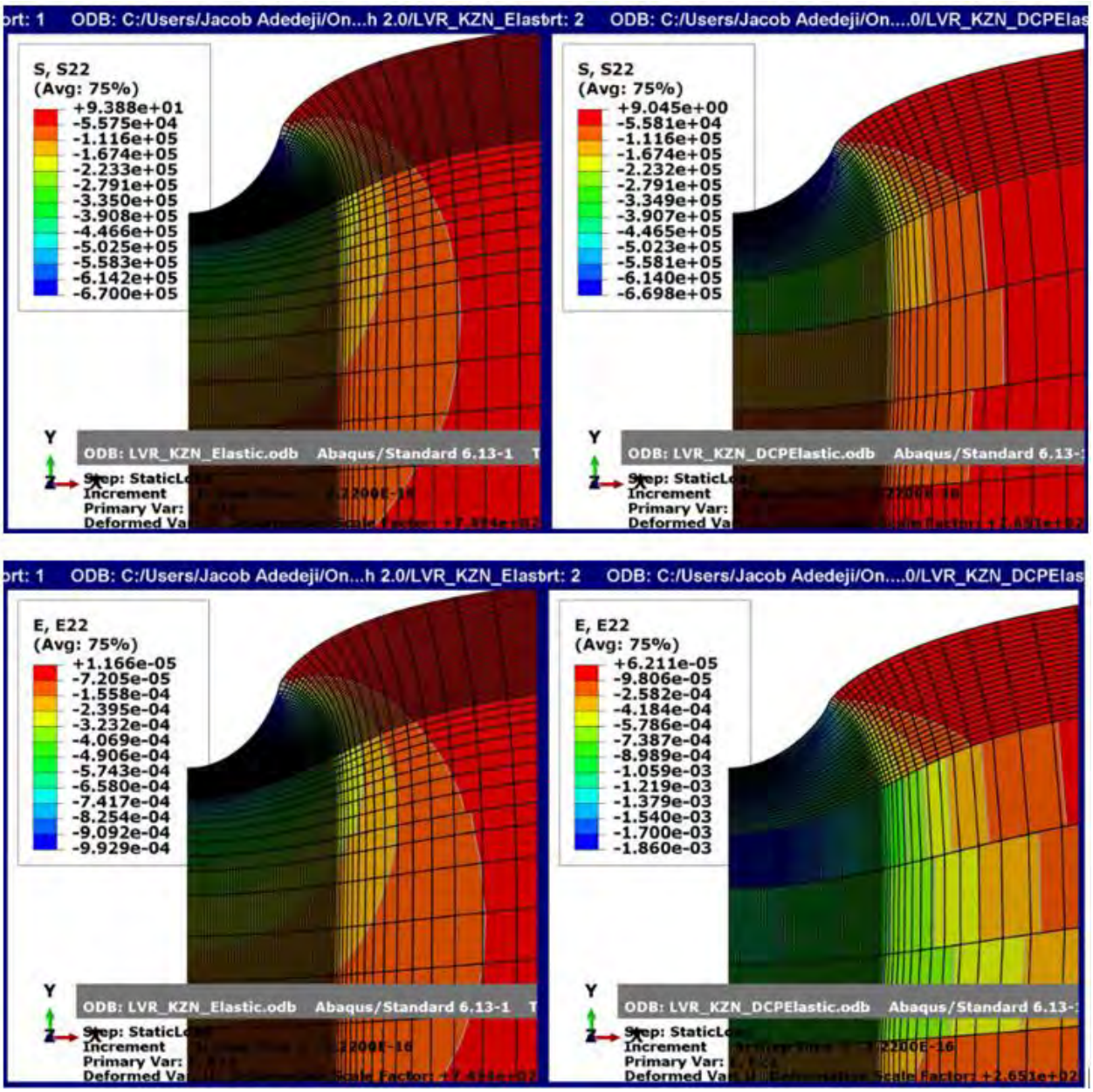

Figure 6-6 Pavement stress and strain responses for the 2D model using elastic and DCP elastic models (KZNS5)

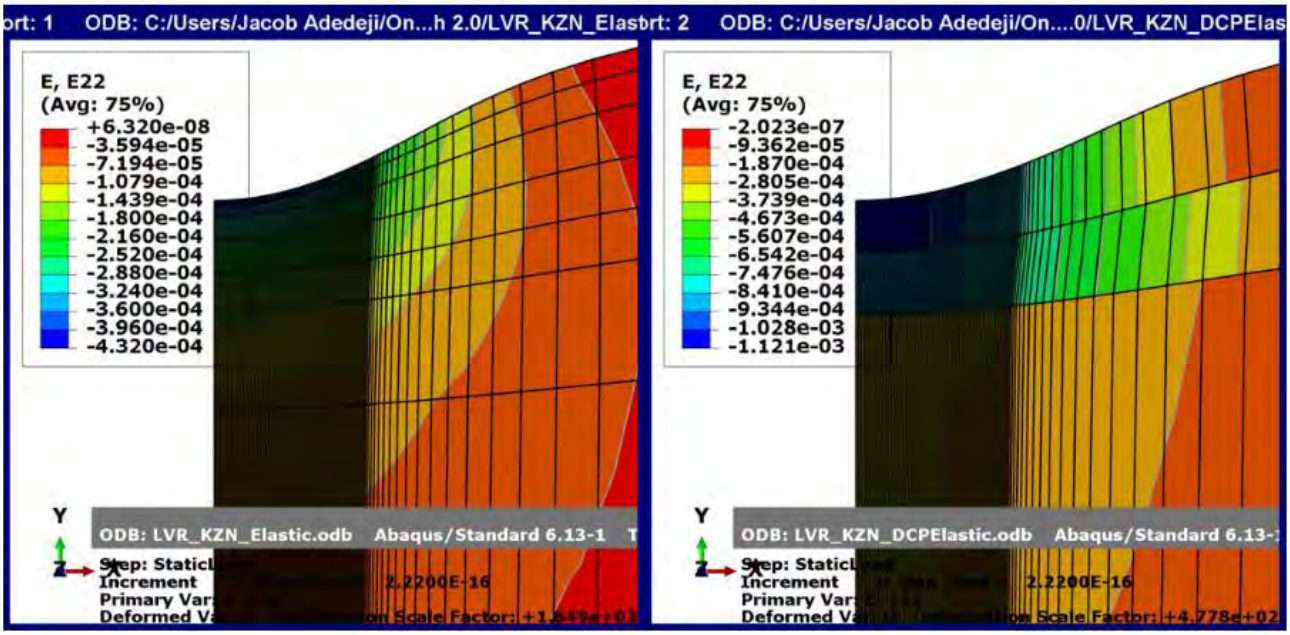

Figure 6-7 Vertical strains on top of the subgrade for the 2D model using the elastic and DCP elastic models (KZNS5)

6.4.2 Comparative Analysis of 2D and 3D models in the FEM

Using Equation 3-22, the pavement life spans were calculated for the rutting criterion, as shown in Table 6-5. Table 6-5 compares the predicted number of load repetitions to failure (Nr) for unsealed low-volume roads (LVRs) via elastic and DCP elastic models in 2D and 3D FEM simulations in two study areas, NCS4 and KZNS5. For both the elastic and DCP elastic models, the 3D models consistently predict higher load repetitions to failure than the 2D models.

Equation 6-1

$$N_r = 1.365x10^{-9}(E_c)^{-4.477}$$

The 3D prediction for KZNS5 in the elastic model is 2.13 × 10⁶ load repetitions, whereas that predicted by the 2D model is 1.58 × 10⁶. For the DCP elastic model, this difference is a 3D prediction of 11.46 × 10³ against 8.29 × 10³ in the 2D model for KZNS5. This implies that 3D models provide a fuller representation of the stress distribution and, thus, a more accurate life estimation for pavements. The significant differences between the elastic and DCP elastic models demonstrate one important point: the importance of material characterization. Although the elastic model of the same modulus may over-predict the life of a pavement, the DCP elastic model, which

allows for different material properties, performs better and provides realistic predictions, especially for unsealed LVRs. Overall, it is also worth noting that, on the basis of the design and use of the asphalt institute model of pavement distress prediction, NCS4 did not meet the desired pavement loading life of 1.488×10^6, as stipulated in the desire criteria (Table 6-1), and most likely met the need to include the surface seal, as suggested by the TRH4 design method (Table 6-2). For this reason, there is a need to carefully select the model for pavement design to ensure an accurate prediction of the performance of the pavement.

Table 6-5 Rutting failure analysis for unsealing LVRs via elastic and DCP elastic models

Model	Fatigue Criterion No. of Load Repetitions to Failure N_r			
	NCS4 2D	NCS4 3D	KZNS5 2D	KZNS5 3D
Elastic	211.80×10^3	288.10×10^3	1.58×10^6	2.13×10^6
DCP Elastic	3.02×10^3	4.05×10^3	8.29×10^3	11.46×10^3

6.4.3 Validation of the FEM

Validation of the FEM was conducted to compare its results (in terms of stress and strain) with those obtained from linear elastic theory (Tsige et al. 2022; Gupta 2017). The validation analysis was performed for Study Area 1 (NCS4) and Study Area 2 (KZNS5) using a granular base and subbase layer of 150 mm each and a subgrade of 2000 mm. Linear elastic properties were applied to all the layers. MePADS, a linear elastic layered analysis program, was employed to validate the FEM results.

Additionally, an axisymmetric model in Abaqus was developed, and the results closely matched those obtained from the layered elastic software. The design model details used in MePADS are highlighted above. The 2D Abaqus model displayed great similarity to those of MePADS (Table 6-6). However, the results of the 3D FEM model revealed a 12% difference in vertical strain on the subgrade compared with those of the other methods, with fewer discrepancies in the other layers, despite the use of a similar mesh configuration. This suggests that while the FEM provides reliable results,

some variations can occur depending on the modelling approach and complexity, emphasizing the need for careful calibration and validation in different contexts.

Table 6-6 Strain Values for Pavement Layers in MePADS, 2D Abaqus and 3D Abaqus Model

Study Area	MePADS	2D Abaqus Model	3D Abaqus Model	Percentage Difference (%) btw MePADS &2D/3DAbaqus
	Vertical Strain Ɛc (10^{-6}) in Subgrade	Vertical Strain Ɛc (10^{-6}) in Subgrade	Vertical Strain Ɛc (10^{-6}) in Subgrade	
NCS4				
Elastic	699	676.5	631.6	3.27/10.13
DCP Elastic	1793	1748	1637	2.54/9.1
KZNS5				
Elastic	453	432	403.7	4.75/11.5
DCP Elastic	1426	1395	1298	2.2/9.4

6.4.4 Modelling Analysis Conclusion

It is from these analyses and findings, therefore, that the comparative evaluation of 2D and 3D FEM modelling of unsealed LVRs would shed some important light on pavement performance and design. The outputs of these NCS4 and KZNS5 study areas with analyses of the granular base and subbase layers revealed large differences in the estimated pavement life through 2D and 3D models, specifically the elastic and DCP elastic models. For all the conditions, there was an increase in the number of load repetitions to failure estimated by the 3D models, which better captures the stress distribution within the pavement structure.

Further evidence of the reliability of these models was their verification against linear elastic theory via MePADS software. However, variation was noted in the 3D FEM results by approximately 12% for the vertical strain on the subgrade. These results underscore the sensitivity of the selection and calibration of pavement models and demonstrate the importance of proper material characterization (Adedeji, 2019). Even if the DCP elastic model yields fewer predicted load repetitions, it is closer to reality and should be considered when designing unsealed LVRs.

Overall, the results clearly identify the importance of advanced modelling techniques, such as the 3D FEM, for improved accuracy in pavement life prediction, especially for

unsealed roads with complex structures. These accurate models may lead to more sustainable and cost-effective pavement designs, particularly for low-volume roads.

6.5 Chapter Summary

This chapter presented a comparative analysis of empirical and mechanistic-empirical pavement design methods for LVRs. Empirical methods such as the CBR, AASHTO 1993, TRH 20, and Odemark approaches were compared with mechanistic models, namely MePADS and 2D/3D FEM simulations, using site-specific datasets. Before performance predictions were undertaken, the FEM models were validated against layered elastic theory in MePADS (Table 6.6), showing close agreement in subgrade strain values (within ~12%). This validation confirmed the reliability of the FEM models and ensured that subsequent comparisons were grounded in robust modelling outputs.

The comparative results revealed differences in design outcomes across methods. For example, TRH 20 uniquely incorporated a gravel wearing course with a thin double surface seal (Table 6.2), while the other empirical methods assumed unsealed granular structures. The FEM analyses further demonstrated that 3D modelling consistently predicted higher pavement lives than 2D models (Table 6.5), reflecting the ability of 3D simulations to capture stress distributions more accurately. When DCP-derived elastic moduli were used, the models provided a more realistic representation of in-situ variability but yielded conservative life estimates (on the order of 10^3 repetitions in wet conditions), aligning with the frequent maintenance observed on unsealed LVRs.

Overall, the findings highlight the need to carefully select and calibrate pavement design methods for LVRs. The results show that while DCP-based models capture realistic field conditions, they may predict premature failure unless supported by surface seals, as suggested by TRH 20. Conversely, uniform modulus designs risk overestimating pavement life. By validating FEM models and systematically comparing outputs across methods, this chapter directly addresses the research aim of evaluating existing LVR design approaches, including DCP-based techniques, and

demonstrates the importance of method selection for cost-effective and sustainable road design.

Chapter 7 : Finite Element Modelling Results

7.1 Introduction

Chapter Seven builds on the evaluations in Chapter Six by developing a finite element model (FEM) for predicting the deformation of low-volume roads (LVRs) and comparing its outputs with conventional design approaches. The FEM simulations were undertaken using both linear elastic and nonlinear constitutive models (Drucker–Prager and Mohr–Coulomb) to capture the behaviour of granular and subgrade layers under loading. This chapter also uses the Asphalt Institute rutting model to estimate the number of load repetitions to failure (Nr) based on subgrade vertical strains, which are then compared with predictions from mechanistic-empirical tools such as MePADS. By linking the FEM analysis to conventional methods already discussed, the chapter provides continuity and enables a direct comparison between advanced modelling outputs and traditional design outcomes.

7.2 Validation of In-Situ Material Characterization through Modelling Triaxial Test Samples

7.2.1 Geometry of the Triaxial Model

In the FEM of a triaxial test via Abaqus, the geometry of the model is designed to simulate a cylindrical soil sample. The consolidated drained triaxial tests were modelled in 3D using a cylindrical sample 300 mm in height and 150 mm in diameter, representing the entire soil sample (Chao, Jommi & Muraro 2023; Tsige et al. 2022; Xiangjing & Jianqing 2010). The commercial finite element program Abaqus®/CAE 6.13 (Abaqus 2013) was used to simulate the experimental response of the samples. The sample is meshed with hexahedral or tetrahedral elements C3D20RP (20-node reduced integration brick element). The boundary conditions replicate the confinement pressure and axial loading, with one end of the cylinder fixed and the opposite end subjected to loading (Figure 7-1).

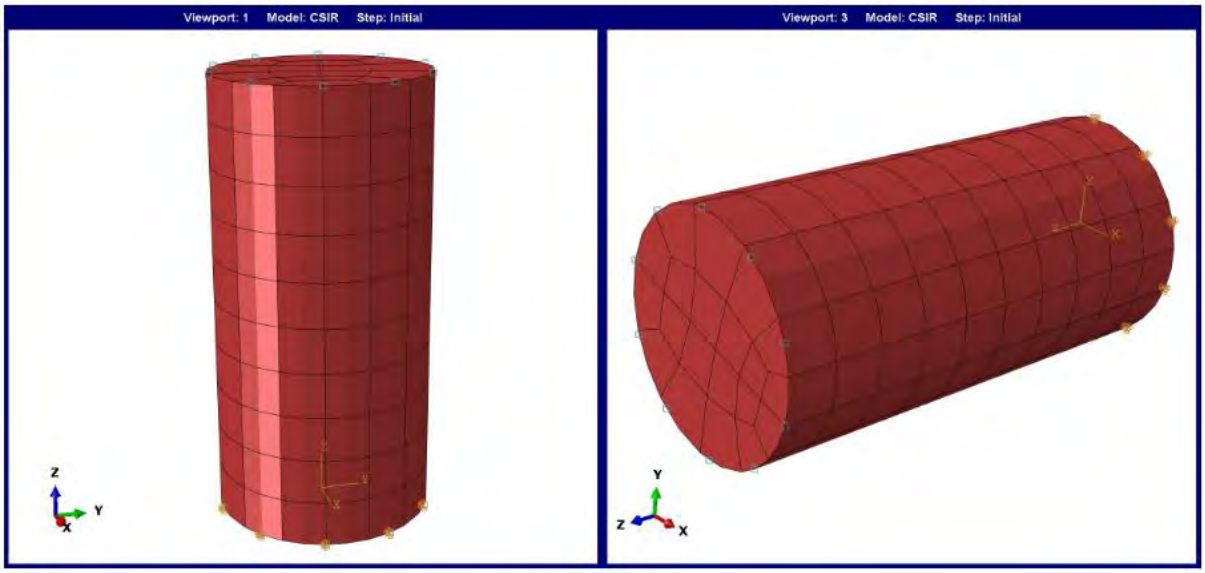

Figure 7-1 Repeated load triaxial test model

7.2.2 Materials Inputs for the Triaxial Model

The soil samples used in the triaxial tests were modelled via three soil constitutive models: elastic, Drucker–Prager (DP), and Mohr-Coulomb (MC) models (Onyelowe et al. 2023; Notash et al. 2022; Abbas et al. 2019; Song, Wang & Bate 2018). The experimental parameters, along with the soil properties obtained from the literature, were carefully adjusted and incorporated into the numerical simulations. Importantly, nonlinear models such as DP and MC require numerous input parameters, which are often not readily available, as highlighted by Sargand, Khoury, Gray & Al-Jhayyish (2014), except where experimental data from triaxial tests are available.

The DP model characterizes soil behaviour via six key input parameters: Young's modulus (E), Poisson's ratio (v), angle of friction (φ), stress ratio (M), dilation angle (ψ), and shear stress. On the other hand, the MC model, which is considered a perfect elastoplastic model, provides a first-order approximation of the non-linear behaviour of the soil. This model is particularly suitable for simulating the behaviour of fine or granular soils. To approximate soil behaviour via the MC model, five input parameters are essential: E, v, φ, cohesion (c), and ψ. The input parameters for these models are summarized in Table 7-1.

Table 7-1 Materials characterization for the triaxial model obtained from laboratory triaxial test results

Elastic model					
General	**KZNS**	**NCS**	**Elastic**	**KZNS**	**NCS**
Density_ρ (kg/m3)	1886	1938	Young's Modulus_E (MPa)	609	384
constant permeability_k (m/sec)	0.0984	0.0984	Poisson's Ratio_ v	0.12	0.02
Specific weight of wetting liquid_γw (kN/m3)	9.81	9.81			
Void Ratio_e0	0.45	0.45			
DP model					
General	**KZNS**	**NCS**	**Plasticity**	**KZNS**	**NCS**
Density_ρ (kg/m3)	1886	1938	Angle of Friction	64,5	57.74
constant permeability_k (m/sec)	0.0984	0.0984	Stress ratio, M	1	1
Specific weight of wetting liquid_γw (kN/m3)	9.81	9.81	Dilation Angle	34,5	27.74
Void Ratio_e0	0.45	0.45			
Elastic			DP Hardening Shear		
Young's Modulus_E (MPa)	609	384	Yield Stress	1E-005	1E-005
Poisson's Ratio_ v	0.12	0.02	Abs Plastic Strain	0	0
MC model					
General	**KZNS**	**NCS**	**Plasticity**	**KZNS**	**NCS**
Density_ρ (kg/m3)	1886	1938	Angle of Friction_ φ	51	38.8
constant permeability_k (m/sec)	0.0984	0.0984	Dilation Angle_ ψ	21	8.8
Specific weight of wetting liquid_γw (kN/m3)	9.81	9.81			
Void Ratio_e0	0.45	0.45			
Elastic			MC Plasticity_Cohesion		
Young's Modulus_E (MPa)	609	384	Yield Stress	5200	135500
Poisson's Ratio_ v	0.12	0.02	Abs Plastic Strain	0	0

7.2.3 Boundary Condition and Analysis Step

In the FEM of a standard consolidated-drained triaxial test, boundary conditions are crucial for accurately replicating the physical test environment (Chao et al., 2023; Xiangjing & Jianqing, 2010). The cylindrical soil sample is subjected to specific boundary conditions to simulate the stress state and loading conditions. The initial stress and pore pressure conditions are specified via the 'geostatic' option in Abaqus, ensuring the initial equilibrium state with negligible displacements during the geostatic step.

A surface-distributed pressure of 210 kPa is applied to the lateral surfaces to replicate the isotropic confining pressure typical in triaxial tests. The bottom surface of the sample is fixed in all directions, simulating the rigid platen of the testing apparatus, whereas the top surface is subjected to controlled vertical displacement, representing the axial load applied during the test. The axial load is introduced as displacement-controlled loading on the top surface, corresponding to a strain rate of 0.2% axial strain per minute.

Drainage conditions are imposed to model the dissipation of pore water pressure, which is characteristic of a consolidated-drained test (Xiangjing & Jianqing 2010). Free drainage is allowed through the top and bottom surfaces by setting the pore pressure degree of freedom (DOF) to zero, while the lateral surfaces are treated as impermeable, preventing any lateral flow. These boundary conditions ensure that the model accurately simulates the triaxial test, providing reliable predictions of soil behaviour under applied loads.

7.2.4 Results of the FEM Simulation Triaxial Test

This analysis compares two triaxial experimental samples, KZNS and NCS, with the experimental results reported in section 5.2.3 via three different material characterization models. The simulation was performed via three different material characterization models: the elastic, DP, and MC constitutive models. In Figure 7-2, the simulation results are displayed as deviatoric stress *versus* axial strain. The experimental triaxial data for the KZNS and NCS samples is also presented in the figure.

The comparison in Figure 7-2 indicates that the DP and MC model predictions are in good agreement with the experimental data for both the KZNS and NCS samples, particularly their stress-strain responses. Importantly, the FEM simulations had a small increase in the failure deviator stress, presumably because the FEM has the ability to continue analysing past the experimental failure point. In this post-peak stage, the axial strain continues to increase even when the deviatoric stress remains constant, because the soil has yielded and entered a plastic deformation regime. In this state, additional strain accumulates at nearly constant stress, reflecting plastic flow

behaviour and the approach to a critical state condition, where further shearing does not mobilise additional strength. This explains why the stress–strain curves plateau while strain growth persists in both the experimental and simulated responses. An example of this type of loading path, an incremental increase in deviator stress, is not modelled explicitly in this work because attention has been given to evaluating various material characterization models to consider the non-linearity of the granular layer in LVRs.

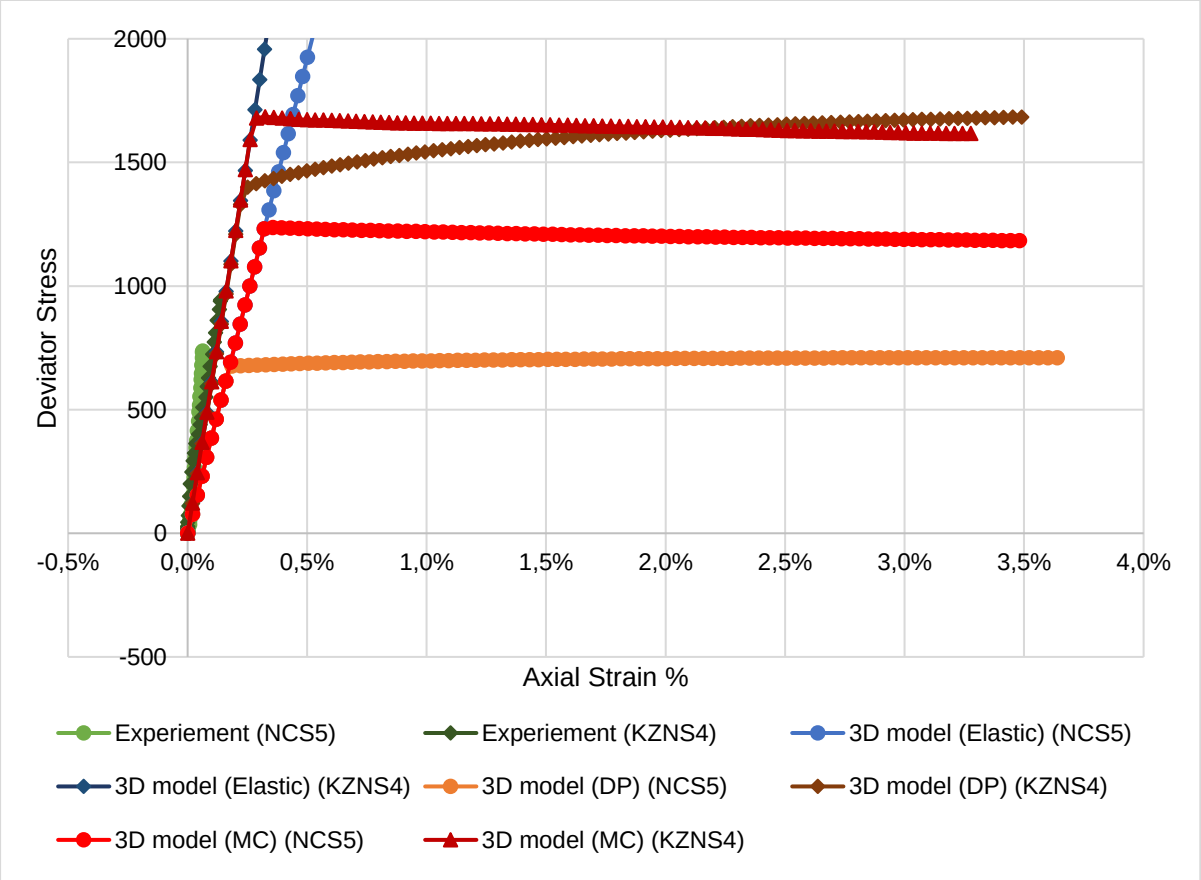

Figure 7-2 Deviatoric stress and axial strain at a confining pressure of 210 kPa for different materials (NCS5 and KZNS4 samples)

With respect to axial strain *versus* volumetric strain (Figure 7-3), the FEM models exhibit typical behaviour that is consistent with the triaxial test results. The DP and MC models, in particular, better fit the experimental data, effectively capturing the non-linear behaviour of the granular materials used in the base layers. This emphasizes that relying on a purely elastic model for predicting real-life performance can be highly

misleading. The DP and MC models provide more reliable simulations of granular material behaviour in complex LVR applications.

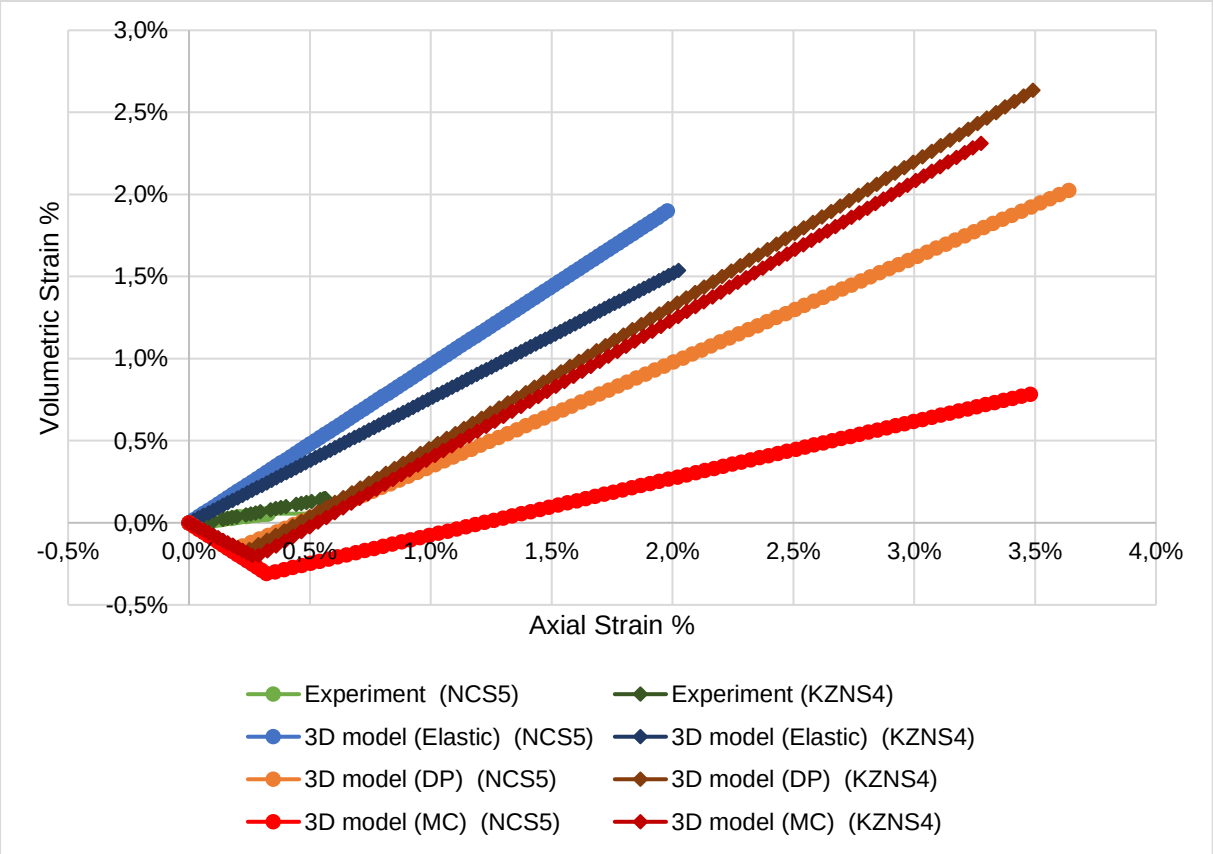

Figure 7-3 Volumetric strain and axial strain at a confining pressure of 210 Kpa for different materials (NCS5 and KZNS4 samples)

Furthermore, Figure 7-4 presents the laboratory sample (NCS4), and Figure 7-5 shows the von Mises stress distribution in the 3D FEM model. Notably, the shear at the edges of the laboratory test is reflected in the maximum von Mises stress in the FEM model, demonstrating a strong correlation between the FEM simulations and experimental results. Additionally, Figure 7-6 and Figure 7-7 illustrate the radial strain and vertical deformation of the sample. Importantly, the elastic model did not exhibit any bulking, which is indicative of non-linear material behaviour, further highlighting the limitations of using an elastic model for such simulations. This observation is consistent with the findings of Islam et al. (2019), where elasto-viscoplastic finite-element models calibrated against triaxial test data were able to reproduce bulging and post-yield deformation characteristics, while purely elastic models could not. Similarly, Hernández-Hernández et al. (2021) found that a hardening soil model better

matched experimental triaxial results at higher moisture contents compared to a simpler MC model, illustrating that non-linear models are necessary to capture actual soil response.

Figure 7-4 Laboratory triaxial test samples before (A) and after (B) testing (NCS5 sample)

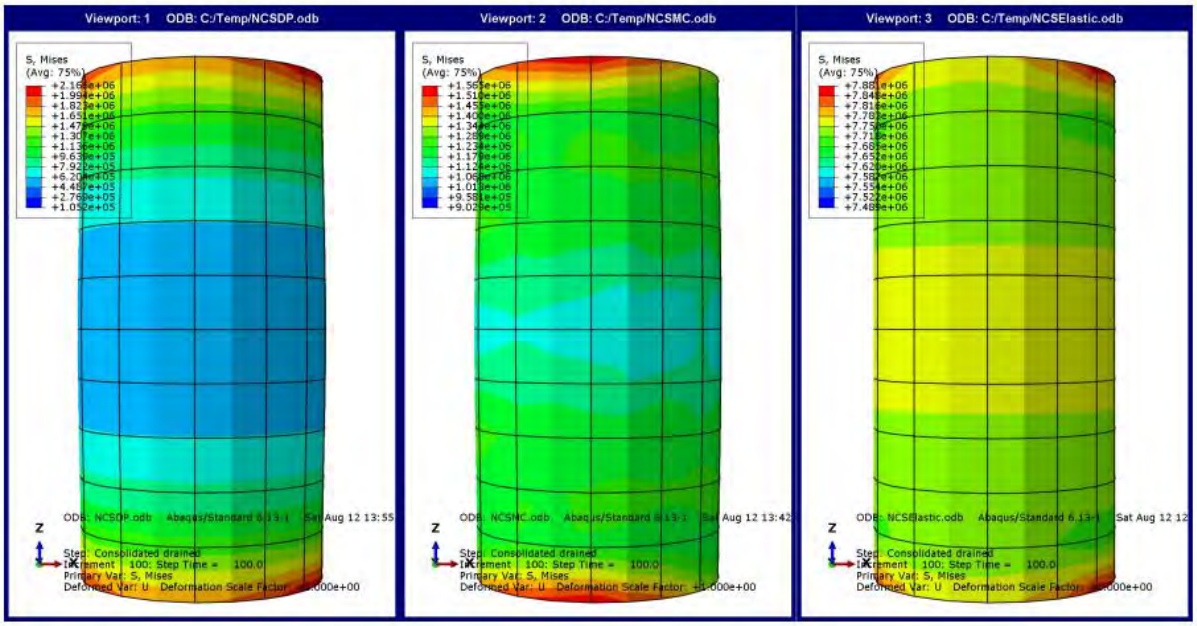

Figure 7-5 von Mises stress for the FEM repeated load triaxial test samples after testing with different material characterizations: (a) Drucker–Prager, (b) Mohr-Coulomb, and (c) elastic (NCS5 samples)

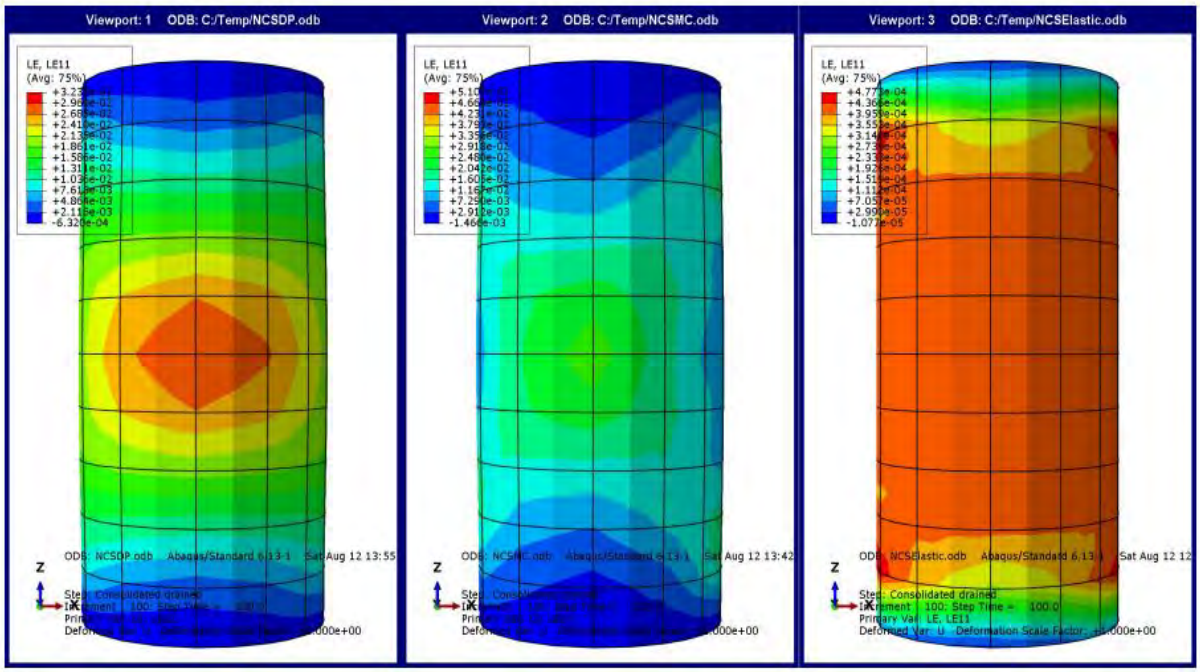

Figure 7-6 Radial strain for FEM repeated load triaxial test samples after testing with different material characterizations: (a) Drucker–Prager, (b) Mohr-Coulomb, and (c) elastic (NCS5 sample)

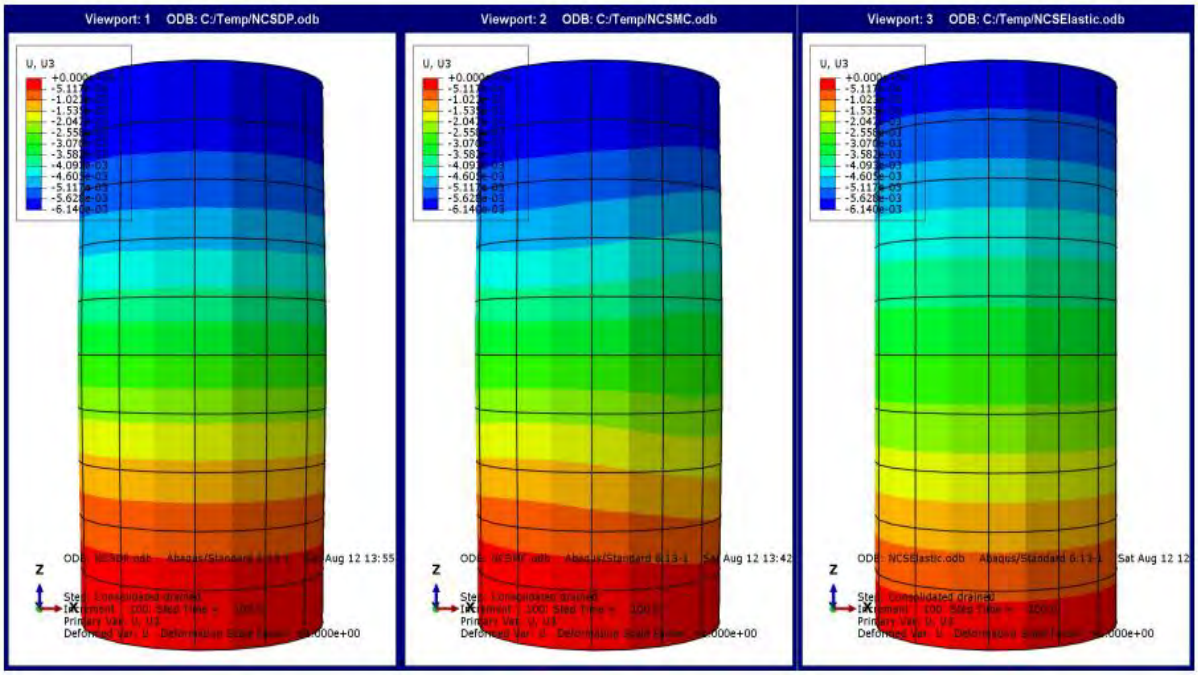

Figure 7-7 Vertical deformations for FEM repeated load triaxial test samples after testing with different material characterizations: (a) Drucker–Prager, (b) Mohr-Coulomb, and (c) elastic (NCS5 sample)

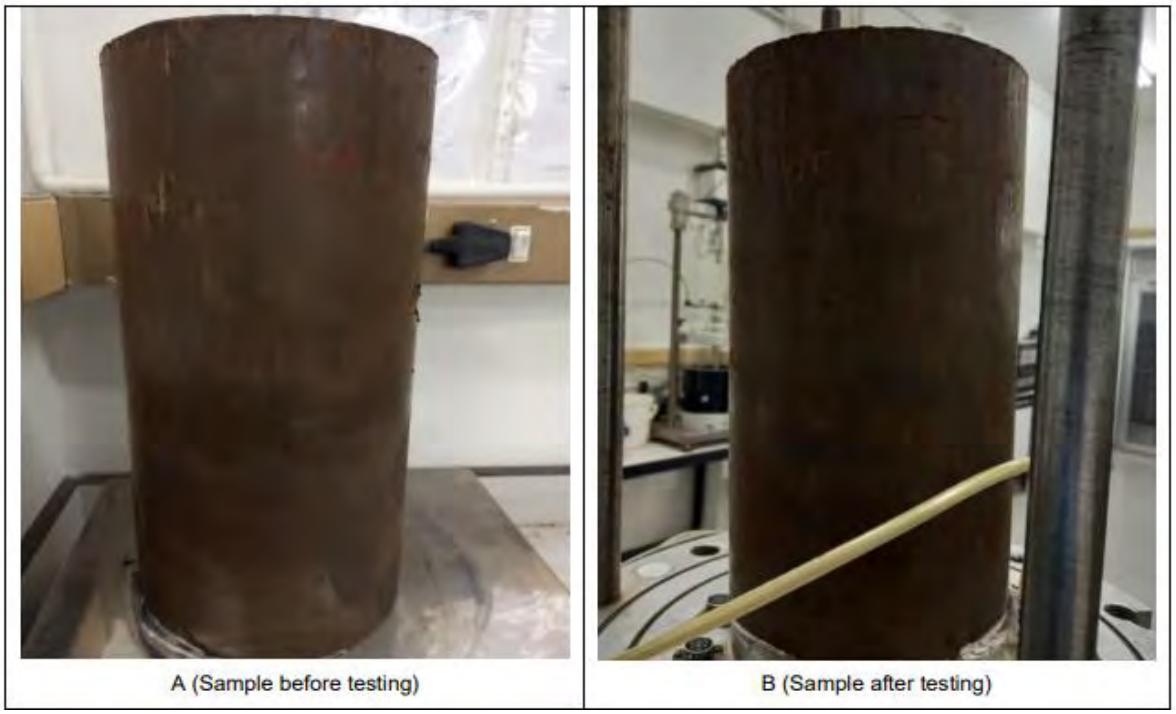

Figure 7-8 Laboratory triaxial test samples before (A) and after (B) testing (KZNS4 sample)

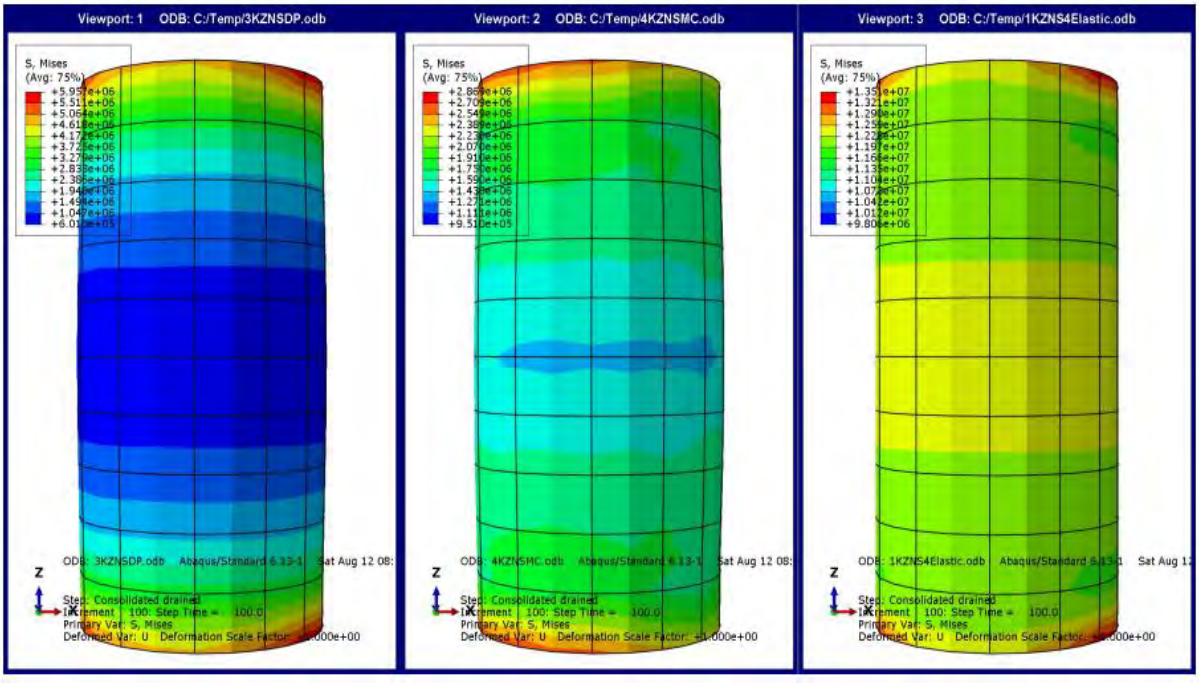

Figure 7-9 von Mises stress for the FEM repeated load triaxial test samples after testing with different material characterizations: (a) Drucker–Prager, (b) Mohr-Coulomb, and (c) elastic (KZNS4 samples)

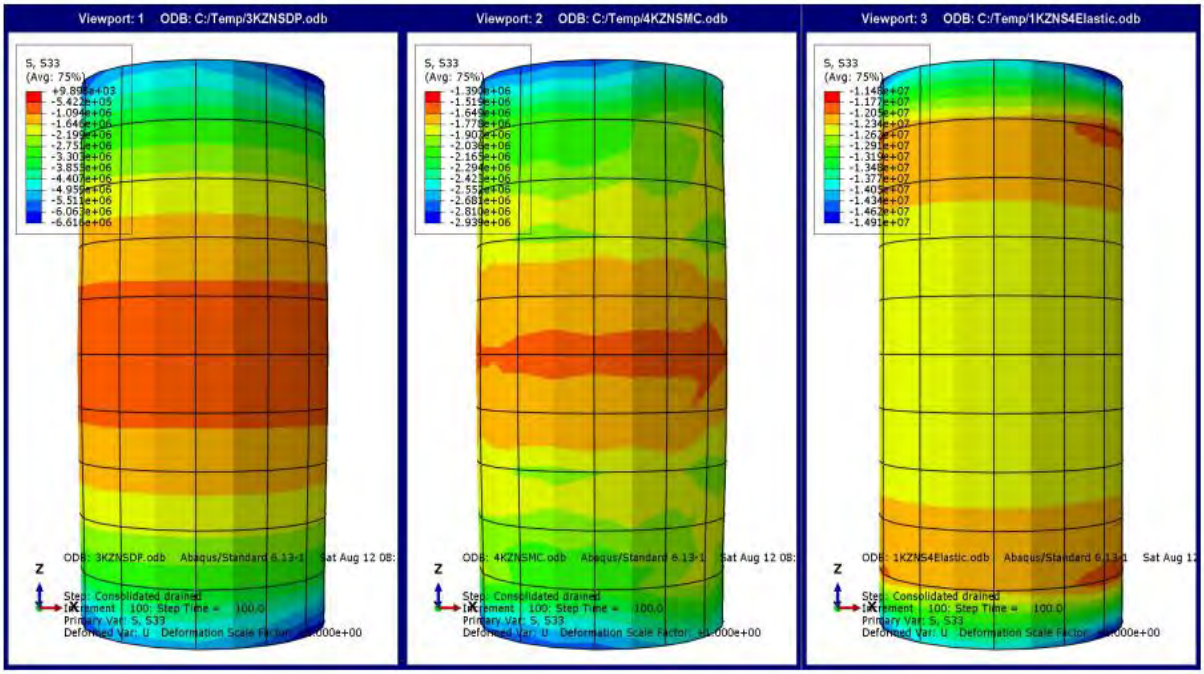

Figure 7-10 Vertical stress for FEM repeated load triaxial test samples after testing with different material characterizations: (a) Drucker–Prager, (b) Mohr-Coulomb, and (c) elastic (KZNS4 sample)

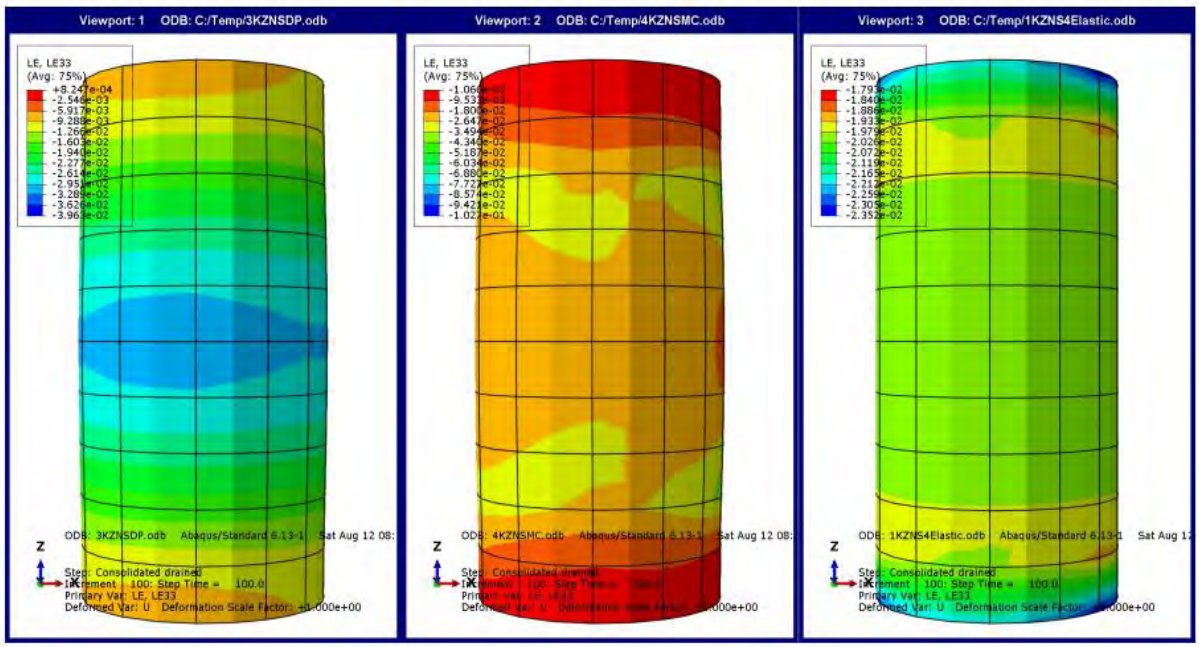

Figure 7-11 Axial strain for FEM repeated load triaxial test samples after testing with different material characterizations: (a) Drucker–Prager, (b) Mohr-Coulomb, and (c) elastic (KZNS4 sample)

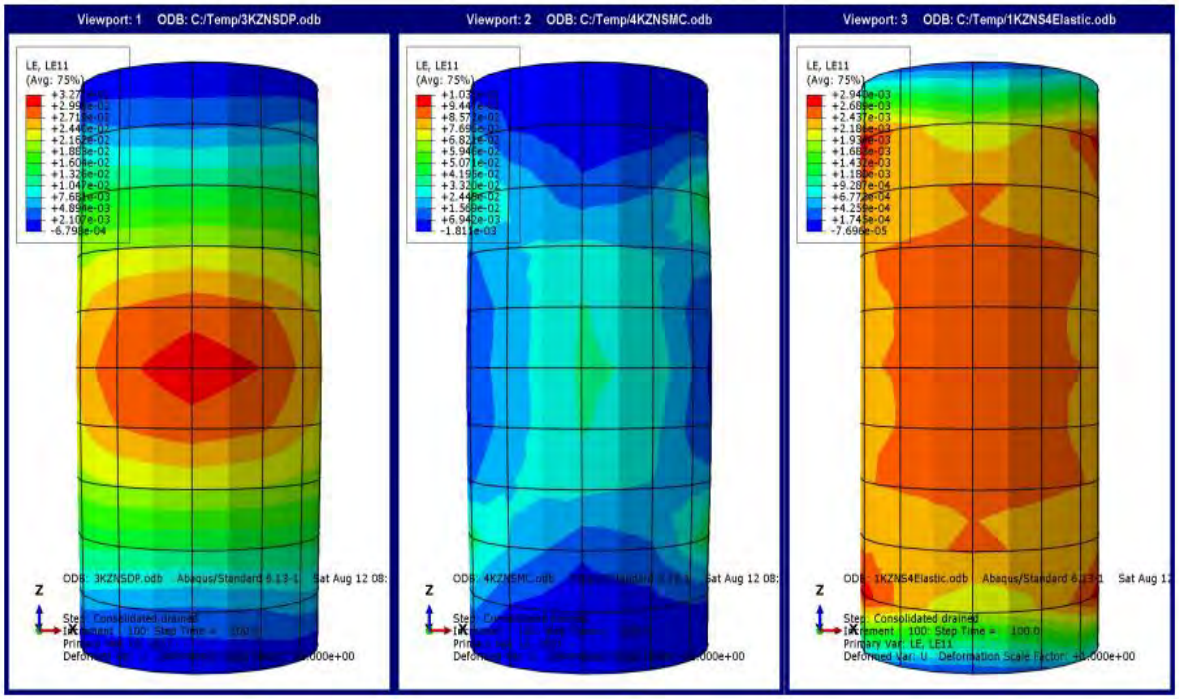

Figure 7-12 Radial strain for FEM repeated load triaxial test samples after testing with different material characterizations: (a) Drucker–Prager, (b) Mohr-Coulomb, and (c) elastic (KZNS4 sample)

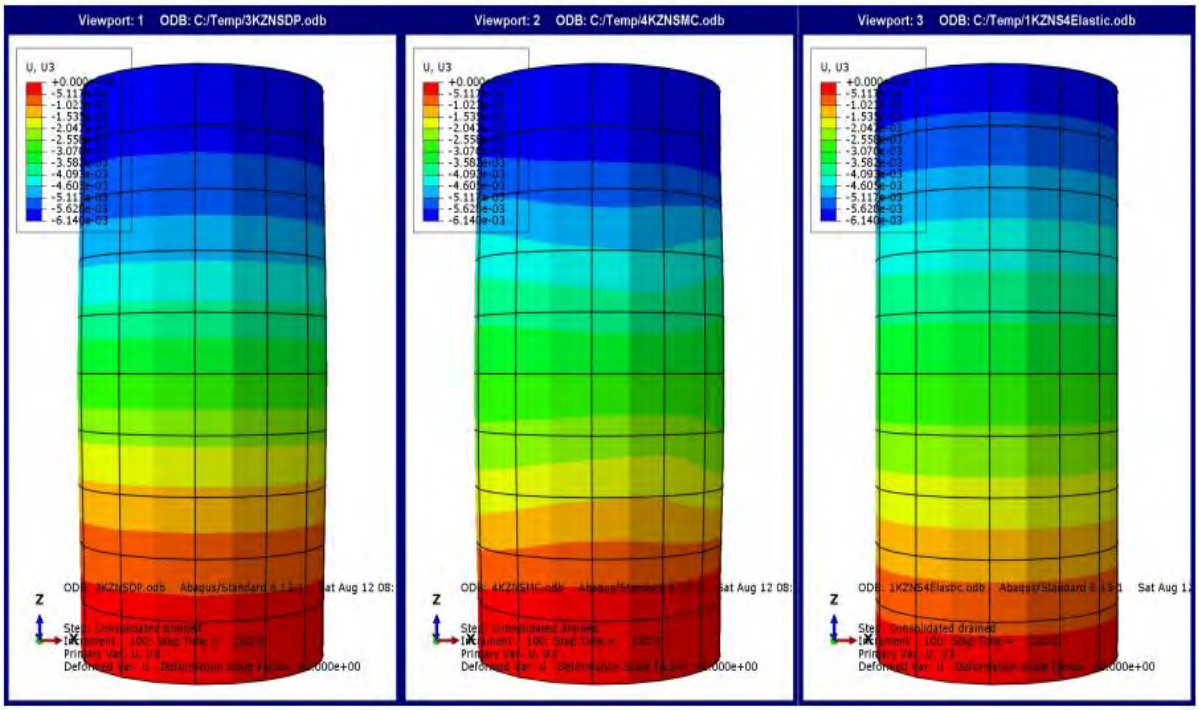

Figure 7-13 Vertical deformations for FEM repeated load triaxial test samples after testing with different material characterizations: (a) Drucker–Prager, (b) Mohr-Coulomb, and (c) elastic (KZNS4 sample)

7.3 2D and 3D Modelling of LVR with Non-Linear Material Characterization for Pavement Layers

Building on the details of the FEM models presented in Section 6.3.1, which covered the model geometry, element types, and mesh size, and Section 6.3.3, which covered boundary conditions, loading, and contact modelling, this section extends the analysis by including nonlinear material characterization, as described in Section 7.2.2. LVRs with a three-layer structure were modelled to evaluate the effects of nonlinear material characterization on the behaviour of the pavement layers. The use of nonlinear material models, particularly the DP and MC models, allows for a more accurate simulation of the complex behaviour of the granular material and subgrade under different loading conditions, providing details on the performance and durability of LVR pavements.

7.3.1 FEM Simulation Results of LVRs

The modelling results, presented in Figure 7-14 to Figure 7-17, display the stress and strain in the subgrade layer for NCS4 and KZNS5. The results generally follow the typical pattern of stress and strain distributions in pavement structures. A notable difference was observed between the 2D and 3D models, with the 2D model showing more stress concentrated near the pavement surface layer (Figure 7-14 and Figure 7-16).

In terms of strain, the pattern differed from that of stress, with three distinct results emerging in the group of 2D and 3D models (elastic, MC, and DP) as well as the DCP elastic model (2D and 3D) (Figure 7-15 and Figure 7-17). These findings indicate that both material characterization and the model geometry, whether 2D or 3D, significantly affect the results generated for LVRs.

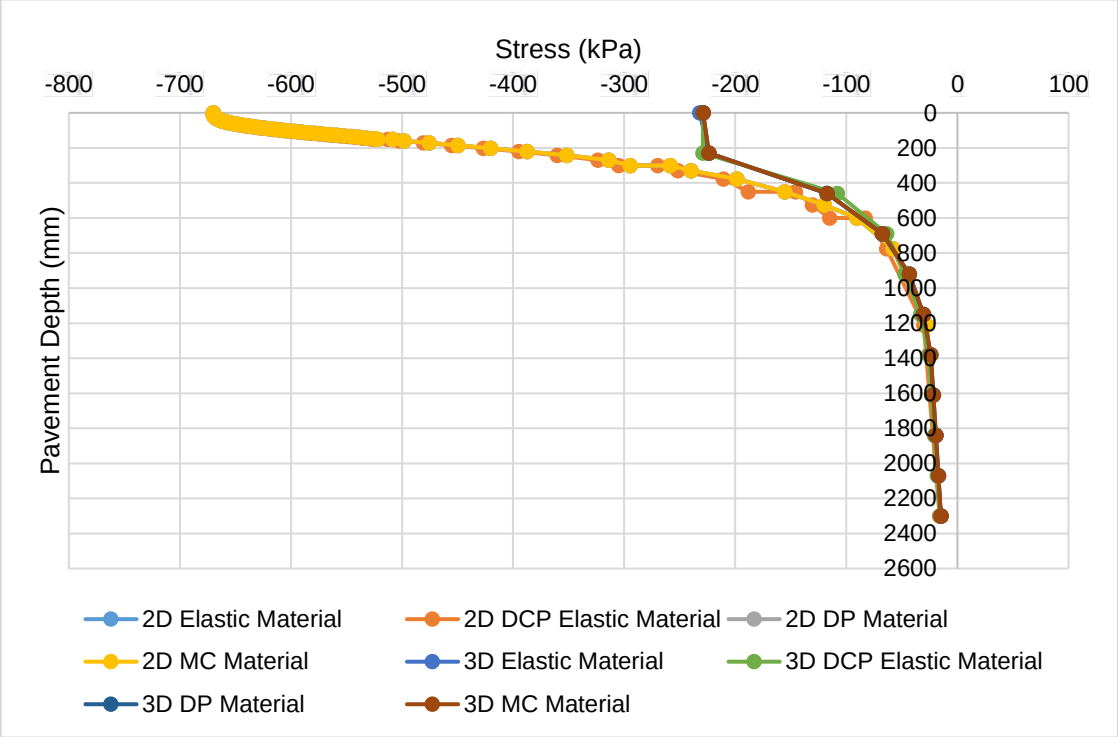

Figure 7-14 Comparative analysis of stress responses for 2D and 3D models using various material models (NCS4)

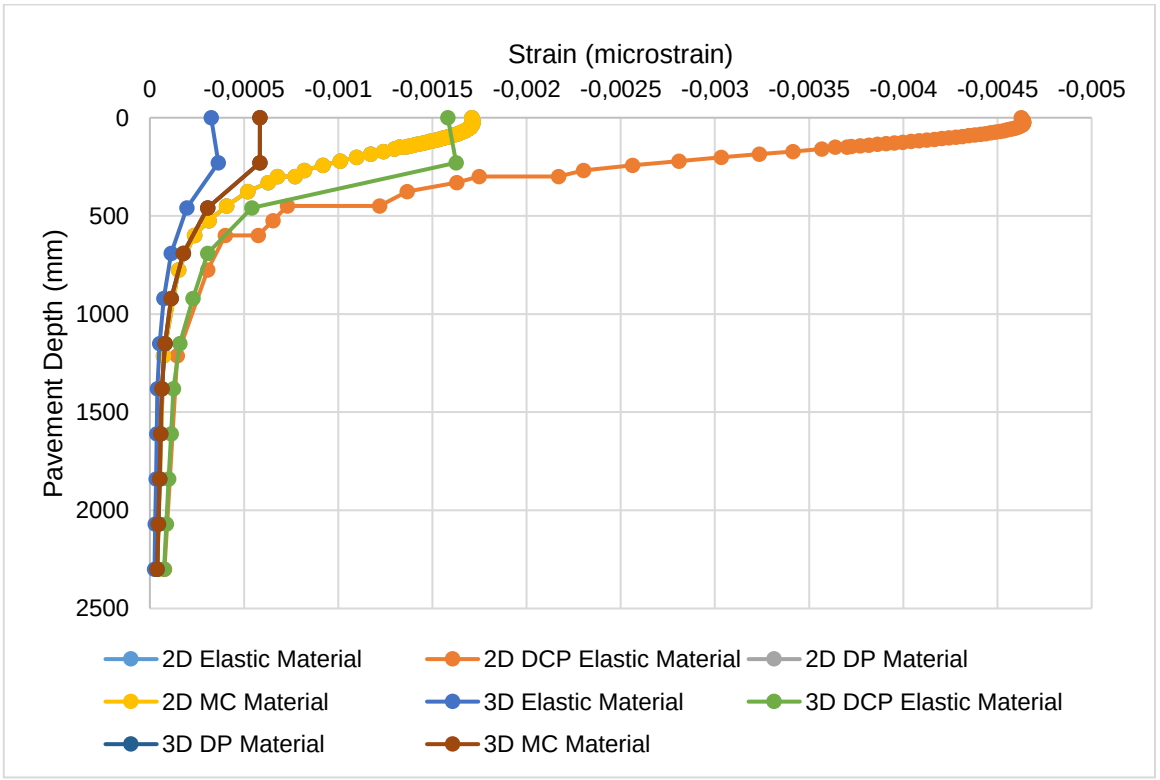

Figure 7-15 Comparative analysis of strain responses for 2D and 3D models using various material models (NCS4)

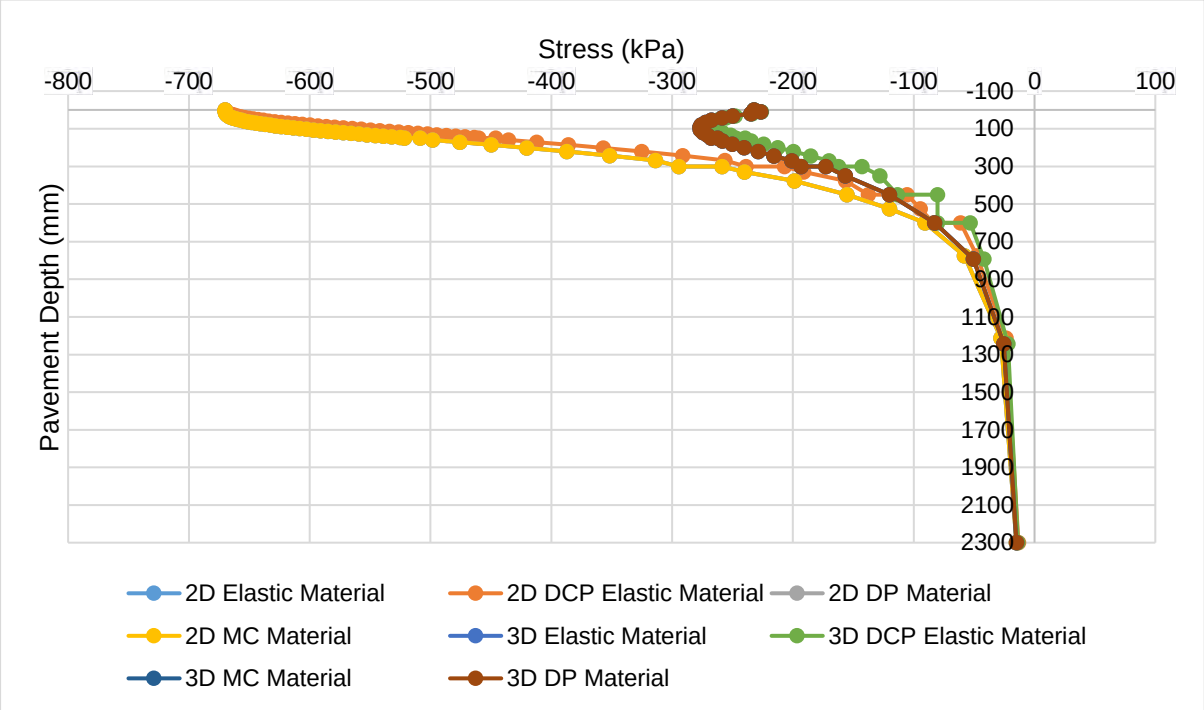

Figure 7-16 Comparative analysis of stress responses for 2D and 3D models using various material models (KZNS5)

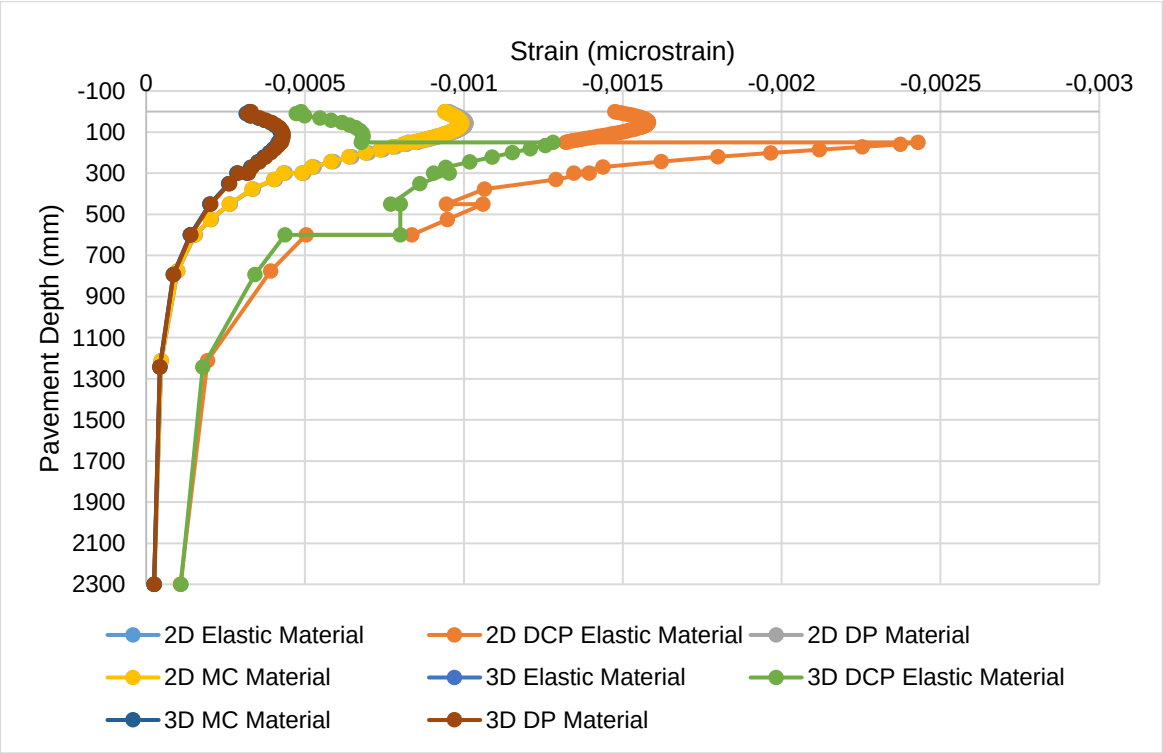

Figure 7-17 Comparative analysis of strain responses for 2D and 3D models using various material models (KZNS5)

7.4 Evaluating Nr Variations Across Material Models

Using the vertical strain on the subgrade layer of the various material models in the FEM models and mePADS analysis, a boxplot analysis was performed to determine the number of repetitions for subgrade rutting failure for each model via the Asphalt Institute damage model (Asphalt Institute 1982) (Equation 3-7).

Equation 7-1

$$\sigma_z = \left[\frac{Nr}{4.783 \times 10^{-5} \times E_4}\right]^{\left\{-\frac{1}{3.734}\right\}}$$

The boxplot (Figure 7-18) provides a clear visualization of the distribution of Nr values across various material characterization models used in LVR pavement design. Each box in the plot represents the interquartile range (IQR), where the middle 50% of the Nr data points lie, with the red line inside each box indicating the median value. The whiskers extend to the smallest and largest data points within 1.5 times the IQR from the lower and upper quartiles, respectively. This boxplot does not display any outliers, suggesting a relatively consistent spread within the models.

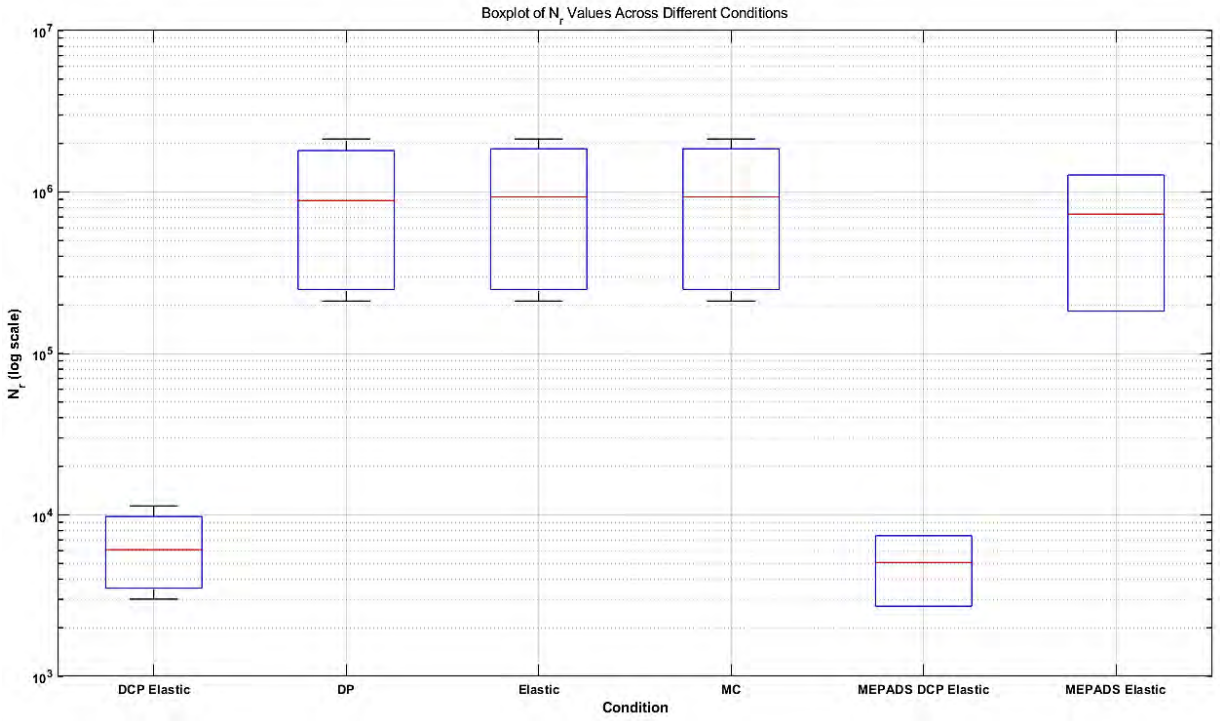

Figure 7-18 Boxplot of Nr values across different conditions

When analysing the different material models, the study revealed considerable variability in the Nr values. The DCP elastic model shows a strong clustering of Nr values at the lower end of the scale, suggesting that this model typically predicts lower resistance, which could indicate less robust performance of LVR pavements under certain conditions. This could imply a more conservative approach or the need for reinforcement when this model is used in design.

In contrast, the DP, elastic and MC models have higher mean Nr values with a wider spread, suggesting that these models predict higher resistance factors. The wider spread indicates variability depending on the specific material and environmental conditions, which may be crucial for the design of LVR pavements to withstand different loads and stresses. These models are likely to be used in scenarios where increased durability is critical and where it is necessary to consider different conditions when designing pavements.

The MEPADS Elastic and MEPADS DCP Elastic models exhibit different behaviours. The MEPADS elastic model lies between the traditional elastic and DP models and

may offer a balance between stiffness and flexibility in pavement design. On the other hand, the MEPADS DCP elastic model is closer to the DCP elastic model, which may indicate that it is tailored to specific conditions where lower resistance is sufficient or where other factors, such as cost or ease of application, take precedence.

Overall, this boxplot highlights the importance of selecting the appropriate material model when designing LVR pavements, as the choice of model significantly affects the predicted performance of the pavement. Understanding these differences helps engineers optimize pavement design in terms of durability, cost efficiency, and suitability for specific traffic and environmental conditions.

7.5 Chapter Summary

Chapter Seven presented a comparative evaluation of FEM and conventional elastic-based methods in predicting LVR performance. The analysis showed that while elastic models are limited in capturing material yielding and bulging behaviour, the nonlinear DP and MC models provided results that were more consistent with observed experimental responses. The validation of the FEM outputs against laboratory triaxial tests confirmed their reliability, whereas the purely elastic approach underestimated critical aspects of deformation.

The rutting predictions, expressed as the number of load repetitions to failure (Nr), highlighted differences across models. The FEM approach, especially when using nonlinear material characterisation, captured variability in pavement life that conventional methods such as MePADS could not. These findings show that relying solely on elastic assumptions may misrepresent the performance of LVR pavements, while FEM provides a more robust framework for understanding deformation mechanisms.

Overall, the chapter demonstrated that FEM not only strengthens the predictive capacity of LVR design but also complements conventional methods by identifying their limitations. The insights from FEM modelling can be used to improve the calibration of mechanistic-empirical approaches, ensuring more reliable, cost-effective, and sustainable pavement structures for low-volume roads.

Chapter 8 : Surface Seal Modelling Results

8.1 Introduction

This chapter presents the modelling of surface seals for low-volume roads, and the FEM was used in this study to model and analyse the structural responses of surface seal models under various conditions. The FEM model was carefully created at the mesoscale, focusing on a thorough depiction of each component aggregate, binder, and base layer within the seal structure. With this detailed method, materials' internal stress and strain can be precisely analysed, providing valuable information on how materials behave under various loadings with various binder properties.

8.1.1 Seal Model Geometry

Given the relative thinness of the seal structures in relation to their lateral dimensions, the model was built in a 2D plane strain environment (Kumbargeri, Boz, Kutay & Heidelberg 2020; Gerber 2016) (Figure 8-1). For the purpose of predicting probable failure mechanisms, this assumption offered a conservative estimate of stress. Within this model, the nominal size is represented by the major axis, the average least dimension (ALD) is represented by the minor axis, and the aggregates are described as ellipses (Gerber & Jenkins 2017; Gerber 2016). Linear elastic characteristics were assumed to simulate how to aggregate and distribute loads and interact with the binder and base layer. Three-node plane stress element (CPS3), a first-order unstructured triangular mesh, was chosen for the model because of its capacity to manage intricate geometries and guarantee precise stress distributions among diverse materials. The mesh was improved to more precisely capture the intricate stress distribution in high-stress concentration locations, such as those around aggregates and adhesive zones.

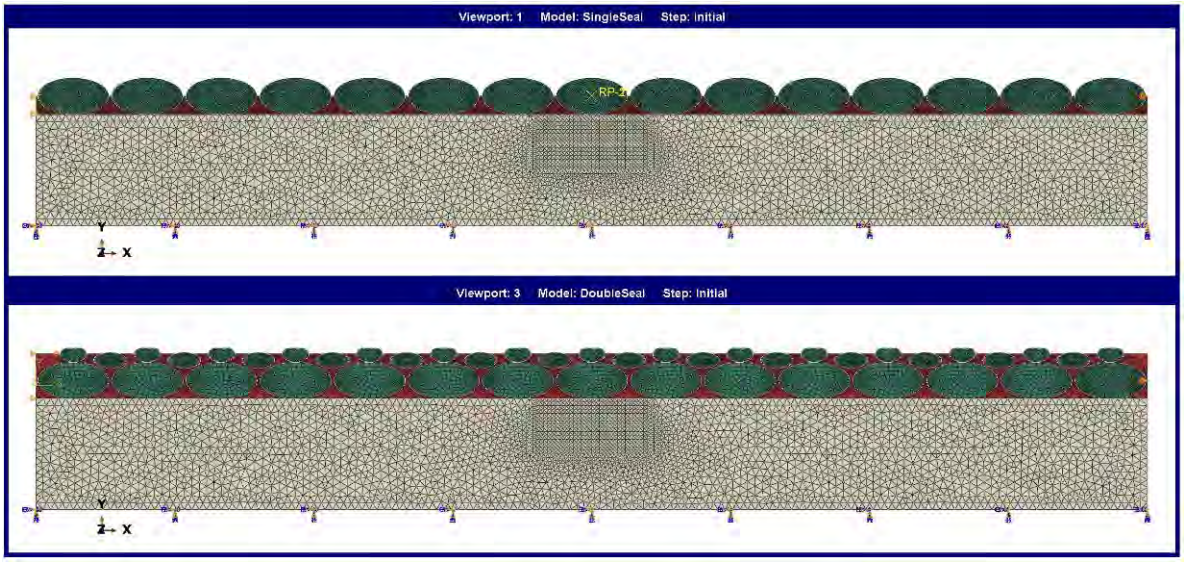

Figure 8-1 Surface seal for single seal and double seal models.

8.1.2 Material Characterization of Surface Seal Layers

The nonlinear behaviour of the granular base, as indicated in Section 7.2.2, was not recorded because of a lack of computational capability. Thus, the material properties have been meticulously simulated to capture both the elastic and viscoelastic reactions of the components for the granular base and binder layer, respectively. The aggregates were treated as dolerite or linear elastic materials with fixed mechanical properties derived from a study by Gerber (2016), with an elastic modulus of 86 GPa and a Poisson's ratio of 0.15. This was crucial for simulating how they distribute loads and interact with binders.

However, because asphalt binders are linear viscoelastic materials, the Prony series coefficient was used to simulate the materials' response to loads over time, including effects that were dependent on temperature (Table 8-1). Through interconversion from the dynamic shear modulus (|G*|) master curve (Kumbargeri, Boz, Kutay & Heidelberg 2020), as in asphalt materials utilizing the Maxwell model, the relaxation modulus Prony series coefficients for the binder were determined.

Table 8-1 Dimensionless Prony series coefficients input into Abaqus® for the binder mixture (Mukandila 2016)

Prony series, virgin, 70-100 penetration grade binder tested at 0◦C	
αi	τi
0.205	0.000184
0.211	0.00117
0.203	0.007
0.198	0.0397
0.141	0.277
0.0368	3.37
0.00423	61.6
0.000259	993
1.00E-09	11200
3.29E-05	73800
G0 = 289 MP a, v = 0.5	

Prony series, virgin, 70-100 penetration grade binder tested at 10◦C	
αi	τi
0.210113382	0.000154292
0.323545218	0.00101028
0.190333926	0.001462246
0.225645499	0.066270833
0.045804251	0.599257126
0.004136786	2.344476277
1.00E-11	43.66544846
0.000419449	381.3050223
4.90E-07	141500.6303
1.00E-11	15615106.52
G0 = 106 MP a, v = 0.5	

Prony series, virgin, 70-100 penetration grade binder tested at 25◦C	
αi	τi
0.61	0.000519
0.258	0.00186
0.0692	0.00399
0.00147	0.0161
0.0591	0.0307
2.90E-05	0.0883
0.00147	0.366
0.000173	3.41
6.75E-05	7.9
3.67E-05	50.1
G0 = 23 MP a, v = 0.5	

8.1.3 Boundary Condition, Loading and Contact Modelling for Sealing

The model was subjected to normal traffic loads for LVRs. These loads were applied as 80 kN vertical forces on the aggregates (Section 6.3.3) and matched shear forces to replicate the rolling resistance Figure 8-2. Section 6.3.3 stated that the sides of the seal model were limited to achieve realistic lateral confinement, mimicking real-world road conditions, whereas the base was fixed to depict the underlying support from the pavement structure. Furthermore, the interaction between the layer interfaces was assumed to be constrained by tie restrictions, which meant that for control purposes, there was no friction and that the layers were completely bonded.

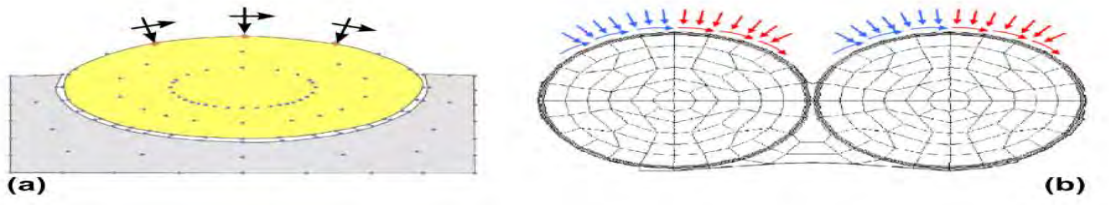

Figure 8-2 Mesoscale model load positions: (a) Section view of Milne's (2004) *3D model and (b) 2D model of* Kringos & Scarpas (2008)

8.1.4 Failure Mechanism in Surface Seal

Several failure processes, including cohesive failure, adhesive failure, and embedment, were simulated via the FEM. To predict the possibility of aggregate dislodgement, adhesive failure was investigated by examining the stress distribution within the adhesive zones between the binder and the aggregates (Figure 8-3) (Gerber & Jenkins 2017; Gerber 2016). The focus of cohesive failure was on the binder itself, specifically how it would break under repeated loading. Shear stress data were utilized to forecast the binder's failure location and timing. To anticipate long-term surface texture loss and structural integrity, the model also included a simulation of the deformation of the base layer, namely, how the aggregates would embed into the base

over time under traffic stresses (Kumbargeri, Boz, Kutay & Heidelberg 2020; Zhou et al. 2024).

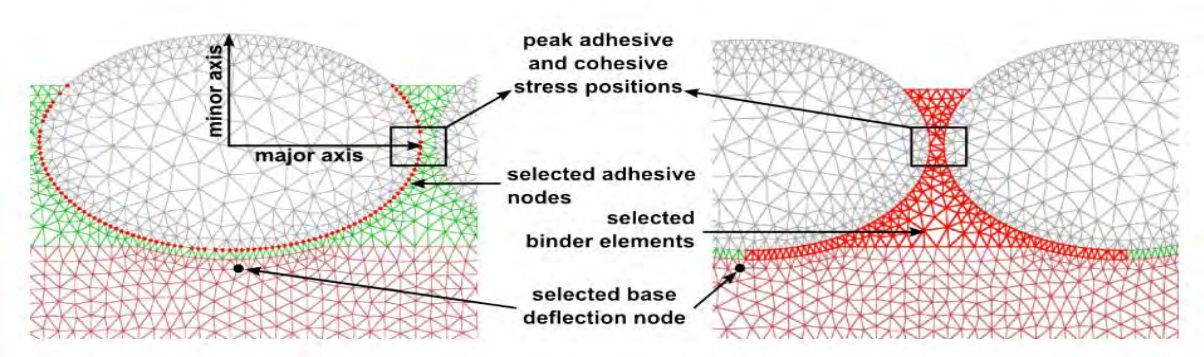

Figure 8-3 Data acquisition locations for the three failure mechanisms (Gerber 2016)

8.2 Seal Modelling Results and Discussions

To estimate probable failure locations and evaluate the overall durability of various seal designs, the FEM produced thorough outputs on the stress and strain within each component of the seal. In addition, the model replicated the deformation patterns of the seal under loading, which was essential for comprehending how well the seal performed in actual circumstances.

8.2.1 Effect of Surfacing (Single or Double Seals) on Pavement Behaviour

Figure 8-4 shows how pavement behaviour is affected by seal surfacing. It shows how a single seal responds structurally to deflection on the pavement surface. The data shows that applying a seal improves the overall stability of the pavement structure by causing a noticeable reduction in deflection within the structure. The effect of aggregate embedment into the base layer, which is controlled by the stiffness of the base material, is further examined by looking at the horizontal strains in the pavement, as shown in Figure 8-5. This embedment is essential to the seal surfacing's failure.

Figure 8-7 and Figure 8-8 provide further details about how binders perform in different scenarios. In particular, when at 10°C (NCDSE), the virgin binder with a penetration grade of 70–100 showed better deflection resistance than at other temperatures modelled in the study. This finding emphasises how significantly binder temperature affects the sealed surface's functionality. At 10 °C, the maximum vertical

deflection in the double seal model was approximately 0.50 mm compared with 0.80 mm at 25 °C, representing a 35–40% reduction in deflection due to increased binder stiffness. These outcomes are consistent with field observations by El-Maaty (2017), who reported that higher asphalt temperatures lead to greater pavement deflections and tensile strains. This alignment between FEM results and experimental findings strengthens confidence in the modelling approach and highlights the importance of selecting binders with appropriate stiffness for in-service temperatures.

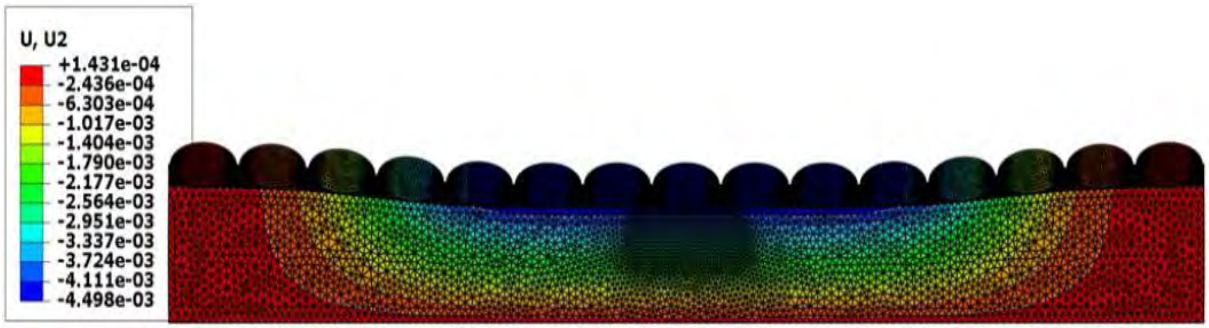

Figure 8-4 Vertical deflection (mm) of a single seal (KZNS)

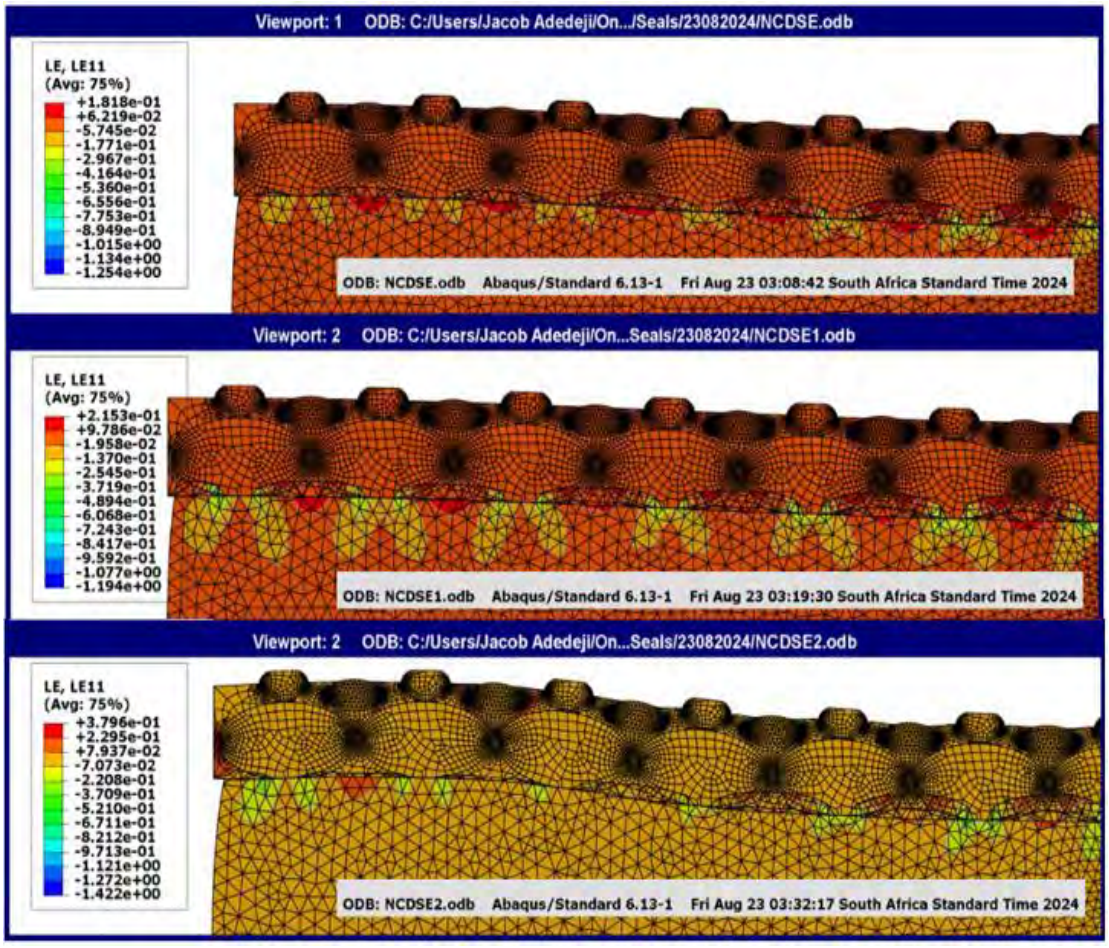

Figure 8-5 Horizontal strain in the pavement for double seal model (NCDS) (a) Virgin binder 70-100 penetration grade tested at 0 °C – (NCDSE); (b) Virgin binder 70-100 penetration grade tested at 10 °C – (NCDSE1); (c) Virgin binder 70-100 penetration grade binder tested at 25 °C – (NCDSE2)

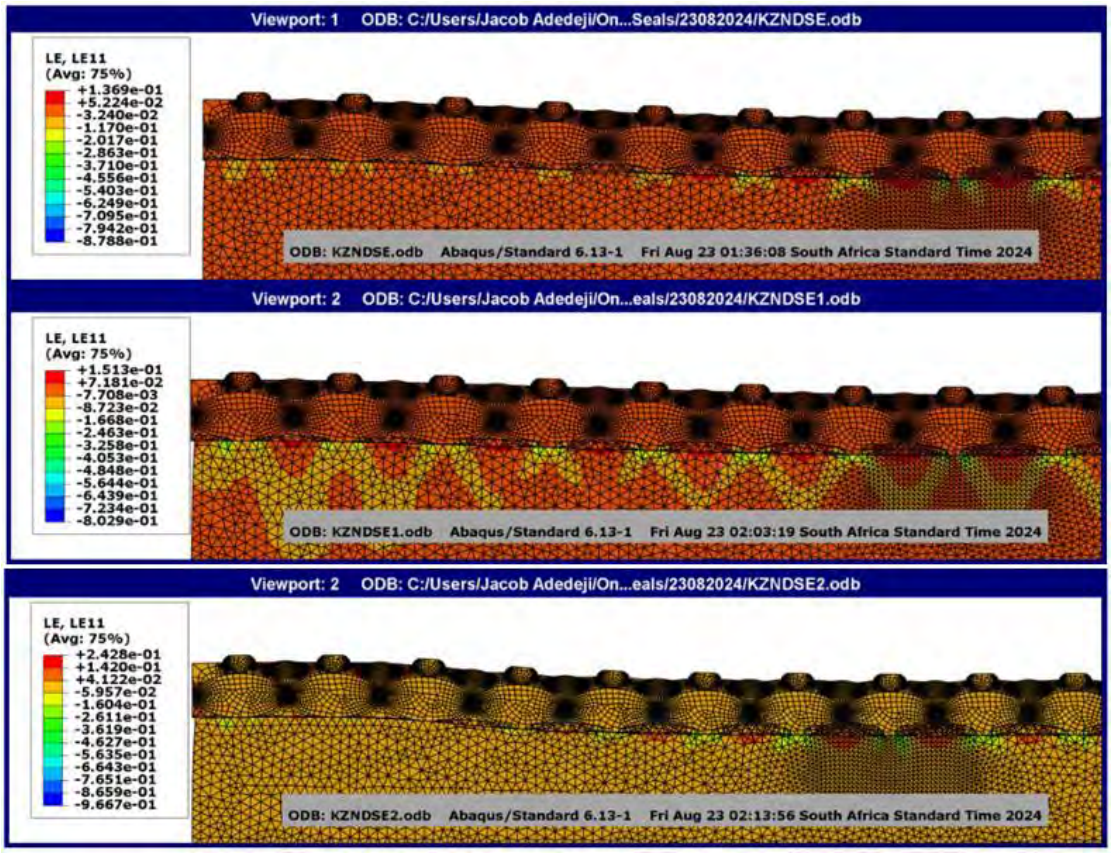

Figure 8-6 Horizontal strain in the pavement for double seal model (KZNDS) (a) Virgin binder 70-100 penetration grade tested at 0 °C – (KZNDSE); (b) Virgin binder 70-100 penetration grade tested at 10 °C – (KZNDSE1); (c) Virgin binder 70-100 penetration grade binder tested at 25 °C – (KZNDSE2)

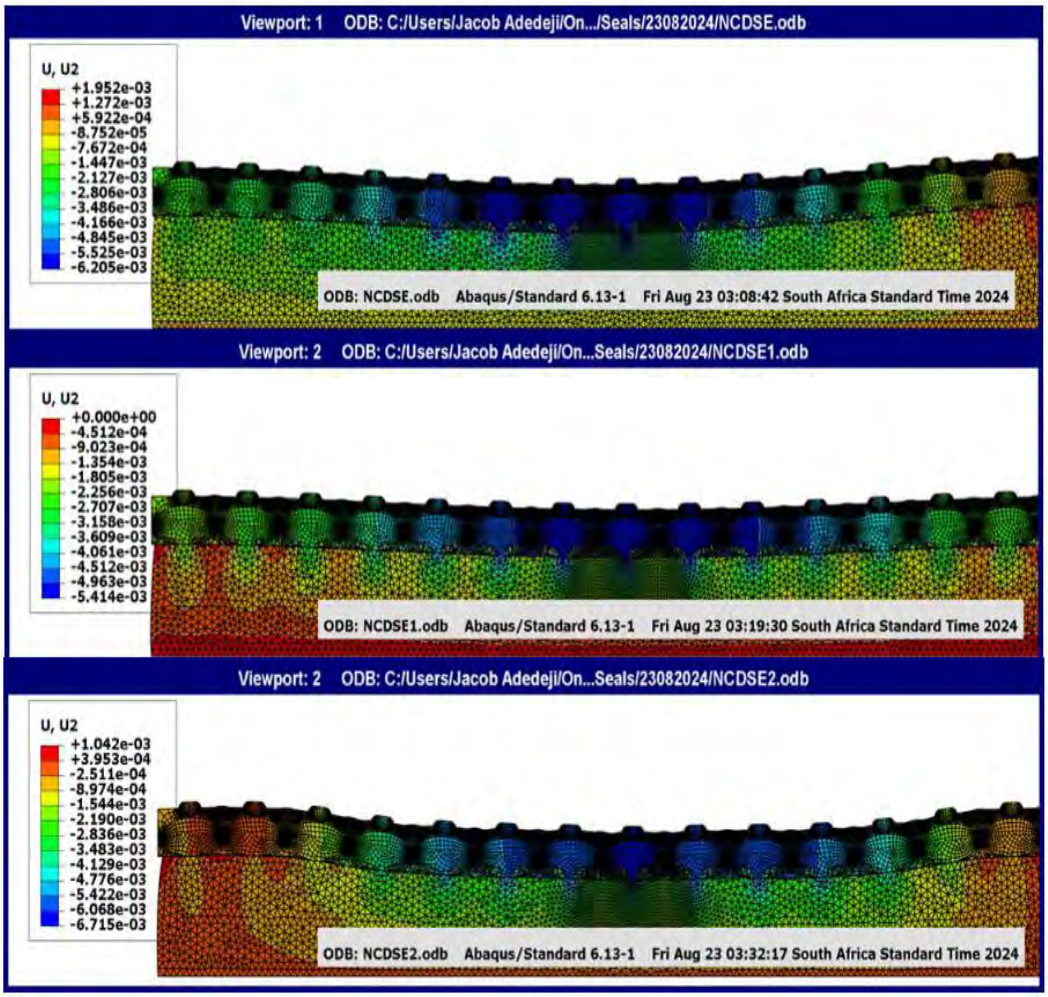

Figure 8-7 Vertical deflection (mm) of the double seal model (NCDS) (a) Virgin binder 70-100 penetration grade tested at 0 °C – (NCDSE); (b) Virgin binder 70-100 penetration grade tested at 10 °C – (NCDSE1); (c) Virgin binder 70-100 penetration grade binder tested at 25 °C – (NCDSE2)

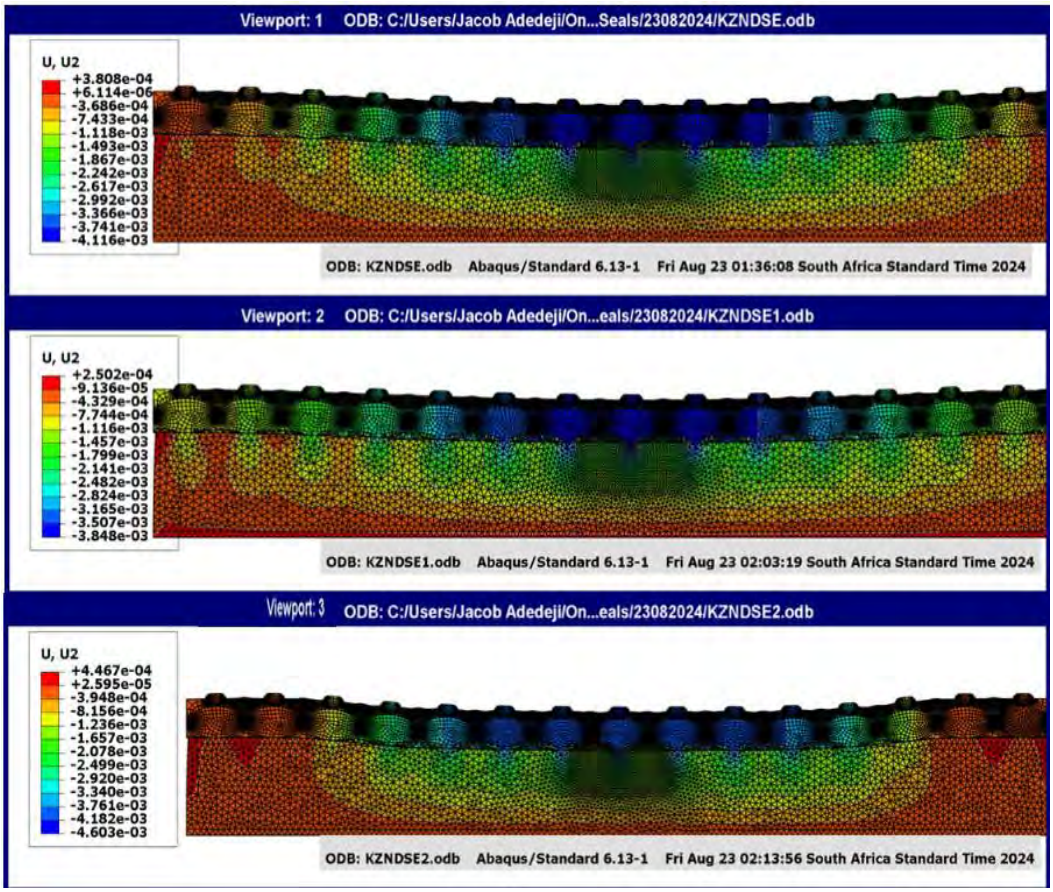

Figure 8-8 Vertical deflection (mm) of the double seal model (KZNDS) (a) Virgin binder 70-100 penetration grade tested at 0 °C – (KZNDSE); (b) Virgin binder 70-100 penetration grade tested at 10 °C – (KZNDSE1); (c) Virgin binder 70-100 penetration grade binder tested at 25 °C – (KZNDSE2)

Table 8-2 presents crest and sag deflections for the NCS and KZNS double seal models under binder test temperatures of 0 °C, 10 °C and 25 °C. The results confirm that deflections are consistently lower in the KZNS models than in the NCS models, and that crest values are much higher than sag values due to localised loading response. For example, at 0 °C the crest deflection was 59.4 mm for NCS compared with 38.1 mm for KZNS, while sag deflections were 6.21 mm and 4.12 mm respectively. At 25 °C, both models showed increased crest deflections (39.5 mm for NCS and 44.7 mm for KZNS), with higher sag values also recorded. These outcomes reinforce the earlier findings from Figures 8-6 and 8-7, showing the clear effect of binder stiffness and temperature on seal performance. The consistency with other

reported studies (Sargand et al. 2023; El-Maaty 2017) strengthens confidence in the modelling approach.

Table 8-2 Pavement Deflection Responses in Double seal

	Pavement Responses	NCS Double Seal		KZNS Double Seal	
		crest	sag	crest	sag
Scenario 1 (Virgin binder 70-100 penetration grade tested at 0◦C)	Deflection (mm)	59.4	6.21	38.1	4.12
Scenario 2 (Virgin binder 70-100 penetration grade tested at 10◦C)	Deflection (mm)	45.1	5.41	25.0	3.85
Scenario 3 (Virgin binder 70-100 penetration grade binder tested at 25◦C)	Deflection (mm)	39.5	6.72	44.7	4.60

8.2.2 Significance of the Seal Surfacing Layer

The FEM results demonstrated that the addition of a seal surfacing layer reduced pavement deflections and horizontal strains compared with unsealed structures, indicating an improvement in structural response. Both the single and double seal models showed this trend, with the double seal achieving the lowest deflections and strains. For example, the maximum sag deflection in the NCS double seal model at 10 °C was 5.41 mm compared with higher values in the unsealed case, while the KZNS double seal produced even lower deflections of 3.85 mm (Table 8-2). These reductions suggest that the seal layer contributes to increased structural capacity by limiting deformation under load.

The FEM outputs also highlighted that binder stiffness plays a critical role in the performance of the seal surfacing. At lower binder temperatures, deflections were reduced by up to 35–40% compared with higher temperature scenarios (Figures 8-6 and 8-7), confirming that a stiffer binder provides greater resistance to deformation. This effect was consistent across both NCS and KZNS models.

Based on these findings, the significance of the seal surfacing in this study lies in its ability to reduce pavement deflections and strains, with double seals and stiffer binders providing the most favourable results. These results, derived directly from the FEM analysis, confirm the contribution of seal surfacing to the structural response of low-volume roads in the context of this study.

8.3 Chapter Summary

This chapter presented the modelling and analysis of surface seals for low-volume roads using FEM at the mesoscale. The model captured the structural responses of surface seals by explicitly representing the interactions between aggregates, binder, and the base layer under different loading conditions. A 2D plane strain approach was adopted, with linear elastic and viscoelastic material properties used to simulate stress distributions and potential failure mechanisms, including cohesive failure, adhesive failure, and aggregate embedment.

The FEM results demonstrated that the inclusion of a surface seal reduced pavement deflections and strains compared with unsealed structures, with double seals providing the greatest improvements. Quantified outputs showed that sag deflections in double seals were consistently lower than in single seals, and that deflections decreased by up to 35 - 40% at lower binder temperatures due to increased binder stiffness. These findings highlight the importance of binder properties and seal thickness in determining sealed pavement performance.

Overall, the chapter established that surface seals contribute to reducing deformation and improving the structural response of low-volume roads. The evidence from the FEM simulations provides a basis for incorporating surface seals into a simplified design model for both new construction and rehabilitation applications.

Chapter 9 : Conclusions and Recommendations

9.1 Introduction

This chapter draws together the findings of the study and presents the overall conclusions and recommendations. This research aims to develop a finite element method (FEM) model that utilises existing Dynamic Cone Penetrometer (DCP) correlations to improve the efficiency and cost-effectiveness of low-volume road design (LVRs). Four specific objectives guided the study: to establish correlations between DCP results and laboratory parameters; to evaluate existing design methods; to develop and apply FEM models for predicting LVR deformation; and to propose a simplified design model that incorporates surface seals for both new construction and rehabilitation.

The conclusions presented here are derived directly from the experimental, analytical, and modelling results reported in Chapters 5 to 8. Each conclusion is structured to address a specific research objective, ensuring that the outcomes are firmly rooted in the study's findings rather than external literature. The recommendations that follow translate these conclusions into practical guidance for engineers, road authorities, and policymakers engaged in the planning, design, and maintenance of LVRs. Finally, directions for further research are outlined to extend and strengthen the contributions of this study.

9.2 Conclusions

9.2.1 Objective 1

To analyse the factors influencing DCP results and establish correlations with laboratory-derived parameters to improve reliability in LVR structural assessments.

The study confirmed that DCP penetration rates are strongly influenced by soil type, density, and moisture content. The KwaZulu-Natal soils (finer, higher plasticity) produced lower CBR values (8.5 - 38%) than the Northern Cape soils (20 - 98%) which were coarser and less plastic. Laboratory testing demonstrated that predicted CBR values from DCP deviated by an average of 28% compared with measured laboratory

CBR, with a minimum deviation of 5.6% for sample NCS5. Similarly, the resilient modulus showed systematic variation with confining pressure, confirming the dependency of strength and stiffness on field conditions. These findings provided the basis for a correlation model linking DCP-derived indices with laboratory CBR and modulus values, thereby improving the reliability of in-situ assessments.

9.2.2 Objective 2

To evaluate existing LVR design methods, including DCP-based approaches, and compare their performance using site-specific datasets.

The comparative analysis of CBR, AASHTO 1993, TRH 20, Odemark, MePADS, and FEM design methods revealed substantial differences in predicted pavement structures and performance. TRH 20 uniquely incorporated a gravel wearing course, while CBR and AASHTO produced thicker granular layers without surfacing. MePADS and FEM provided outputs more consistent with measured site conditions. Validation of FEM against MePADS elastic theory showed agreement within ~12% in subgrade strains, strengthening confidence in the modelling results. Overall, the evaluation confirmed that empirical methods are limited by assumptions that risk over- or under-design, whereas mechanistic-empirical methods, particularly when incorporating DCP data, capture material variability more realistically.

9.2.3 Objective 3

To develop a FEM model for predicting LVR deformation and compare its outputs with empirical and mechanistic-empirical design approaches.

The FEM models (Appendix D), developed in Abaqus, successfully simulated pavement behaviour under traffic loading using both linear elastic and non-linear constitutive models. Validation against laboratory triaxial results and MePADS confirmed reliability, with 3D FEM consistently predicting 30 - 35% longer pavement life than 2D FEM due to better representation of stress distribution. Incorporating DCP-derived moduli into FEM produced more conservative life predictions, particularly under wetter conditions, which aligns with observed frequent maintenance needs for unsealed roads. The FEM thus provided a more realistic tool for predicting deformation

mechanisms (rutting, yielding, bulging) than conventional elastic-layer designs, demonstrating its value for improving design reliability.

9.2.4 Objective 4

To develop a simplified design model for low-volume roads, incorporating both new construction and rehabilitation options, including the use of surface seals as alternative wearing courses.

The mesoscale FEM modelling of surface seals showed that both single and double seals reduced pavement deflections and strains relative to unsealed pavements. Double seals provided the greatest improvement, with sag deflections reduced by up to 20% compared with single seals. Binder stiffness was also shown to be critical: at 10 °C, deflections in double seals were 35 - 40% lower than at 25 °C, confirming the sensitivity of performance to temperature and binder properties. The modelling also demonstrated the role of adhesive, cohesive, and embedment mechanisms in governing seal durability. Collectively, these findings form the basis of a simplified design framework which supports the use of surface seals as cost-effective wearing courses in both new construction and rehabilitation of LVRs.

9.3 Recommendations

Based on the findings of this study, the following suggestions can be made to improve LVR designs in developing countries, particularly in South Africa:

- Adoption of FEM in LVR Design: This study highlights the major advantages of developing LVRs with FEM. Designers of roads in underdeveloped nations should consider the use of the FEM in their designs. Pavement performance can be predicted more precisely by the FEM, especially when nonlinear material behaviour is taken into consideration.
- Use of DCP Results for Pavement Assessment: An efficient and economical way to assess the in-situ strength of LVRs is via the DCP test. DCP testing should be routinely used in both the rehabilitation of old LVRs and the design of new LVRs. The accuracy of structural assessments can be improved by including DCP data in the FEM.

- Improvement in Data Collection and Analysis: Extending the sample size of test samples and performing comprehensive material characterization are essential steps in increasing the dependability of FEM forecasts. By using this method, the correlation between the predicted and actual pavement performance will be improved, and the data variability will decrease.
- Surface Seal Implementation: Given the importance of surface seals in prolonging the life of LVRs, it is advised that, while unsealed roads are rebuilt, economical surface seal solutions should be considered. Surface sealing can reduce maintenance costs, improve traffic safety, and reduce negative environmental effects such as dust production.

9.4 Further Studies

This study paves the way for further research on LVR design and maintenance, with the goal of improving LVR design, construction, and maintenance to make them more long-lasting, affordable, and sustainable. These can be listed as follows:

- Expansion of FEM application: Future studies should explore the use of the FEM in a broader range of LVR situations, including different soil types and climate zones. This will facilitate the creation of more broadly applicable models in various circumstances.
- Incorporation of Additional Materials in the FEM: While unbound granular aggregates were the focus of this investigation, other stabilizer materials—which are frequently utilized in FEM analyses in South Africa—should be considered in subsequent research. A more thorough knowledge of how various materials function in low-volume traffic situations will result from this.
- Development of a Standardized Framework for LVR Design: To facilitate the adoption of these techniques by practitioners, a standardized design framework that combines DCP results with the FEM is needed. This framework should also include guidelines for surface seal selection and application.

These recommendations and future research directions are aimed at advancing the design, construction, and maintenance of LVRs, ensuring that they become more durable, cost-effective, and sustainable over the long term.

References

Abaqus. 2019. *Analysis User's Guide (6.13).* Available from: https://classes.engineering.wustl.edu/2009/spring/mase5513/abaqus/docs/v6.6/books/usb/default.htm [Accessed 2 April 2024].

Abbas, A, Ruddock, F, Alkhaddar, R, Rothwell, G, Carnacina, I & Andoh, R. 2019. Experimental data used to validate the FE model of the structural performance of two flexible pipes laid in a single trench. *Data in Brief*. 27. doi.org/10.1016/j.dib.2019.104594.

Adedeji, JA. 2015. Simulation of flexible pavement utilizing fly ash as alternative stabilizer. Central University of Technology, Free State.

Adedeji, JA & Hassan, MM. 2018. Performance Evaluation of Ultra-Thin Pavement Seals in Low-Volume Roads. *Sustainable Civil Infrastructures*. (October). doi.org/10.1007/978-3-030-01908-2_1.

Adedeji, JA, Abejide, SO & Mostafa, MMH. 2021. Comparative Study on the Design Methods for Fly Ash- Flexible Pavement. In: *6th International Conference on Road and Rail Infrastructure*. 1033–1040.

Adeniyi, JO, Akinrinmade, Y & Abiodun, AL. 2018. Analysis of Road Transport Impact On Rural Development in Nigeria: A Study On Akure North Local Government Area, Ondo State. *International Journal of New Technology and Research*. 4(3):263103.

Adu-Osei, A. 2001. Characterization Of Unbound Granular Layers In Flexible Pavements: Research Report ICAR-502-3. *Texas Transportation Institute the Texas A&M University System College Station, Texas*.

Ahmad, H. 2023. Two-dimensional study of the inclusions of skirt sand and deep cement piles to improve the load-displacement behaviour of circular foundations on soft clay soil. *Heliyon*. 9(2):e13627. doi.org/10.1016/j.heliyon.2023.e13627.

Ahmad, H & Mahboubi, A. 2023. Effect of strip footing on the stress-strain behaviour of soil-geogrid interaction: A new simple concept. *Geosynthetics: Leading the Way to a Resilient Planet*. 1034–1040. doi.org/10.1201/9781003386889-127.

Al-Azzawi, AA. 2012. Finite element analysis of flexible pavements strengthed with geogrid. *ARPN Journal of Engineering and Applied Sciences*. 7(10):1295–1299.

Al-Khateeb, LA, Saoud, A & Al-Msouti, MF. 2011. Rutting prediction of flexible pavements using finite element modeling. *Jordan Journal of Civil Engineering*. 5(2):173–190.

Alaswadko, N, Hassan, R, Meyer, D & Mohammed, B. 2019. Modelling roughness progression of sealed granular pavements: a new approach. *International Journal of Pavement Engineering*. 20(2):222–232. doi.org/10.1080/10298436.2017.1283689.

Ameri, M, Salehabadi, EG, Nejad, FM & Rostami, T. 2012. Assessment of analytical techniques of flexible pavements by final element method and theory of multi-layer system. *J. Basic Appl. Sci. Res*. 2(11):11743–11748.

American Association of State Highway and Transportation Officials (AASHTO), 2002. *AASHTO Guide for Design of Pavement Structures*. Washington, D.C.: AASHTO.

Van Amsterdam, E. 2014. *Construction Methods for Civil Engineering*. Juta Limited. Available from: https://books.google.co.za/books?id=ye%5C_IngEACAAJ.

Aneke, FI. 2018. Behaviour Of Unsaturated Soils of Road Pavement Structure Under Cyclic Loading. Bloemfontein: Central University of Technology, Free State.

Apronti, D, Ksaibati, K, Gerow, K & Hepner, JJ. 2016. Estimating traffic volume on Wyoming low volume roads using linear and logistic regression methods. *Journal of Traffic and Transportation Engineering (English Edition)*. 3(6):493–506. doi.org/10.1016/j.jtte.2016.02.004.

Araya, AA. 2011. Characterization of Unbound Granular Materials for Pavements. IHE/TUDelft, the Netherlands.

Asphalt Institute. 1982. *Research and Development of the Asphalt Institute's Thickness Design Manual*. Asphalt Institute.

Austroads. 2012. *Pavement design: A guide to the structural design of road pavements*. Sydney: Austroads.

Bareither, CA, Benson, CH & Edil, TB. 2008. Comparison of shear strength of sand

backfills measured in small-scale and large-scale direct shear tests. *Canadian Geotechnical Journal*. 45(9):1224–1236. doi.org/10.1139/T08-058.

Balaguera, A., Carvajal, G.I., Albertí, J. and Fullana-i-Palmer, P., 2018. Life cycle assessment of road construction alternative materials: A literature review. *Resources, Conservation and Recycling*, 132:37-48.

Berg, CN, Deichmann, U, Liu, Y & Selod, H. 2017. Transport Policies and Development. *Journal of Development Studies*. 53(4):465–480. doi.org/10.1080/00220388.2016.1199857.

Berg, CN, Blankespoor, B & Selod, H. 2018. Roads and Rural Development in Sub-Saharan Africa. *The Journal of Development Studies*. 54(8):856–874.

Biswas, PP, Sahis, MK, Mondal, GC & Majumdar, D. 2016. Design of Low Volume Rural Roads with Unbound Granular Materials using Odemark's Method. *International Journal of Engineering Research and*. V5(06):404–408. doi.org/10.17577/ijertv5is060520.

Brito, L. 2011. Brito, Lelio (2011) Design methods for low volume roads. PhD thesis, University of Nottingham.

Brown, SF. 2013. An introduction to asphalt pavement design in the UK. *Proceedings of the Institution of Civil Engineers: Transport*. 166(4):189–202. doi.org/10.1680/tran.11.00076.

Burningham, S., & Stankevich, N. (2005). *Why road maintenance is important and how to get it done* (No. Transport Note No. TRN-4).

Campbell, AE. 2009. Federal road management for sub-Saharan African nations: A Nigerian case study. *ProQuest Dissertations and Theses*. 137. Available from: https://proxy.library.carleton.ca/login?url=https://www.proquest.com/dissertations-theses/federal-road-management-sub-saharan-african/docview/305140765/se-2?accountid=9894%0Ahttps://ocul-crl.primo.exlibrisgroup.com/discovery/openurl?institution=01OCUL_CRL.

Cary, CE & Zapata, CE. 2011. Resilient modulus for unsaturated unbound materials. *Road Materials and Pavement Design*. 12(3):615–638. doi.org/10.3166/rmpd.12.615-

638.

Chao, C, Jommi, C & Muraro, S. 2023. Numerical investigation of the equipment set-up in triaxial testing of soft soils.

Chen, J, Hossain, M & Latorella, TM. 1999. Use of falling weight deflectometer and dynamic cone penetrometer in pavement evaluation. *Transportation Research Record*. 1655(1):145–151.

Chowdary, V, Ramulu, G, Shankar, S & Prasad, C. 2012. Influence of unbound material properties on rutting potential of low volume roads. *J. Elixir Cem. Concrete Comp*. 42:6377–6382.

Committee of Land Transport Officials (COLTO), 1998. Standard Specifications for Road and Bridge Works for State Road Authorities. Pretoria: COLTO

Committee of State Road Authorities (CSRA), 1984. TMH6: Technical Methods for Highways No. 6: Pavement Design. Pretoria: Department of Transport, South Africa.

Committee of State Road Authorities. 1990. *The structural design, construction and maintenance of unpaved roads*. National Institute for Transport and Road Research.

Cook, JR, Petts, RC & Rolt, J. 2013. Low Volume Rural Road Surfacing and Pavements: A Guide to Good Practice. (June):134. Available from: http://r4d.dfid.gov.uk/pdf/outputs/AfCap/AFCAP-GEN-099-Rural-Road-Surfacing-and-Pavements-Guideline.pdf.

Daleiden, JF, Killingsworth, BM, Simpson, AL & Zamora, RA. 1994. Analysis of procedures for establishing in situ subgrade moduli. *Transportation Research Record*. 1462.

De Beer, M & van Rensburg, Y. 2016. *Improvements to the WinDCP software for Pavement Design of Low Volume Roads - Final Development report*.

Debrah, E.K. and Anochie-Boateng, J.K., 2022. Environmentally optimised design of road surfacing alternatives for steep slope sections on rural roads. Southern African Transport Conference.

Department for Transport. 2018. *Statistical data set Road length statistics (RDL)*.

Available from: https://www.gov.uk/government/statistical-data-sets/road-length-statistics-rdl [Accessed 10 October 2021].

Dione, A, Fall, M, Yves, B, Benboudjema, F & Michou, A. 2015. Implementation of Resilient Modulus - CBR relationship in Mechanistic-Empirical (M. -E) Pavement Design, Revue du Cames – Sci. Appl. & de l'Ing., Vol. 1(2), pp. 65-71, 20. *Cames Sai*. 1(January):65–71.

Djenane, M, Demagh, R & Hammoud, F. 2022. Rotation of Stresses in French Wheel Tracking Test. *Civil Engineering Journal (Iran)*. 8(3):438–453. doi.org/10.28991/CEJ-2022-08-03-03.

Doré, G. 2014. *Pavement design for low volume roads*. Available from: http://ctep.ca/wp-content/uploads/2017/05/Pavement-Design-for-Low-volume-Roads-Dore.pdf. [Accessed 10 October 2021].

DoT, CR. 1996.

Douglas, RA. 2018. *Low-volume road engineering: Design, construction, and maintenance*. CRC Press.

Drumm, EC, Boateng-Poku, Y & Johnson Pierce, T. 1990. Estimation of subgrade resilient modulus from standard tests. *Journal of Geotechnical Engineering*. 116(5):774–789.

Dudziński, PA. 2019. Method for predicting dynamic shear strength in soils – Part I: Proposal for a new criterion. *Journal of Terramechanics*. 86:31–37. doi.org/10.1016/j.jterra.2019.08.005.

Duris, L & Hrubesova, E. 2020. Numerical simulation of the interaction between fibre concrete slab and subsoil—the impact of selected determining factors. *Sustainability (Switzerland)*. 12(23):1–17. doi.org/10.3390/su122310036.

Ekwulo, EO & Eme, DB. 2009. Fatigue and rutting strain analysis of flexible pavements designed using CBR methods. *African Journal of Environmental Science and Technology*. 3(12):412–421.

El-Ashwah, AS, Mousa, E, El-Badawy, SM & Abo-Hashema, MA. 2022. Advanced

characterization of unbound granular materials for pavement structural design in Egypt. *International Journal of Pavement Engineering*. 23(2):476–488. doi.org/10.1080/10298436.2020.1754416.

El-Badawy, SM & Kamel, MA. 2011. Assessment and Improvement of the Accuracy of the Odemark Transformation Method. *International Journal of Advanced Engineering Sciences and Technologies*. 5(2):105–110.

El-Maaty, A.E.A. 2017. Temperature change implications for flexible pavement performance and life. *International Journal of Transportation Engineering and Technology*, *3*(1): 1-11.

Ethiopian Roads Authority. 2018. *Road sector development program: 21 years performance assessment*.

Fabrice, PKR, Abejide, SO, Adedeji, JA & Mostafa, MMH. 2020. Evaluating the Performance of Warm Mix Asphalt Incorporating Recycled Asphalt Pavement Treated Bases. *Transportation Research Procedia*. doi.org/10.1016/j.trpro.2020.02.106.

Faiz, A, Faiz, A, Wang, W & Bennett, C. 2012. Sustainable Rural Roads for Livelihoods and Livability. *Procedia - Social and Behavioral Sciences*. 53:1–8. doi.org/10.1016/j.sbspro.2012.09.854.

Federation of Canadian Municipalities and National Research Council. 2005. Dust control for unpaved roads. *Infraguide*. 10(October):1–42.

Fiorentini, N, Huang, J, Cuciniello, G, Leandri, P & Losa, M. 2023. Comparing the Performance of Historical and Regular Stone Pavement Structures in Urban Trafficked Areas through the Finite Element Method (FEM) †. *Infrastructures*. 8(7). doi.org/10.3390/infrastructures8070115.

Fouche, N. 2021. Geotechnical Characterisation of the Upper Quaternary Sands of the Cape Flats. Stellenbosch University. Available from: https://scholar.sun.ac.za.

Franzen, T & Thorpe, D. 2020. Sustainable development and management of low-volume road networks in Australia. In: *Sustainable Ecological Engineering Design: Selected Proceedings from the International Conference of Sustainable Ecological Engineering Design for Society (SEEDS) 2019*. 51–63.

Garber, NJ & Hoel, LA. 2018. *Traffic and highway engineering*. Cengage Learning.

Garcia, K.E., Cruz, O.G.D., Muhi, M.M. and Tabaroei, A., 2024. The role of dynamic cone penetrometer testing in assessing pavement subgrade strength: a literature review. *GEOMATE Journal*, *26*(117), 132-142.

Geoffroy, DN. 1998. *Thin-surfaced Pavements*. V. 260. Transportation Research Board.

George, KP. 2004. Prediction of Resilient Modulus From Soil Index Properties. Report No. FHWA/MS-DOT-RD-04-172. (November):72.

George, KP & Uddin, W. 2000. *Subgrade characterization for highway pavement design*.

Gerald, H, Andrewski, D & Gallivan, V. 2009. Design and Construction of Highways for Very Heavy Trucks. In: *Proceedings International Conference of Perpetual Pavements*. Ohio University. Columbus. CD-ROM.

Gerber, JAK. 2016. Numerical modelling of performance and failure criteria for surfacing seals. Stellenbosch University.

Gerber, J & Jenkins, K. 2017. Finite element modelling and damage quantification of chip seals. *Road Materials and Pavement Design*. 18(2):350–361. doi.org/10.1080/14680629.2016.1213512.

Gkyrtis, K. 2023. Pavement Analysis with the Consideration of Unbound Granular Material Nonlinearity. *Designs*. 7(6). doi.org/10.3390/designs7060142.

Gobena, JA & Lollo, LC. 2016. Design of Low Volume Road in Dallo Manna, Ethiopia. *International Journal of Research in Engineering and Technology*. 05(02):79–81. doi.org/10.15623/ijret.2016.0502015.

Goh, ATC, Teh, CI & Wong, KS. 1997. Analysis of Piles Subjected to Embankment Induced Lateral Soil Movements. *Journal of Geotechnical and Geoenvironmental Engineering*. 123(9):792–801. doi.org/10.1061/(asce)1090-0241(1997)123:9(792).

Groenewald, M & Wijk, I Van. 2010. Ultra Thin Reinforced Concrete Pavements (UTRCP)-innovative technology which offers cost and socio-economic benefits for

infrastructure provision. *Satc 2010*. (August):188–200. Available from: http://137.215.9.22/handle/2263/14866.

Gudishala, R. 2004. Development of Resilient Modulus Prediction Models for Base and Subgrade Pavement Layers From In Situ Devices Test Results. Louisiana State University. Available from: http://digitalcommons.lsu.edu/gradschool_theses.

Guirguis, M & Buss, A. 2017. Performance Evaluation of Emulsion and Hot Asphalt Cement Chip Seal Pavements. *Journal of Materials in Civil Engineering*. 29(11). doi.org/10.1061/(asce)mt.1943-5533.0002057.

Gungor, OE, Al-Qadi, IL, Gamez, A & Hernandez, JA. 2017. Development of adjustment factors for MEPDG pavement responses utilizing finite-element analysis. *Journal of Transportation Engineering*. 143(7). doi.org/10.1061/JTEPBS.0000040.

Gupta, A. 2017. Finite Element Analysis of Granular Pavements Considering Material Nonlinearity. *Asian Transport Studies*. 4(3):550–564.

Gupta, A & Kumar, A. 2014. Comparative structural analysis of flexible pavements using finite element method. *International Journal on Pavement Engineering & Asphalt Technology*. 15(1):11–19.

Gupta, A, Kumar, P & Rastogi, R. 2011. Pavement deterioration and maintenance model for low volume roads. *International Journal of Pavement Research and Technology*. 4(4):195–202.

Hadi, MNS & Bodhinayake, BC. 2003. Non-linear finite element analysis of flexible pavements. *Advances in Engineering Software*. 34(11–12):657–662. doi.org/10.1016/S0965-9978(03)00109-1.

Hall, KD & Bettis, JW. 2001. Development of Comprehensive Low-Volume Pavement Design Procedures.

Hall, KD & Thompson, MR. 1994. Soil-property-based subgrade resilient modulus estimation for flexible pavement design. *Transportation Research Record*. (1449).

Hamim, OF & Hoque, MS. 2019. Prediction of pavement life of flexible pavements under the traffic loading conditions of Bangladesh. *Airfield and Highway Pavements*

2019: Design, Construction, Condition Evaluation, and Management of Pavements - Selected Papers from the International Airfield and Highway Pavements Conference 2019. (July):21–31. doi.org/10.1061/9780784482452.003.

El Hariri, A, Elawad Eltayeb Ahmed, A & Kiss, P. 2023. Review on soil shear strength with loam sand soil results using direct shear test. *Journal of Terramechanics*. 107:47–59. doi.org/10.1016/j.jterra.2023.03.003.

Hassan, AB. 1996. The effects of material parameters on Dynamic Cone Penetrometer results for fine-grained soils and granular materials. Oklahoma State University.

Henning, T, Kadar, P & Bennett, CR. 2006. Surfacing Alternatives for Unsealed Rural Roads. (30):8. Available from: http://documents1.worldbank.org/curated/en/613681468161665541/pdf/356760TRN02900Success0Transport0Note.pdf.

Herath, A, Mohammad, LN, Gaspard, K, Gudishala, R & Abu-Farsakh, MY. 2005. The Use of Dynamic Cone Penetrometer to Predict Resilient Modulus of Subgrade Soils. 1–16. doi.org/10.1061/40776(155)2.

Hernandez, JA & Al-Qadi, IL. 2015. Airfield pavement response caused by heavy aircraft takeoff advanced modeling for consideration of wheel interaction. *Transportation Research Record*. 2471:40–47. doi.org/10.3141/2471-06.

Hernández-Hernández, V.A., Joya-Cárdenas, D.R., Equihua-Anguiano, L.N., Leal-Vaca, J.C., Peña, J.A., Pérez-Moreno, L., Saldaña-Robles, N. and Saldaña-Robles, A., 2021. Experimental and numerical analysis of triaxial compression test for a clay soil. *Chilean journal of agricultural research*, *81*(3), pp.357-367.

Hoffmann, P & Potgieter, CJ. 2007. Bitumen rubber chip and spray seals in South Africa. *SATC 2007 - 26th Annual Southern African Transport Conference: The Challenges of Implementing Policy*. (July):225–238.

Horak, E. 2008. Benchmarking the structural condition of flexible pavements with deflection bowl parameters. *Journal of the South African Institution of Civil Engineering*. 50(2):2–9.

Hossain, MS. 2009. Estimation of subgrade resilient modulus for Virginia soil. *Transportation research record*. 2101(1):98–109.

Hossain, MS & Kim, WS. 2013. Estimation of Subgrade Resilient Modulus Using Unconfined Compression Test. *Final Report VCTIR 15-R12*. 37.

Hossain, MS & Kim, WS. 2015. Estimation of subgrade resilient modulus for fine-grained soil from unconfined compression test. *Transportation Research Record*. 2473(1):126–135.

Hossain, N, Singh, D & Zaman, M. 2015. Development of rut prediction models from an instrumented in-service test section on interstate-35. *International Journal of Pavement Research and Technology*. 8(5):305–314. doi.org/10.6135/ijprt.org.tw/2015.8(5).305.

Huang, YH. 2004. *Pavement analysis and design*. V. 2. Pearson Prentice Hall Upper Saddle River, NJ.

Van Huyssteen, CW, Turner, DP & Le Roux, PAL. 2013. Principles of soil classification and the future of the South African system. *South African Journal of Plant and Soil*. 30(1):23–32. doi.org/10.1080/02571862.2013.771752.

Hwayyis, K, Hassan, R & Fahey, MT. 2022. Factors affecting performance of sprayed seals in rural Victoria. *International Journal of Pavement Engineering*. 23(7):2278–2292. doi.org/10.1080/10298436.2020.1851030.

Ikechukwu, AF. 2018. Behaviour of unsaturated soils for road pavement structure under cyclic loading. Central University of Technology, Free State.

Ikechukwu, AF, Emeka, O & Hassan, MM. 2019. *Resilient Modulus Prediction of Subgrade Soil Using Dynamic Cone Penetrometer*. V. 1. Springer International Publishing. doi.org/10.1007/978-3-030-01941-9_6.

Indian Road Congress. 2012. *IRC 37: Guidelines for the design of flexible pavements (Third Revision)*. New Delhi-110 022.

Islam, KM, Gassman, S & Rahman, MM. 2020. Field and Laboratory Characterization of Subgrade Resilient Modulus for Pavement Mechanistic-Empirical Pavement Design

Guide Application. *Transportation Research Record*. 2674(8):921–930. doi.org/10.1177/0361198120926171.

Islam, M.N., Gnanendran, C.T. and Massoudi, M., 2019. Finite element simulations of an elasto-viscoplastic model for clay. Geosciences, 9(3), p.145.

Jagtap, PS & Nagrale, PP. 2013. Benefits of mechanistic approach for low volume rural roads. In: *Proceedings of Indian Geotechnical Conference, Roorkee*. 1–8.

Jain, S, Joshi, YP & Goliya, SS. 2013. Design of Rigid and Flexible Pavements by Various Methods & Their Cost Analysis of Each Method. *International Journal of Engineering Research and Applications*. 3(5):119–123.

Jameson, GW. 1996. *Origins of AUSTROADS design procedures for granular pavements (No. ARR292).*

Janoo, VC & Bayer II, JJ. 2001. The Effect of Aggregate Angularity on Base Course Performance. (September 2001).

Janoo, V, Bayer Jr, JJ & Benda, CC. 2004. Effect of aggregate angularity on base material properties. *Journal of materials in civil engineering*. 16(6):614–622.

Jawad, AA, Almuhanna, RR & Shaban, AM. 2020. Three-dimensional finite element analysis for determining subgrade reaction modulus of subgrade soils. *IOP Conference Series: Materials Science and Engineering*. 745(1). doi.org/10.1088/1757-899X/745/1/012137.

Ji, R, Siddiki, N, Nantung, T & Kim, D. 2014. Evaluation of resilient modulus of subgrade and base materials in Indiana and its implementation in MEPDG. *The Scientific World Journal*. 2014. doi.org/10.1155/2014/372838.

Jihanny, J, Subagio, BS, Yang, SH, Karsaman, RH & Hariyadi, ES. 2021. The Overload Impact on Design Life of Flexible Pavement. *International Journal of GEOMATE*. 20(78):65–72. doi.org/10.21660/2021.78.j2020.

Jin, D, Yin, L, Xin, K & You, Z. 2023. Comparison of asphalt emulsion-based chip seal and hot rubber asphalt-based chip seal. *Case Studies in Construction Materials*. 18(May):e02175. doi.org/10.1016/j.cscm.2023.e02175.

Jing, P, Nowamooz, H & Chazallon, C. 2017. Effect of anisotropy on the resilient behaviour of a granular material in low traffic pavement. *Materials*. 10(12). doi.org/10.3390/ma10121382.

Jooste, F. 2004. A Re-evaluation of some aspects of the Mechanistic-Empirical Design Approach. In: *The 8th Conference on Asphalt Pavements for Southern Africa (CAPSA'04)*. Available from: https://www.researchgate.net/publication/344603018.

Kakwagh, V V. 2018. The impact of roads on rural development in Katsina-Ala, Logo and Ukum local government areas of Benue state-Nigeria. *International Journal of Sociology and Anthropology Research*. 4(1):10–15.

Kannemeyer, L. 2013. Asset Management General Status Overview. *Presentation: SANRAL, South Africa*. 1–14.

Khajeh, A, Jamshidi Chenari, R & Payan, M. 2020. A Simple Review of Cemented Non-conventional Materials: Soil Composites. *Geotechnical and Geological Engineering*. 38(2):1019–1040. doi.org/10.1007/s10706-019-01090-x.

Khalid, U, Rehman, Z ur, Mujtaba, H & Farooq, K. 2022. 3D response surface modeling based in-situ assessment of physico-mechanical characteristics of alluvial soils using dynamic cone penetrometer. *Transportation Geotechnics*. 36(November 2021):100781. doi.org/10.1016/j.trgeo.2022.100781.

Kim, M. 2007. *Three-dimensional finite element analysis of flexible pavements considering nonlinear pavement foundation behavior*. University of Illinois at Urbana-Champaign.

Kim, D & Siddiki, NZ. (in press). Simplification of Resilient Modulus Testing for Subgrades. *Joint Transportation Research Program*. (February 2006):FHWA/IN/JTRP-2005/23.

Kleyn, EG, De Wet, LF & Savage, PF. 1989. Development of an equation for the strength-balance of road pavement structures. *Civil engineer in South Africa*. 31(2):45–50.

Kodippily, S, Henning, T & Ingham, JM. 2012. Detecting flushing of thin-sprayed seal pavements using pavement management data. *Journal of transportation engineering*.

138(5):665–673. doi.org/10.2307/3615019.

Kozicki, J, Niedostatkiewicz, M, Tejchman, J & Muhlhaus, HB. 2013. Discrete modelling results of a direct shear test for granular materials versus FE results. *Granular Matter*. 15(5):607–627. doi.org/10.1007/s10035-013-0423-y.

Kringos, N & Scarpas, A. 2008. Physical and mechanical moisture susceptibility of asphaltic mixtures. *International Journal of Solids and Structures*. 45(9):2671–2685. doi.org/10.1016/j.ijsolstr.2007.12.017.

Kumbargeri, Y, Boz, I, Kutay, ME & Heidelberg, A. 2020. A study on the effects of aggregate shape and percent embedment on chip seal performance via image-based finite element analysis. *International Journal of Pavement Engineering*. 21(8):1002–1011. doi.org/10.1080/10298436.2019.1654104.

Kumbargeri, YS, Kutay, ME & Boz, I. 2018. Effect of percent embedment on chip seal performance using fe modeling. *Advances in Materials and Pavement Performance Prediction - Proceedings of the International AM3P Conference, 2018*. (April):583–586. doi.org/10.1201/9780429457791-141.

Lakshmi, SM, priya, MR, K, S & N, U. 2019. Establishment of Correlation between CBR and Resilient Modulus of Subgrade. *International Journal of Civil Engineering*. 6(5):44–49. doi.org/10.14445/23488352/ijce-v6i5p107.

Lee, C, Kim, KS, Woo, W & Lee, W. 2014. Soil Stiffness Gauge (SSG) and Dynamic Cone Penetrometer (DCP) tests for estimating engineering properties of weathered sandy soils in Korea. *Engineering Geology*. 169:91–99. doi.org/10.1016/j.enggeo.2013.11.010.

Lekarp, F, Isacsson, U & Dawson, A. 2000. State of the art. I: Resilient response of unbound aggregates. *Journal of transportation engineering*. 126(1):66–75.

Li, D, Zhao, L, Cheng, X, Huang, F & Zuo, S. 2020. Active Stability Analysis of 3D Shallow Tunnel Face with Longitudinally Inclined Ground Surface Based on Nonlinear Mohr-Coulomb Failure Criterion. *International Journal of Geomechanics*. 20(11):1–12. doi.org/10.1061/(asce)gm.1943-5622.0001844.

Liu, Z, Gu, X, Ren, H, Wang, X & Dong, Q. 2022. Three-dimensional finite element

analysis for structural parameters of asphalt pavement: A combined laboratory and field accelerated testing approach. *Case Studies in Construction Materials*. 17(June):e01221. doi.org/10.1016/j.cscm.2022.e01221.

Livneh, M, Ishai, I & Livneh, NA. 1992. Automated DCP device versus manual DCP device. *Road and Transport Research*. 1(4).

Livneh, M, Ishai, I & Livneh, NA. 1995. Effect of vertical confinement on dynamic cone penetrometer strength values in pavement and subgrade evaluations. *Transportation Research Record*. (1473):1–8.

Mamatha, KH & Dinesh, S V. 2017. Resilient modulus of black cotton soil. *International Journal of Pavement Research and Technology*. 10(2):171–184. doi.org/10.1016/j.ijprt.2017.01.008.

Mamlouk, M & Mobasher, B. 2004. Cracking Resistance of Asphalt Rubber Mix Versus Hot-Mix Asphalt. *Road Materials and Pavement Design*. 5(4):435–451. doi.org/10.1080/14680629.2004.9689980.

Mathew, BS & Isaac, KP. 2014. doi.org/10.1080/10298436.2013.806807.

Mathur, U, Kumar, N, Pandey, TN & Choudhary, A. 2017. Study of Index Properties of the Soil. *Ijariie*. (3):656–661.

Merritt, DK, Lyon, C & Persaud, B. 2015. Evaluation of Pavement Safety Performance. *Federal Highway Administration Report FHWA-HRT-14-065*. 159.

Milne, TI. 2004. Towards a performance related seal design method for bitumen and modified road seal binders. University of Stellenbosch.

Mohammad, LN, Herath, A, Abu-Farsakh, MY, Gaspard, K & Gudishala, R. 2007. Prediction of Resilient Modulus of Cohesive Subgrade Soils from Dynamic Cone Penetrometer Test Parameters. *Journal of Materials in Civil Engineering*. 19(11):986–992. doi.org/10.1061/(asce)0899-1561(2007)19:11(986).

Mohammadi, SD, Nikoudel, MR, Rahimi, H & Khamehchiyan, M. 2008. Application of the Dynamic Cone Penetrometer (DCP) for determination of the engineering parameters of sandy soils. *Engineering Geology*. 101(3–4):195–203.

doi.org/10.1016/j.enggeo.2008.05.006.

Mostafa Hassan, M. 2018. Road Maintenance in Africa: Approaches and Perspectives. *E3S Web of Conferences*. 38. doi.org/10.1051/e3sconf/20183801005.

Mousavi, HS, Gabr, MA & Borden, RH. 2018. Resilient modulus prediction of soft low-plasticity Piedmont residual soil using dynamic cone penetrometer. *Journal of Rock Mechanics and Geotechnical Engineering*. 10(2):323–332. doi.org/10.1016/j.jrmge.2017.10.007.

Mukandila, E. 2016. Investigation of Rheological Response, Cohesion and Adhesion Fatigue Damage of Bituminous Road Seal Materials Investigation of Rheological Response, Cohesion and Adhesion Fatigue Damage of. University of Pretoria.

Nakamura, S, Bundervoet, T & Nuru, M. 2020. Rural roads, poverty, and resilience: Evidence from Ethiopia. *The Journal of Development Studies*. 56(10):1838–1855.

NCHRP. 2004. Guide for mechanistic empirical design of new and rehabilitated pavement structures. *NCHRP Report*.

Netterberg, F & Elsmere, D. 2015. Untreated aeolian sand base course for low-volume road proven by 50-year old road experiment. *Journal of the South African Institution of Civil Engineering*. 57(2):50–68. doi.org/10.17159/2309-8775/2015/v57n2a7.

Ngezahayo, E, Burrow, M & Ghataora, G. 2021. Calibration of the Simple Rainfall Simulator for Investigating Soil Erodibility in Unpaved Roads. *International Journal of Civil Infrastructure*. 4. doi.org/10.11159/ijci.2021.018.

Nguyen, BT & Mohajerani, A. 2012. Development of a New Dynamic Lightweight Penetrometer for the Determination of Mechanical Properties of Fine-Grained Soils. *Journal of Civil Engineering and Architecture*. 6(11). doi.org/10.17265/1934-7359/2012.10.020.

Nguyen, BT & Mohajerani, A. 2016. Resilient modulus of fine-grained soil and a simple testing and calculation method for determining an average resilient modulus value for pavement design. *Transportation Geotechnics*. 7:59–70. doi.org/10.1016/j.trgeo.2016.05.001.

Nguyen, BT & Mohajerani, A. 2017. Possible estimation of resilient modulus of fine-grained soils using a dynamic lightweight cone penetrometer. *International Journal of Pavement Engineering*. 18(6):473–484. doi.org/10.1080/10298436.2015.1095899.

Nkomo, SL, Desai, S & Peerbhay, K. 2016. Assessing the conditions of rural road networks in South Africa using visual observations and field-based manual measurements: A case study of four rural communities in Kwa-Zulu Natal. *Review of Social Sciences*. 1(2):42–55. doi.org/10.18533/rss.v1i2.24.

Notash, HN, Dabiri, R, Hajialilue Bonab, M, Khodadadi, L & Behrouz Sarand, F. 2022. A finite element modeling of drained triaxial test on loose sand using different constitutive models. *AUT Journal of Civil Engineering*. 6(3):339–358. doi.org/10.22060/ajce.2023.22031.5817.

Obe, RKD, de Brito, J, Silva, R V & Lye, CQ. 2019. Use of Recycled Aggregates in Geotechnical Applications. *Sustainable Construction Materials: Recycled Aggregates*. 419–450.

Onyelowe, KC, Ebid, AM, Ramani Sujatha, E, Fazel-Mojtahedi, F, Golaghaei-Darzi, A, Kontoni, DPN & Nooralddin-Othman, N. 2023. Extensive overview of soil constitutive relations and applications for geotechnical engineering problems. *Heliyon*. 9(3):e14465. doi.org/10.1016/j.heliyon.2023.e14465.

Otto, A, Rolt, J & Mukura, K. 2020. The impact of drainage on the performance of low volume sealed roads. *Sustainability (Switzerland)*. 12(15). doi.org/10.3390/su12156101.

Ozdemir, U, Kutay, ME, Hibner, D, Lanotte, M & Kumbargeri, YS. 2018. Quantification of Aggregate Embedment in Chip Seals Using Image Processing. *Journal of Transportation Engineering, Part B: Pavements*. 144(4):04018047. doi.org/10.1061/jpeodx.0000068.

Ozel, MR & Mohajerani, A. 2011. Prediction of subgrade resilient modulus for flexible pavement design. *Scientific Research and Essays*. 6(21):4567–4576. doi.org/10.5897/sre11.846.

Paige-green, P. 2007. Local Government Note: New perspectives of unsealed roads

in South Africa. *REAAA (NZ) Low Volume Roads Workshop*. 16(3):18–20.

Paige-green, P. 2015. An alternative philosophy on the deterioration and design of low volume roads. Available from: https://assets.publishing.service.gov.uk/media/57a09dcde5274a31e0001a64/61280-PaigeGreen_2015_AlternativePhilosophyon_DeteriorationandDesignLVR_AFCAP_CAPSA_150714.pdf.

Paige-Green, P. 2003. Strength and behavior of materials for low-volume roads as affected by moisture and density. *Transportation research record*. 1819(1):104–109.

Paige-Green, P. 2005. Practical aspects of low cost sealing of roads. 1–11. Available from: http://www.ssatp.org/sites/ssatp/files/publications/HTML/LVSR/English/Miscellaneous/02-Paige-Green-CSIR-LowCostSeals-2005.pdf.

Paige-Green, P. 2011. Applying the dynamic cone penetrometer (DCP) design method to low volume roads. 422–430. Available from: http://researchspace.csir.co.za/dspace/handle/10204/5271.

Paige-Green, P & Pinard, MI. 2012. Optimum Design of Sustainable Sealed Low Volume Roads Using the Dynamic Cone. In: *25th ARRB Conference – Shaping the future: Linking policy, research and outcomes*. 1–11.

Paige-Green, P & Van Zyl, GD. 2019. A Review of the DCP-DN Pavement Design Method for Low Volume Sealed Roads: Development and Applications. *Journal of Transportation Technologies*. 09(04):397–422. doi.org/10.4236/jtts.2019.94025.

Papagiannakis, AT & Masad, EA. 2012. *Pavement Design and Materials*. John Wiley & Sons. doi.org/10.1002/9780470259924.

Park, JS & Park, D. 2017. Vertical bearing capacity of bucket foundation in sand overlying clay. *Ocean Engineering*. 134(December 2016):62–76. doi.org/10.1016/j.oceaneng.2017.02.015.

Parker, F, Hammons, M & Hall, J. 1998. Development of an automated dynamic cone penetrometer for evaluating soils and pavement materials. *Road and Transport Research*.

Paul, S, Biswas, PP, Mondal, GC & Sahis, MK. 2024. Mechanistic-Empirical Design of Low Volume Flexible Road Pavement by Limiting Vertical Interface Stress and Strain on Subgrade. 482–491. doi.org/10.1007/978-3-031-63588-5_46.

Pavement Interactive. 2024. *Bituminous Surface Treatments*. Available from: https://pavementinteractive.org/ [Accessed 12 June 2023].

Peddaiah, S, Burman, A & Sreedeep, S. 2018. Experimental Study on Effect of Waste Plastic Bottle Strips in Soil Improvement. *Geotechnical and Geological Engineering*. 36(5):2907–2920. doi.org/10.1007/s10706-018-0512-0.

Peng, Y & He, Y. 2009. Structural characteristics of cement-stabilized soil bases with 3D finite element method. *Frontiers of Architecture and Civil Engineering in China*. 3(4):428–434. doi.org/10.1007/s11709-009-0059-5.

Pezo, R, Nazarian, S & Picornell, M. 1996. An Approach to Relate Laboratory and Field Moduli of Base Materials. (July).

Pinard, MI & van Zyl, G. 2019. *Evaluation of Cost-Effectiveness and Value-for-Money of DCP-DN Pavement Design Method for Low-Volume Roads in Comparison with Conventional Designs*.

Pinard, M, Paige-Green, P, Hongve, J & Mukandila, E. 2021. A Proposed Framework for Optimised Utilisation of Materials for Low Volume Roads Using the Dynamic Cone Penetrometer. *Journal of Transportation Technologies*. 11(01):14–36. doi.org/10.4236/jtts.2021.111002.

Pinard, MI, Ellis, SD, Eriksson, CH, Johansen, R, Toole, T, Beger, R, Gumbie, ME, Lotter, HJS, et al. 2003. *SADC Guideline on Low-Volume Sealed Roads*. V. 56. Gaborone: Southern Africa Transport Communications Commission (SATCC) and Southern African Development Community (SADC). doi.org/10.1016/S0007-1226(03)00027-4.

Pinard, MI, Paige-Green, P & Hongve, J. 2015. Developments in low volume roads technology: challenging conventional paradigms. In: *Asphalt Pavements for Southern Africa (CAPSA15), 11th, 2015,*. Sun City, South Africa. 12p. Available from: https://trid.trb.org/view/1404854.

Du Plessis, L & Paige-Green, P. 2009. THE USE AND INTERPRETATION OF THE DYNAMIC CONE PENETROMETER (DCP) TEST P Paige-Green and L Du Plessis CSIR Built Environment Pretoria SEPTEMBER 2009. (September).

Du Plessis, L, Kilian, A & Mngaza, K. 2014. Ultra-Thin Reinforced Concrete Pavements (UTCRP): Addressing the design issues. *33rd Southern African Transport Conference*. (July):179–190.

Pooni, J, Robert, D, Giustozzi, F, Gunasekara, C & Setunge, S. 2022. A review on soil stabilisation of unsealed road pavements from an Australian perspective. *Road Materials and Pavement Design*. doi.org/10.1080/14680629.2022.2060122.

Praticò, FG, Vaiana, R & Iuele, T. 2015. Macrotexture modeling and experimental validation for pavement surface treatments. *Construction and Building Materials*. 95:658–666. doi.org/10.1016/j.conbuildmat.2015.07.061.

Praticò, FG, Vaiana, R & Iuele, T. 2016. Surface performance characterization of single-layer surface dressing: A macrotexture prediction model. *RILEM Bookseries*. 11:459–470. doi.org/10.1007/978-94-017-7342-3_37.

La Ragione, L, Prantil, VC & Sharma, I. 2008. A simplified model for inelastic behavior of an idealized granular material. *International Journal of Plasticity*. 24(1):168–189. doi.org/10.1016/j.ijplas.2007.06.001.

Rahim, AM. 2005. Subgrade soil index properties to estimate resilient modulus for pavement design. *International Journal of Pavement Engineering*. 6(3):163–169.

Rahim, AM & George, KP. 2002. Automated dynamic cone penetrometer for subgrade resilient modulus characterization. *Transportation research record*. 1806(1):70–77.

Rahim, AM & George, KP. 2004. Subgrade soil index properties to estimate resilient modulus. In: *CD-ROM of Transportation Research Board Annual Meeting*.

Rahman, MT, Mahmud, K & Ahsan, S. 2011. Stress-Strain Characteristics of Flexible Pavement by Finite Element Method. *International Journal of Civil and Structural Engineering*. 2(September 2011):233–240.

Rao, C, Titus-Glover, L, Bhattacharya, B, Darter, MI, Stanley, M, Quintus & Von, HL.

2012. *Estimation of key PCC, base, subbase, and pavement engineering properties from routine tests and physical characteristics.*

Rensburg, J Van & Krygsman, S. 2020. Funding for roads in South Africa: Understanding the principles of fair and efficient road user charges. *Transportation Research Procedia*. 48(2019):1835–1847. doi.org/10.1016/j.trpro.2020.08.218.

Riverson, J, Gaviria, J & Thriscutt, S. 1991. *Rural roads in sub-Saharan Africa: lessons from World Bank experience*.

Roads and Transportation Association of Canada. 1986. *Manual of geometric design standards for Canadian roads*. Roads and Transportation Association of Canada.

Roads Authority Malawi. 2020. *Low Volume Roads Manual; Volumes 1: Pavement Design.* V. 1.

Robert, DJ. 2017. A Modified Mohr-Coulomb Model to Simulate the Behavior of Pipelines in Unsaturated Soils. *Computers and Geotechnics*. 91:146–160. doi.org/10.1016/j.compgeo.2017.07.004.

Robertson, P. 2012. Interpretation of In-situ Tests - Some Insights. *Proceedings of the Fourth International Conference on Site Characterization*. 1–22.

Rodriguez-Roa, F. 2003. Observed and predicted behavior of Maipo River sand. *Soils and foundations*. 43(5):1–11.

Rojimol, J & Umashankar, B. 2022. Three-Dimensional Analysis of Geogrid Reinforced Flexible Pavement Using Finite Difference Program Flac3D. *International Journal of GEOMATE*. 22(92):41–47. doi.org/10.21660/2022.92.1720.

Roy, S. & Bhalla, SK. 2017. Role of Geotechnical Properties of Soil on Civil Engineering Structures. *Resources and Environment*. 7(4):103–109. doi.org/10.5923/j.re.20170704.03.

Roy, T, Chattopadhyay, B & Roy, S. 2010. California bearing ratio, evaluation, and estimation: a study on comparison. In: *Proceedings of the Indian Geotechnical Conference*. 19–22. Available from: http://gndec.ac.in/~igs/ldh/conf/2010/articles/005.pdf.

Sadek, MA, Chen, Y & Liu, J. 2011. Simulating shear behavior of a sandy soil under different soil conditions. *Journal of Terramechanics*. 48(6):451–458. doi.org/10.1016/j.jterra.2011.09.006.

Sagar, CP, Badiger, M, Mamatha, KH & Dinesh, S V. 2022. Prediction of CBR using dynamic cone penetrometer index. *Materials Today: Proceedings*. 60:223–228. doi.org/10.1016/j.matpr.2021.12.467.

Sahis, MK & Biswas, PP. 2021. Optimization of bituminous pavement thickness using mechanistic-empirical strain-based design approach. *Civil Engineering Journal (Iran)*. 7(5):804–815. doi.org/10.28991/cej-2021-03091691.

Sahoo, UC & Reddy, KS. 2010. Effect of nonlinearity in granular layer on critical pavement responses of low volume roads. *International Journal of Pavement Research and Technology*. 3(6):320–325.

Salgado, R & Yoon, S. 2003. Dynamic cone penetration test (DCPT) for subgrade assessment. *Joint Transportation Research Program*. (February):108. doi.org/10.5703/1288284313196.This.

Sandberg, U, Kragh, J, Goubert, L, Bendtsen, H, Bergiers, A, Biligiri, KP, Karlsson, R, Nielsen, E, et al. 2011. Optimization of thin asphalt layers - State-of-the-Art Review. *Era-Net Road*. 1(Final Version):140. Available from: http://www.diva-portal.org/smash/get/diva2:674027/FULLTEXT02.pdf.

Sanchez, L.H., 2021. Probability of failure analysis in flexible pavements through the reliability concept (Doctoral dissertation, Universidade de São Paulo).

Sargand, S., Green, R., Russ, A., Buss, A. & Guirguis, M.I.N.A.S. 2023. Best Practices for Chip Sealing Low-Volume Roads in Ohio. *Transportation Research Circular*, 69-95.

Sargand, S, Khoury, I, Gray, J & Al-Jhayyish, A. 2014. Incorporating Chemical Stabilization of the Subgrade in Pavement Design and Construction Practices (Final Report No. FHWA/OH-2014/12). (October).

Saudy, M, Breakah, T, El-Badawy, S & Khedr, S. 2021. Development of a flexible pavement design catalogue based on mechanistic–empirical pavement design

approach: Egyptian case study. *Innovative Infrastructure Solutions*. 6(4):1–18. doi.org/10.1007/s41062-021-00573-2.

Scala, AJ. 1985. Simple methods of flexible pavement design using cone penetrometers. In: *Golden Jubilee of the International Society for Soil Mechanics and Foundation Engineering: Commemorative Volume*. Institution of Engineers, Australia Barton, ACT. 1–12.

Selsal, Z, Karakas, AS & Sayin, B. 2022. Effect of pavement thickness on stress distribution in asphalt pavements under traffic loads. *Case Studies in Construction Materials*. 16(February):e01107. doi.org/10.1016/j.cscm.2022.e01107.

Shafabakhsh, GA, Motamedi, M & Family, A. 2013. Influence of asphalt concrete thickness on settlement of flexible pavements. *Electronic Journal of Geotechnical Engineering*. 18 C:473–483.

Sinha, AK, Chandra, S & Kumar, P. 2014. Finite element analysis of flexible pavement with different subbase materials. *Indian Highways*. 42(2).

Sivakugan, N, Das, BM, Lovisa, J & Patra, CR. 2014. Determination of c and Φ of rocks from indirect tensile strength and uniaxial compression tests. *International Journal of Geotechnical Engineering*. 8(1):59–65. doi.org/10.1179/1938636213Z.00000000053.

Song, X, Wang, K & Bate, B. 2018. A hierarchical thermo-hydro-plastic constitutive model for unsaturated soils and its numerical implementation. *International Journal for Numerical and Analytical Methods in Geomechanics*. 42(15):1785–1805. doi.org/10.1002/nag.2811.

South African Institution of Civil Engineering (SAICE). 2022. *SAICE 2022 Infrastructure Report Card for South Africa:* Available from: http://saice.org.za/downloads/saice-reportcard.pdf.

South African National Roads Agency Ltd. 2013. *South African Pavement Engineering Manual Chapter 10 - Pavement Design*. Available from: www.nra.co.za.

Springer Nature Limited. 2021. Angola. In: *The Statesman's Yearbook 2021: The Politics, Cultures and Economies of the World*. London: Palgrave Macmillan UK. 98–181

102. doi.org/10.1057/978-1-349-95972-3_15.

Stefanow, D & Dudziński, PA. 2021. Soil shear strength determination methods – State of the art. *Soil and Tillage Research*. 208(February 2020). doi.org/10.1016/j.still.2020.104881.

Steyn, WJ, Maina, J & Repsold, A. 2013. Comparison of isotropic and cross-anisotropic analysis of pavement structures. *International Journal of Pavement Research and Technology*. 6(4):336–343. doi.org/10.6135/ijprt.org.tw/2013.6(4).336.

Sukumaran, B. 2004. *Three dimensional finite element modeling of flexible pavements*.

Sukumaran, B, Kyatham, V, Shah, A & Sheth, D. 2002. Suitability of using California bearing ratio test to predict resilient modulus. In: *Proceedings: Federal aviation administration airport technology transfer conference*. 9.

Tapia Romero, MA, Dehonor Gomez, M & Lugo Uribe, LE. 2020. Prony series calculation for viscoelastic behavior modeling of structural adhesives from DMA data. *Ingeniería Investigación y Tecnología*. 21(2):1–10. doi.org/10.22201/fi.25940732e.2020.21n2.014.

Taskiran, T. 2010. Prediction of California bearing ratio (CBR) of fine grained soils by AI methods. *Advances in Engineering Software*. 41(6):886–892. doi.org/10.1016/j.advengsoft.2010.01.003.

Terefe, AL, Lorenzo, P & Bedi, A. 2012. Graduate School of Development Studies Impact of Road on Rural Poverty Evidence Form Fifteen Rural Villages in Ethiopia. Available from: https://thesis.eur.nl/.../Lulit Akilu Terefe_Final_Masters Research Paper.

Theyse, HL & Muthen, M. 2000. Pavement analysis and design software (pads) based on the South African mechanistic-empirical design method. In: *SATC*.

Theyse, H., De Beer, M & Rust, FC. 1996. Overview of South African Mechanistic. *Transportation Research Record*. (1):6–17.

Theyse, HL, de Beer, M, Maina, JW & Kannemeyer, L. 2011. Interim Revision of the

South African Mechanistic-Empirical Pavement. In: *Conference on Asphalt Pavements for Southern Africa (CAPSA11)*. 1–20.

Tiliouine, B & Sandjak, K. 2014. Numerical simulation of granular materials behaviour for unbound base layers used in Algerian pavement structures. *International Journal of Civil & Structural Engineering*. 4(3):419–429.

TMH1. 1986. *Standard methods of testing road construction materials. Method A6.*

Toohey, NM, Mooney, MA & Bearce, RG. 2013. Relationship between Resilient Modulus and Unconfined Compressive Strength for Lime-Stabilized Soils. *Journal of Geotechnical and Geoenvironmental Engineering*. 139(11):1982–1985. doi.org/10.1061/(asce)gt.1943-5606.0000925.

TRH 20. 2009. *Draft TRH 20 Unsealed roads: design, construction and maintenance*.

Tsige, D, Korita, M & Beyene, A. 2022. Deformation analysis of cement modified soft clay soil using finite element method (FEM). *Heliyon*. 8(6):e09613. doi.org/10.1016/j.heliyon.2022.e09613.

Usman, AB. 2014. Analysis of Condition of Rural Road Transport in Kwara State, Nigeria. *European Scientific Journal*. 10(5):1857–7881.

Vakili, AH, Salimi, M & Shamsi, M. 2021. Application of the dynamic cone penetrometer test for determining the geotechnical characteristics of marl soils treated by lime. *Heliyon*. 7(9):e08062. doi.org/10.1016/j.heliyon.2021.e08062.

Vásquez-Varela, LR & García-Orozco, FJ. 2020. An overview of asphalt pavement design for streets and roads. *Revista Facultad de Ingenieria*. (98):10–26. doi.org/10.17533/udea.redin.20200367.

Vaughan, K. 2014. *Inverted Pavements.*

Walubita, L.F. and van de Ven, MF. 2009. Stresses and Strains in Pavements. In: *South African Transport Conference Organised by: Conference Planners, "Action in Transport for the New Millennium."* 1–8.

Wang, J. 2001. Three-Dimensional Finite Element Analysis of Flexible Pavements. University of Maine. Available from:

http://www.library.umaine.edu/theses/pdf/WangJ2001.pdf.

Weinert, HH. 1980. *Natural road construction materials of Southern Africa*. CSIR.

Wondemu, KA & Weiss, J. 2012. Rural roads and development: Evidence from Ethiopia. *European Journal of Transport and Infrastructure Research*. 12(4):417–439. doi.org/10.18757/ejtir.2012.12.4.2977.

Xiangjing, H & Jianqing, J. 2010. Finite element analysis of triaxial tests of a new composite reinforced soil. In: *2010 International Conference on Intelligent Computation Technology and Automation, ICICTA 2010*. V. 2. IEEE. 319–322. doi.org/10.1109/ICICTA.2010.67.

Yan, K, Xu, H & Shen, G. 2014. Novel approach to resilient modulus using routine subgrade soil properties. *International Journal of Geomechanics*. 14(6):4014025.

Yetkin Yildirim, PE. 2015. Texas Considers Ultra-Thin HMA Alternatives to Seal Coats. *Pavement Preservation Journal*. 8(1).

Yin, H. 2013. The Impact of Strain Gage Instrumentation on Localized Strain Responses in Asphalt Concrete Pavements. *International Journal of Pavement Research and Technology*. 6(3).

Yu, HS & Carter, JP. 2002. Rigorous Similarity Solutions for Cavity Expansion in Cohesive-Frictional Soils. *International Journal of Geomechanics*. 2(2):233–258. doi.org/10.1061/(asce)1532-3641(2002)2:2(233).

Zafar, R, Nassar, W & Elbella, A. 2005. Interaction Between Pavement Instrumentation and Hot-Mix-Asphalt in Flexible Pavements. *Engineering*. 10(1):49–55.

Zhalehjoo, N, Tolooiyan, A, Mackay, R & Bodin, D. 2018. The effect of instrumentation on the determination of the resilient modulus of unbound granular materials using advanced repeated load triaxial testing. *Transportation Geotechnics*. 14:190–201. doi.org/10.1016/j.trgeo.2018.01.003.

Zheng, N, Bi, J, Dong, S, Lei, J, He, Y, Cui, Z & Chen, LG. 2022. Testing and evaluation for long-term skid resistance of asphalt pavement composite seal using

texture characteristics. *Construction and Building Materials*. 356(January):129241. doi.org/10.1016/j.conbuildmat.2022.129241.

Zhou, Y, Peng, Z, Wang, J, Wei, J, Liu, H, Wang, D & Li, J. 2024. A review on adhesion behavior of chip seal pavement and aggregate. *Journal of Traffic and Transportation Engineering (English Edition)*. 11(3):441–466. doi.org/10.1016/j.jtte.2023.11.003.

Zumrawi, MME. 2014. Prediction of In-situ CBR of Subgrade Cohesive Soils from Dynamic Cone Penetrometer and Soil Properties. *International Journal of Engineering and Technology*. 6(5):439–442. doi.org/10.7763/ijet.2014.v6.738.

Zumrawi, M & Awad, M. 2017. Estimation of Subgrade Resilient Modulus from Soil Index Properties. *World Academy of Science, Engineering and Technology, International Science Index 129, International Journal of Environmental, Chemical, Ecological, Geological and Geophysical Engineering*. 11(9):830–836.

van Zyl, GD, Visser, AT & du Plessis, JA. 1995. Guidelines for Structural Design of Low-Volume Rural Roads in Southern Africa. In: *6th Int Conf on Low Volume Roads, Minneapolis, Minnesota*. 108–117.

Van Zyl, G, Beukes, M, Bredenhann, S, Fourie, G & Greyling, A. 2021. *MANUAL 40: Design and Construction of Surface Treatments Manual 40/TRH3 Second Edition-February 2021*.

Appendices

Appendix A

SUMMARISED DESIGN PROCEDURE

CBR Summary Design Procedure

Step 1.

Determine the expected traffic volume. This is obtained from traffic survey data.

Step 2.

Determine the cumulative number of vehicles expected to use the road over its design lifetime.

Step 3.

Determine the “equivalent number of standard axles” by multiplying the different axle loads by suitable equivalency factors. This yields the cumulative number of standard axles.

Step 4.

Determine the subbase thickness. For this purpose, the CBR of the subgrade is determined, and by entering the graph along the horizontal scales with the appropriate number of standard axles and the subgrade CBR value, the subbase thickness is read off.

Step 5.

Determine the base and surfacing thicknesses. The thickness of the base-course will depend on the type of material used, and this is also obtained from the appropriate curves.

AASHTO 1993 Summary Design Procedure

Determine the required structural number (SN)

Step 1.

Estimate the future traffic, W18.

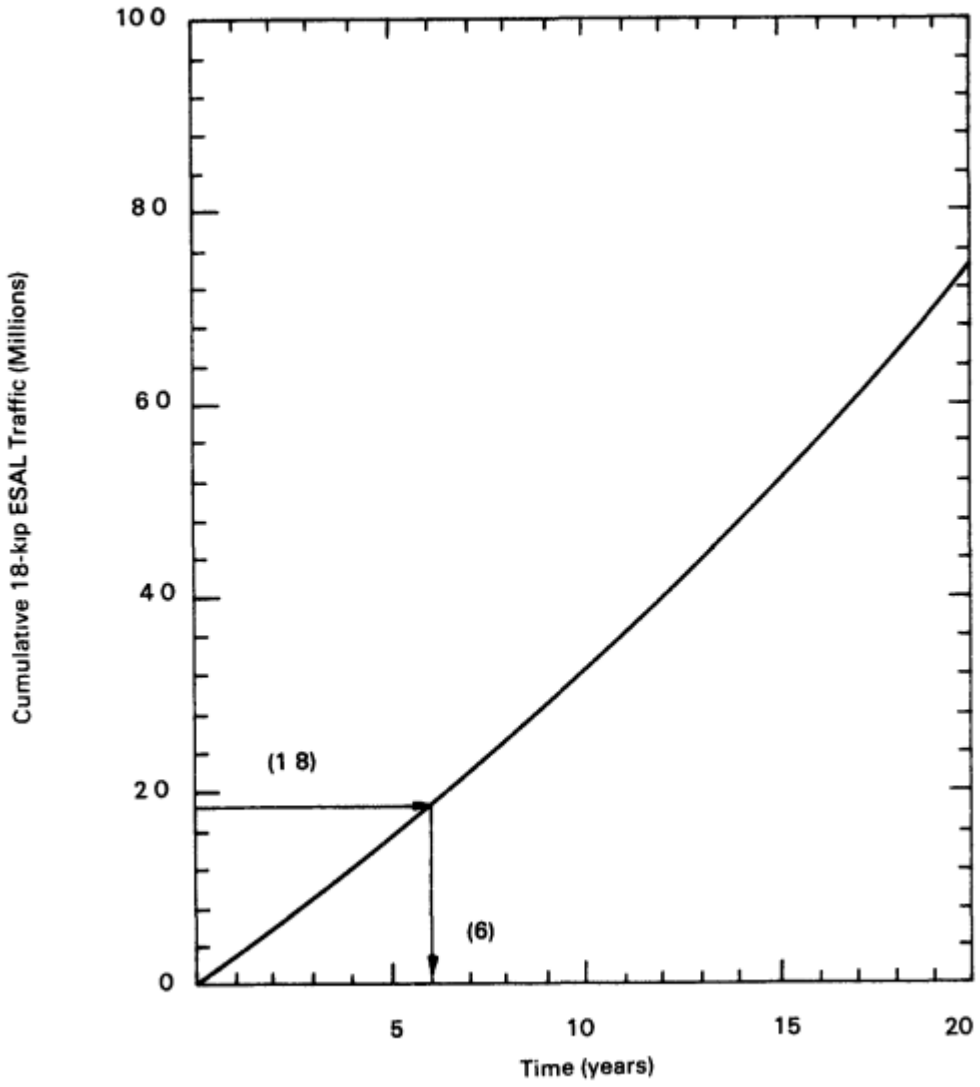

Figure 2.1. Example Plot of Cumulative 18-kip ESAL Traffic Versus Time

Step 2.

Ascertain the reliability (R)

Step 3.

The overall standard deviation (So) is 0.35 for rigid pavements and 0.45 for flexible pavements.

Step 4.

Join the two plots above and project to intercept the turning line, TL1.

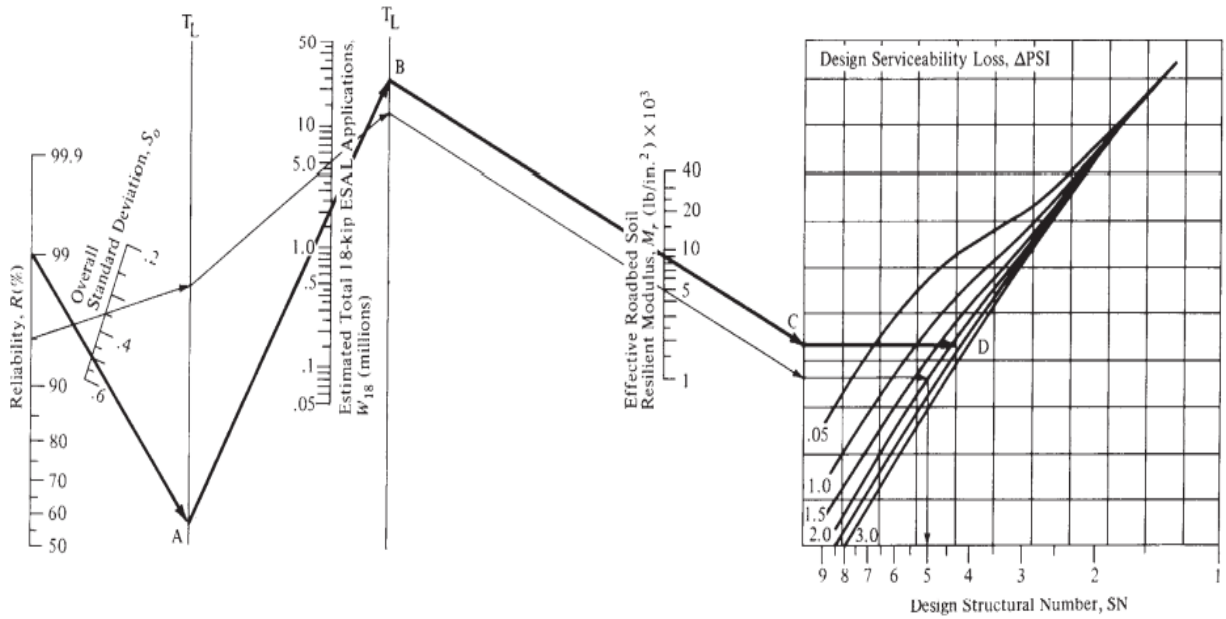

Figure A- 1 Design chart for flexible pavements based on the use of mean values for each input

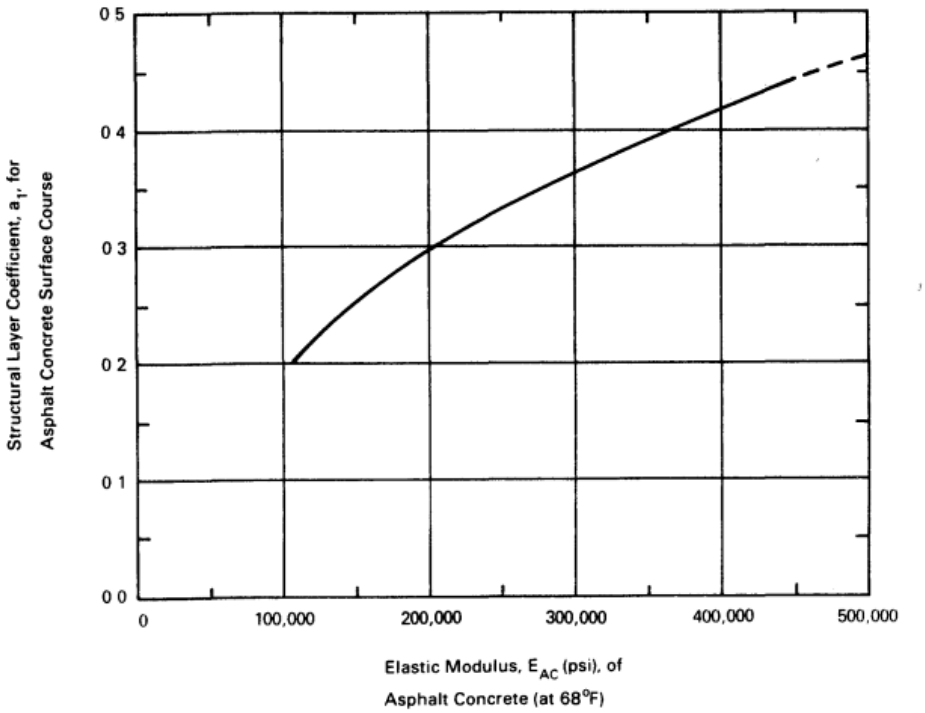

Figure A- 2 Chart for estimating the structural layer coefficient of dense-graded asphalt concrete on the basis of the elastic (resilient) modulus

Step 5.

A plot of the traffic nomograph–cumulative E80s during the analysis period.

Step 6.

TL1 is projected to intercept the traffic on the nomograph and project to join the turning line TL2.

Step 7.

Ascertain the effective, resilient modulus MR.

Step 8.

Join TL2 to intercept the Mr value and project to locate the PSI.

Step 9.

Read horizontally and, locate the PSI and read down vertically to determine the structural number (SN)

Appendix B1

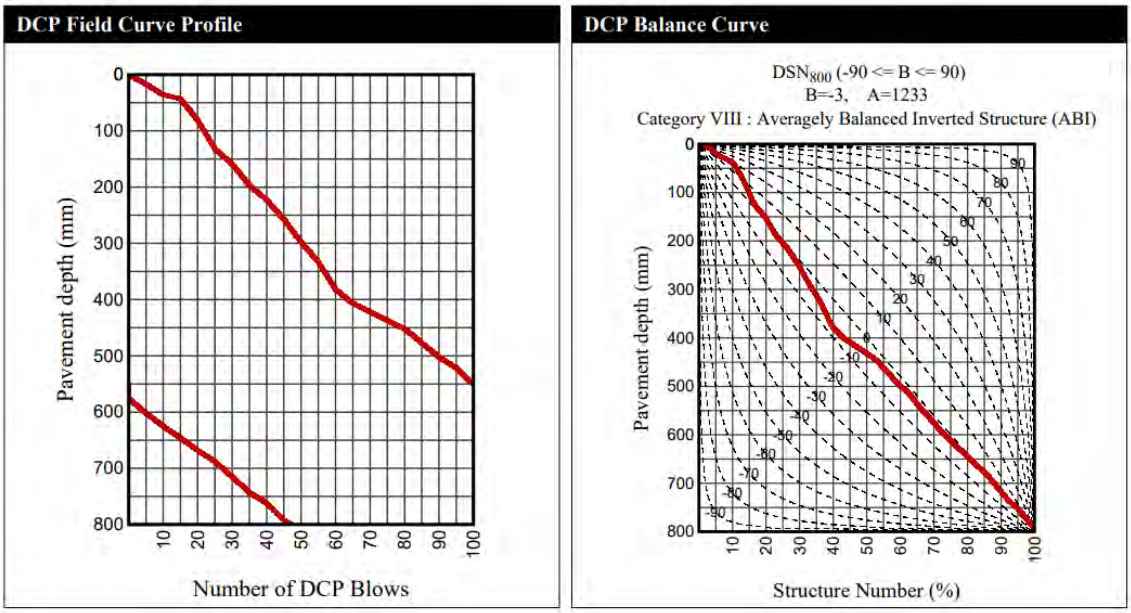

Figure B1- 1 Penetration against the number of blows and the DSN curve for NCS3

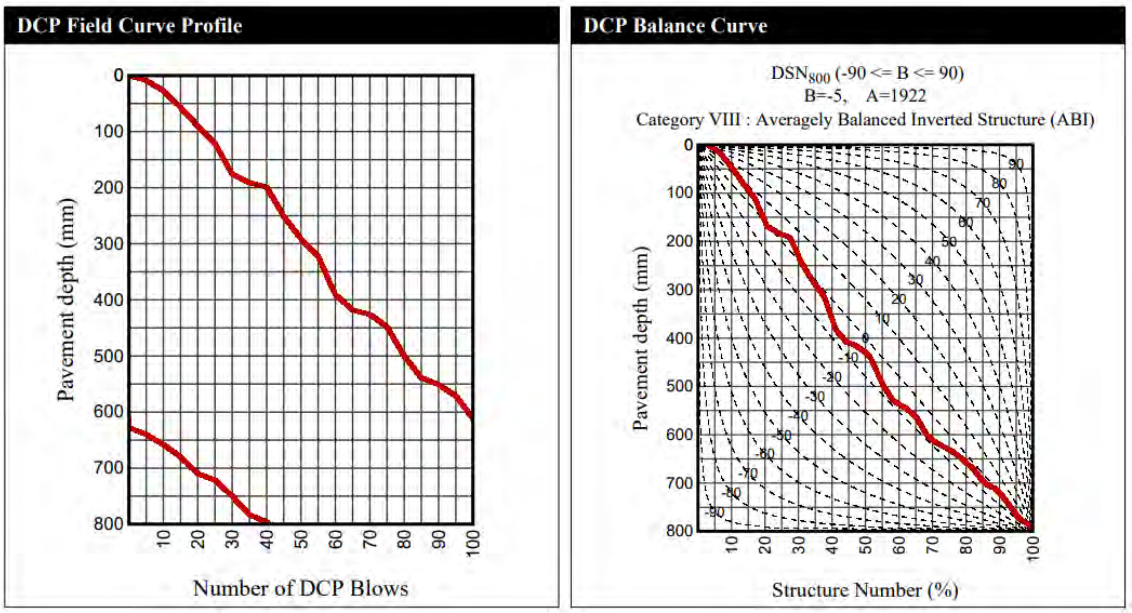

Figure B1- 2 Penetration against the number of blows and the DSN curve for NCS4

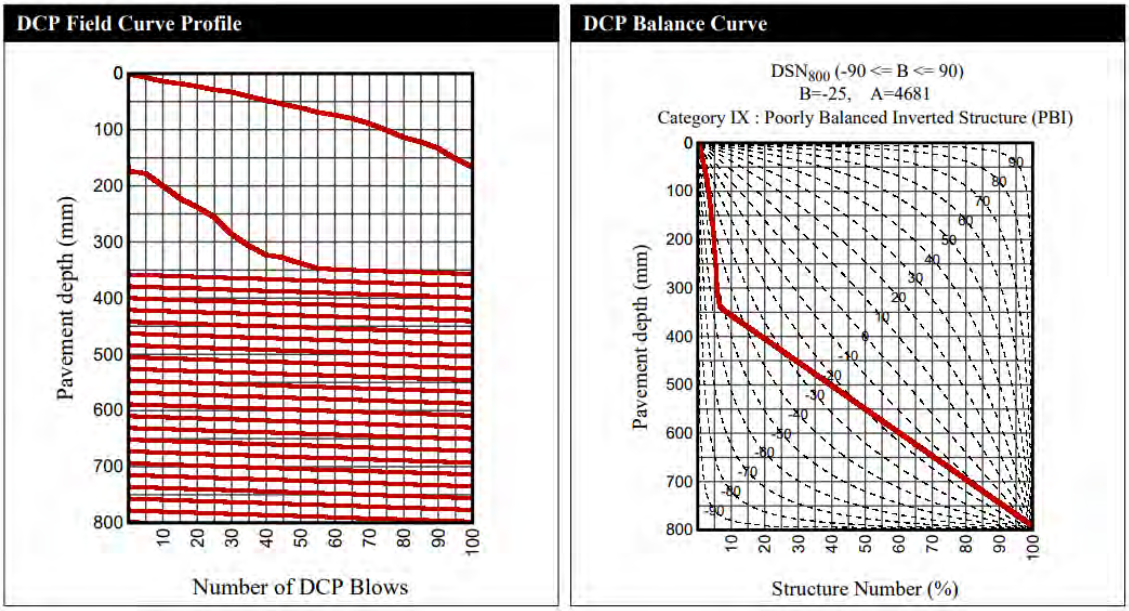

Figure B1- 3 Penetration against the number of blows and the DSN curve for NCS5

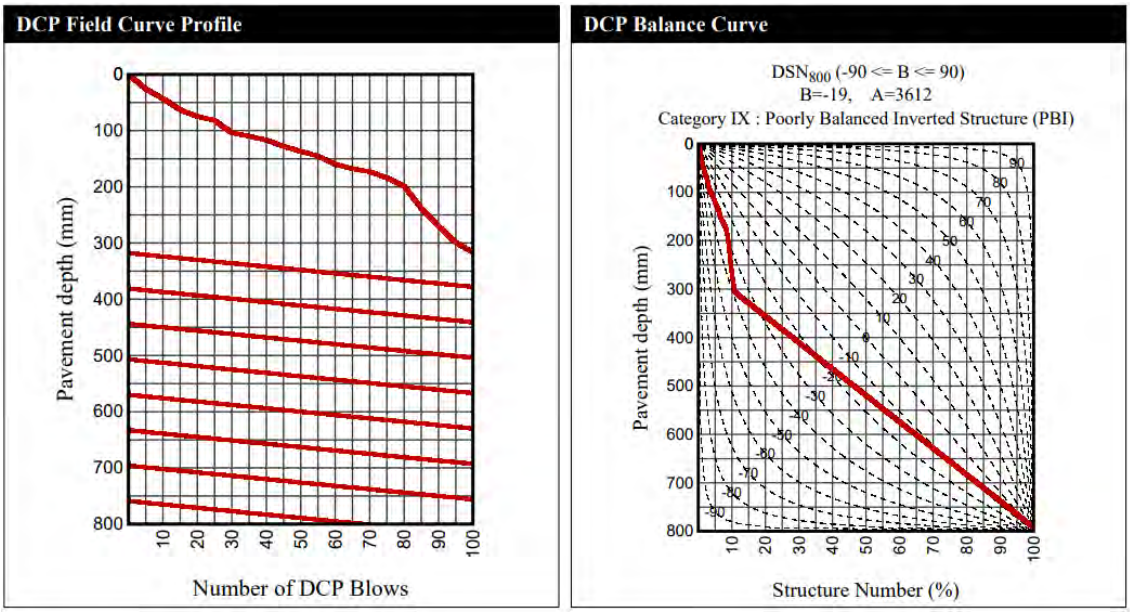

Figure B1- 4 Penetration against the number of blows and the DSN curve for NCS6

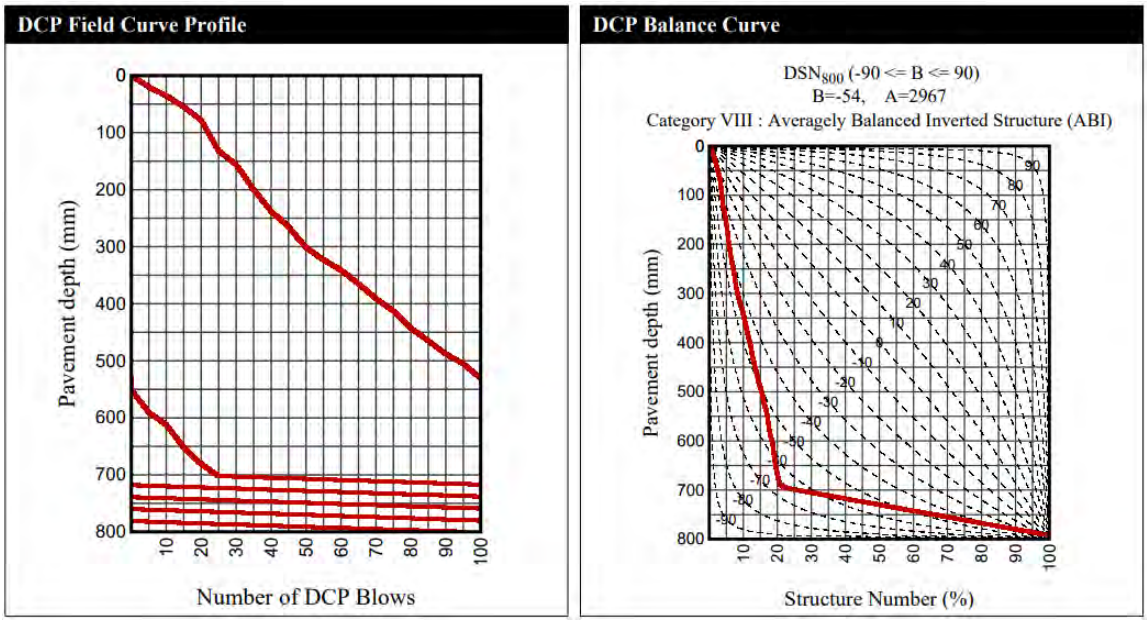

Figure B1- 5 Penetration against no blows and the DSN curve for NCS7

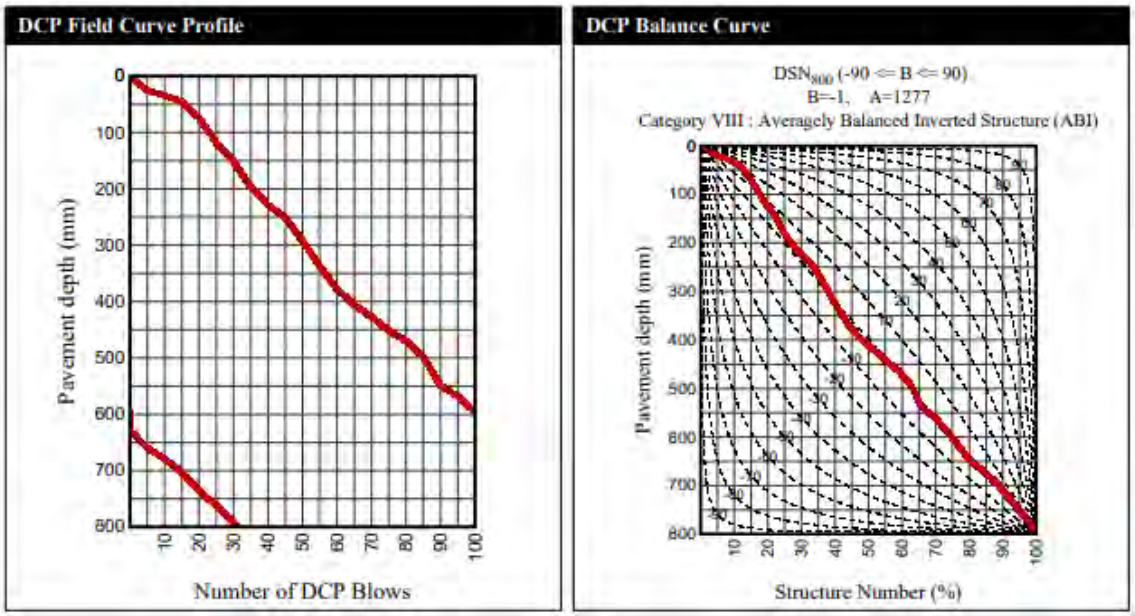

Figure B1- 6 Penetration against the number of blows and the DSN curve for NCS8

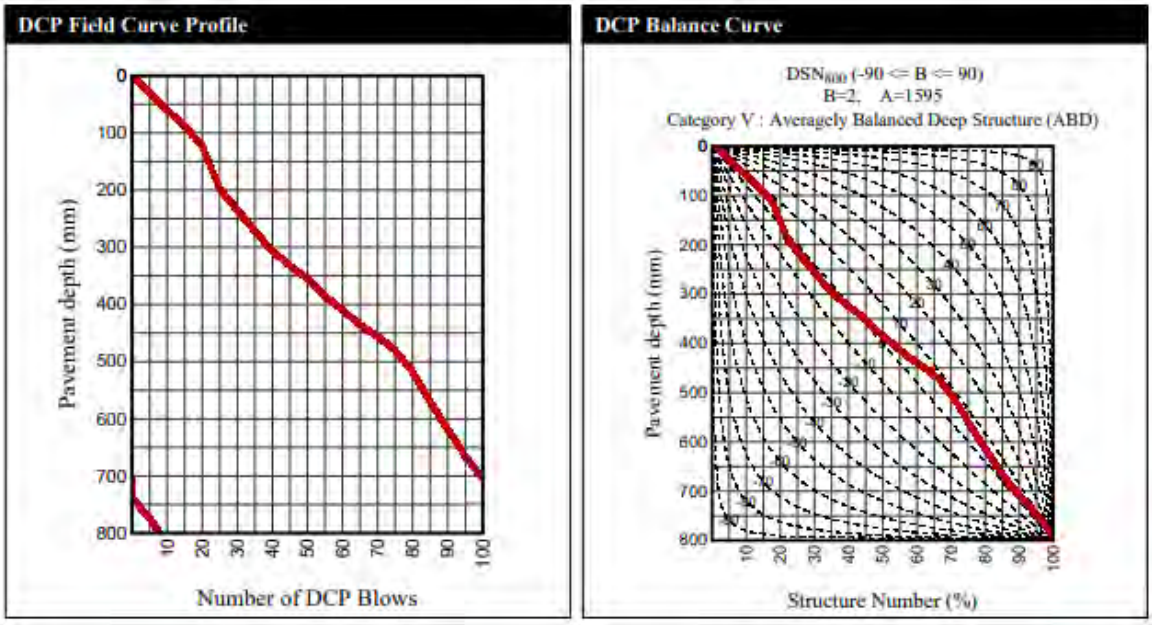

Figure B1- 7 Penetration against the number of blows and the DSN curve for KZNS3

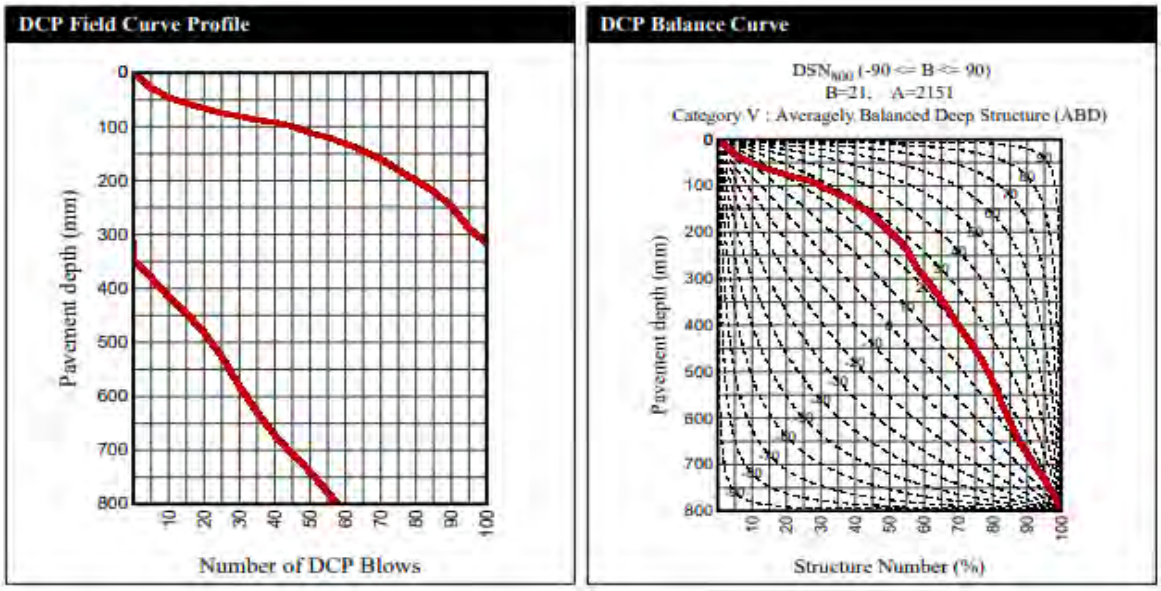

Figure B1- 8 Penetration against the number of blows and the DSN curve for KZNS4

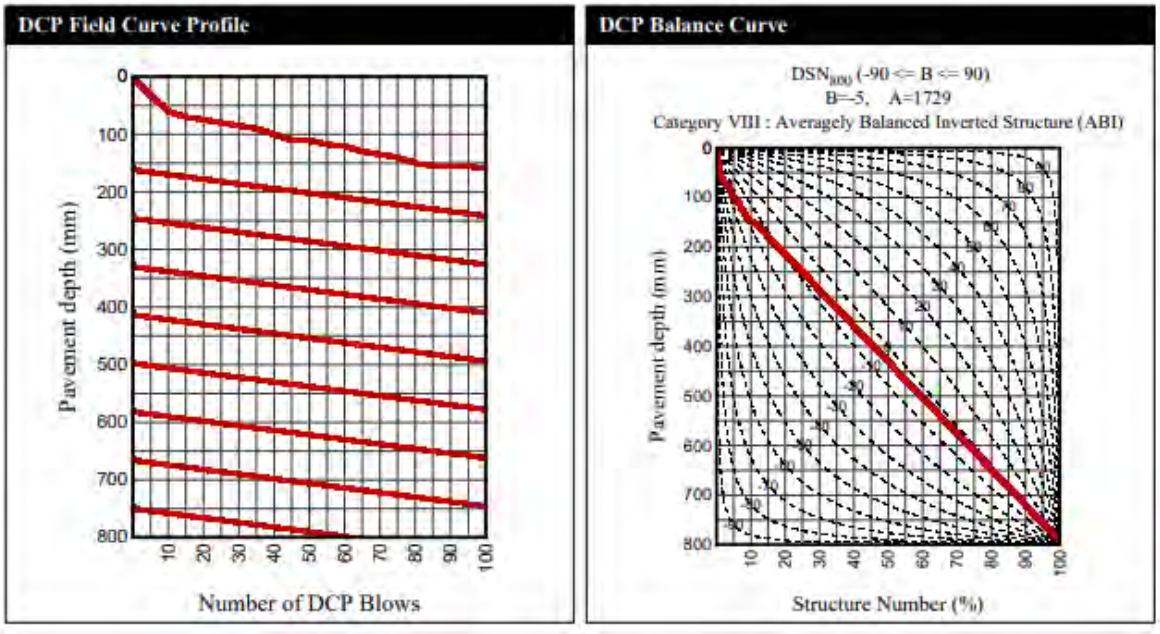

Figure B1- 9 Penetration against no blows and the DSN curve for KZNS5

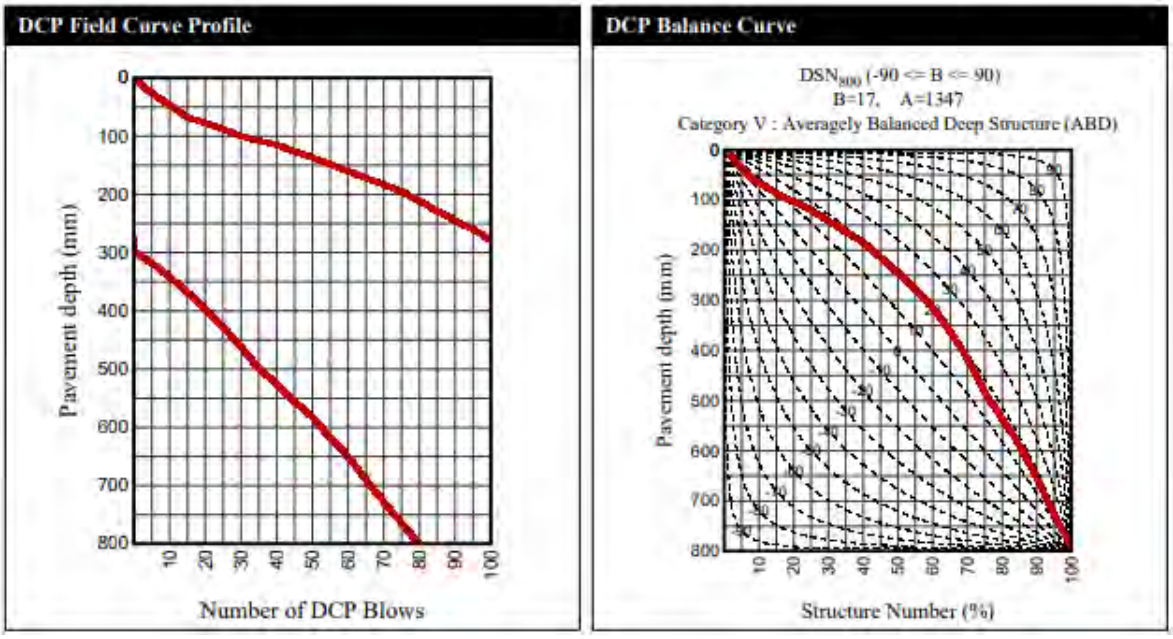

Figure B1- 10 Penetration against the number of blows and the DSN curve for KZNS6

Appendix B2

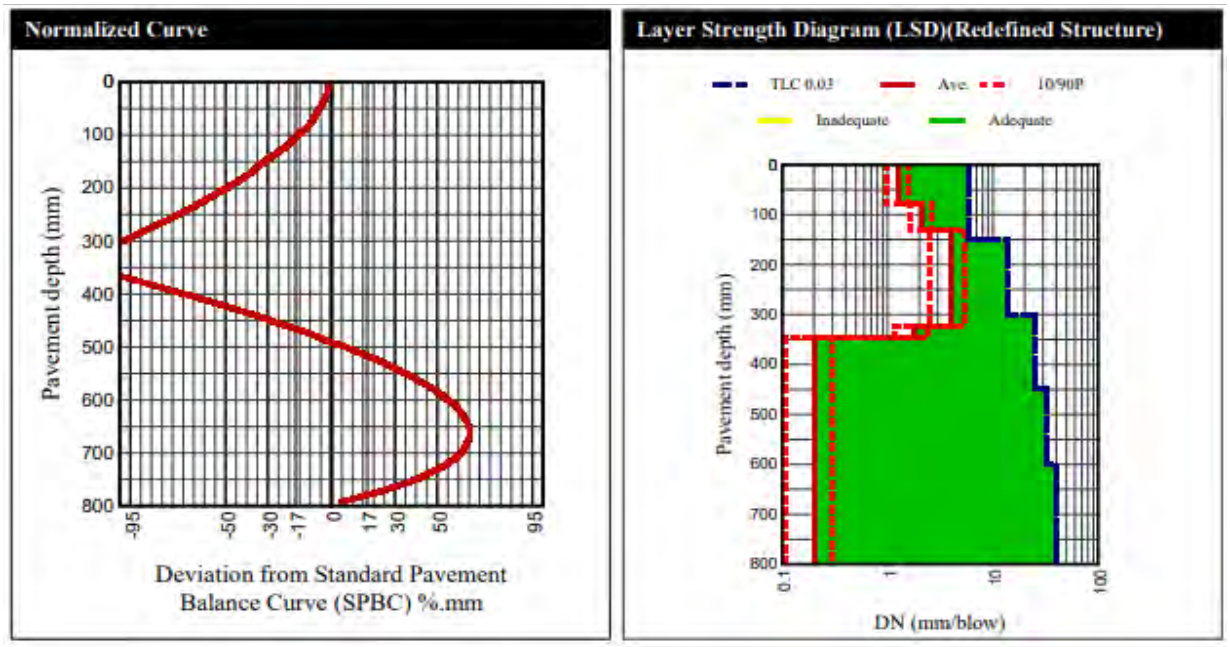

Figure B2- 1 Normalized curve and layer strength diagram NCS3

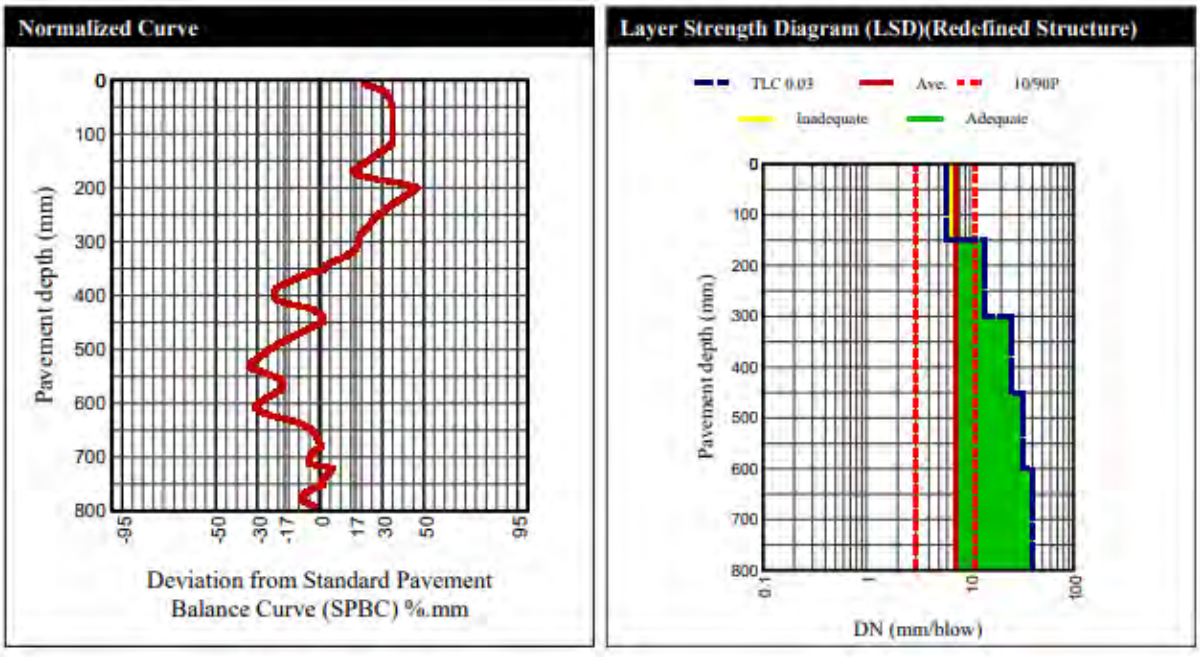

Figure B2- 2 Normalized curve and layer strength diagram NCS4

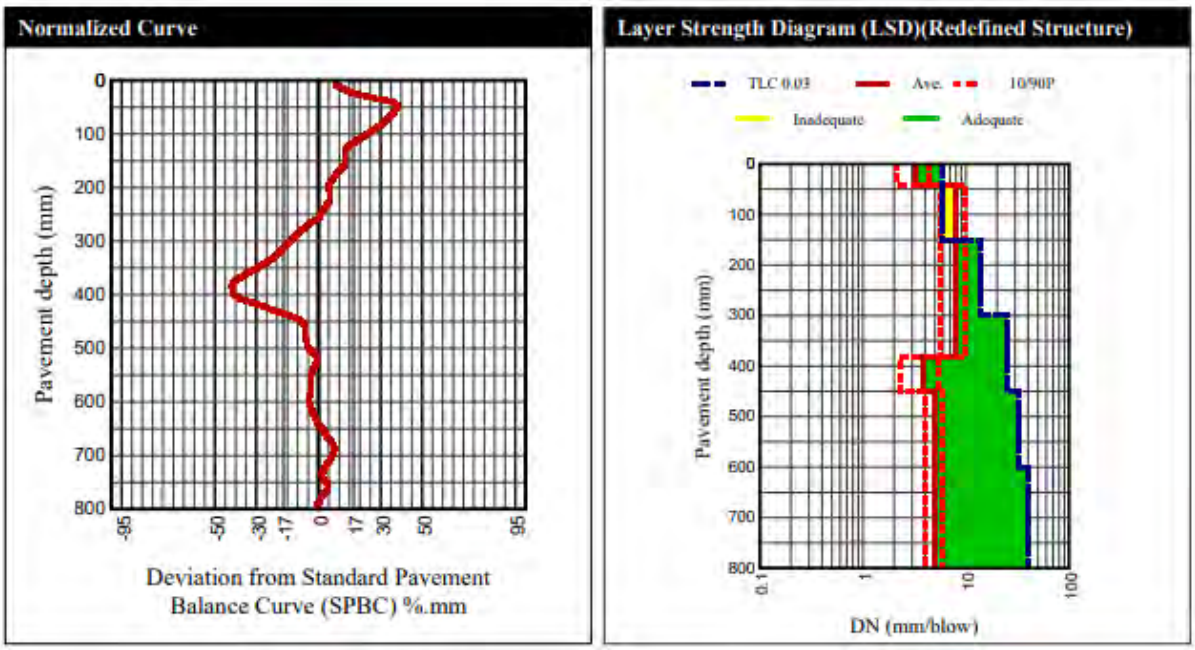

Figure B2- 3 Normalized curve and layer strength diagram NCS5

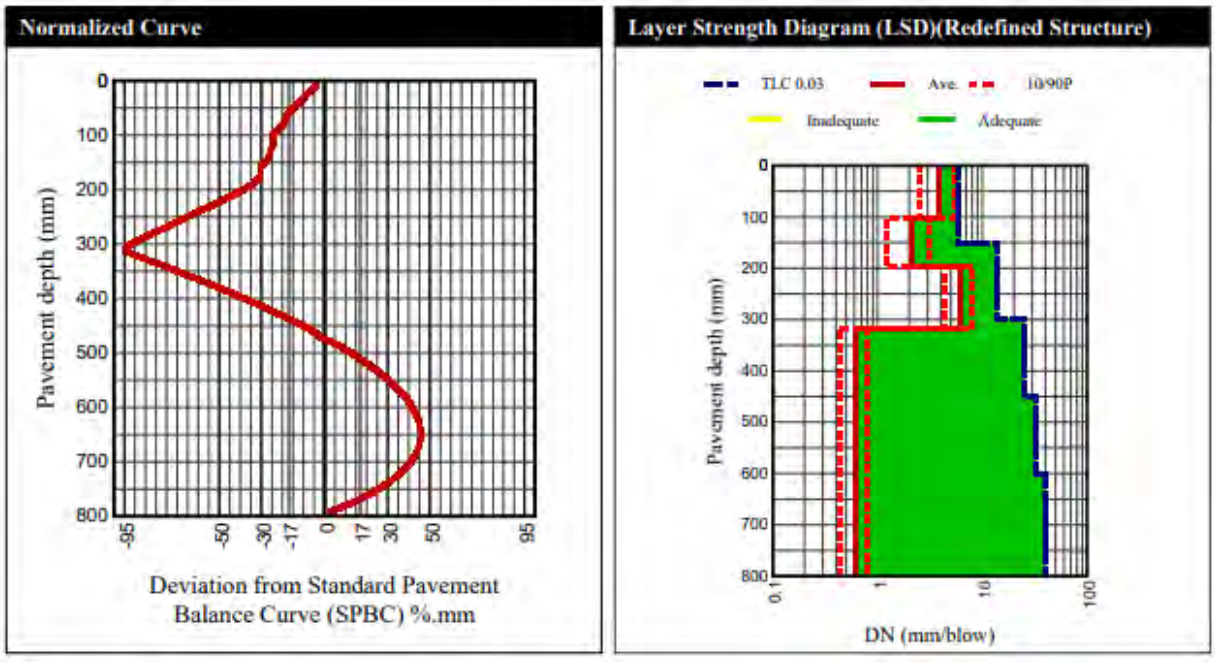

Figure B2- 4 Normalized curve and layer strength diagram NCS6

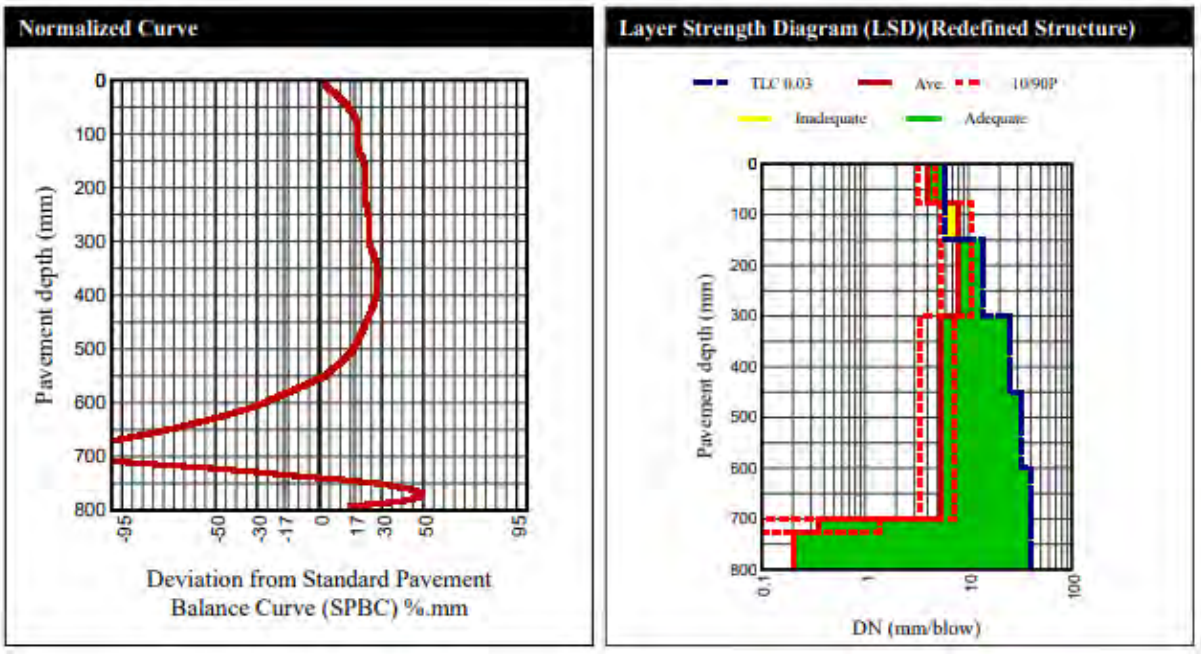

Figure B2- 5 Normalized curve and layer strength diagram NCS7

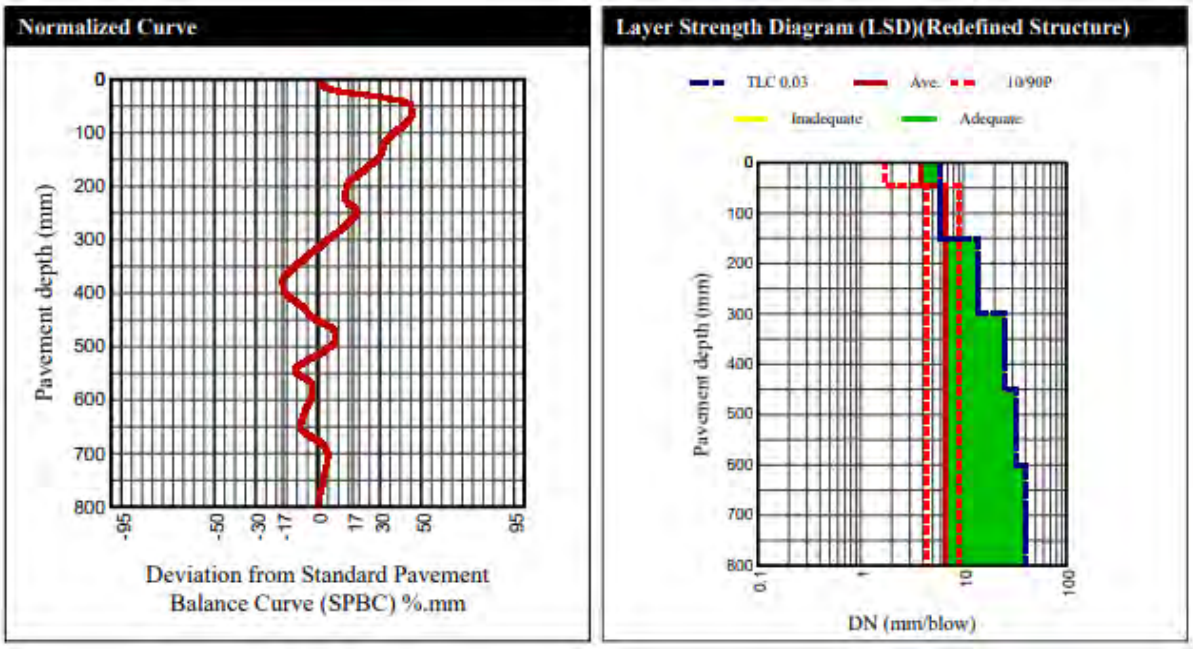

Figure B2- 6 Normalized curve and layer strength diagram NCS8

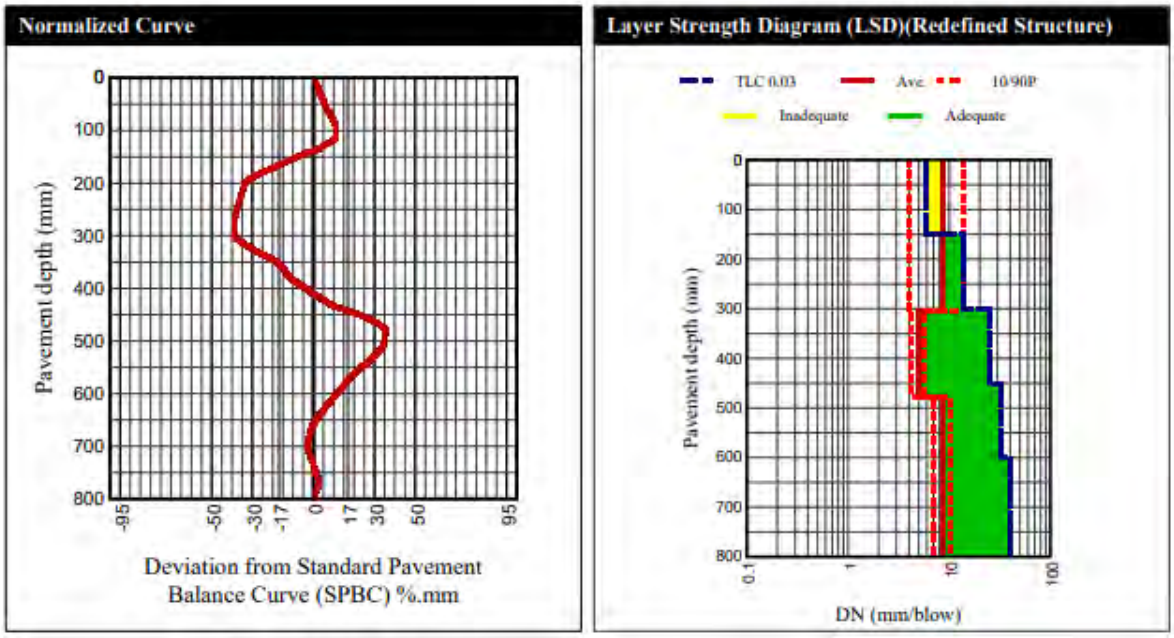

Figure B2- 7 Normalized curve and layer strength diagram of KZNS3

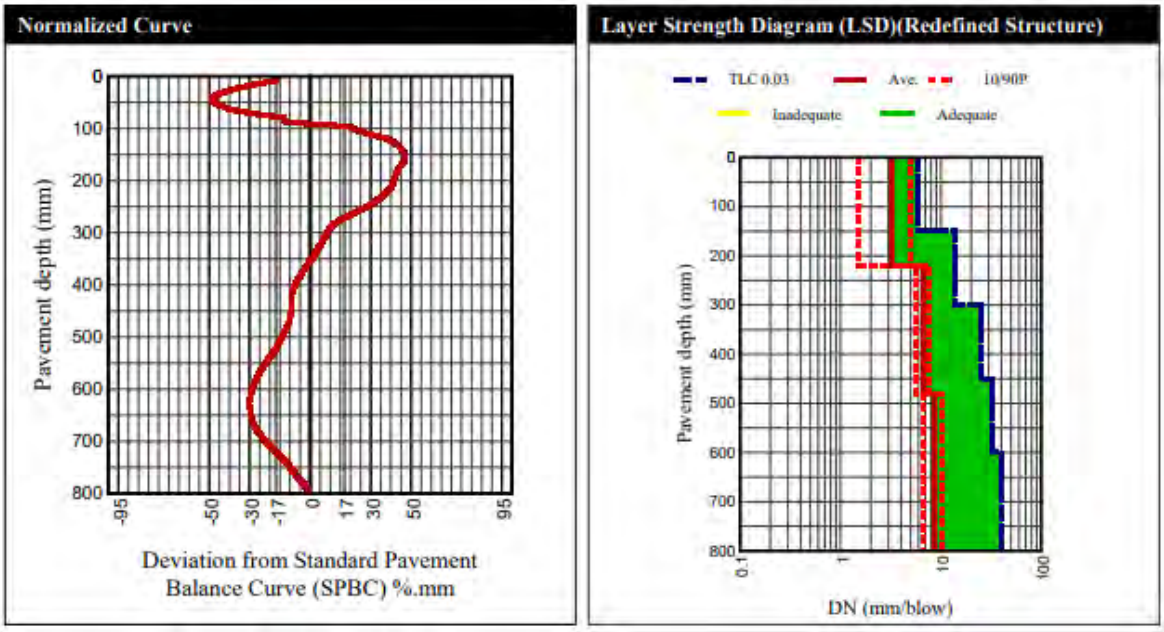

Figure B2- 8 Normalized curve and layer strength diagram of KZNS4

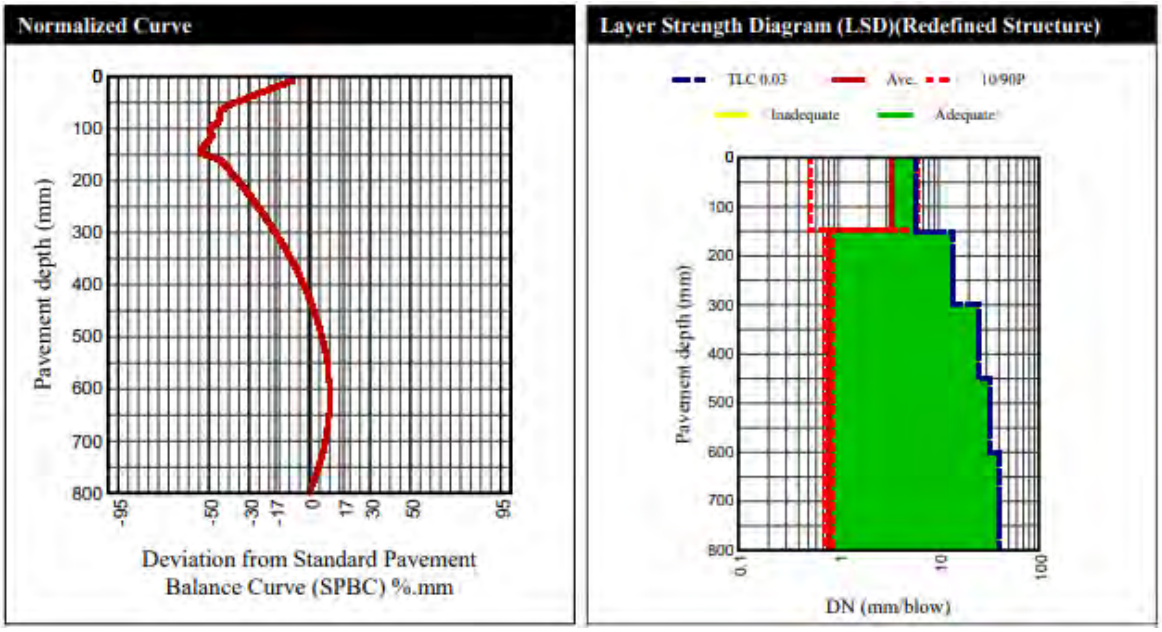

Figure B2- 9 Normalized curve and layer strength diagram of KZNS5

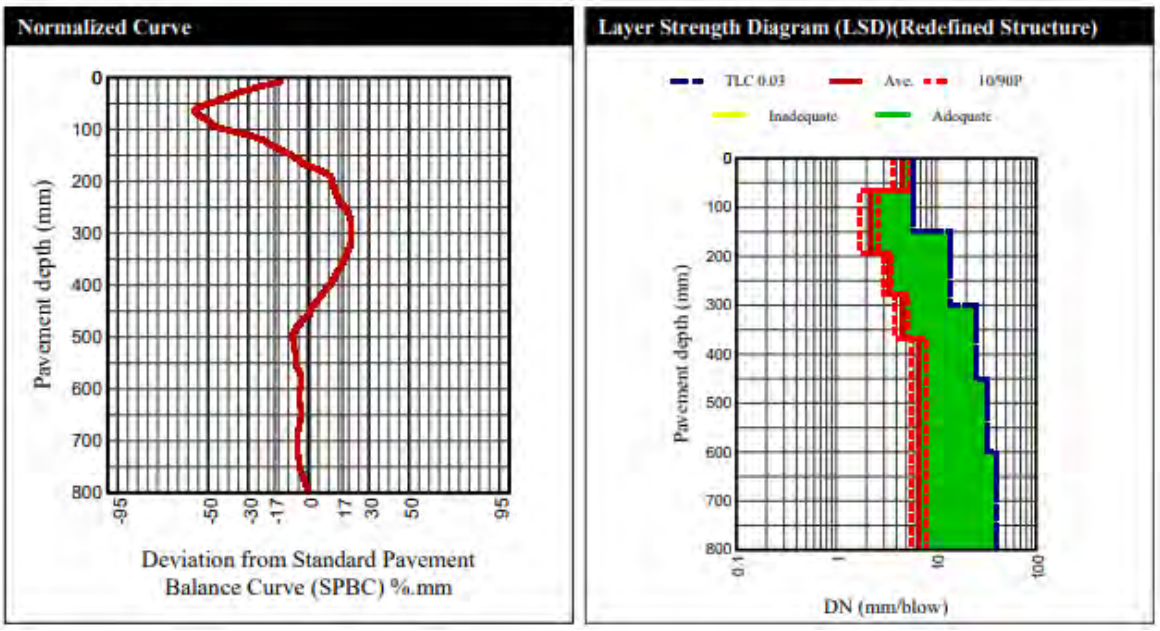

Figure B2- 10 Normalized curve and layer strength diagram of KZNS6

Appendix B3

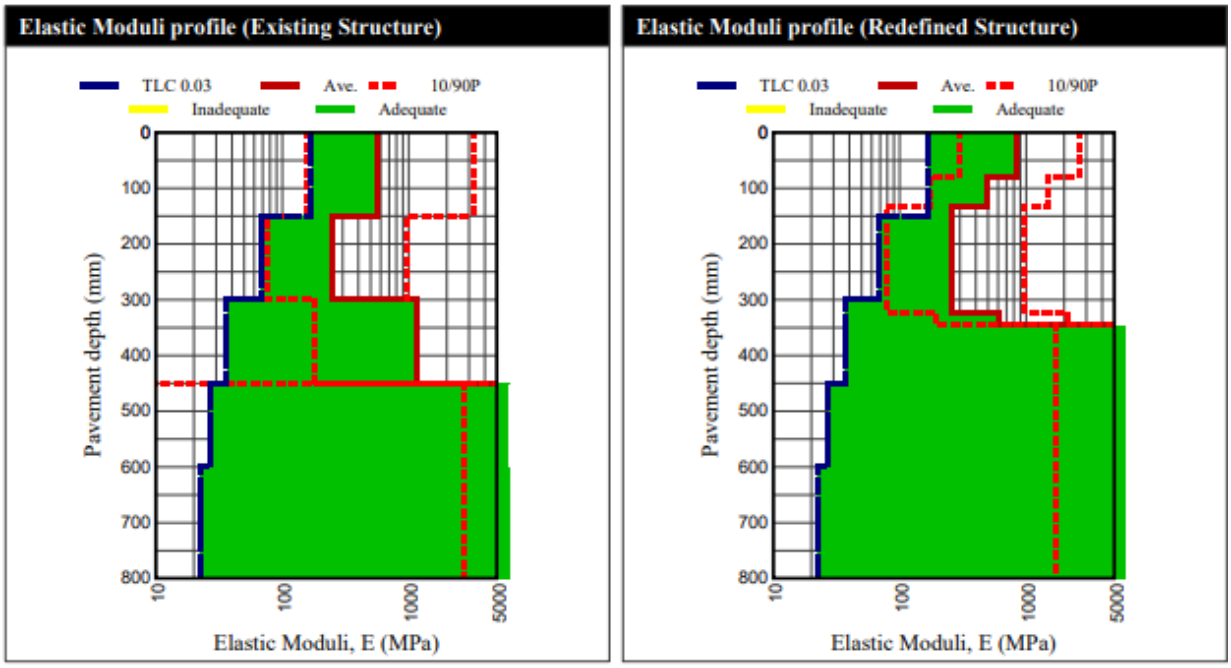

Figure B3- 1 Elastic moduli versus the pavement depth NCS3

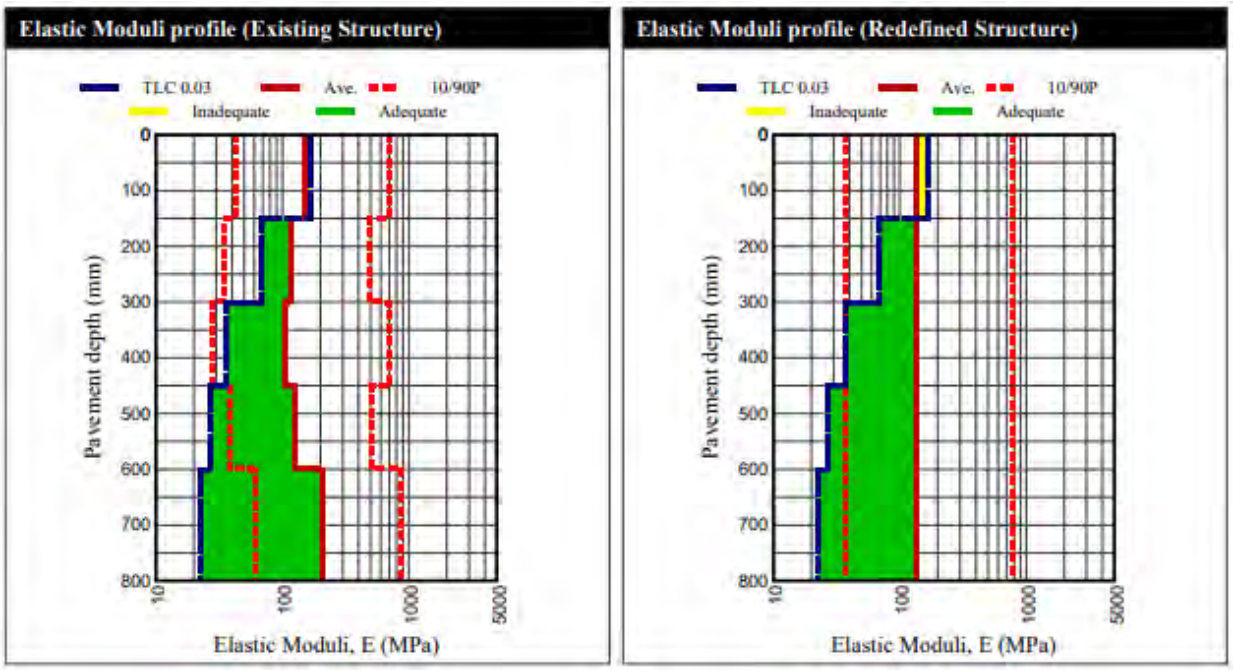

Figure B3- 2 Elastic moduli versus the pavement depth NCS4

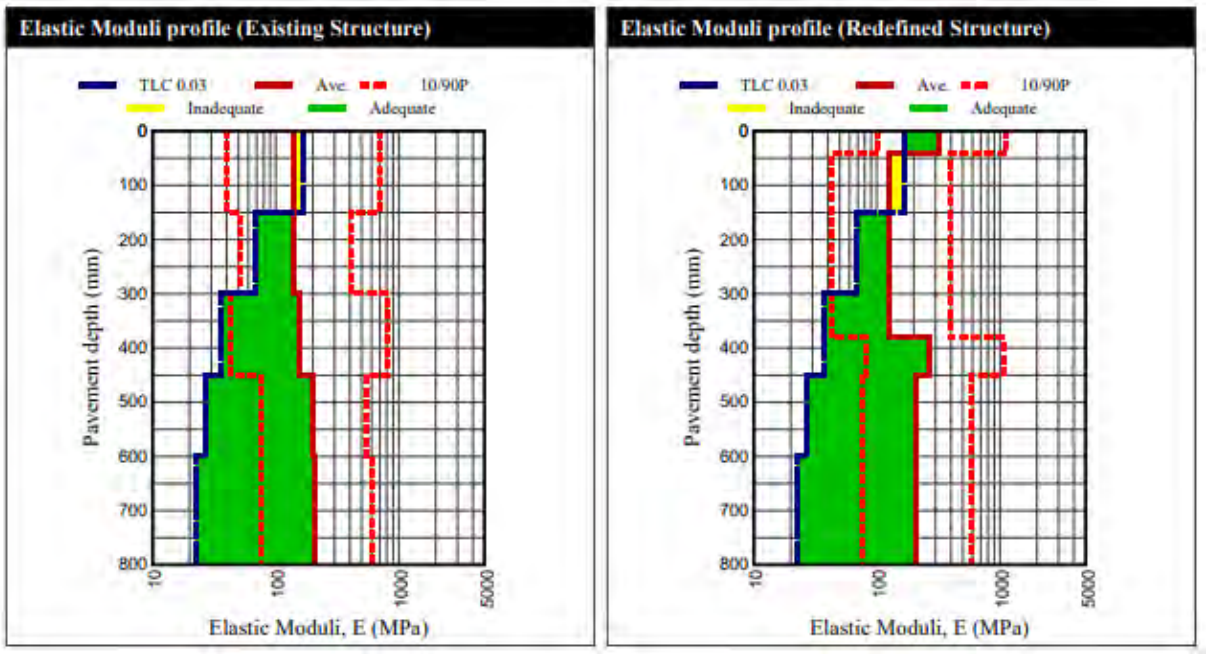

Figure B3- 3 Elastic moduli versus the pavement depth NCS5

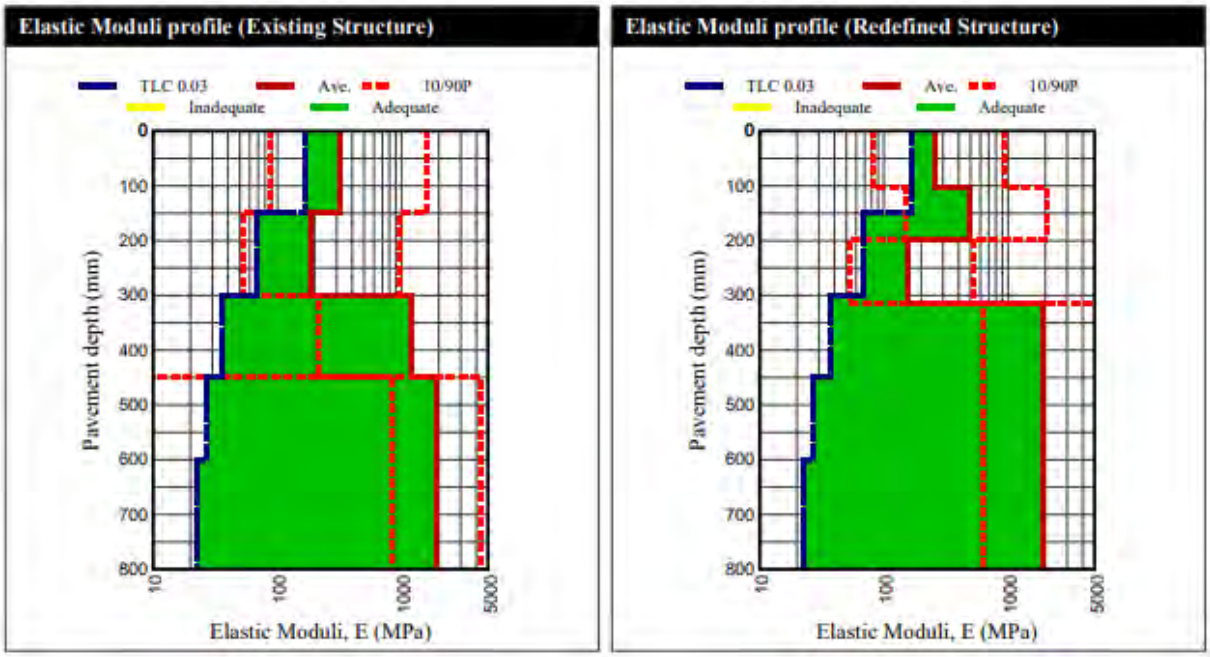

Figure B3- 4 Elastic moduli versus the pavement depth NCS6

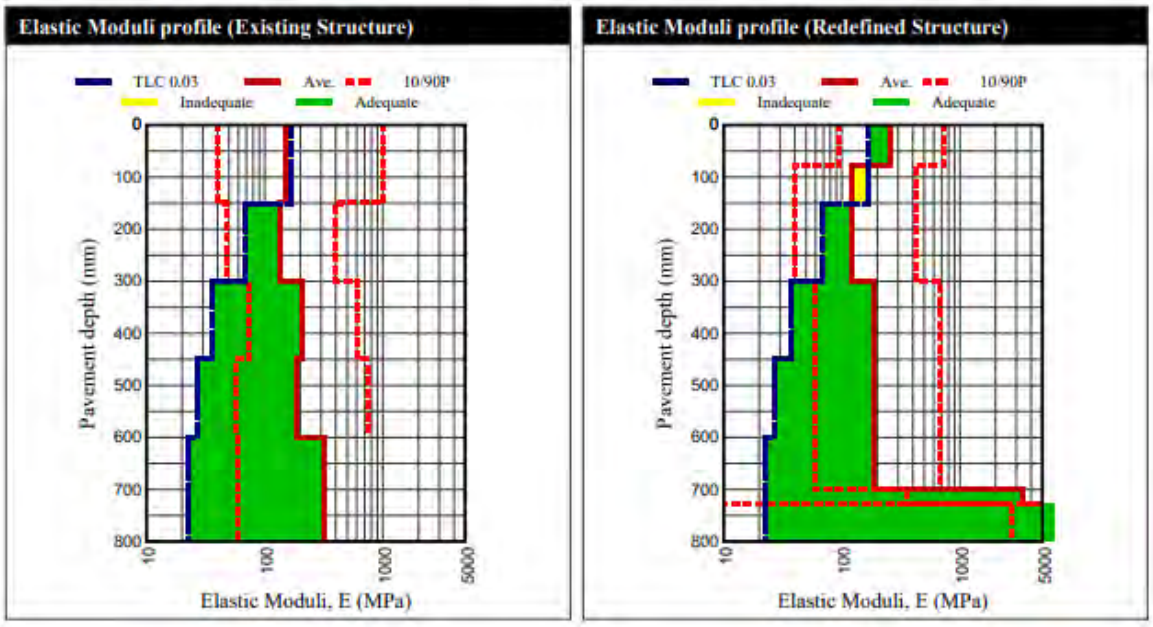

Figure B3- 5 Elastic moduli versus the pavement depth NCS7

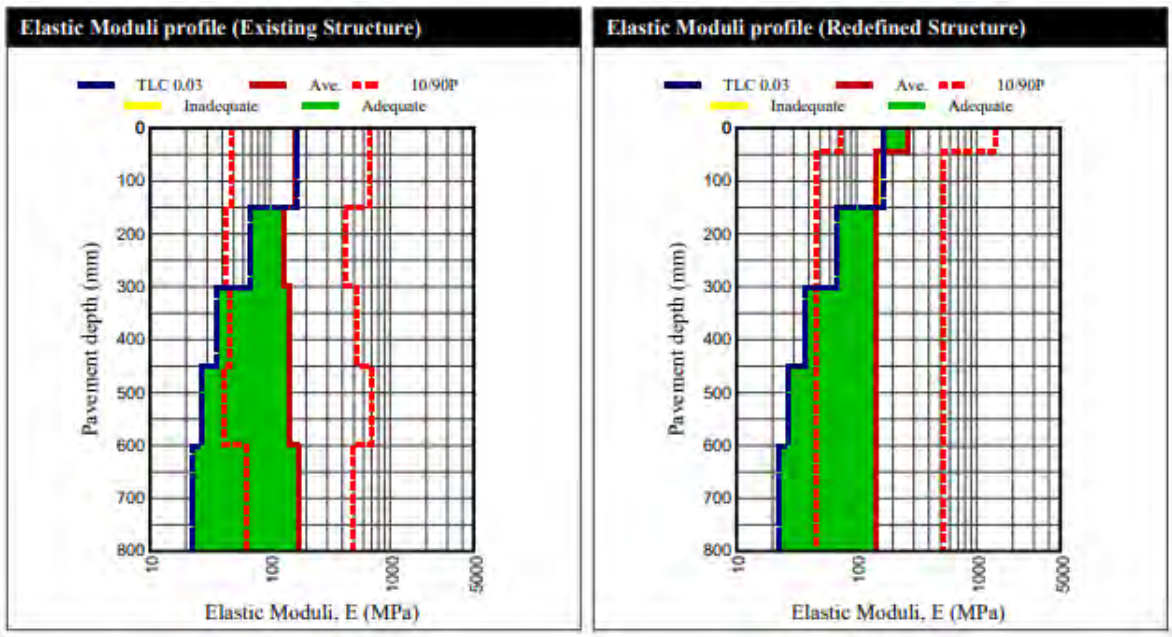

Figure B3- 6 Elastic moduli versus the pavement depth NCS8

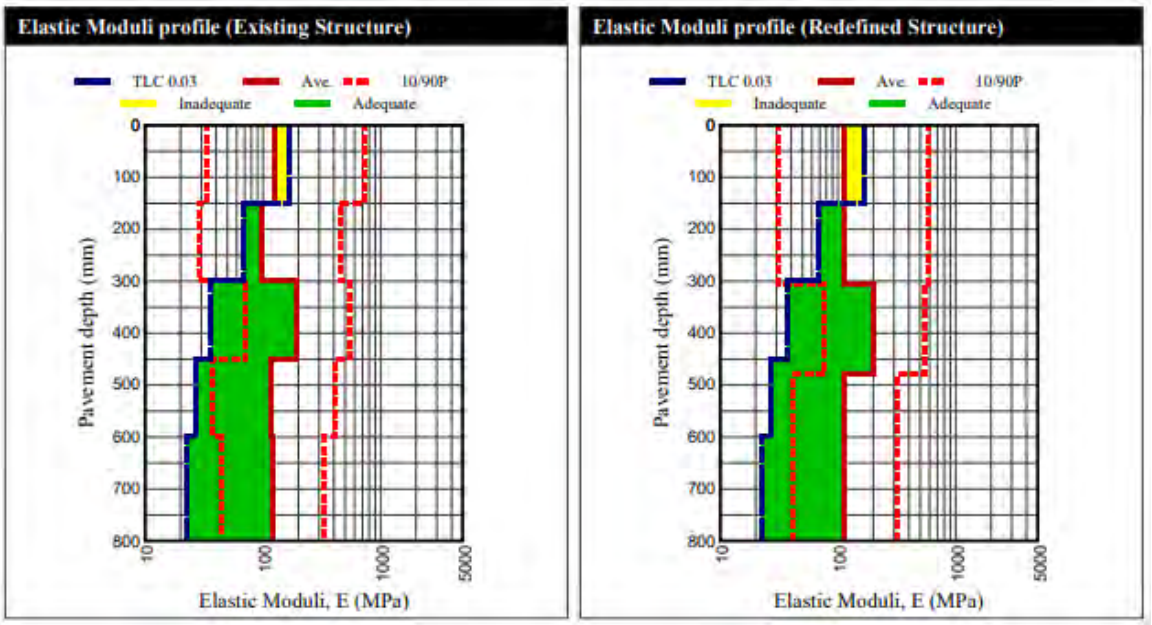

Figure B3- 7 Elastic moduli versus pavement depth for KZNS3

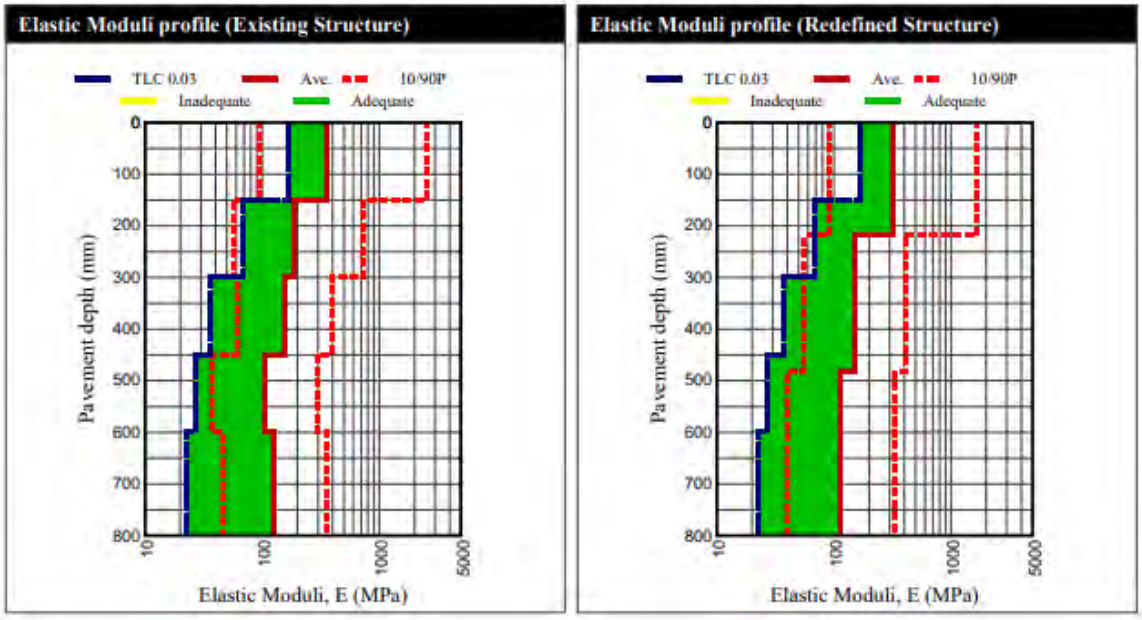

Figure B3- 8 Elastic moduli versus pavement depth for KZNS4

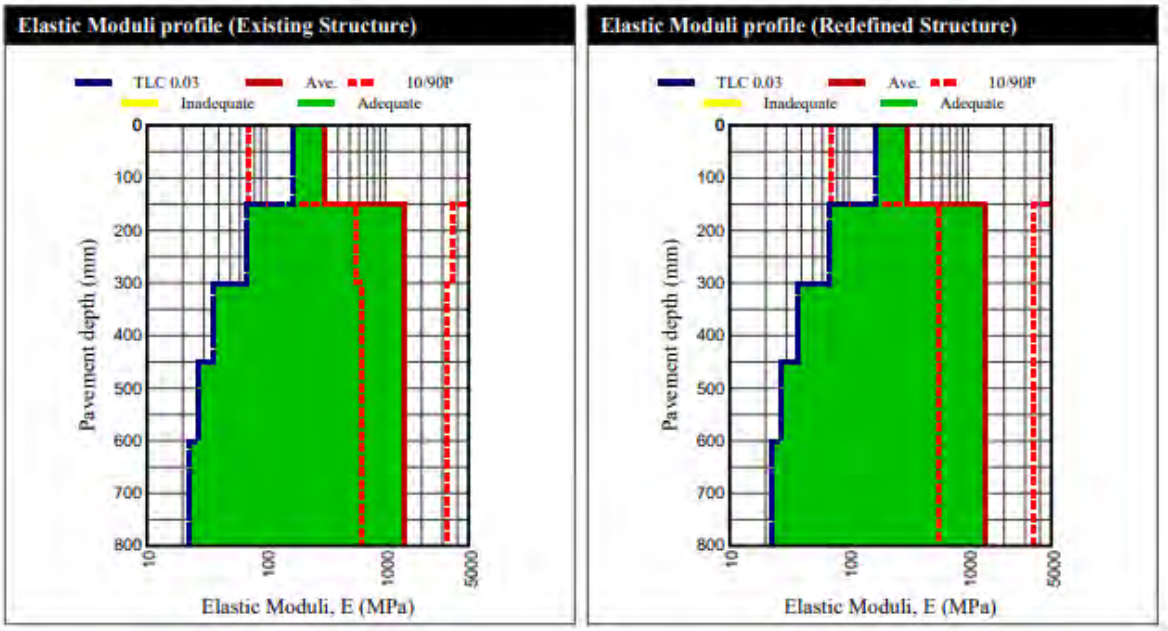

Figure B3- 9 Elastic moduli versus pavement depth for KZNS5

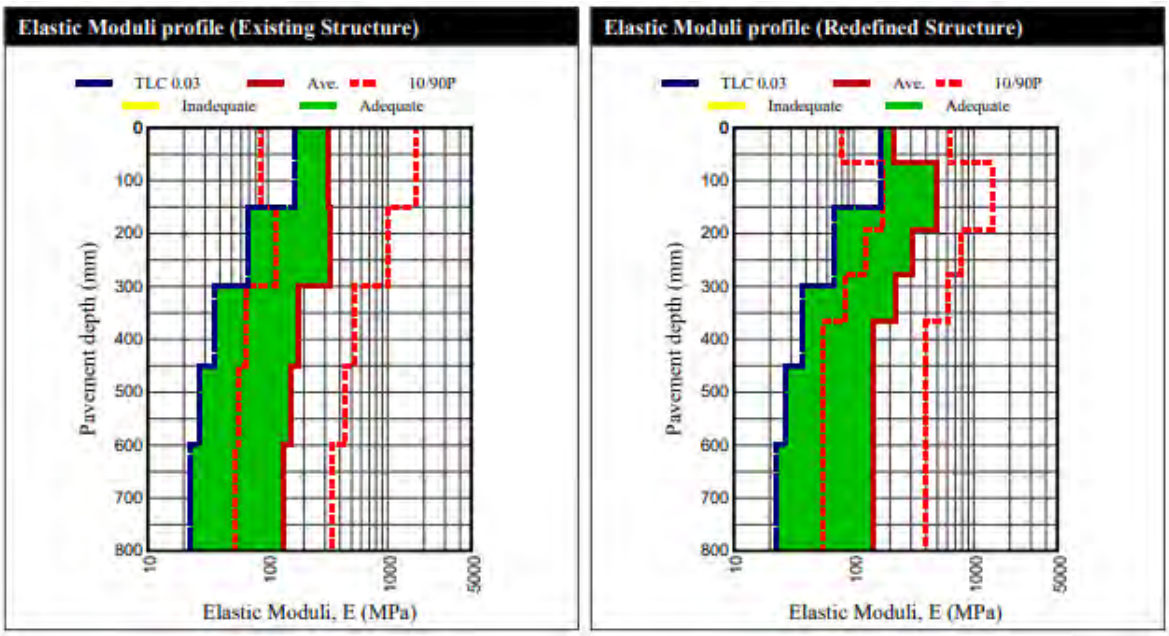

Figure B3- 10 Elastic moduli versus pavement depth for KZNS6

Appendix C

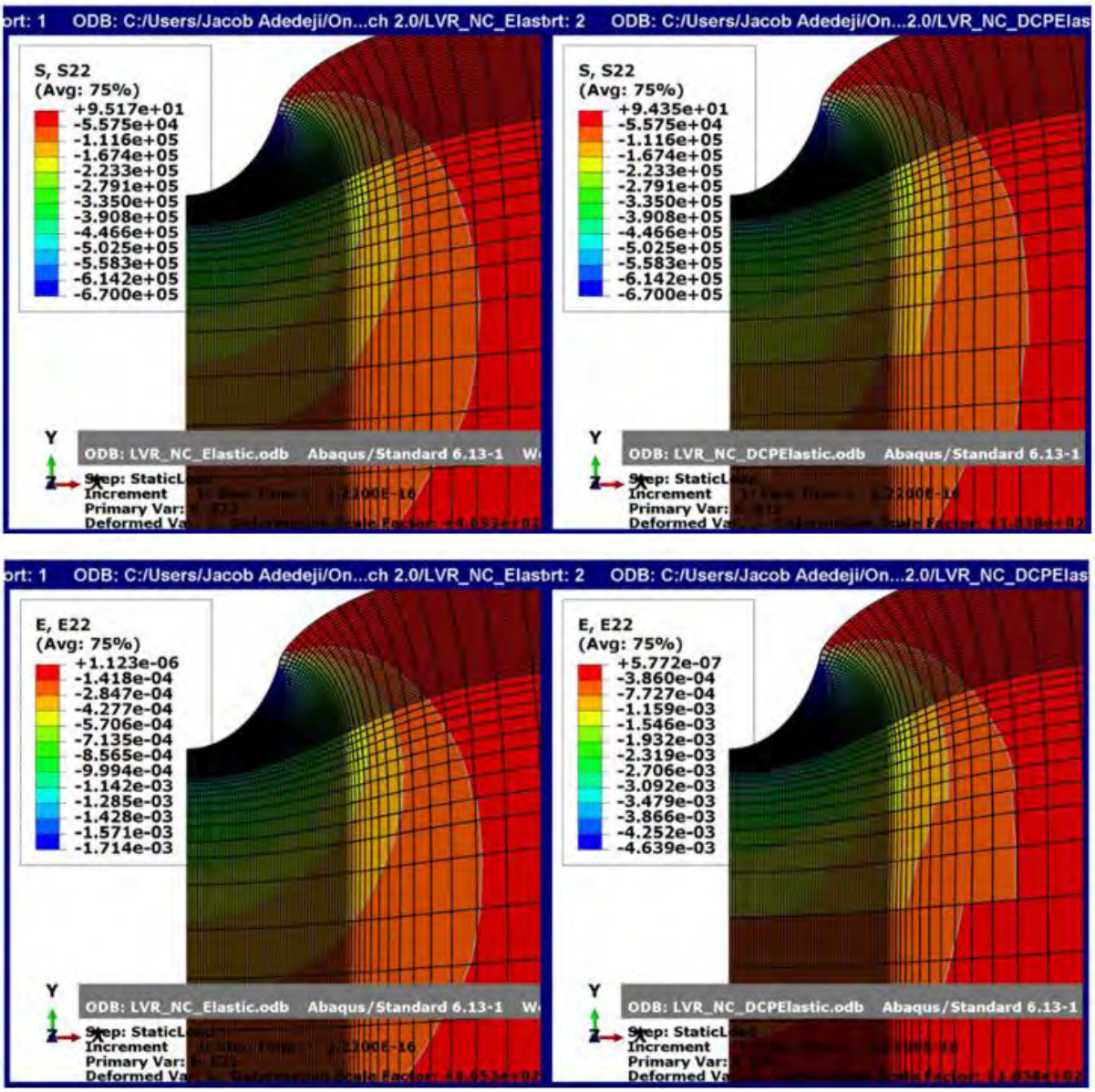

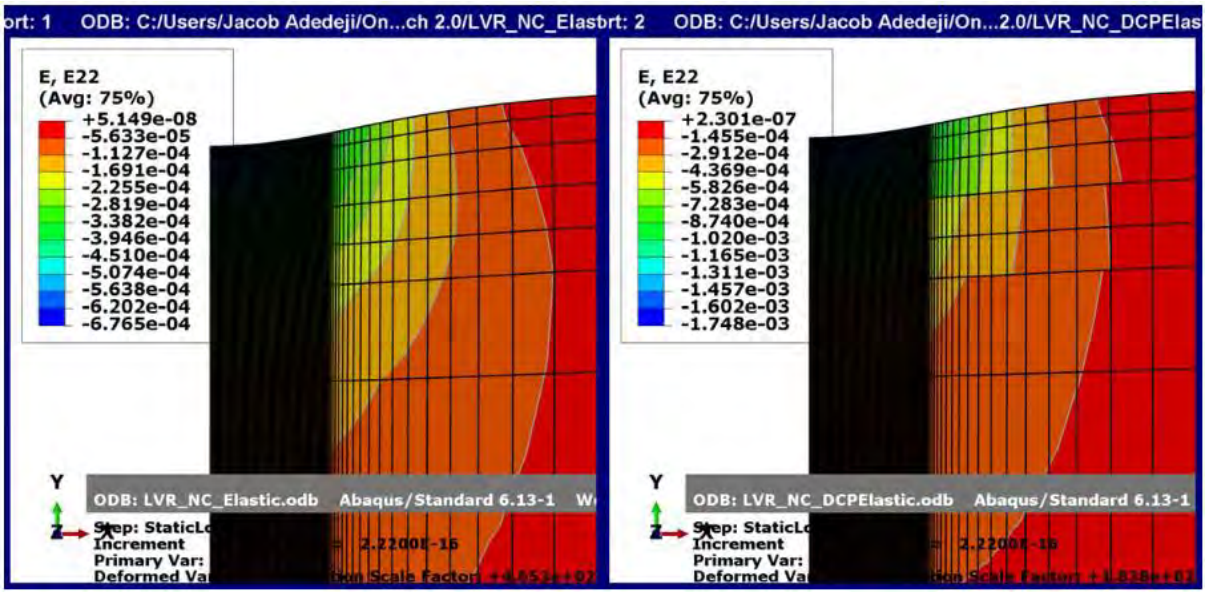

Appendix D

Abaqus DCP Model

```
# -*- coding: mbcs -*-
# Do not delete the following import lines
from abaqus import *
from abaqusConstants import *
import __main__
import section
import regionToolset
import displayGroupMdbToolset as dgm
import part
import material
import assembly
import step
import interaction
import load
import mesh
import optimization
import job
import sketch
import visualization
import xyPlot
import displayGroupOdbToolset as dgo
import connectorBehavior

# =========================
# ===== INPUT PARAMETERS ==
# =========================
# Edit only this section to change material properties, tyre pressure, and mesh
controls.
INPUT = {
"materials" : {
"TopLayer" : { "rho" : 1 9 3 8 . 0 , "E" : 1 4 2 e6 , "nu" : 0 . 0 2 } ,
"Base" : { "rho" : 1 9 3 8 . 0 , "E" : 1 4 1 e6 , "nu" : 0 . 0 2 } ,
"SubgradeL1" : { "rho" : 1 9 3 8 . 0 , "E" : 1 5 5 e6 , "nu" : 0 . 0 2 } ,
"SubgradeL2" : { "rho" : 1 9 3 8 . 0 , "E" : 2 0 1 e6 , "nu" : 0 . 0 2 } ,
"SubgradeL3" : { "rho" : 1 9 3 8 . 0 , "E" : 2 0 9 e6 , "nu" : 0 . 0 2 } ,
} ,
# Uniform tyre contact pressure (Pa)
"tyre_pressure" : 6 . 7 0 e5 ,
}

def __apply_inputs__ ( ) :
# Materials (if they already exist, overwrite their density & elastic props)
try :
mm = mdb . models [ 'Model-1' ] . materials
for mname , props in INPUT [ "materials" ] . items ( ) :
if mname in mm . keys ( ) :
mm [ mname ] . Density ( table = ( ( props [ "rho" ] , ) , ) )
mm [ mname ] . Elastic ( table = ( ( props [ "E" ] , props [ "nu" ] ) , ) )
except Exception as _e :
pass
# Pressure (if the load exists, update magnitude)
```

```
try :
mdb . models [ 'Model-1' ] . loads [ 'TyreLoad' ] . setValues ( magnitude =
INPUT [ "tyre_pressure" ] )
except Exception as _e :
pass
# ====================================
s = mdb . models [ 'Model-1' ] . ConstrainedSketch ( name = '__profile__' ,
sheetSize = 2 0 0 . 0 )
g , v , d , c = s . geometry , s . vertices , s . dimensions , s . constraints
s . sketchOptions . setValues ( viewStyle = AXISYM )
s . setPrimaryObject ( option = STANDALONE )
s . ConstructionLine ( point1 = ( 0 . 0 , - 1 0 0 . 0 ) , point2 = ( 0 . 0 ,
1 0 0 . 0 ) )
s . FixedConstraint ( entity = g [ 2 ] )
session . viewports [ 'Viewport: 1' ] . view . setValues ( nearPlane = 8 1 . 4
7 5 4 ,
farPlane = 1 0 7 . 0 8 6 , width = 1 2 3 . 8 9 3 , height = 6 1 . 0 8 2 6 ,
cameraPosition = (
2 3 . 3 5 9 8 , 1 6 . 5 1 8 2 , 9 4 . 2 8 0 9 ) , cameraTarget = ( 2 3 . 3 5
9 8 , 1 6 . 5 1 8 2 , 0 ) )
s . rectangle ( point1 = ( 0 . 0 , 0 . 0 ) , point2 = ( 7 0 . 0 , 5 . 0 ) )
s . CoincidentConstraint ( entity1 = v [ 0 ] , entity2 = g [ 2 ] , addUndoState
= False )
s . ObliqueDimension ( vertex1 = v [ 2 ] , vertex2 = v [ 3 ] , textPoint = ( 7
8 . 5 2 1 8 6 5 8 4 4 7 2 6 6 ,
- 0 . 5 1 5 3 7 3 2 2 9 9 8 0 4 6 9 ) , value = 0 . 1 5 )
s . HorizontalDimension ( vertex1 = v [ 1 ] , vertex2 = v [ 3 ] , textPoint = (
6 9 . 9 6 7 3 3 0 9 3 2 6 1 7 2 ,
- 4 . 9 8 4 8 3 0 8 5 6 3 2 3 2 4 ) , value = 3 . 0 )
session . viewports [ 'Viewport: 1' ] . view . setValues ( nearPlane = 9 3 . 3
2 8 6 ,
farPlane = 9 5 . 2 3 3 2 , width = 8 . 1 4 0 9 3 , height = 4 . 0 1 3 6 9 ,
cameraPosition = (
5 . 6 2 5 2 3 , 0 . 7 8 9 4 8 3 , 9 4 . 2 8 0 9 ) , cameraTarget = ( 5 . 6 2
5 2 3 , 0 . 7 8 9 4 8 3 , 0 ) )
session . viewports [ 'Viewport: 1' ] . view . setValues ( cameraPosition = ( 1
. 2 9 6 3 2 ,
- 0 . 3 1 3 4 6 5 , 9 4 . 2 8 0 9 ) , cameraTarget = ( 1 . 2 9 6 3 2 , - 0 .
3 1 3 4 6 5 , 0 ) )
session . viewports [ 'Viewport: 1' ] . view . setValues ( nearPlane = 9 3 . 8
8 0 4 ,
farPlane = 9 4 . 6 8 1 4 , width = 3 . 4 2 3 4 5 , height = 1 . 6 8 7 8 5 ,
cameraPosition = (
1 . 0 7 5 4 2 , - 0 . 2 4 7 2 8 3 , 9 4 . 2 8 0 9 ) , cameraTarget = ( 1 . 0
7 5 4 2 , - 0 . 2 4 7 2 8 3 , 0 ) )
s . offset ( distance = 0 . 1 9 5 , objectList = ( g [ 3 ] , ) , side = RIGHT
)
s . undo ( )
p = mdb . models [ 'Model-1' ] . Part ( name = 'TopLayer' , dimensionality =
AXISYMMETRIC ,
type = DEFORMABLE_BODY )
p = mdb . models [ 'Model-1' ] . parts [ 'TopLayer' ]
p . BaseShell ( sketch = s )
s . unsetPrimaryObject ( )
p = mdb . models [ 'Model-1' ] . parts [ 'TopLayer' ]
session . viewports [ 'Viewport: 1' ] . setValues ( displayedObject = p )
```

```
del mdb . models [ 'Model-1' ] . sketches [ '__profile__' ]
p = mdb . models [ 'Model-1' ] . parts [ 'TopLayer' ]
f , e , d1 = p . faces , p . edges , p . datums
t = p . MakeSketchTransform ( sketchPlane = f [ 0 ] , sketchPlaneSide = SIDE1 ,
origin = ( 1 . 5 ,
0 . 0 7 5 , 0 . 0 ) )
s1 = mdb . models [ 'Model-1' ] . ConstrainedSketch ( name = '__profile__' ,
sheetSize = 6 . 0 ,
gridSpacing = 0 . 1 5 , transform = t )
g , v , d , c = s1 . geometry , s1 . vertices , s1 . dimensions , s1 .
constraints
s1 . setPrimaryObject ( option = SUPERIMPOSE )
p = mdb . models [ 'Model-1' ] . parts [ 'TopLayer' ]
p . projectReferencesOntoSketch ( sketch = s1 , filter = COPLANAR_EDGES )
s1 . offset ( distance = 0 . 1 9 5 , objectList = ( g [ 5 ] , ) , side = LEFT
)
p = mdb . models [ 'Model-1' ] . parts [ 'TopLayer' ]
f = p . faces
pickedFaces = f . getSequenceFromMask ( mask = ( '[#1 ]' , ) , )
e1 , d2 = p . edges , p . datums
p . PartitionFaceBySketch ( faces = pickedFaces , sketch = s1 )
s1 . unsetPrimaryObject ( )
del mdb . models [ 'Model-1' ] . sketches [ '__profile__' ]
s = mdb . models [ 'Model-1' ] . ConstrainedSketch ( name = '__profile__' ,
sheetSize = 2 0 0 . 0 )
g , v , d , c = s . geometry , s . vertices , s . dimensions , s . constraints
s . sketchOptions . setValues ( viewStyle = AXISYM )
s . setPrimaryObject ( option = STANDALONE )
s . ConstructionLine ( point1 = ( 0 . 0 , - 1 0 0 . 0 ) , point2 = ( 0 . 0 ,
1 0 0 . 0 ) )
s . FixedConstraint ( entity = g [ 2 ] )
s . rectangle ( point1 = ( 0 . 0 , 0 . 0 ) , point2 = ( 2 8 . 7 5 , 3 . 7 5 )
)
s . CoincidentConstraint ( entity1 = v [ 0 ] , entity2 = g [ 2 ] , addUndoState
= False )
s . VerticalDimension ( vertex1 = v [ 2 ] , vertex2 = v [ 3 ] , textPoint = (
3 3 . 5 1 2 7 6 3 9 7 7 0 5 0 8 ,
0 . 1 9 1 0 5 7 2 0 5 2 0 0 1 9 5 ) , value = 0 . 1 5 )
s . ObliqueDimension ( vertex1 = v [ 0 ] , vertex2 = v [ 3 ] , textPoint = ( 2
9 . 2 3 0 8 1 3 9 8 0 1 0 2 5 ,
5 . 9 3 9 0 2 4 9 2 5 2 3 1 9 3 ) , value = 3 . 0 )
session . viewports [ 'Viewport: 1' ] . view . setValues ( nearPlane = 8 6 . 9
4 3 4 ,
farPlane = 1 0 1 . 6 1 8 , width = 6 2 . 7 2 7 , height = 3 0 . 9 2 6 ,
cameraPosition = ( 1 4 . 3 7 1 3 ,
1 5 . 5 3 7 2 , 9 4 . 2 8 0 9 ) , cameraTarget = ( 1 4 . 3 7 1 3 , 1 5 . 5 3
7 2 , 0 ) )
p = mdb . models [ 'Model-1' ] . Part ( name = 'Base' , dimensionality =
AXISYMMETRIC ,
type = DEFORMABLE_BODY )
p = mdb . models [ 'Model-1' ] . parts [ 'Base' ]
p . BaseShell ( sketch = s )
s . unsetPrimaryObject ( )
p = mdb . models [ 'Model-1' ] . parts [ 'Base' ]
session . viewports [ 'Viewport: 1' ] . setValues ( displayedObject = p )
del mdb . models [ 'Model-1' ] . sketches [ '__profile__' ]
```

```
p = mdb . models [ 'Model-1' ] . parts [ 'Base' ]
f1 , e , d1 = p . faces , p . edges , p . datums
t = p . MakeSketchTransform ( sketchPlane = f1 [ 0 ] , sketchPlaneSide = SIDE1
, origin = (
1 . 5 , 1 . 2 7 5 , 0 . 0 ) )
s1 = mdb . models [ 'Model-1' ] . ConstrainedSketch ( name = '__profile__' ,
sheetSize = 6 . 5 7 , gridSpacing = 0 . 1 6 , transform = t )
g , v , d , c = s1 . geometry , s1 . vertices , s1 . dimensions , s1 .
constraints
s1 . setPrimaryObject ( option = SUPERIMPOSE )
p = mdb . models [ 'Model-1' ] . parts [ 'Base' ]
p . projectReferencesOntoSketch ( sketch = s1 , filter = COPLANAR_EDGES )
s1 . offset ( distance = 0 . 1 9 5 , objectList = ( g [ 5 ] , ) , side = LEFT
)
p = mdb . models [ 'Model-1' ] . parts [ 'Base' ]
f = p . faces
pickedFaces = f . getSequenceFromMask ( mask = ( '[#1 ]' , ) , )
e1 , d2 = p . edges , p . datums
p . PartitionFaceBySketch ( faces = pickedFaces , sketch = s1 )
s1 . unsetPrimaryObject ( )
del mdb . models [ 'Model-1' ] . sketches [ '__profile__' ]
s = mdb . models [ 'Model-1' ] . ConstrainedSketch ( name = '__profile__' ,
sheetSize = 2 0 0 . 0 )
g , v , d , c = s . geometry , s . vertices , s . dimensions , s . constraints
s . sketchOptions . setValues ( viewStyle = AXISYM )
s . setPrimaryObject ( option = STANDALONE )
s . ConstructionLine ( point1 = ( 0 . 0 , - 1 0 0 . 0 ) , point2 = ( 0 . 0 ,
1 0 0 . 0 ) )
s . FixedConstraint ( entity = g [ 2 ] )
s . rectangle ( point1 = ( 0 . 0 , 0 . 0 ) , point2 = ( 3 0 . 0 , 7 . 5 ) )
s . CoincidentConstraint ( entity1 = v [ 0 ] , entity2 = g [ 2 ] , addUndoState
= False )
s . ObliqueDimension ( vertex1 = v [ 1 ] , vertex2 = v [ 2 ] , textPoint = ( 3
0 . 1 8 8 6 1 5 7 9 8 9 5 0 2 ,
1 2 . 1 4 2 2 7 5 8 1 0 2 4 1 7 ) , value = 3 . 0 )
s . VerticalDimension ( vertex1 = v [ 2 ] , vertex2 = v [ 3 ] , textPoint = (
1 1 . 4 2 6 9 1 2 3 0 7 7 3 9 3 ,
1 . 3 8 6 1 7 9 9 2 4 0 1 1 2 3 ) , value = 2 . 0 )
p = mdb . models [ 'Model-1' ] . Part ( name = 'Subgrade' , dimensionality =
AXISYMMETRIC ,
type = DEFORMABLE_BODY )
p = mdb . models [ 'Model-1' ] . parts [ 'Subgrade' ]
p . BaseShell ( sketch = s )
s . unsetPrimaryObject ( )
p = mdb . models [ 'Model-1' ] . parts [ 'Subgrade' ]
session . viewports [ 'Viewport: 1' ] . setValues ( displayedObject = p )
del mdb . models [ 'Model-1' ] . sketches [ '__profile__' ]
p = mdb . models [ 'Model-1' ] . parts [ 'Subgrade' ]
f , e , d1 = p . faces , p . edges , p . datums
t = p . MakeSketchTransform ( sketchPlane = f [ 0 ] , sketchPlaneSide = SIDE1 ,
origin = ( 1 . 5 ,
2 . 8 3 3 3 3 3 , 0 . 0 ) )
s1 = mdb . models [ 'Model-1' ] . ConstrainedSketch ( name = '__profile__' ,
sheetSize = 9 . 7 3 , gridSpacing = 0 . 2 4 , transform = t )
g , v , d , c = s1 . geometry , s1 . vertices , s1 . dimensions , s1 .
constraints
```

```
s1 . setPrimaryObject ( option = SUPERIMPOSE )
p = mdb . models [ 'Model-1' ] . parts [ 'Subgrade' ]
p . projectReferencesOntoSketch ( sketch = s1 , filter = COPLANAR_EDGES )
s1 . offset ( distance = 0 . 1 9 5 , objectList = ( g [ 5 ] , ) , side = LEFT
)
session . viewports [ 'Viewport: 1' ] . view . setValues ( nearPlane = 6 . 7 1
2 8 6 ,
farPlane = 7 . 7 0 9 3 5 , width = 4 . 8 2 0 5 2 , height = 2 . 3 7 6 6 4 ,
cameraPosition = (
1 . 6 6 2 1 , 2 . 9 6 4 0 1 , 7 . 2 1 1 1 ) , cameraTarget = ( 1 . 6 6 2 1 ,
2 . 9 6 4 0 1 , 0 ) )
s1 . offset ( distance = 0 . 1 5 , objectList = ( g [ 4 ] , ) , side = LEFT )
s1 . offset ( distance = 0 . 1 5 , objectList = ( g [ 8 ] , ) , side = LEFT )
p = mdb . models [ 'Model-1' ] . parts [ 'Subgrade' ]
f = p . faces
pickedFaces = f . getSequenceFromMask ( mask = ( '[#1 ]' , ) , )
e1 , d2 = p . edges , p . datums
p . PartitionFaceBySketch ( faces = pickedFaces , sketch = s1 )
s1 . unsetPrimaryObject ( )
del mdb . models [ 'Model-1' ] . sketches [ '__profile__' ]
session . viewports [ 'Viewport: 1' ] . partDisplay . setValues (
sectionAssignments = ON ,
engineeringFeatures = ON )
session . viewports [ 'Viewport: 1' ] . partDisplay . geometryOptions . setValues
(
referenceRepresentation = OFF )
mdb . models [ 'Model-1' ] . Material ( name = 'TopLayer' )
mdb . models [ 'Model-1' ] . materials [ 'TopLayer' ] . Density ( table = ( ( 1
9 3 8 . 0 , ) , ) )
mdb . models [ 'Model-1' ] . materials [ 'TopLayer' ] . Elastic ( table = ( ( 1
4 2 0 0 0 0 0 0 . 0 , 0 . 0 2 ) ,
) )
mdb . models [ 'Model-1' ] . Material ( name = 'Base' )
mdb . models [ 'Model-1' ] . materials [ 'Base' ] . Density ( table = ( ( 1 9 3
8 . 0 , ) , ) )
mdb . models [ 'Model-1' ] . materials [ 'Base' ] . Elastic ( table = ( ( 1 4 1
0 0 0 0 0 0 . 0 , 0 . 0 2 ) , ) )
mdb . models [ 'Model-1' ] . Material ( name = 'SubgradeL1' )
mdb . models [ 'Model-1' ] . materials [ 'SubgradeL1' ] . Density ( table = ( (
1 9 3 8 . 0 , ) , ) )
mdb . models [ 'Model-1' ] . materials [ 'SubgradeL1' ] . Elastic ( table = ( (
1 5 5 0 0 0 0 0 0 . 0 ,
0 . 0 2 ) , ) )
mdb . models [ 'Model-1' ] . Material ( name = 'SubgradeL2' )
mdb . models [ 'Model-1' ] . materials [ 'SubgradeL2' ] . Density ( table = ( (
1 9 3 8 . 0 , ) , ) )
mdb . models [ 'Model-1' ] . materials [ 'SubgradeL2' ] . Elastic ( table = ( (
2 0 1 0 0 0 0 0 0 . 0 ,
0 . 0 2 ) , ) )
mdb . models [ 'Model-1' ] . Material ( name = 'SubgradeL3' )
mdb . models [ 'Model-1' ] . materials [ 'SubgradeL3' ] . Density ( table = ( (
1 9 3 8 . 0 , ) , ) )
mdb . models [ 'Model-1' ] . materials [ 'SubgradeL3' ] . Elastic ( table = ( (
2 0 9 0 0 0 0 0 0 . 0 ,
0 . 0 2 ) , ) )
mdb . models [ 'Model-1' ] . HomogeneousSolidSection ( name = 'TopLayer' ,
```

```
material = 'TopLayer' , thickness = None )
mdb . models [ 'Model-1' ] . HomogeneousSolidSection ( name = 'Base' , material
= 'Base' ,
thickness = None )
mdb . models [ 'Model-1' ] . HomogeneousSolidSection ( name = 'SubgradeL1' ,
material = 'SubgradeL1' , thickness = None )
mdb . models [ 'Model-1' ] . HomogeneousSolidSection ( name = 'SubgradeL2' ,
material = 'SubgradeL2' , thickness = None )
mdb . models [ 'Model-1' ] . HomogeneousSolidSection ( name = 'SubgradeL3' ,
material = 'SubgradeL3' , thickness = None )
p = mdb . models [ 'Model-1' ] . parts [ 'TopLayer' ]
session . viewports [ 'Viewport: 1' ] . setValues ( displayedObject = p )
p = mdb . models [ 'Model-1' ] . parts [ 'TopLayer' ]
f = p . faces
faces = f . getSequenceFromMask ( mask = ( '[#3 ]' , ) , )
region = p . Set ( faces = faces , name = 'TopLayer' )
p = mdb . models [ 'Model-1' ] . parts [ 'TopLayer' ]
p . SectionAssignment ( region = region , sectionName = 'TopLayer' , offset = 0
. 0 ,
offsetType = MIDDLE_SURFACE , offsetField = '' ,
thicknessAssignment = FROM_SECTION )
p = mdb . models [ 'Model-1' ] . parts [ 'Base' ]
session . viewports [ 'Viewport: 1' ] . setValues ( displayedObject = p )
p = mdb . models [ 'Model-1' ] . parts [ 'Base' ]
f = p . faces
faces = f . getSequenceFromMask ( mask = ( '[#3 ]' , ) , )
region = p . Set ( faces = faces , name = 'Base' )
p = mdb . models [ 'Model-1' ] . parts [ 'Base' ]
p . SectionAssignment ( region = region , sectionName = 'Base' , offset = 0 . 0
,
offsetType = MIDDLE_SURFACE , offsetField = '' ,
thicknessAssignment = FROM_SECTION )
p = mdb . models [ 'Model-1' ] . parts [ 'TopLayer' ]
session . viewports [ 'Viewport: 1' ] . setValues ( displayedObject = p )
p = mdb . models [ 'Model-1' ] . parts [ 'Subgrade' ]
session . viewports [ 'Viewport: 1' ] . setValues ( displayedObject = p )
p = mdb . models [ 'Model-1' ] . parts [ 'Subgrade' ]
f = p . faces
faces = f . getSequenceFromMask ( mask = ( '[#12 ]' , ) , )
region = p . Set ( faces = faces , name = 'SubgradeL1' )
p = mdb . models [ 'Model-1' ] . parts [ 'Subgrade' ]
p . SectionAssignment ( region = region , sectionName = 'SubgradeL1' , offset =
0 . 0 ,
offsetType = MIDDLE_SURFACE , offsetField = '' ,
thicknessAssignment = FROM_SECTION )
p = mdb . models [ 'Model-1' ] . parts [ 'Subgrade' ]
f = p . faces
faces = f . getSequenceFromMask ( mask = ( '[#24 ]' , ) , )
region = p . Set ( faces = faces , name = 'SubgradeL2' )
p = mdb . models [ 'Model-1' ] . parts [ 'Subgrade' ]
p . SectionAssignment ( region = region , sectionName = 'SubgradeL2' , offset =
0 . 0 ,
offsetType = MIDDLE_SURFACE , offsetField = '' ,
thicknessAssignment = FROM_SECTION )
p = mdb . models [ 'Model-1' ] . parts [ 'Subgrade' ]
f = p . faces
```

```
faces = f . getSequenceFromMask ( mask = ( '[#9 ]' , ) , )
region = p . Set ( faces = faces , name = 'SubgradeL3' )
p = mdb . models [ 'Model-1' ] . parts [ 'Subgrade' ]
p . SectionAssignment ( region = region , sectionName = 'SubgradeL3' , offset =
0 . 0 ,
offsetType = MIDDLE_SURFACE , offsetField = '' ,
thicknessAssignment = FROM_SECTION )
a = mdb . models [ 'Model-1' ] . rootAssembly
session . viewports [ 'Viewport: 1' ] . setValues ( displayedObject = a )
session . viewports [ 'Viewport: 1' ] . assemblyDisplay . setValues (
optimizationTasks = OFF , geometricRestrictions = OFF , stopConditions = OFF )
a = mdb . models [ 'Model-1' ] . rootAssembly
a . DatumCsysByThreePoints ( coordSysType = CYLINDRICAL , origin = ( 0 . 0 , 0
. 0 , 0 . 0 ) ,
point1 = ( 1 . 0 , 0 . 0 , 0 . 0 ) , point2 = ( 0 . 0 , 0 . 0 , - 1 . 0 ) )
p = mdb . models [ 'Model-1' ] . parts [ 'Base' ]
a . Instance ( name = 'Base-1' , part = p , dependent = ON )
p = mdb . models [ 'Model-1' ] . parts [ 'Subgrade' ]
a . Instance ( name = 'Subgrade-1' , part = p , dependent = ON )
p = mdb . models [ 'Model-1' ] . parts [ 'TopLayer' ]
a . Instance ( name = 'TopLayer-1' , part = p , dependent = ON )
a = mdb . models [ 'Model-1' ] . rootAssembly
e1 = a . instances [ 'TopLayer-1' ] . edges
e2 = a . instances [ 'Base-1' ] . edges
a . EdgeToEdge ( movableAxis = e1 [ 4 ] , fixedAxis = e2 [ 6 ] , flip = ON ,
clearance = 0 . 0 )
a = mdb . models [ 'Model-1' ] . rootAssembly
e1 = a . instances [ 'Base-1' ] . edges
e2 = a . instances [ 'Subgrade-1' ] . edges
a . EdgeToEdge ( movableAxis = e1 [ 4 ] , fixedAxis = e2 [ 7 ] , flip = ON ,
clearance = 0 . 0 )
session . viewports [ 'Viewport: 1' ] . view . setValues ( nearPlane = 9 . 7 4
2 7 4 ,
farPlane = 1 2 . 2 2 4 5 , width = 1 0 . 8 1 9 8 , height = 4 . 8 4 8 7 1 ,
viewOffsetX = 0 . 0 4 7 9 7 8 3 ,
viewOffsetY = - 0 . 1 3 2 7 6 8 )
session . viewports [ 'Viewport: 1' ] . partDisplay . setValues (
sectionAssignments = OFF ,
engineeringFeatures = OFF )
session . viewports [ 'Viewport: 1' ] . partDisplay . geometryOptions . setValues
(
referenceRepresentation = ON )
p1 = mdb . models [ 'Model-1' ] . parts [ 'TopLayer' ]
session . viewports [ 'Viewport: 1' ] . setValues ( displayedObject = p1 )
p = mdb . models [ 'Model-1' ] . parts [ 'TopLayer' ]
s = p . edges
side1Edges = s . getSequenceFromMask ( mask = ( '[#18 ]' , ) , )
p . Surface ( side1Edges = side1Edges , name = 'TopLayerBase' )
p = mdb . models [ 'Model-1' ] . parts [ 'TopLayer' ]
s = p . edges
side1Edges = s . getSequenceFromMask ( mask = ( '[#2 ]' , ) , )
p . Surface ( side1Edges = side1Edges , name = 'TyrePath' )
p1 = mdb . models [ 'Model-1' ] . parts [ 'Base' ]
session . viewports [ 'Viewport: 1' ] . setValues ( displayedObject = p1 )
p = mdb . models [ 'Model-1' ] . parts [ 'Base' ]
s = p . edges
```

```
side1Edges = s . getSequenceFromMask ( mask = ( '[#18 ]' , ) , )
p . Surface ( side1Edges = side1Edges , name = 'BaseBase' )
p = mdb . models [ 'Model-1' ] . parts [ 'Base' ]
s = p . edges
side1Edges = s . getSequenceFromMask ( mask = ( '[#42 ]' , ) , )
p . Surface ( side1Edges = side1Edges , name = 'BaseTope' )
p1 = mdb . models [ 'Model-1' ] . parts [ 'Subgrade' ]
session . viewports [ 'Viewport: 1' ] . setValues ( displayedObject = p1 )
p = mdb . models [ 'Model-1' ] . parts [ 'Subgrade' ]
s = p . edges
side1Edges = s . getSequenceFromMask ( mask = ( '[#4080 ]' , ) , )
p . Surface ( side1Edges = side1Edges , name = 'SubgradeTop' )
p = mdb . models [ 'Model-1' ] . parts [ 'Subgrade' ]
s = p . edges
side1Edges = s . getSequenceFromMask ( mask = ( '[#1002 ]' , ) , )
p . Surface ( side1Edges = side1Edges , name = 'SubgradeBase' )
session . viewports [ 'Viewport: 1' ] . partDisplay . setValues (
sectionAssignments = ON ,
engineeringFeatures = ON )
session . viewports [ 'Viewport: 1' ] . partDisplay . geometryOptions . setValues
(
referenceRepresentation = OFF )
a = mdb . models [ 'Model-1' ] . rootAssembly
a . regenerate ( )
a = mdb . models [ 'Model-1' ] . rootAssembly
session . viewports [ 'Viewport: 1' ] . setValues ( displayedObject = a )
session . viewports [ 'Viewport: 1' ] . assemblyDisplay . setValues (
adaptiveMeshConstraints = ON )
mdb . models [ 'Model-1' ] . StaticLinearPerturbationStep ( name = 'TyreLoading'
,
previous = 'Initial' )
session . viewports [ 'Viewport: 1' ] . assemblyDisplay . setValues (
step = 'TyreLoading' )
session . viewports [ 'Viewport: 1' ] . assemblyDisplay . setValues (
interactions = ON ,
constraints = ON , connectors = ON , engineeringFeatures = ON ,
adaptiveMeshConstraints = OFF )
a = mdb . models [ 'Model-1' ] . rootAssembly
region1 = a . instances [ 'TopLayer-1' ] . surfaces [ 'TopLayerBase' ]
a = mdb . models [ 'Model-1' ] . rootAssembly
region2 = a . instances [ 'Base-1' ] . surfaces [ 'BaseTope' ]
mdb . models [ 'Model-1' ] . Tie ( name = 'TopLayerBase' , master = region1 ,
slave = region2 ,
positionToleranceMethod = COMPUTED , adjust = ON , tieRotations = ON ,
thickness = ON )
a = mdb . models [ 'Model-1' ] . rootAssembly
region1 = a . instances [ 'Base-1' ] . surfaces [ 'BaseBase' ]
a = mdb . models [ 'Model-1' ] . rootAssembly
region2 = a . instances [ 'Subgrade-1' ] . surfaces [ 'SubgradeTop' ]
mdb . models [ 'Model-1' ] . Tie ( name = 'BaseSubgrade' , master = region1 ,
slave = region2 ,
positionToleranceMethod = COMPUTED , adjust = ON , tieRotations = ON ,
thickness = ON )
session . viewports [ 'Viewport: 1' ] . assemblyDisplay . setValues ( loads = ON
, bcs = ON ,
predefinedFields = ON , interactions = OFF , constraints = OFF ,
```

```
engineeringFeatures = OFF )
a = mdb . models [ 'Model-1' ] . rootAssembly
region = a . instances [ 'TopLayer-1' ] . surfaces [ 'TyrePath' ]
mdb . models [ 'Model-1' ] . Pressure ( name = 'TyreLoad' , createStepName =
'TyreLoading' ,
region = region , distributionType = UNIFORM , field = '' , magnitude = 6 7 0 0
0 0 . 0 )
a = mdb . models [ 'Model-1' ] . rootAssembly
e1 = a . instances [ 'TopLayer-1' ] . edges
edges1 = e1 . getSequenceFromMask ( mask = ( '[#20 ]' , ) , )
region = a . Set ( edges = edges1 , name = 'TopLayerSide' )
mdb . models [ 'Model-1' ] . DisplacementBC ( name = 'TopLayer' ,
createStepName = 'TyreLoading' , region = region , u1 = 0 . 0 , u2 = UNSET ,
ur3 = UNSET , amplitude = UNSET , fixed = OFF , distributionType = UNIFORM ,
fieldName = '' , localCsys = None )
session . viewports [ 'Viewport: 1' ] . view . setValues ( nearPlane = 1 0 . 4
7 9 3 ,
farPlane = 1 1 . 4 8 8 , width = 4 . 3 2 4 3 , height = 1 . 9 3 7 8 6 ,
viewOffsetX = 0 . 9 1 6 4 5 3 ,
viewOffsetY = 1 . 1 1 9 4 8 )
a = mdb . models [ 'Model-1' ] . rootAssembly
e1 = a . instances [ 'Base-1' ] . edges
edges1 = e1 . getSequenceFromMask ( mask = ( '[#20 ]' , ) , )
region = a . Set ( edges = edges1 , name = 'BaseSide' )
mdb . models [ 'Model-1' ] . DisplacementBC ( name = 'Base' , createStepName =
'TyreLoading' ,
region = region , u1 = 0 . 0 , u2 = UNSET , ur3 = UNSET , amplitude = UNSET ,
fixed = OFF ,
distributionType = UNIFORM , fieldName = '' , localCsys = None )
a = mdb . models [ 'Model-1' ] . rootAssembly
e1 = a . instances [ 'Subgrade-1' ] . edges
edges1 = e1 . getSequenceFromMask ( mask = ( '[#4 ]' , ) , )
region = a . Set ( edges = edges1 , name = 'SubgradeSide' )
mdb . models [ 'Model-1' ] . DisplacementBC ( name = 'Subgrade' ,
createStepName = 'TyreLoading' , region = region , u1 = 0 . 0 , u2 = UNSET ,
ur3 = UNSET , amplitude = UNSET , fixed = OFF , distributionType = UNIFORM ,
fieldName = '' , localCsys = None )
session . viewports [ 'Viewport: 1' ] . view . setValues ( nearPlane = 1 0 . 2
3 7 ,
farPlane = 1 1 . 7 3 0 2 , width = 7 . 1 9 3 5 8 , height = 3 . 2 2 3 6 8 ,
viewOffsetX = - 0 . 2 4 1 3 6 6 ,
viewOffsetY = 1 . 1 2 5 6 1 )
a = mdb . models [ 'Model-1' ] . rootAssembly
e1 = a . instances [ 'Subgrade-1' ] . edges
edges1 = e1 . getSequenceFromMask ( mask = ( '[#1002 ]' , ) , )
region = a . Set ( edges = edges1 , name = 'SubgradeBase' )
mdb . models [ 'Model-1' ] . DisplacementBC ( name = 'SubgradeBase' ,
createStepName = 'TyreLoading' , region = region , u1 = 0 . 0 , u2 = 0 . 0 ,
ur3 = 0 . 0 ,
amplitude = UNSET , fixed = OFF , distributionType = UNIFORM , fieldName = '' ,
localCsys = None )
session . viewports [ 'Viewport: 1' ] . assemblyDisplay . setValues ( mesh = ON
, loads = OFF ,
bcs = OFF , predefinedFields = OFF , connectors = OFF )
session . viewports [ 'Viewport: 1' ] . assemblyDisplay . meshOptions . setValues
(
```

```
meshTechnique = ON )
p = mdb . models [ 'Model-1' ] . parts [ 'Subgrade' ]
session . viewports [ 'Viewport: 1' ] . setValues ( displayedObject = p )
session . viewports [ 'Viewport: 1' ] . partDisplay . setValues (
sectionAssignments = OFF ,
engineeringFeatures = OFF , mesh = ON )
session . viewports [ 'Viewport: 1' ] . partDisplay . meshOptions . setValues (
meshTechnique = ON )
p = mdb . models [ 'Model-1' ] . parts [ 'TopLayer' ]
session . viewports [ 'Viewport: 1' ] . setValues ( displayedObject = p )
p = mdb . models [ 'Model-1' ] . parts [ 'TopLayer' ]
e = p . edges
pickedEdges1 = e . getSequenceFromMask ( mask = ( '[#8 ]' , ) , )
pickedEdges2 = e . getSequenceFromMask ( mask = ( '[#2 ]' , ) , )
p . seedEdgeByBias ( biasMethod = SINGLE , end1Edges = pickedEdges1 ,
end2Edges = pickedEdges2 , minSize = 0 . 0 0 2 5 , maxSize = 0 . 0 0 2 5 ,
constraint = FINER )
p = mdb . models [ 'Model-1' ] . parts [ 'TopLayer' ]
e = p . edges
pickedEdges1 = e . getSequenceFromMask ( mask = ( '[#8 ]' , ) , )
pickedEdges2 = e . getSequenceFromMask ( mask = ( '[#2 ]' , ) , )
p . seedEdgeByBias ( biasMethod = SINGLE , end1Edges = pickedEdges1 ,
end2Edges = pickedEdges2 , minSize = 0 . 0 0 2 5 , maxSize = 0 . 0 0 2 5 ,
constraint = FINER )
p = mdb . models [ 'Model-1' ] . parts [ 'TopLayer' ]
e = p . edges
pickedEdges1 = e . getSequenceFromMask ( mask = ( '[#40 ]' , ) , )
pickedEdges2 = e . getSequenceFromMask ( mask = ( '[#10 ]' , ) , )
p . seedEdgeByBias ( biasMethod = SINGLE , end1Edges = pickedEdges1 ,
end2Edges = pickedEdges2 , minSize = 0 . 0 0 2 5 , maxSize = 0 . 5 , constraint
= FINER )
p = mdb . models [ 'Model-1' ] . parts [ 'TopLayer' ]
e = p . edges
pickedEdges1 = e . getSequenceFromMask ( mask = ( '[#4 ]' , ) , )
pickedEdges2 = e . getSequenceFromMask ( mask = ( '[#21 ]' , ) , )
p . seedEdgeByBias ( biasMethod = SINGLE , end1Edges = pickedEdges1 ,
end2Edges = pickedEdges2 , minSize = 0 . 0 0 5 , maxSize = 0 . 0 0 5 ,
constraint = FINER )
p = mdb . models [ 'Model-1' ] . parts [ 'TopLayer' ]
e = p . edges
pickedEdges1 = e . getSequenceFromMask ( mask = ( '[#4 ]' , ) , )
pickedEdges2 = e . getSequenceFromMask ( mask = ( '[#21 ]' , ) , )
p . seedEdgeByBias ( biasMethod = SINGLE , end1Edges = pickedEdges1 ,
end2Edges = pickedEdges2 , minSize = 0 . 0 0 5 , maxSize = 0 . 0 0 5 ,
constraint = FINER )
p = mdb . models [ 'Model-1' ] . parts [ 'TopLayer' ]
p . generateMesh ( )
session . viewports [ 'Viewport: 1' ] . view . setValues ( nearPlane = 5 . 6 1
5 2 1 ,
farPlane = 6 . 4 0 6 3 7 , width = 3 . 7 9 9 9 7 , height = 1 . 7 0 8 3 1 ,
viewOffsetX = - 0 . 1 6 4 5 7 ,
viewOffsetY = 0 . 3 7 5 1 9 3 )
p = mdb . models [ 'Model-1' ] . parts [ 'Base' ]
session . viewports [ 'Viewport: 1' ] . setValues ( displayedObject = p )
p = mdb . models [ 'Model-1' ] . parts [ 'Base' ]
e = p . edges
```

```
pickedEdges1 = e . getSequenceFromMask ( mask = ( '[#8 ]' , ) , )
pickedEdges2 = e . getSequenceFromMask ( mask = ( '[#2 ]' , ) , )
p . seedEdgeByBias ( biasMethod = SINGLE , end1Edges = pickedEdges1 ,
end2Edges = pickedEdges2 , minSize = 0 . 0 0 2 5 , maxSize = 0 . 0 0 2 5 ,
constraint = FINER )
p = mdb . models [ 'Model-1' ] . parts [ 'Base' ]
e = p . edges
pickedEdges1 = e . getSequenceFromMask ( mask = ( '[#40 ]' , ) , )
pickedEdges2 = e . getSequenceFromMask ( mask = ( '[#10 ]' , ) , )
p . seedEdgeByBias ( biasMethod = SINGLE , end1Edges = pickedEdges1 ,
end2Edges = pickedEdges2 , minSize = 0 . 0 0 2 5 , maxSize = 0 . 5 , constraint
= FINER )
p = mdb . models [ 'Model-1' ] . parts [ 'Base' ]
e = p . edges
pickedEdges1 = e . getSequenceFromMask ( mask = ( '[#4 ]' , ) , )
pickedEdges2 = e . getSequenceFromMask ( mask = ( '[#21 ]' , ) , )
p . seedEdgeByBias ( biasMethod = SINGLE , end1Edges = pickedEdges1 ,
end2Edges = pickedEdges2 , minSize = 0 . 0 1 , maxSize = 0 . 0 3 , constraint =
FINER )
session . viewports [ 'Viewport: 1' ] . view . setValues ( nearPlane = 5 . 5 9
4 8 1 ,
farPlane = 6 . 4 2 6 7 7 , width = 3 . 9 9 5 0 8 , height = 1 . 7 9 6 0 3 ,
viewOffsetX = - 0 . 3 1 6 8 4 2 ,
viewOffsetY = 0 . 1 0 1 5 2 4 )
p = mdb . models [ 'Model-1' ] . parts [ 'Base' ]
e = p . edges
pickedEdges1 = e . getSequenceFromMask ( mask = ( '[#21 ]' , ) , )
pickedEdges2 = e . getSequenceFromMask ( mask = ( '[#4 ]' , ) , )
p . seedEdgeByBias ( biasMethod = SINGLE , end1Edges = pickedEdges1 ,
end2Edges = pickedEdges2 , minSize = 0 . 0 1 , maxSize = 0 . 0 3 , constraint =
FINER )
session . viewports [ 'Viewport: 1' ] . view . setValues ( nearPlane = 5 . 6 8
1 2 8 ,
farPlane = 6 . 3 4 0 3 , width = 3 . 1 6 7 3 6 , height = 1 . 4 2 3 9 2 ,
viewOffsetX = - 0 . 6 2 1 9 6 3 ,
viewOffsetY = 0 . 0 7 4 0 8 9 5 )
p = mdb . models [ 'Model-1' ] . parts [ 'Subgrade' ]
session . viewports [ 'Viewport: 1' ] . setValues ( displayedObject = p )
p = mdb . models [ 'Model-1' ] . parts [ 'Subgrade' ]
e = p . edges
pickedEdges1 = e . getSequenceFromMask ( mask = ( '[#3400 ]' , ) , )
pickedEdges2 = e . getSequenceFromMask ( mask = ( '[#4000 ]' , ) , )
p . seedEdgeByBias ( biasMethod = SINGLE , end1Edges = pickedEdges1 ,
end2Edges = pickedEdges2 , minSize = 0 . 0 0 2 5 , maxSize = 0 . 0 0 2 5 ,
constraint = FINER )
p = mdb . models [ 'Model-1' ] . parts [ 'Subgrade' ]
e = p . edges
pickedEdges1 = e . getSequenceFromMask ( mask = ( '[#3400 ]' , ) , )
pickedEdges2 = e . getSequenceFromMask ( mask = ( '[#4000 ]' , ) , )
p . seedEdgeByBias ( biasMethod = SINGLE , end1Edges = pickedEdges1 ,
end2Edges = pickedEdges2 , minSize = 0 . 0 0 2 5 , maxSize = 0 . 0 0 2 5 ,
constraint = FINER )
p = mdb . models [ 'Model-1' ] . parts [ 'Subgrade' ]
e = p . edges
pickedEdges1 = e . getSequenceFromMask ( mask = ( '[#80 ]' , ) , )
pickedEdges2 = e . getSequenceFromMask ( mask = ( '[#2a ]' , ) , )
```

```
p . seedEdgeByBias ( biasMethod = SINGLE , end1Edges = pickedEdges1 ,
end2Edges = pickedEdges2 , minSize = 0 . 0 0 2 5 , maxSize = 0 . 5 , constraint
= FINER )
p = mdb . models [ 'Model-1' ] . parts [ 'Subgrade' ]
e = p . edges
pickedEdges1 = e . getSequenceFromMask ( mask = ( '[#50 ]' , ) , )
pickedEdges2 = e . getSequenceFromMask ( mask = ( '[#8000 ]' , ) , )
p . seedEdgeByBias ( biasMethod = SINGLE , end1Edges = pickedEdges1 ,
end2Edges = pickedEdges2 , minSize = 0 . 0 3 , maxSize = 0 . 0 8 , constraint =
FINER )
p = mdb . models [ 'Model-1' ] . parts [ 'Subgrade' ]
e = p . edges
pickedEdges1 = e . getSequenceFromMask ( mask = ( '[#300 ]' , ) , )
pickedEdges2 = e . getSequenceFromMask ( mask = ( '[#10000 ]' , ) , )
p . seedEdgeByBias ( biasMethod = SINGLE , end1Edges = pickedEdges1 ,
end2Edges = pickedEdges2 , minSize = 0 . 0 8 , maxSize = 0 . 1 7 5 5 ,
constraint = FINER )
p = mdb . models [ 'Model-1' ] . parts [ 'Subgrade' ]
e = p . edges
pickedEdges1 = e . getSequenceFromMask ( mask = ( '[#5 ]' , ) , )
pickedEdges2 = e . getSequenceFromMask ( mask = ( '[#800 ]' , ) , )
p . seedEdgeByBias ( biasMethod = SINGLE , end1Edges = pickedEdges1 ,
end2Edges = pickedEdges2 , minSize = 0 . 1 7 5 5 , maxSize = 1 . 0 , constraint
= FINER )
p = mdb . models [ 'Model-1' ] . parts [ 'Base' ]
session . viewports [ 'Viewport: 1' ] . setValues ( displayedObject = p )
p = mdb . models [ 'Model-1' ] . parts [ 'Base' ]
p . generateMesh ( )
p = mdb . models [ 'Model-1' ] . parts [ 'Subgrade' ]
session . viewports [ 'Viewport: 1' ] . setValues ( displayedObject = p )
p = mdb . models [ 'Model-1' ] . parts [ 'Subgrade' ]
p . generateMesh ( )
session . viewports [ 'Viewport: 1' ] . view . setValues ( nearPlane = 7 . 1 4
3 5 9 ,
farPlane = 8 . 2 2 3 9 1 , width = 4 . 6 2 3 6 6 , height = 2 . 0 7 8 6 1 ,
viewOffsetX = - 0 . 1 2 6 3 5 3 ,
viewOffsetY = 0 . 0 9 0 9 9 4 6 )
a = mdb . models [ 'Model-1' ] . rootAssembly
session . viewports [ 'Viewport: 1' ] . setValues ( displayedObject = a )
a1 = mdb . models [ 'Model-1' ] . rootAssembly
a1 . regenerate ( )
session . viewports [ 'Viewport: 1' ] . view . setValues ( nearPlane = 1 0 . 4
2 7 8 ,
farPlane = 1 1 . 5 3 9 4 , width = 4 . 7 5 1 8 , height = 2 . 1 3 6 2 2 ,
viewOffsetX = - 0 . 2 7 0 4 7 4 ,
viewOffsetY = 1 . 4 4 1 7 8 )
session . viewports [ 'Viewport: 1' ] . assemblyDisplay . setValues ( mesh = OFF
,
adaptiveMeshConstraints = ON )
session . viewports [ 'Viewport: 1' ] . assemblyDisplay . meshOptions . setValues
(
meshTechnique = OFF )
mdb . models [ 'Model-1' ] . fieldOutputRequests [ 'F-Output-1' ] . setValues (
variables = (
'S' , 'E' , 'LE' , 'U' , 'RF' , 'CF' ) )
```

```
session . viewports [ 'Viewport: 1' ] . assemblyDisplay . setValues (
interactions = ON ,
constraints = ON , connectors = ON , engineeringFeatures = ON ,
adaptiveMeshConstraints = OFF )
session . viewports [ 'Viewport: 1' ] . view . setValues ( nearPlane = 1 0 . 2
7 1 7 ,
farPlane = 1 1 . 6 9 5 5 , width = 6 . 8 6 2 3 , height = 3 . 0 7 5 2 2 ,
viewOffsetX = 0 . 5 8 3 2 3 ,
viewOffsetY = 1 . 1 4 6 6 3 )
session . viewports [ 'Viewport: 1' ] . assemblyDisplay . setValues ( loads = ON
, bcs = ON ,
predefinedFields = ON , interactions = OFF , constraints = OFF ,
engineeringFeatures = OFF )
session . viewports [ 'Viewport: 1' ] . assemblyDisplay . setValues ( mesh = ON
, loads = OFF ,
bcs = OFF , predefinedFields = OFF , connectors = OFF )
session . viewports [ 'Viewport: 1' ] . assemblyDisplay . meshOptions . setValues
(
meshTechnique = ON )
session . viewports [ 'Viewport: 1' ] . assemblyDisplay . setValues ( mesh = OFF
,
adaptiveMeshConstraints = ON )
session . viewports [ 'Viewport: 1' ] . assemblyDisplay . meshOptions . setValues
(
meshTechnique = OFF )
session . viewports [ 'Viewport: 1' ] . assemblyDisplay . setValues (
adaptiveMeshConstraints = OFF )
session . viewports [ 'Viewport: 1' ] . partDisplay . setValues (
sectionAssignments = ON ,
engineeringFeatures = ON , mesh = OFF )
session . viewports [ 'Viewport: 1' ] . partDisplay . meshOptions . setValues (
meshTechnique = OFF )
p = mdb . models [ 'Model-1' ] . parts [ 'Subgrade' ]
session . viewports [ 'Viewport: 1' ] . setValues ( displayedObject = p )
session . viewports [ 'Viewport: 1' ] . partDisplay . setValues (
sectionAssignments = OFF ,
engineeringFeatures = OFF )
session . viewports [ 'Viewport: 1' ] . partDisplay . geometryOptions . setValues
(
referenceRepresentation = ON )
a = mdb . models [ 'Model-1' ] . rootAssembly
session . viewports [ 'Viewport: 1' ] . setValues ( displayedObject = a )
mdb . Job ( name = 'LVR_DCP' , model = 'Model-1' , description = '' , type =
ANALYSIS ,
atTime = None , waitMinutes = 0 , waitHours = 0 , queue = None , memory = 9 0 ,
memoryUnits = PERCENTAGE , getMemoryFromAnalysis = True ,
explicitPrecision = SINGLE , nodalOutputPrecision = SINGLE , echoPrint = OFF ,
modelPrint = OFF , contactPrint = OFF , historyPrint = OFF , userSubroutine = ''
,
scratch = '' , multiprocessingMode = DEFAULT , numCpus = 4 , numDomains = 4 ,
numGPUs = 2 )
mdb . jobs [ 'LVR_DCP' ] . submit ( consistencyChecking = OFF )


# Apply user inputs for materials and pressure
__apply_inputs__ ( )
```

Abaqus Seal Model

```
# -*- coding: mbcs -*-
# Parametric 2D FEM for surface seals on LVRs — Single vs Double Seal
# Builds two models:
#   1) Model-SingleSeal  -> JOB_SingleSeal
#   2) Model-DoubleSeal  -> JOB_DoubleSeal
#  Edit ONLY the INPUTS block. Run in Abaqus/CAE or with: abaqus cae
noGUI=Seal2D_parametric.py
from abaqus import *
from abaqusConstants import *
import regionToolset , mesh , part , material , assembly , step , interaction ,
load , job , sketch
# ==========================
# ========= INPUTS ========
# ==========================
INPUTS = {
# Naming
"base_model_name" : "Model-SingleSeal" ,
"double_model_name" : "Model-DoubleSeal" ,
"single_job_name" : "JOB_SingleSeal" ,
"double_job_name" : "JOB_DoubleSeal" ,
# Geometry [m]
"width" : 0 . 3 0 , # model width (x)
"base_thk" : 0 . 1 0 , # base thickness (y)
"seal1_thk" : 0 . 0 1 0 , # single seal OR top seal in double
"seal2_thk" : 0 . 0 1 0 , # bottom seal in double
"edge_buffer" : 0 . 0 5 , # unused here; reserved for future
# Load / contact band
"tyre_pressure" : 5 5 0 e3 , # Pa
"contact_width" : 0 . 1 0 , # width of loaded band, centered
# Materials (linear elastic)
"materials" : {
"BASE" : { "E" : 2 5 0 e6 , "nu" : 0 . 3 5 , "rho" : 2 0 0 0 . 0 } ,
"SEAL" : { "E" : 1 5 0 0 e6 , "nu" : 0 . 4 5 , "rho" : 1 1 0 0 . 0 } , #
effective binder+chips
} ,
# Mesh
"mesh" : {
"size_base" : 0 . 0 1 ,
"size_seal" : 0 . 0 0 5
} ,
# Step & output
"step_name" : "LoadStep" ,
"nlgeom" : False ,
"field_outputs" : ( "S" , "E" , "U" , "RF" , "CF" , "LE" ) ,
"history_outputs" : ( )
}
# ==========================
# ======== Helpers ========
# ==========================
def ensure_new_model ( name ) :
if name in mdb . models . keys ( ) :
del mdb . models [ name ]
return mdb . Model ( name = name )

def make_layer ( model , part_name , width , thk ) :
s = model . ConstrainedSketch ( name = '__%s__' % part_name , sheetSize = max (
1 . 0 , width * 5 ) )
s . rectangle ( point1 = ( 0 . 0 , 0 . 0 ) , point2 = ( width , thk ) )
p = model . Part ( name = part_name , dimensionality = TWO_D_PLANAR , type =
DEFORMABLE_BODY )
p . BaseShell ( sketch = s )
```

```
del model . sketches [ '__%s__' % part_name ]
return p

def make_materials ( model , matdict ) :
for n , pr in matdict . items ( ) :
if n in model . materials . keys ( ) :
del model . materials [ n ]
m = model . Material ( name = n )
m . Density ( table = ( ( pr [ "rho" ] , ) , ) )
m . Elastic ( table = ( ( pr [ "E" ] , pr [ "nu" ] ) , ) )
if n in model . sections . keys ( ) :
del model . sections [ n ]
model . HomogeneousSolidSection ( name = n , material = n , thickness = None )

def assign_section_and_type ( p , sec_name ) :
region = p . Set ( faces = p . faces , name = 'SET_%s' % sec_name )
p . SectionAssignment ( region = region , sectionName = sec_name , offset = 0 .
0 ,
offsetType = MIDDLE_SURFACE , thicknessAssignment = FROM_SECTION )
et = mesh . ElemType ( elemCode = CPS4R , elemLibrary = STANDARD ) # 2D
quadrilateral, reduced
p . setElementType ( regions = ( region , ) , elemTypes = ( et , ) )

def seed_and_mesh ( p , size ) :
p . seedPart ( size = size , deviationFactor = 0 . 1 , minSizeFactor = 0 . 1 )
p . generateMesh ( )

def top_edge_of_part ( p ) :
return max ( p . edges , key = lambda e : e . pointOn [ 0 ] [ 1 ] )

def bottom_edge_of_part ( p ) :
return min ( p . edges , key = lambda e : e . pointOn [ 0 ] [ 1 ] )

def partition_top_edge_for_band ( model , p , width , thk , band_width ) :
"" " Partition the face vertically at x0 and x1 so the TOP edge has 3 segments
.
Creates a surface 'S_LOAD' on the middle top segment for pressure application .
"" "
x0 = 0 . 5 * width - 0 . 5 * band_width
x1 = 0 . 5 * width + 0 . 5 * band_width
f = p . faces [ 0 ]
t = p . MakeSketchTransform ( sketchPlane = f , sketchPlaneSide = SIDE1 , origin
= ( 0 . 0 , 0 . 0 , 0 . 0 ) )
s = model . ConstrainedSketch ( name = '__partBand__' , sheetSize = max ( 1 . 0
, width * 5 ) , transform = t )
# draw two vertical lines
s . Line ( point1 = ( x0 , 0 . 0 ) , point2 = ( x0 , thk ) )
s . Line ( point1 = ( x1 , 0 . 0 ) , point2 = ( x1 , thk ) )
p . PartitionFaceBySketch ( faces = ( f , ) , sketch = s )
del model . sketches [ '__partBand__' ]

# After partition, find the TOP edge segments and pick the middle one by x centroid
top_y = max ( [ e . pointOn [ 0 ] [ 1 ] for e in p . edges ] )
top_edges = [ e for e in p . edges if abs ( e . pointOn [ 0 ] [ 1 ] - top_y
) < 1 e - 9 ]
# Middle edge has x centroid ~ center of band
xc_mid = 0 . 5 * ( x0 + x1 )
e_mid = min ( top_edges , key = lambda e : abs ( e . pointOn [ 0 ] [ 0 ] -
xc_mid ) )
p . Surface ( name = 'S_LOAD' , side1Edges = ( e_mid , ) )

def define_bot_top_surfaces ( p ) :
```

```
p . Surface ( name = 'S_BOT' , side1Edges = ( bottom_edge_of_part ( p ) , ) )
p . Surface ( name = 'S_TOP' , side1Edges = ( top_edge_of_part ( p ) , ) )

def build_assembly_single ( model , width , base_thk , seal1_thk ) :
a = model . rootAssembly
iB = a . Instance ( name = 'Base-1' , part = model . parts [ 'Base' ] ,
dependent = ON )
iS1 = a . Instance ( name = 'Seal1-1' , part = model . parts [ 'Seal1' ] ,
dependent = ON )
a . translate ( instanceList = ( 'Seal1-1' , ) , vector = ( 0 . 0 , base_thk ,
0 . 0 ) )
return a

def build_assembly_double ( model , width , base_thk , seal1_thk , seal2_thk ) :
a = model . rootAssembly
iB = a . Instance ( name = 'Base-1' , part = model . parts [ 'Base' ] ,
dependent = ON )
iS2 = a . Instance ( name = 'Seal2-1' , part = model . parts [ 'Seal2' ] ,
dependent = ON )
iS1 = a . Instance ( name = 'Seal1-1' , part = model . parts [ 'Seal1' ] ,
dependent = ON )
a . translate ( instanceList = ( 'Seal2-1' , ) , vector = ( 0 . 0 , base_thk ,
0 . 0 ) )
a . translate ( instanceList = ( 'Seal1-1' , ) , vector = ( 0 . 0 , base_thk +
seal2_thk , 0 . 0 ) )
return a

def tie_stack ( model , a , upper , lower ) :
model . Tie ( name = 'Tie_%s_%s' % ( upper , lower ) ,
master = a . instances [ upper ] . surfaces [ 'S_BOT' ] ,
slave = a . instances [ lower ] . surfaces [ 'S_TOP' ] ,
positionToleranceMethod = COMPUTED , adjust = ON , tieRotations = ON , thickness
= ON )

def add_bcs_and_loads ( model , a , width , step_name , p_load ) :
# Fix bottom of Base (y=0)
e_bot = min ( a . instances [ 'Base-1' ] . edges , key = lambda e : e . pointOn
[ 0 ] [ 1 ] )
set_bottom = a . Set ( edges = ( e_bot , ) , name = 'SET_BOTTOM' )
model . DisplacementBC ( name = 'BC_FixBottom' , createStepName = step_name ,
region = set_bottom , u1 = 0 . 0 , u2 = 0 . 0 )

# X-symmetry at left edge x=0 (optional)
left_edges = [ e for e in a . instances [ 'Base-1' ] . edges if abs ( e .
pointOn [ 0 ] [ 0 ] - 0 . 0 ) < 1 e - 9 ]
if left_edges :
set_left = a . Set ( edges = tuple ( left_edges ) , name = 'SET_LEFT' )
model . XsymmBC ( name = 'BC_XSYM' , createStepName = step_name , region =
set_left )

# Apply pressure on topmost instance using part-defined S_LOAD surface
top_inst_name = None ; top_y = - 1 e9
for nm , inst in a . instances . items ( ) :
e_top = max ( inst . edges , key = lambda e : e . pointOn [ 0 ] [ 1 ] )
y = e_top . pointOn [ 0 ] [ 1 ]
if y > top_y :
top_y = y ; top_inst_name = nm
model . Pressure ( name = 'TyrePressure' , createStepName = step_name ,
region = a . instances [ top_inst_name ] . surfaces [ 'S_LOAD' ] ,
magnitude = p_load , distributionType = UNIFORM )

def make_step_and_outputs ( model , step_name , nlgeom , fvars , hvars ) :
```

```
if step_name in model . steps . keys ( ) :
del model . steps [ step_name ]
model . StaticStep ( name = step_name , previous = 'Initial' , nlgeom = nlgeom
)
# Field output
model . fieldOutputRequests [ 'F-Output-1' ] . setValues ( variables = fvars )
if hvars :
model . historyOutputRequests [ 'H-Output-1' ] . setValues ( variables = hvars )

def make_job ( model_name , job_name , ncpus = 4 , ndomains = 4 , mem_pct = 9
0 ) :
if job_name in mdb . jobs . keys ( ) :
del mdb . jobs [ job_name ]
mdb . Job ( name = job_name , model = model_name , type = ANALYSIS ,
memory = mem_pct , memoryUnits = PERCENTAGE ,
multiprocessingMode = DEFAULT , numCpus = ncpus , numDomains = ndomains )

# =========================
# ===== Build Single ======
# =========================
M1 = ensure_new_model ( INPUTS [ "base_model_name" ] )
W = INPUTS [ "width" ]
tB = INPUTS [ "base_thk" ]
tS1 = INPUTS [ "seal1_thk" ]

make_materials ( M1 , INPUTS [ "materials" ] )
pB = make_layer ( M1 , 'Base' , W , tB )
pS1 = make_layer ( M1 , 'Seal1' , W , tS1 )

assign_section_and_type ( pB , 'BASE' )
assign_section_and_type ( pS1 , 'SEAL' )

# Partition top edge of Seal1 for load band and define surfaces
partition_top_edge_for_band ( M1 , pS1 , W , tS1 , INPUTS [ "contact_width" ] )
define_bot_top_surfaces ( pB )
define_bot_top_surfaces ( pS1 )

seed_and_mesh ( pB , INPUTS [ "mesh" ] [ "size_base" ] )
seed_and_mesh ( pS1 , INPUTS [ "mesh" ] [ "size_seal" ] )

a1 = build_assembly_single ( M1 , W , tB , tS1 )
tie_stack ( M1 , a1 , 'Seal1-1' , 'Base-1' )

make_step_and_outputs ( M1 , INPUTS [ "step_name" ] , INPUTS [ "nlgeom" ] ,
INPUTS [ "field_outputs" ] , INPUTS [ "history_outputs" ] )
add_bcs_and_loads ( M1 , a1 , W , INPUTS [ "step_name" ] , INPUTS [ "tyre_pressure"
] )

make_job ( M1 . name , INPUTS [ "single_job_name" ] )

# =========================
# ===== Build Double ======
# =========================
M2 = ensure_new_model ( INPUTS [ "double_model_name" ] )
W = INPUTS [ "width" ]
tB = INPUTS [ "base_thk" ]
tS1 = INPUTS [ "seal1_thk" ]
tS2 = INPUTS [ "seal2_thk" ]

make_materials ( M2 , INPUTS [ "materials" ] )
pB = make_layer ( M2 , 'Base' , W , tB )
```

```
pS2 = make_layer ( M2 , 'Seal2' , W , tS2 ) # bottom
pS1 = make_layer ( M2 , 'Seal1' , W , tS1 ) # top

assign_section_and_type ( pB , 'BASE' )
assign_section_and_type ( pS2 , 'SEAL' )
assign_section_and_type ( pS1 , 'SEAL' )

# Partition top edge of Seal1 (topmost) for load band and define surfaces
partition_top_edge_for_band ( M2 , pS1 , W , tS1 , INPUTS [ "contact_width" ] )
define_bot_top_surfaces ( pB )
define_bot_top_surfaces ( pS2 )
define_bot_top_surfaces ( pS1 )

seed_and_mesh ( pB , INPUTS [ "mesh" ] [ "size_base" ] )
seed_and_mesh ( pS2 , INPUTS [ "mesh" ] [ "size_seal" ] )
seed_and_mesh ( pS1 , INPUTS [ "mesh" ] [ "size_seal" ] )

a2 = build_assembly_double ( M2 , W , tB , tS1 , tS2 )
tie_stack ( M2 , a2 , 'Seal1-1' , 'Seal2-1' )
tie_stack ( M2 , a2 , 'Seal2-1' , 'Base-1' )

make_step_and_outputs ( M2 , INPUTS [ "step_name" ] , INPUTS [ "nlgeom" ] ,
INPUTS [ "field_outputs" ] , INPUTS [ "history_outputs" ] )
add_bcs_and_loads ( M2 , a2 , W , INPUTS [ "step_name" ] , INPUTS [ "tyre_pressure"
] )

make_job ( M2 . name , INPUTS [ "double_job_name" ] )

print ( "Built models:" , M1 . name , "and" , M2 . name )
print ( "Jobs:" , INPUTS [ "single_job_name" ] , "and" , INPUTS [ "double_job_name"
] )
print ( "Edit the INPUTS dict at the top to change geometry, materials, loads, and
mesh." )
```